



2013 | Faculteit Wetenschappen



DOCTORAATSPROEFSCHRIFT



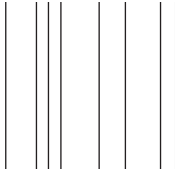
Limit cycles in slow-fast codimension 3 bifurcations

Proefschrift voorgelegd tot het behalen van de graad van doctor
in de wetenschappen, wiskunde, te verdedigen door

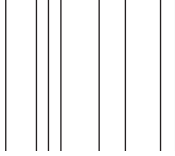
Renato Huzak

Promoter: prof. dr. P. De Maesschalck

Copromoter: prof. dr. F. Dumortier



D/2013/2451/59



Words of thanks

I am truly grateful to Professor Michael Deleuze, my supervisor, for his help, encouragement and stimulating scientific discussions over these three years of work which brought me to the achievement of this thesis. I really appreciate his professionalism and dedication to his research and his doctoral students. Working with him has been a privilege.

I also truly appreciated the widespread and fascinating discussions with Dr. Balázs Hajgató. I would like to thank him for his very constructive suggestions, comments and help.

It is also a pleasure to thank my colleagues Reza Shojaei, Filippo Morini, and Abolfazl Shiroudi for interesting discussions and exchange of ideas.

Nele and Renato I would like to thank you for your help.

Last but not least, I would like to give a special thank to my dear wife Ines for being very supportive, encouraging, and patient. Hvala ti Ines!

I also would like to thank my family for being very supportive.

Contents

1	General introduction	5
1.1	References	10
2	Theoretical methods.....	12
2.1	Electronic structure theory	12
2.1.1	Hartree-Fock theory	17
2.1.1.1	Restricted closed-shell Hartree-Fock theory.....	23
2.1.1.2	Unrestricted open-shell Hartree-Fock theory	26
2.2	Electron correlation treatments.....	28
2.2.1	Full configuration interaction	28
2.2.2	Many body perturbation theory.....	31
2.2.3	Coupled cluster theory.....	35
2.3	Density functional theory	40
2.3.1	The Kohn-Sham theory.....	42
2.3.2	Exchange, correlation and hybrid functionals.....	47
2.3.2.1	Local density approximation	48
2.3.2.2	Gradient expansion approximation	49
2.3.2.3	Hybrid methods.....	50
2.3.3	The self-interaction problem.....	51

2.3.4	Computational implementation: LCAO ansatz in the Kohn-Sham equations	52
2.4	Basis sets.....	55
2.5	Finite field method	58
2.6	Born-Oppenheimer molecular dynamics	59
2.6.1	Hellmann-Feynman theorem	66
2.7	Translation symmetry: Bloch theorem, Bloch orbitals and Bloch functions.....	67
2.8	References	73
3	Half-metallicity and spin-contamination of the electronic ground state of graphene nanoribbons and related systems: an impossible compromise?	80
3.1	Context and scientific motivation	80
3.2	Crystalline orbital analysis of spin-contamination in extended periodic systems	88
3.3	Methodology and computational details.....	98
3.4	Naphthalene: the smallest half-metallic graphene nanoisland?.....	102
3.5	Spin-contamination and half-metallicity as a function of system size	117
3.6	Further considerations on spontaneous spin flips and symmetry breakings.....	126
3.7	Conclusions and outlook for the future	130

3.8	References	135
4	Focal point analysis of the singlet-triplet energy gap of octacene and larger acenes	143
4.1	Introduction	143
4.2	Methodology.....	146
4.3	Results and discussion	151
4.4	Conclusions and further challenges to theoreticians.....	168
4.5	References	173
4.6	Appendix.....	181
5	Benchmark theoretical study of the ionization energies, electron affinities and singlet-triplet energy gaps of azulene, phenanthrene, pyrene, chrysene and perylene.....	186
5.1	Introduction	186
5.2	Computational details	190
5.3	Results and discussion	192
5.3.1	The electronic ground state.....	192
5.3.2	Singlet-triplet energy gap	194
5.3.3	Electron affinities	200
5.3.4	Ionization energies.....	206
5.4	Conclusions	213
5.5	References	215

6	Benchmark theoretical study of the electric polarizabilities of naphthalene, anthracene and tetracene	221
6.1	Introduction	221
6.2	Computational details	224
6.3	Results and discussion	229
6.3.1	Convergence of molecular polarizabilities towards the CCSD(T)/CBS level	229
6.3.2	Naphthalene.....	233
6.3.3	Anthracene	235
6.3.4	Tetracene	237
6.3.5	Vibrational corrections to electronic polarizabilities.....	238
6.4	Conclusions	240
6.5	References	241
7	Summary and conclusions.....	249
7.1	References	253
8	Samenvatting en conclusies	254
8.1	References	259
	List of publications	260
	List of attended conferences.....	261

1 General introduction

Polycyclic Aromatic Hydrocarbons (PAHs) represent a large class of π -conjugated compounds, which are of great importance in many research areas, such as astrophysics, material sciences (organic opto-electronics), environmental chemistry, and other research areas of physics and chemistry. PAHs are very important from a practical point of view, since they have found applications in a large variety of industrial branches. They are for instance involved in the production of skin conditioning agents [1], of dyes, drugs, and pesticides [2], of UV-filters, paints and sensitizers [2].

PAHs have been identified in the interstellar medium, as well as in interplanetary dust particles [3], and in the atmosphere of Titan and Jupiter [4]. They have also been unambiguously characterized in meteoritic samples [5]. There is a consensus in the literature about the association of the interstellar infrared (IR) emission bands to the molecular vibrations of complex mixtures of molecular PAHs of different sizes, structures and charge states, or of PAHs as subunits of larger carbonaceous grains. PAHs are also considered to contribute to major diffuse interstellar absorption bands [6]. PAHs constitute the building blocks of interstellar dust grains, and play an important role in mediating energetic and chemical processes in the interstellar medium. Many questions, such as the formation mechanisms of PAHs and related species, their size distribution, their charge and hydrogenation state, etc., remain open. These questions have motivated numerous (observational, experimental, and theoretical) studies and have led to the conjecture that many unidentified spectral features of interstellar origin could be ascribed to PAHs. Therefore, the understanding of the molecular properties of PAHs in all their relevant ionization

and hydrogenation states is of great relevance for unraveling the physics and chemistry of the interstellar medium.

One of the most important and attractive research fields, where PAHs appear to be very promising materials, is organic opto-electronics [7]. Organic semiconductors have been subject to intensive research for the last few decades, since they are key components in organic field-effect transistors (OFET) [8], which are essential for the next generation of electronic devices, such as flexible sensors [9], electronic papers [10], radio-frequency identification (RFID) tags [11], etc. The ability to replace inorganic semiconductors by organic materials will decrease manufacturing costs and enable the fabrication of electronic devices over large areas, or on lightweight, flexible substrates. Among organic semiconductors, *n*-acenes and their derivatives have found widespread application as active elements in a variety of electronic devices, due to their excellent charge carrier transport properties [12].

The performance of organic semiconducting devices depends upon many physical processes, such as charge transport, charge collections at the electrodes, molecular packaging in the bulk material, absorption and emission properties [13]. Accurate quantum-mechanical studies of basic properties of individual PAH molecules, such as their electronic excitation energies and electric polarizabilities, can significantly contribute to a better understanding of the electronic and optical properties of organic semiconductors with promising applications in optoelectronics.

Polycyclic Aromatic Hydrocarbons (PAHs) are characterized by extremely low band gaps and are therefore subject to particularly strong electron correlation effects. Accurate quantum mechanical insights into their properties

requires thus high level and large scale treatments of electronic correlation, requiring prohibitively expensive computational means. As shall be shown in this thesis, theoretical studies at benchmark levels of the electronic properties of these systems are interesting, not only because of the computational challenge they represent, but also because “getting the right numbers for the right reasons” has lead us to revise well-established views on the electronic structure and properties of these systems.

A new field of research which is currently raising great excitement among material scientists with regards to future applications of large PAHs, referred to as zig-zag graphene nanoribbons (ZGNRs) and zig-zag graphene nanoislands (ZGNIs), is spintronics (i.e. *spin transport electronics*) - a new technology where it is not the electric charge but the electron spin that carries information. This excitement stems from the recent theoretical prediction that (extended) ZGNRs (Figure 1) of finite width (thus, with one-dimensional periodicity) [14] and finite ZGNIs such as bisanthrene [15] (Figure 2) should be half-metallic, i.e. that electrons with one spin orientation should behave in a metallic way whereas the electrons of opposite spin would behave according to an insulating regime, when an electric field is applied perpendiculary to the zig-zag edge. This prediction was drawn on the ground of “first principle” calculations employing (spin-unrestricted) Density Functional Theory (DFT) [16] along with the local spin density approximation (LSDA) [17]. Due to a localization of frontier electrons of opposite spin on opposite zig-zag edges, a band gap opens in a given spin-band system in a presence of an external perpendicular electric field, whereas electrons in the opposite spin-band system are lifted from the occupied (valence) to the unoccupied (conduction) bands (Figure 3).

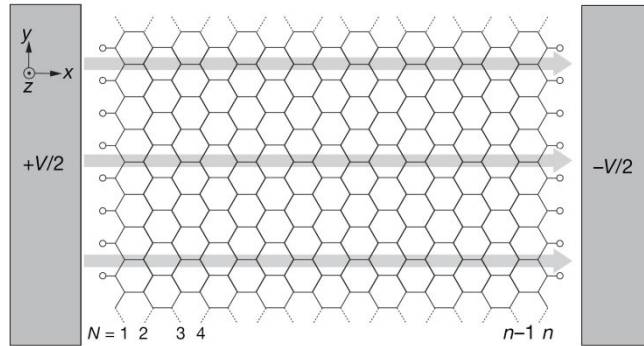


Figure 1. Extended zig-zag graphene nanoribbon (ZGNR) of finite width with one-dimensional periodicity in the presence of an external electric field perpendicular to the zig-zag edge.

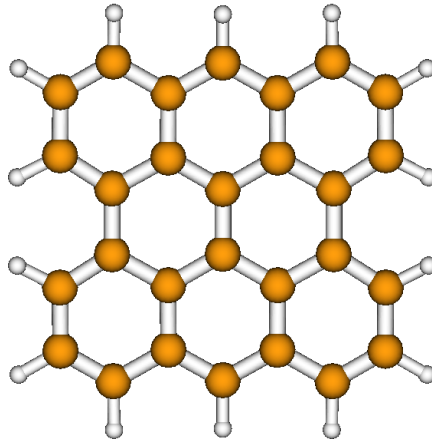


Figure 2. Molecular structure of a phenanthro[1,10,9,8-opqra]perylene, alias bisanthrene [$C_{28}H_{14}$].

The views that ZGNRs are half-metallic systems have never been experimentally confirmed so far. As shall be shown within this thesis, such views are incompatible with basic principles and postulates of (non-relativistic) quantum mechanics.

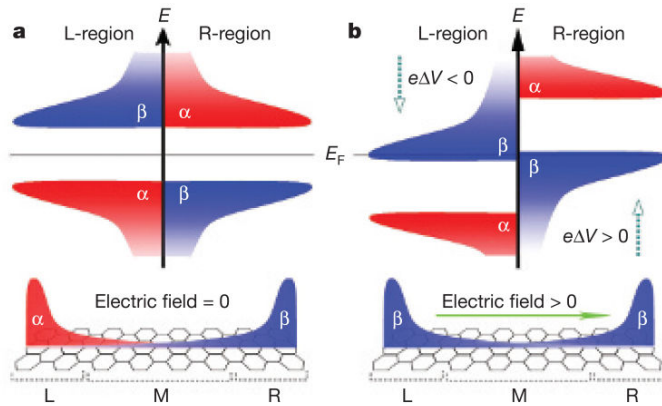


Figure 3. Schematic density-of-states diagram of the electronic states of a ZGNR in the absence (a) and in the presence (b) of an external electric field perpendicular to zig-zag edge. Figure is taken from ref. [14].

The half-metallicity of ZGNRs and ZGNIs is a most important and topical issue. Indeed, by virtue of the resemblance of the spin-polarization (up or down) with the information zero or one in regular electronics, monitoring spin transports in appropriate materials offers opportunities for a new generation of devices combining microelectronics with spin-dependent effects (“spintronics” [18]) due to interactions between the spin of the carrier and local magnetic fields. Spin-field effect transistors and light emitting diodes, spin resonant tunnelling devices, optical switches operating at terahertz frequency, modulators, encoders, decoders, or quantum bits for quantum computation and communication are already envisioned.

In the first part of the present thesis, we re-investigate the issue of Half-Metallicity of ZGNRs and related finite systems. To this end, the influence of an external electric field on the molecular and electronic structure of large but finite model PAHs is comparatively studied on DFT and many-body quantum mechanically grounds. The scaling properties of the spin-contamination arising with symmetry breakings of the electron densities into “singlet open-shell”

states is investigated analytically using the formalism of crystalline orbitals for extended periodic systems with periodicity in one dimension, and computationally, at various theoretical levels, using Hartree-Fock and Density Functional Theories. We then proceed with benchmark calculations of the singlet-triplet excitation energies, ionization energies, electron affinities and polarizabilities of model PAH compounds to demonstrate that highly accurate insights into main physico-chemical properties of these systems are amenable using symmetry restricted spin-densities.

1.1 References

- [1] F. A. Anderson, *Int. J. Toxicol.* **18**, 27 (1999).
- [2] R. G. Harvey, *Polycyclic Aromatic Hydrocarbons*, (Wiley-VCH, New York, 1997).
- [3] S. J. Clemett, C. R. Maechling, R. N. Zare, P. D. Swan, R. M. Walker, *Science*, **262** 721 (1993).
- [4] C. Sagan, B. N. Khare, W. R. Thompson, G. D. McDonald, M. R. Wing, J. L. Bada, T. Vo-Dinh, E. T. Arakawa, *Astrophys. J.* **414**, 399 (1993).
- [5] J. H. Hahn, R. Zenobi, J. L. Bada, R. N. Zare, *Science* **239**, 1523 (1988).
- [6] A. Léger, L. d'Hendecourt, *Astron. Astrophys.* **146**, 81 (1985); G. P. van der Zwet, L. Allamandola, *Astron. Astrophys.* **146** 76 (1985); M. K. Crawford, A. G. G. M. Tielens, L. J. Allamandola, *Astrophys. J. Lett.* **293**, L45 (1985). F. Salama, G. A. Galazutdinov, J. Krelowski, L. J. Allamandola, F. A. Musaev, *Astrophys. J.* **526** 265 (1999).
- [7] J. E. Anthony, *Angew. Chem. Int. Ed.* **47**, 452 (2008).

- [8] M. Halik, H. Klauk, U. Zschieschang, T. Kriem, G. Schmid, W. Radlik, K. Wussow, *Appl. Phys. Lett.* **81**, 289 (2002).
- [9] Z.-T. Zhu, J.T. Mason, R. Dieckmann, G.G. Malliaras, *Appl. Phys. Lett.* **81**, 4643 (2002).
- [10] L. Zhou, A. Wanga, S.-C. Wu, J. Sun, S. Park, T. N. Jackson, *Appl. Phys. Lett.* **88**, 083502 (2006).
- [11] R. Rotzoll, S. Mohapatra, V. Olariu, R. Wenz, M. Grigas, K. Dimmler, *Appl. Phys. Lett.* **88**, 123502 (2006).
- [12] Y.-Y. Lin, D. J. Gundlach, S. F. Nelson, T. N. Jackson, *IEEE Electron Device Lett.* **18**, 606 (1997).
- [13] J.-L. Brédas, D. Beljonne, V. Coropceanu, J. Cornil, *Chem. Rev.* **104**, 4971 (2004); J. C. Sancho-Garcia, *Chem. Phys.* **331**, 321 (2007).
- [14] Y.-W. Son, M. L. Cohen, and S. G. Louie, *Nature (London)*, **444**, 347 (2006).
- [15] O. Hod, V. Barone, G. E. Scuseria, *Phys. Rev. B*, **77**, 035411 (2008)
- [16] (a) R. G. Parr, W. Yang, *Density Functional Theory of Atoms and Molecules* (Oxford University Press, New York, 1989); (b) R. M. Dreizler, E. K. U. Gross, *Density Functional Theory* (Springer-Verlag, Berlin Heidelberg, New York, 1990); (c) W. Koch, M. Holthausen, *A Chemist's Guide to Density Functional Theory*, Second Ed. (Wiley-VCH, Weinheim, 2001).
- [17] J. P. Perdew, A. Zunger, *Phys. Rev. B*, **23**, 5048 (1981).
- [18] S. A. Wolf, D. D. Awschalom, R. A. Buhrman, J. M. Daughton, S. von Molnár, M. L. Roukes, A. Y. Chtchelkanova, D. M. Treger, *Science*, **294**, 1488 (2001).

2 Theoretical methods

2.1 Electronic structure theory

The central equation of quantum mechanics, from which practically all molecular properties can be derived, is the non-relativistic time-independent Schrödinger equation [1-5]:

$$\hat{H}\Psi = E\Psi, \quad (1)$$

where \hat{H} represents the Hamiltonian operator for a system of nuclei and electrons, Ψ is the total wave function depending on the Cartesian coordinates of these particles, and E is the total energy of the system. The Hamiltonian \hat{H} contains two terms, describing the kinetic and potential energy contributions. In atomic units, the Hamiltonian \hat{H} is given by:

$$\hat{H} = \hat{T} + \hat{V}, \quad (2)$$

where

$$\hat{T} = -\frac{1}{2} \sum_i^{\text{electrons}} \nabla_i^2 - \frac{1}{2} \sum_A^{\text{nuclei}} \frac{1}{M_A} \nabla_A^2, \quad (3)$$

and

$$\hat{V} = \sum_i \sum_A \frac{Z_A}{r_{iA}} + \sum_{i>j} \frac{1}{r_{ij}} + \sum_{A<B} \frac{Z_A Z_B}{R_{AB}}. \quad (4)$$

In the above equations, ∇_i^2 and ∇_A^2 represent the Laplacian operators for the i -th electron and A -th nucleus, respectively. $r_{iA} = |\mathbf{r}_i - \mathbf{R}_A|$ and $r_{ij} = |\mathbf{r}_i - \mathbf{r}_j|$ are the interdistances between the electron i and the nucleus A , and between the i -th

and j -th electrons, respectively, while Z_A and Z_B denote the nuclear charges of atoms A and B. $R_{AB} = \mathbf{R}_A - \mathbf{R}_B$ is the corresponding interdistance. The two terms in eq. (3) represent the kinetic energy operators for electrons and nuclei. The first term in eq. (4) represents the Coulomb attraction between electrons and nuclei, and the last two terms in the same equation represent the repulsion between electrons and between nuclei, respectively.

The Schrödinger equation can be analytically solved only for very small and specific systems, such as hydrogenoid atoms (H, H⁺, Li²⁺, ...etc.). In general, a number of approximations has to be introduced in order for the equation to be solved numerically. The first central approximation to quantum chemistry is the Born-Oppenheimer approximation [6]. Nuclei are much heavier than electrons, and move therefore much more slowly than electrons. Therefore, the Schrödinger equation can, to a very good approximation, be separated into two equations, a first one which describes the electronic wave function for a fixed nuclear geometry, and a second one which describes nuclear motions in the average field of electrons.

Within the framework of the Born-Oppenheimer approximation, on the time scale of the electronic motions, the Hamiltonian terms corresponding to the kinetic energy of the nuclei and the repulsion energy of the nuclei can be considered as constants. Since any constant added to an operator does not have any effect on the eigenfunctions of the operator, these two terms can be neglected. The remaining terms describe the motions of N electrons in the field of M fixed atomic charges, and define the so-called electronic Hamiltonian:

$$\hat{H}_{elec} = -\sum_{i=1}^N \frac{1}{2} \nabla_i^2 - \sum_{i=1}^N \sum_{A=1}^M \frac{Z_A}{r_{iA}} + \sum_{i=1}^N \sum_{j>i}^N \frac{1}{r_{ij}}, \quad (5)$$

where

$$-\sum_{A=1}^M \frac{Z_A}{r_{iA}} = v(\mathbf{r}_i) \quad (6)$$

represents an “external” potential generated by the charges Z_A of the M fixed nuclei. The solution of the Schrödinger equation involving the electronic Hamiltonian,

$$\hat{H}_{elec} \Psi_{elec} = E_{elec} \Psi_{elec} \quad (7)$$

is the electronic wave function:

$$\Psi_{elec} = \Psi_{elec} \{(\mathbf{r}_i); (\mathbf{R}_A)\}, \quad (8)$$

which depends explicitly on the electron coordinates \mathbf{r}_i and *parametrically* on the nuclear coordinates \mathbf{R}_A . Thus, the electronic energy E_{elec} depends also parametrically on the nuclear coordinates.

In order to obtain the total energy for a system of fixed nuclei, one has at last to account for nuclear repulsions:

$$E_{tot} = E_{elec} + \sum_{A=1}^M \sum_{B>A}^M \frac{Z_A Z_B}{R_{AB}}. \quad (9)$$

After solving eq. (7) and obtaining the total energy from eq. (9), it is then possible to investigate the motions of nuclei using the same assumptions as used in the formulation of the electronic problem, considering that $E_{tot}(\{\mathbf{R}_A\})$ provides a potential energy function for nuclear motions:

$$\hat{H}_{nucl} \Psi_{nucl} = E \Psi_{nucl}, \quad (10)$$

together with:

$$\hat{H}_{nucl} = -\frac{1}{2} \sum_{A=1}^M \frac{1}{M_A} \nabla^2 + E_{tot}(\{\mathbf{R}_A\}). \quad (11)$$

Solving the nuclear Schrödinger equation $\hat{H}_{nucl} \Psi_{nucl} = E \Psi_{nucl}$ enables us therefore to study the rotational, vibrational and translational motions of the molecule, and to calculate the Born-Oppenheimer approximation to the total energy E , which includes electronic, vibrational, rotational, and translational contributions. The total wave function in this approximation is:

$$\Psi(\{\mathbf{r}_i\}; \{\mathbf{R}_A\}) = \Psi_{elec}(\{\mathbf{r}_i\}; \{\mathbf{R}_A\}) \Psi_{nucl}(\{\mathbf{R}_A\}). \quad (12)$$

The electronic Hamiltonian of a molecule containing N electrons depends on the $3N$ Cartesian coordinates of the electrons, but does not completely describe the states of electrons. In order to specify these states completely, one has to account for an additional property of the electron, namely, its spin. In this purpose, we introduce for each electron two orthonormal spin functions $\alpha(\omega)$ and $\beta(\omega)$, corresponding to spin up and spin down, respectively. In a non-relativistic context, an electron is described by three spatial coordinates \mathbf{r} and by one spin coordinate ω . The wave function of an electron, which describes both its spatial distribution and its spin, is referred to as a *spin orbital* $\chi_i(\mathbf{x}_i)$, which is obtained as a product of a space function $\psi(\mathbf{r}_i)$ and a spin function $\sigma(\omega)$:

$$\chi_i(\mathbf{x}_i) = \psi(\mathbf{r}_i) \sigma(\omega). \quad (13)$$

In the above equation, the four coordinates are denoted collectively by $\mathbf{x} = \{\mathbf{r}, \omega\}$. The electronic wave function obtained upon solving the electronic Schrödinger equation [eq. (7)] must satisfy an independent postulate of quantum mechanics, the so-called *Pauli's exclusion principle* or *antisymmetry principle*. Specifically, a many electron wave function has to be antisymmetric with respect to the interchange of the spin-space coordinates of any two electrons:

$$\Psi_{elec}(\mathbf{x}_1, \mathbf{x}_2, \dots, \mathbf{x}_i, \dots, \mathbf{x}_j, \dots, \mathbf{x}_N) = -\Psi_{elec}(\mathbf{x}_1, \mathbf{x}_2, \dots, \mathbf{x}_j, \dots, \mathbf{x}_i, \dots, \mathbf{x}_N). \quad (14)$$

The *antisymmetry principle* ensures the indistinguishability of electrons, upon any interchange of their spin-space coordinates.

For a system of N independent and non-interacting electrons occupying N spin-orbitals $(\chi_i, \chi_j, \dots, \chi_k)$, the electronic wave function can be expanded as a normalized antisymmetric product of these spin orbitals, which are assumed to be orthonormal. In a first approximation, the electronic wave function Ψ_{elec} is therefore usually written in the form of a determinant, referred to as a Slater determinant:

$$\Psi_{elec} = \frac{1}{\sqrt{N!}} \begin{vmatrix} \chi_i(1) & \chi_j(1) & \cdots & \chi_k(1) \\ \chi_i(2) & \chi_j(2) & \cdots & \chi_k(2) \\ \vdots & \vdots & & \vdots \\ \chi_i(N) & \chi_j(N) & \cdots & \chi_k(N) \end{vmatrix}, \quad (15)$$

where, from here and henceforth, for the purpose of simplifying notations, 1 stands for \mathbf{x}_1 , 2 stands for \mathbf{x}_2 , ...etc.

One way to find approximate solutions $\tilde{\Psi}$ to the Schrödinger equation ($\hat{H}\Psi = E\Psi$) is by means of the variation principle, which states:

$$E[\tilde{\Psi}] = \frac{\langle \tilde{\Psi} | \hat{H} | \tilde{\Psi} \rangle}{\langle \tilde{\Psi} | \tilde{\Psi} \rangle} \geq E_0, \quad (16)$$

where E_0 is the exact ground-state energy of the system, $\tilde{\Psi}$ is any arbitrary (variational) function which depends on the same coordinates as the exact solution of the Schrödinger equation, and \hat{H} is the Hamiltonian of the system under consideration (in this case $\hat{H} = \hat{H}_{elec}$). It follows that the expectation value of the Hamiltonian operator corresponding to the variational function $\tilde{\Psi}$ is an upper bound to the exact ground state energy. The equality is valid only when $\tilde{\Psi} = \Psi_0$, where Ψ_0 is the exact solution of the Schrödinger equation for the ground state.

2.1.1 Hartree-Fock theory

The Hartree-Fock (HF) method [7, 8] is a variational method which expresses the variational wave function of the electronic ground state (Ψ_0) in the form of a single Slater determinant. In other words, with this method one seeks the Slater determinant which results in the lowest mean energy value associated to the electronic Hamiltonian [eq. (5)]. The main purpose of the Hartree-Fock approximation is to reduce the complicated many electron problem into a one electron problem in which electron-electron repulsions are treated in an average way. The HF equation is derived by finding the set of orthonormal

spin orbitals used to expand the electronic wave function in the form of a single Slater determinant, which minimizes the electronic energy of the system:

$$\hat{f}(1)\chi_i(1) = \varepsilon_i\chi_i(1). \quad (17)$$

In this equation ε_i is the energy corresponding to the spin orbital χ_i , and $\hat{f}(1)$ is an effective one-electron operator for electron 1, the so-called Fock operator, which is given by:

$$\hat{f}(1) = \hat{h}(1) + v^{HF}(1). \quad (18)$$

The first term $\hat{h}(1)$ in eq. (18) is the one-electron operator defined as:

$$\hat{h}(1) = -\frac{1}{2}\nabla_1^2 - \sum_{A=1} \frac{Z_A}{r_{1A}}, \quad (19)$$

where the first term accounts for the kinetic energy and the second term for the nuclear-electronic attraction. The second term in eq. (18) is the Hartree-Fock potential:

$$v^{HF}(1) = \sum_j [\hat{J}_j(1) - \hat{K}_j(1)], \quad (20)$$

where the summation \sum_j runs over all occupied spin orbitals of the system under consideration. $\hat{J}_j(1)$ is a local operator, referred to as the Coulomb operator:

$$\hat{J}_j(1) = \int \chi_j^*(2) \frac{1}{r_{12}} \chi_j(2) d\mathbf{x}_2, \quad (21)$$

whereas $\hat{K}_j(1)$ represents a non-local operator, referred to as the exchange operator, which is defined via its action on the spin orbital $\chi_j(1)$, according to:

$$\hat{K}_j(1)\chi_i(1) = \left[\int \chi_j^*(2) \frac{1}{r_{12}} \chi_i(2) d\mathbf{x}_2 \right] \chi_j(1). \quad (22)$$

Since the Coulomb and exchange operators depend on the eigenfunctions of the Fock operator, it is clear that the Hartree-Fock equation can only be solved iteratively. Solving the Hartree-Fock eigenvalue problem [eq. (17)] yields a set of orthonormal spin-orbitals $\{\chi_i\}$ with orbital energies $\{\varepsilon_i\}$. The first N spin orbitals with the lowest orbital energies are called the occupied spin orbitals; these will be denoted by indices i, j, k, \dots . Once these orbitals are known, the Fock operator becomes a well defined Hermitian operator with an infinite number of eigenfunctions. The remaining spin orbitals are called the virtual or unoccupied spin orbitals; these will be labeled by indices r, s, t, \dots

In order to clarify the physical significance of the energies of occupied and virtual spin-orbitals, one has to consider the expression for the corresponding energies:

$$\varepsilon_i = \langle i | \hat{h} | i \rangle + \sum_{j \neq i} (\langle ij | ij \rangle - \langle ij | ji \rangle), \quad (23)$$

$$\varepsilon_r = \langle r | \hat{h} | r \rangle + \sum_j (\langle rj | rj \rangle - \langle rj | jr \rangle), \quad (24)$$

with $\langle ij | kl \rangle$ a bielectron integral of the form:

$$\iint d\mathbf{x}_1 d\mathbf{x}_2 \chi_i^*(1) \chi_j(2) \frac{1}{r_{12}} \chi_k^*(1) \chi_l(2). \quad (25)$$

The first contribution ($\langle i | \hat{h} | i \rangle$) to the energy of an electron associated with the spin orbital $|\chi_i\rangle$ is associated with the kinetic energy and attraction to the nuclei, while the $\langle ij | ij \rangle$ and $-\langle ij | ji \rangle$ contributions correspond to the Coulomb and exchange interactions with each of the remaining $N-1$ electrons occupying the spin orbitals $|\chi_j\rangle$ ($j \neq i$), respectively. The energy ε_r associated with the virtual spin orbital includes the kinetic energy and nuclear attraction in the same way ($\langle r | \hat{h} | r \rangle$) as in the case of occupied orbitals, but Coulomb and exchange interactions are included with respect to all N electrons of the Hartree-Fock ground state $|\Psi_0\rangle$. Performing the summation over the orbital energies ε_i which correspond to the N electrons in the ground state, the following expression is obtained:

$$\sum_i^N \varepsilon_i = \sum_i^N \langle i | \hat{h} | i \rangle + \sum_i^N \sum_j^N (\langle ij | ij \rangle - \langle ij | ji \rangle). \quad (26)$$

The above expression can be further reduced to:

$$\sum_i^N \varepsilon_i = \sum_i^N \langle i | \hat{h} | i \rangle + \sum_i^N \sum_j^N \langle ij || ij \rangle, \quad (27)$$

where $\langle ij || ij \rangle$ stands for the anti-symmetrised bielectron interaction $\langle ij | ij \rangle - \langle ij | ji \rangle$. The expectation value of the total ground state energy is:

$$E_0 = \langle \Psi_0 | \hat{H} | \Psi_0 \rangle = \sum_i^N \langle i | \hat{h} | i \rangle + \frac{1}{2} \sum_i^N \sum_j^N \langle ij || ij \rangle. \quad (28)$$

Upon comparing between eqs. (27) and (28), it is clear that:

$$E_0 \neq \sum_i^N \varepsilon_i. \quad (29)$$

When summing the occupied spin-orbital energies, the electron-electron interaction (Coulomb and exchange interaction) is counted twice, whereas in the correct expression for the total electronic energy of the ground state [eq. (28)], a factor 1/2 prevents such overcounting.

In order to find the physical significance of orbital energies within the framework of Hartree-Fock theory, one has to investigate the processes of subtracting and adding one electron to the N -electron ground state

$|^N \Psi_0 \rangle = |\chi_1 \chi_2 \dots \chi_k \dots \chi_N \rangle$ under the assumption that the initial and final states

in these processes possess the same set of spin-orbitals (i.e. relaxation effect are neglected). Removing one electron corresponding to the spin orbital χ_k

from the N -electron state, one obtains the $(N-1)$ -electron state

$|^{N-1} \Psi_k \rangle = |\chi_1 \chi_2 \dots \chi_{k-1} \chi_{k+1} \dots \chi_N \rangle$. In order to evaluate the corresponding

ionization potential, one has to determine the total energies of these two single determinants and calculate their difference. The electronic energy of the N -

electron system in its ground state is:

$${}^N E_0 = \sum_i \langle i | \hat{h} | i \rangle + \frac{1}{2} \sum_i \sum_j \langle ij || ij \rangle, \quad (30)$$

while for the $(N-1)$ -electron system, one finds:

$${}^{N-1}E_k = \sum_{i \neq k} \langle i | \hat{h} | i \rangle + \frac{1}{2} \sum_{i \neq k} \sum_{j \neq k} \langle ij | ij \rangle. \quad (31)$$

Therefore, the ionization potential is:

$$\begin{aligned} IP &= {}^{N-1}E_k - {}^N E_0 \\ &= -\langle k | \hat{h} | k \rangle - \sum_j \langle kj | kj \rangle \\ &= -\varepsilon_k. \end{aligned} \quad (32)$$

According to eq. (32), the energy of the spin orbital χ_k corresponds to the energy (with opposite sign) needed to remove an electron from this spin orbital in the single determinant approximation and under the assumption that relaxation effects can be neglected.

When adding one electron to the virtual orbital χ_r , one has to consider the $(N+1)$ -electron single determinant $|\Psi_r^{N+1}\rangle = |\chi_r \chi_1 \chi_2 \dots \chi_N\rangle$ with an electronic energy ${}^{N+1}E_r$. By means of the same procedure as that used for evaluating the ionization potential, one finds for the electron affinity (EA):

$$\begin{aligned} EA &= {}^N E_0 - {}^{N+1}E_r \\ &= -\langle r | \hat{h} | r \rangle - \sum_i \langle ri | ri \rangle \\ &= -\varepsilon_r. \end{aligned} \quad (33)$$

Thus, the electron affinity for adding an electron to the virtual spin orbital χ_r is equal to the orbital energy, after a change of a sign, under the assumption that the occupied spin orbitals in the $(N+1)$ -electron state ($|\Psi_r^{N+1}\rangle$) are identical to those of the neutral system in its electronic ground state ($|\Psi_0^N\rangle$). This

conclusion, along with the corresponding statement about ionization potentials, is referred to as Koopmans' theorem [1, 9].

2.1.1.1 Restricted closed-shell Hartree-Fock theory

At this stage, one has to specify in details the form of the spin orbitals prior to proceeding further, towards the actual calculation of the Hartree-Fock wave function. Two types of spin-orbitals are considered in quantum mechanical calculations: the restricted and the unrestricted spin-orbitals. Spin orbitals obtained under the restriction that the same spatial function applies to both α (spin-up) and β (spin-down) functions are referred to as restricted spin orbitals. The restricted Hartree-Fock formalism is devised for obtaining the Hartree-Fock solution for closed-shell systems with an even number of electrons (N), which are paired in such a way that $n=N/2$ spatial functions $\psi_i(\mathbf{r}_1)$ (molecular orbitals) are doubly occupied. Since the spatial function is the same for spin-up (α) and spin-down (β) orbitals associated to the same energy level, the calculation of molecular orbitals is equivalent to the problem of solving an integro-differential equation of the form:

$$\hat{f}(\mathbf{r}_1)\psi_i(\mathbf{r}_1) = \varepsilon_i\chi_i(\mathbf{r}_1), \quad (34)$$

with $\hat{f}(\mathbf{r}_1)$ the closed-shell Fock operator:

$$\hat{f}(\mathbf{r}_1) = \int d\omega_1 \alpha^*(\omega_1) \hat{f}(\mathbf{x}_1) \alpha(\omega_1). \quad (35)$$

In order to solve eq. (34), Roothaan [10] introduced a set of known basis functions and in this way converted the Hartree-Fock equation into a set of

simple algebraic equations, which can be solved by means of standard matrix diagonalization techniques.

In this purpose, molecular orbitals $\psi_i(\mathbf{r})$ are expanded as linear combinations of K known basis functions $\{\phi_\mu(\mathbf{r})|\mu=1,2,\dots,K\}$, usually referred to as atomic orbitals:

$$\psi_i = \sum_{\mu=1}^K c_{\mu i} \phi_\mu, \quad i = 1, 2, \dots, K. \quad (36)$$

This important approximation is known as the LCAO (linear combination of atomic orbitals) approximation. In order to avoid truncation errors in the expansion, one should use a complete basis set $\{\phi_\mu\}$, corresponding formally to an infinite number of basis functions. In practice, finite basis sets of K basis functions have to be used. As the basis set approaches completeness ($K \rightarrow \infty$) molecular orbitals converge to the exact eigenfunctions of the Fock operator. In practice, once a finite set of basis functions is chosen, one has to determine the set of expansion coefficients $c_{\mu i}$ in order to obtain the Hartree-Fock molecular orbitals.

By substituting eq. (36) into the Hartree-Fock equation [eq. (34)], one obtains a matrix equation, which is usually referred to as the Hartree-Fock-Roothaan matrix equation:

$$\mathbf{FC} = \mathbf{SC}\epsilon, \quad (37)$$

where \mathbf{F} denotes the Fock matrix:

$$F_{\mu\nu} = \int \phi_{\mu}^*(\mathbf{r}_1) \hat{f}(\mathbf{r}_1) \phi_{\nu}(\mathbf{r}_1) d\mathbf{r}_1, \quad \mu, \nu = 1, 2, \dots, K, \quad (38)$$

and \mathbf{S} is the overlap matrix:

$$S_{\mu\nu} = \int \phi_{\mu}^*(\mathbf{r}_1) \phi_{\nu}(\mathbf{r}_1) d\mathbf{r}_1, \quad \mu, \nu = 1, 2, \dots, K. \quad (39)$$

\mathbf{C} represents a $K \times K$ square matrix containing the expansion coefficients $c_{\mu i}$,

and $\boldsymbol{\varepsilon}$ is a diagonal matrix containing the orbital energies ε_i .

The basis functions used in molecular calculations are not orthogonal to each other [$(\mathbf{S} \neq \mathbf{1})$], and have therefore to be orthogonalized so that eq. (37) can be solved by means of standard diagonalization techniques. Orthogonalization procedures are described in details in the book by Szabo and Ostlund [1]. Upon orthonormalizing the basis set, the transformed Roothaan equation is obtained:

$$\mathbf{F}'\mathbf{C}' = \mathbf{C}'\boldsymbol{\varepsilon}. \quad (40)$$

In order to solve the transformed equation, use has to be made of an iterative procedure referred to as the Self Consistent Field (SCF) approach. An SCF calculation starts with an initial guess of the LCAO expansion coefficients [$c_{\mu i}$ in eq. (36)], and a first determination from these coefficients of the Fock matrix (\mathbf{F}) and transformed Fock matrix (\mathbf{F}'). By diagonalizing this matrix, new LCAO coefficients and orbital energies are obtained. The iterative procedure proceeds further by reevaluating the Fock matrix and transformed Fock matrix from which new LCAO coefficients are obtained. This procedure is repeated until self-consistency is reached.

2.1.1.2 Unrestricted open-shell Hartree-Fock theory

When dealing with systems possessing one or several unpaired electrons, the Hartree-Fock-Roothaan equation needs to be modified. Within the frame of a spin-unrestricted Hartree-Fock (UHF) treatment, different spatial orbitals ψ_i^α and ψ_i^β are associated to spin-up (α) and spin-down (β) electrons:

$$\chi_i(\mathbf{x}) = \begin{cases} \psi_i^\alpha(\mathbf{r})\alpha(\omega) \\ \psi_i^\beta(\mathbf{r})\beta(\omega) \end{cases} \quad (41)$$

To find solutions to the spin-unrestricted Hartree-Fock (UHF) equations, one has to convert the integro-differential equations into matrix equations by introducing a finite set of K basis functions:

$$\psi_i^\alpha = \sum_{\mu=1}^K c_{\mu i}^\alpha \phi_\mu, \quad i = 1, 2, \dots, K, \quad (42)$$

$$\psi_i^\beta = \sum_{\mu=1}^K c_{\mu i}^\beta \phi_\mu, \quad i = 1, 2, \dots, K. \quad (43)$$

The final form of the matrix equations, obtained by using the above expressions for molecular orbitals, is:

$$\begin{aligned} \mathbf{F}^\alpha \mathbf{C}^\alpha &= \mathbf{S} \mathbf{C}^\alpha \boldsymbol{\varepsilon}^\alpha, \\ \mathbf{F}^\beta \mathbf{C}^\beta &= \mathbf{S} \mathbf{C}^\beta \boldsymbol{\varepsilon}^\beta. \end{aligned} \quad (44)$$

These equations represent a generalization of the Hartree-Fock-Roothaan equation. They are called the Pople-Nesbet equations. These equations can be solved in essentially the same way Hartree-Fock-Roothaan equation is solved. From the explicit expression of the Fock matrix elements [1], one can see that the \mathbf{F}^α and \mathbf{F}^β matrices depend on both the \mathbf{C}^α and \mathbf{C}^β expansion

coefficients. The matrix equations in eq. (44) are thus coupled and have to be solved iteratively.

Spin-unrestricted determinants have a serious limitation, they are not eigenfunctions of the spin operator \hat{S}^2 . One cannot obtain spin-adapted solutions by simply combining a small number of spin-unrestricted determinants. Spin-unrestricted wave functions are contaminated by components of higher spin multiplicity and therefore the expectation values of the \hat{S}^2 operator are always too large if the number of α spin electrons (N^α) is larger or equal to the number of β spin electrons (N^β). The expectation value of the \hat{S}^2 operator for an unrestricted one-determinantal wave function is given by:

$$\langle \hat{S}^2 \rangle_{UHF} = \langle \hat{S}^2 \rangle_{EXACT} + N^\beta - \sum_i^{N^\alpha} \sum_j^{N^\beta} |S_{ij}^{\alpha\beta}|^2, \quad (45)$$

along with:

$$\langle \hat{S}^2 \rangle_{EXACT} = \left(\frac{N^\alpha - N^\beta}{2} \right) \left(\frac{N^\alpha - N^\beta}{2} + 1 \right). \quad (46)$$

When $N^\alpha = N^\beta$, we note from eq. (45) that the expectation value of the \hat{S}^2 operator can differ from the exact value (0) for a singlet state ($S=0$) if space functions associated to spin-up and spin-down electrons localize in different regions of space. Such a situation will be referred further to as a symmetry breaking situation.

2.2 Electron correlation treatments

The Hartree-Fock method neglects the instantaneous correlation of electronic motions, due to the use of the mean field approximation. However, some correlation between electrons with the same spin is already taken into account by virtue of the determinantal form of the wave function resulting in the exclusion principle, which prevents two electrons with the same spin to have the same space coordinates. The error in the electronic energy due to the neglect of the remaining electron correlation is called the *correlation energy* and is defined as the difference between the exact non-relativistic energy of the system and the HF energy:

$$E_{corr} = E - E_{HF} < 0. \quad (47)$$

Rigorous enough treatments of electronic correlation are crucial for accurate calculations of molecular properties, obtained as energy differences or energy derivatives.

2.2.1 Full configuration interaction

The Configuration Interaction (CI) method is conceptually, but not computationally, the simplest method to deal with electronic correlation. Although this method originates from the 1930's, its first applications began to appear only around forty years later, when sufficient computer capabilities became available. Since the publication in 1977 of a review article on CI by Shavitt [11], important improvements to the CI approach have been made, which are gathered and discussed in the book by McWeeny [3]. A more recent review of CI can be found in the paper by Bauschlicher *et al*, published in 1990 [12].

The general idea of this method is to represent the exact electronic wave function as a linear combination of N -electron trial functions (Slater determinants) representing the ground and electronically excited states, and to optimize the expansion coefficients in a variational way.

A fundamental theorem in configuration interaction (CI) theory was formulated by Löwdin [13]. This theorem states that every normalizable antisymmetric wave function can be expanded as a sum of an infinite series of Slater determinants constructed from a complete basis set of one-electron functions, which defines an exact solution to the many-electron problem.

Suppose we have solved the Hartree-Fock problem in the finite basis set and have obtained a set of $2K$ spin orbitals $\{\chi_i\}$. The determinant constructed from the N lowest energy spin orbitals is denoted by $|\Psi_0\rangle$. In addition to $|\Psi_0\rangle$, a large number of further N -electron determinants can be constructed by distributing N electrons among $2K$ spin orbitals. We can describe these other determinants by stating how they differ from $|\Psi_0\rangle$. Thus, if the occupied spin orbitals χ_i, χ_j, \dots are replaced by virtual ones such as χ_r, χ_s, \dots then the set of possible determinants contains singly excited determinants $|\Psi_i^r\rangle$, which differ from $|\Psi_0\rangle$ by having the spin orbital χ_i replaced by χ_r , doubly excited determinants $|\Psi_{ij}^{rs}\rangle$ where the χ_i and χ_j spin-orbitals are replaced by χ_r and χ_s spin-orbitals, and so on until the N -tuply excited determinants. In general

any excited determinant can be written as $|\Psi_{ijk\dots}^{rst\dots}\rangle$. The form of a full CI trial wave function is:

$$|\Phi_0\rangle = c_0 |\Psi_0\rangle + \sum_i c_i^r |\Psi_i^r\rangle + \sum_{\substack{i<j \\ r<s}} c_{ij}^{rs} |\Psi_{ij}^{rs}\rangle + \sum_{\substack{i<j<k \\ r<s<t}} c_{ijk}^{rst} |\Psi_{ijk}^{rst}\rangle + \dots, \quad (48)$$

where the c represents unknown expansion coefficients. The successive restrictions on summation indices (e.g. $i < j < k \dots$ and $r < s < t \dots$) prevent the repetition of the same excited determinant in the CI expansion. The energies of the electronic ground state and excited states are obtained by means of the linear variational method, as eigenvalues of the matrix representation of the N -electron Hamiltonian in the basis of the N -electron functions used in the expansion of eq. (48), which is called the full CI matrix. The corresponding method is referred to as Full Configuration Interaction (FCI). The lowest eigenvalue of the full CI matrix represents the exact ground state energy E_0^{exact} . Within the subspace spanned by the one-electron basis, the difference in between E_0^{exact} and the Hartree-Fock ground state energy (E_0^{HF}) is called *the basis set correlation energy*. The basis set correlation energy obtained from a FCI calculation forms a benchmark for judging all other approaches to the correlation energy performed with the same basis set.

When basis set approaches completeness, the FCI result approaches the exact solution of the non-relativistic Schrödinger equation. The method consists in the diagonalization of an N -electron Hamiltonian in a basis of N -electron Slater determinants. These determinantal trial functions are constructed by selecting N orbitals from both occupied and virtual Hartree-Fock orbitals. The

number of the N -electron Slater determinants, which can be generated from the HF spin orbitals, scales like $(2K)!/[N!(2K-N)!]$, where N is the number of electrons and $2K$ is the number of spin orbitals. The problem of a FCI treatment is its feasibility due to the exceedingly large number of excited determinants to consider, even for small systems. For larger systems, one has to restrict the CI expansion to given classes of electronically excited determinants (e.g. singly and doubly excited determinants in a SDCI treatment). An important consequence of such approximations is the loss of size consistency in the computed energies.

2.2.2 Many body perturbation theory

Many body perturbation theory (MBPT) is a systematic procedure for obtaining the correlation energy, which is not variational, but which is size consistent at each level. The general frame of MBPT was devised by Rayleigh and Schrödinger and hence it is referred to as Rayleigh-Schrödinger Perturbation Theory (RSPT). RSPT employing the Hartree-Fock Hamiltonian as a zeroth-order Hamiltonian of an N -electron system is more specifically referred to as Møller-Plesset Perturbation Theory (MPPT) [14].

The basic idea of RSPT is to divide the total Hamiltonian in two parts: a zeroth-order part or unperturbed part \hat{H}_0 (the Hartree-Fock Hamiltonian in the case of MPPT), and a perturbation \hat{V} , representing the difference between the N -electron Hamiltonian and the unperturbed Hamiltonian \hat{H}_0 . It is assumed that

the unperturbed Hamiltonian \hat{H}_0 has known eigenfunctions ($|\Psi_i^{(0)}\rangle$) and eigenenergies ($E_i^{(0)}$):

$$\hat{H}_0|\Psi_i^{(0)}\rangle = E_i^{(0)}|\Psi_i^{(0)}\rangle. \quad (49)$$

The eigenvalue problem of interest has therefore the form:

$$\hat{H}|\Phi_i\rangle = (\hat{H}_0 + \hat{V})|\Phi_i\rangle = \varepsilon_i|\Phi_i\rangle. \quad (50)$$

For a small enough perturbation \hat{V} , it is reasonable to expect that the zeroth-order approximations $|\Psi_i^{(0)}\rangle$ and $E_i^{(0)}$ are close to the exact solutions $|\Phi_i\rangle$ and ε_i of the electronic Schrödinger equation. In order to devise the procedure which would systematically improve the eigenfunctions and eigenvalues of \hat{H}_0 towards the eigenvalues and eigenfunctions of the total Hamiltonian \hat{H} , one has to introduce an ordering parameter λ :

$$\hat{H} = \hat{H}_0 + \lambda\hat{V}, \quad (51)$$

and expand the eigenvalues and eigenfunctions of \hat{H} in a Taylor series, as a function of this parameter:

$$\varepsilon_i = E_i^{(0)} + \lambda E_i^{(1)} + \lambda^2 E_i^{(2)} + \dots, \quad (52)$$

$$\Phi_i = |\Psi_i^{(0)}\rangle + \lambda|\Psi_i^{(1)}\rangle + \lambda^2|\Psi_i^{(2)}\rangle + \dots, \quad (53)$$

where $E_i^{(n)}$ denotes the n -th order energy, and $|\Psi_i^{(n)}\rangle$ the n -th order wave function.

The main objective of RSPT is to express the higher order energies in terms of zeroth-order energies and of matrix elements of the perturbation \hat{V} , over unperturbed wave functions ($\langle \Psi_i^{(0)} | \hat{V} | \Psi_j^{(0)} \rangle$). Following the mathematical derivation outlined in the book by Szabo and Ostlund [1], the expressions for the n -th-order energies are obtained:

$$E_i^{(0)} = \langle \Psi_i^{(0)} | \hat{H}_0 | \Psi_i^{(0)} \rangle, \quad (54a)$$

$$E_i^{(1)} = \langle \Psi_i^{(0)} | \hat{V} | \Psi_i^{(0)} \rangle, \quad (54b)$$

$$E_i^{(2)} = \langle \Psi_i^{(0)} | \hat{V} | \Psi_i^{(1)} \rangle, \quad (54c)$$

$$E_i^{(3)} = \langle \Psi_i^{(0)} | \hat{V} | \Psi_i^{(2)} \rangle, \quad (54d)$$

and so on until infinite order in the correlation potential.

Upon expanding the exact wave function Φ_i under the constraint of intermediate normalization $\langle \Psi_i^{(0)} | \Phi_i \rangle = 0$, which implies that at all orders $\langle \Psi_i^{(0)} | \Psi_i^{(n)} \rangle = 0$, the higher order energies are obtained in terms of zeroth-order energies $E_i^{(0)}$ and zeroth-order wave functions $\Psi_i^{(0)}$. For example, at second-order, we have:

$$E_i^{(2)} = \sum_{n \neq i} \frac{\langle \Psi_i^{(0)} | \hat{V} | \Psi_n^{(0)} \rangle \langle \Psi_n^{(0)} | \hat{V} | \Psi_i^{(0)} \rangle}{E_i^{(0)} - E_n^{(0)}} = \sum_{n \neq i} \frac{\left| \langle \Psi_i^{(0)} | \hat{V} | \Psi_n^{(0)} \rangle \right|^2}{E_i^{(0)} - E_n^{(0)}}, \quad (55)$$

and at third-order we have:

$$\begin{aligned}
E_i^{(3)} = & \sum_{n,m \neq i} \frac{\langle \Psi_i^{(0)} | \hat{V} | \Psi_n^{(0)} \rangle \langle \Psi_n^{(0)} | \hat{V} | \Psi_m^{(0)} \rangle \langle \Psi_m^{(0)} | \hat{V} | \Psi_i^{(0)} \rangle}{(E_i^{(0)} - E_n^{(0)})(E_i^{(0)} - E_m^{(0)})} - \\
& - E_i^{(i)} \sum_{n \neq i} \frac{\left| \langle \Psi_i^{(0)} | \hat{V} | \Psi_n^{(0)} \rangle \right|^2}{(E_i^{(0)} - E_n^{(0)})^2}.
\end{aligned} \tag{56}$$

Within the frame of MPPT, the Hartree-Fock Hamiltonian ($\hat{H}_0 = \sum_i [\hat{h}(i) + \hat{v}^{HF}(i)]$) is employed as a zeroth-order Hamiltonian, and the corresponding perturbation operator reads as follows:

$$\hat{V} = \sum_{i < j} r_{ij}^{-1} - \hat{V}^{HF} = \sum_{i < j} r_{ij}^{-1} - \sum_i \hat{v}^{HF}(i). \tag{57}$$

Since the Hartree-Fock energy corresponds to the sum of the zeroth-order ($\sum_i \varepsilon_i$) and first-order perturbation energies ($-\frac{1}{2} \sum_{ij} \langle ij || ij \rangle$), the first contribution to the correlation energy arises from the second-order of Møller-Plesset theory (MP2). Because of the rules by Slater, and Brillouin's theorem which forbids couplings of singly excited states with the electronic ground state, the only terms that contribute to eq. (55) are the doubly excited determinants $|\Psi_{ij}^{rs}\rangle$. It follows therefore that:

$$E_0^{(2)} = \frac{1}{4} \sum_{ijrs} \frac{|\langle ij || rs \rangle|^2}{\varepsilon_i + \varepsilon_j - \varepsilon_r - \varepsilon_s}. \tag{58}$$

By means of a similar procedure one obtains the following expression for the third-order perturbation energy (MP3):

$$\begin{aligned}
E_0^{(3)} = & \frac{1}{8} \sum_{ijklrs} \frac{\langle ij || rs \rangle \langle kl || ij \rangle \langle rs || kl \rangle}{(\varepsilon_i + \varepsilon_j - \varepsilon_r - \varepsilon_s)(\varepsilon_k + \varepsilon_l - \varepsilon_r - \varepsilon_s)} \\
& + \frac{1}{8} \sum_{ijrstu} \frac{\langle ij || rs \rangle \langle rs || tu \rangle \langle tu || ij \rangle}{(\varepsilon_i + \varepsilon_j - \varepsilon_r - \varepsilon_s)(\varepsilon_i + \varepsilon_j - \varepsilon_t - \varepsilon_u)} \\
& + \sum_{ijkrt} \frac{\langle ij || rs \rangle \langle ks || tj \rangle \langle rt || ik \rangle}{(\varepsilon_i + \varepsilon_j - \varepsilon_r - \varepsilon_s)(\varepsilon_i + \varepsilon_k - \varepsilon_r - \varepsilon_t)}.
\end{aligned} \tag{59}$$

Expressions for the higher orders of Møller-Plesset theory such as MP4 [15, 16], MP5 and MP6 [17, 18] are also available. From a computational point of view, the cost of Møller-Plesset theory scales as N^5 , N^6 and N^7 for MP2, MP3 and MP4, respectively, where N represents the number of basis set functions. With a MP4 calculation, the most demanding step is the one related to calculating the triple contribution. This is the reason why there are two implementations of the MP4 approach: the MP4(SDQ) approach [19], which neglects the triple contributions, and the MP4(SDTQ) approach, which is the complete one.

2.2.3 Coupled cluster theory

Due to the high accuracy of the obtained results, Coupled Cluster (CC) theory is widely used as benchmark. The method is based on the *exponential Ansatz* introduced by Coester and Kümmel [20, 21]. The exact CC ground state can be written by applying upon the reference wave function Ψ_0 (usually, the Hartree-Fock wave function) an excitation operator \hat{T} using:

$$\Psi_{CC} = e^{\hat{T}} \Psi_0 = \left(1 + \hat{T} + \frac{1}{2!} \hat{T}^2 + \frac{1}{3!} \hat{T}^3 + \dots \right) \Psi_0. \tag{60}$$

Now, one has to find the cluster operator \hat{T} , such that the wave operator $e^{\hat{T}}$ turns the HF wave function into an exact solution of the Schrödinger equation.

The cluster operator is defined as a sum:

$$\hat{T} = \hat{T}_1 + \hat{T}_2 + \hat{T}_3 + \dots + \hat{T}_{l_{MAX}}, \quad (61)$$

where \hat{T}_l denotes the excitation operators defined by considering the action of annihilation ($\hat{i}, \hat{j}, \hat{k}, \dots$) and creation ($\hat{r}^\dagger, \hat{s}^\dagger, \hat{t}^\dagger, \dots$) operators, with the subscript l indicating the rank of the excitation. For instance, single and double excitation operators are defined as follows:

$$\hat{T}_1 = \sum_{i,r} t_i^r \hat{r}^\dagger \hat{i}, \quad (62)$$

$$\hat{T}_2 = \frac{1}{4} \sum_{\substack{ij \\ rs}} t_{ij}^{rs} \hat{s}^\dagger \hat{r}^\dagger \hat{i} \hat{j}, \quad (63)$$

where the indices i, j, k, \dots correspond to occupied Hartree-Fock spin orbitals, while r, s, t, \dots correspond to unoccupied ones. The unknown $t_{ij}^{rs\dots}$ coefficients represent the *cluster amplitudes*, whose optimization is crucial to practical applications of coupled cluster theory. Since the structure of the wave operator is well-defined, one obtains these amplitudes by solving the Schrödinger equation:

$$\hat{H}e^{\hat{T}}\Psi_0 = Ee^{\hat{T}}\Psi_0. \quad (64)$$

After mathematically manipulating this equation, as outlined in [22] and expressing the operators in terms of commutators, one obtains the fundamental equation of the CC method:

$$\begin{aligned}
& \langle \begin{smallmatrix} rs\dots \\ ij\dots \end{smallmatrix} | \hat{H} + [\hat{H}, \hat{T}] + \frac{1}{2!} [[\hat{H}, \hat{T}], \hat{T}] + \frac{1}{3!} [[[\hat{H}, \hat{T}], \hat{T}], \hat{T}] \\
& + \frac{1}{4!} [[[[\hat{H}, \hat{T}], \hat{T}], \hat{T}], \hat{T}] | \Psi_0 \rangle = 0,
\end{aligned} \tag{65}$$

where the $\langle \begin{smallmatrix} rs\dots \\ ij\dots \end{smallmatrix} |$ represent the determinants obtained from the reference state by considering the action of the $\hat{i}, \hat{j}, \hat{k} \dots$ annihilation and $\hat{r}^\dagger, \hat{s}^\dagger, \hat{t}^\dagger \dots$ creation operators. The Coupled Cluster equations are nonlinear, since the searched amplitudes appear in powers higher than one (up to fourth order). These equations must therefore be solved iteratively. The initial amplitudes are usually obtained from eq. (64) after neglecting the non-linear terms. The iterative procedure starts by inserting these amplitudes in eq. (65) and proceeds further until self-consistency is achieved.

In the CC expansion with double electronic excitations ($\hat{T} = \hat{T}_2$) [CCD approach], eq. (64) reduces to:

$$\begin{aligned}
& \langle \begin{smallmatrix} rs \\ ij \end{smallmatrix} | \hat{H} \Psi_0 \rangle + \langle \begin{smallmatrix} rs \\ ij \end{smallmatrix} | \hat{H} \hat{T}_2 \Psi_0 \rangle + \frac{1}{2} \langle \begin{smallmatrix} rs \\ ij \end{smallmatrix} | \hat{H} \hat{T}_2^2 \Psi_0 \rangle \\
& - \langle \begin{smallmatrix} rs \\ ij \end{smallmatrix} | \hat{T}_2 \hat{H} \Psi_0 \rangle - \langle \begin{smallmatrix} rs \\ ij \end{smallmatrix} | \hat{T}_2 \hat{H} \hat{T}_2 \Psi_0 \rangle = 0.
\end{aligned} \tag{66}$$

For each amplitude t_{ij}^{rs} , one equation has to be solved iteratively. From the obtained amplitudes, one can then expand the CCD ground state wave function as follows:

$$\Psi_{CCD} = \Psi_0 + \sum_{\substack{i < j \\ r < s}} t_{ij}^{rs} \Psi_{ij}^{rs} + \sum_{\substack{r < j < k < l \\ r < s < t < u}} t_{ij}^{rs} t_{kl}^{tu} \Psi_{ijkl}^{rstu} + \dots \tag{67}$$

The corresponding energy reads:

$$E_{CCD} = \langle \Psi_0 | e^{-\hat{T}_2} \hat{H} e^{\hat{T}_2} \Psi_0 \rangle. \tag{68}$$

The CCSD method takes single and double electronic excitations into account ($\hat{T} = \hat{T}_1 + \hat{T}_2$). If only single excitations are included, there would not be any dynamic correlation effect. The \hat{T}_2 operator certainly accounts for most of the dynamic correlation effects. In this model, equations for amplitudes t_i^r and t_{ij}^{rs} are obtained [23-30]. The computational cost for the CCD and CCSD methods scales like N^6 , where N represents the number of basis functions.

In the CCSDT method also the triple excitations are included ($\hat{T} = \hat{T}_1 + \hat{T}_2 + \hat{T}_3$). At this level, the computational cost scales like N^8 . Thus, the CCSDT approach is extremely expensive and the use of large basis sets is impossible unless in the case of calculations upon atoms or small molecules. Going beyond CCSDT, the models (CCSDTQ, CCSDTQ5,...) become too demanding and practically intractable, except in the case of exceedingly small systems.

In order to reduce the computational cost of CCSDT calculations, the effect of triple excitations can be accounted for by means of perturbation theory. This approximation is known as CCSD(T) theory [31]. It includes perturbative triple corrections and a single and triple interaction term. The triple correction is obtained by means of a formula similar to that used in fourth-order Møller-Plesset (MP4) perturbation theory using the cluster amplitudes corresponding to the double excitations t_{ij}^{rs} obtained from the CCSD wave function. The CCSD(T) method provides a very good single-reference correlation treatment in conjunction with a very good compromise between the computational cost and the achieved accuracy.

Coupled cluster methods are single-reference methods, where the Hartree–Fock determinant is usually used as the reference function. Therefore, one has to be very careful about multi-reference (or static correlation) effects. If these effects are sufficiently large i.e. if two or more determinants of comparable weight dominate in the expansion of the electronic wave function, the results of the CC method become unreliable. In order to assess the influence of multi-reference effects, Lee and Taylor [32] devised a method for identifying the extent of near-degeneracy effects. The quantity, which measures the importance of the multi-reference effects, is called the T_1 diagnostic, which is defined as:

$$T_1 = \frac{\|\mathbf{t}_1\|}{\sqrt{N}}, \quad (69)$$

where \mathbf{t}_1 is the vector of single excitation amplitudes and N corresponds to the number of electrons. The finally retained threshold for the T_1 diagnostic has been set to 0.08 [33]: as long as the T_1 value remains below 0.08, a single-reference treatment should be valid. Further energy-based criteria have been more recently devised by Karton *et al* [34] for recognizing these situations where static or dynamical correlation dominates. According to Karton *et al*, the targets are dominated by dynamical correlation if the percentage of the total atomization energy which is accounted for by perturbative triple excitations (%TAE[(T)]) is below 2 %.

2.3 Density functional theory

Density Functional Theory (DFT) is based upon the idea that the energy of an electronic system can be expressed in terms of its density. DFT is based on two theorems due to Hohenberg and Kohn. The one-electron density $\rho(\mathbf{r})$ for a N -electron system is obtained by carrying out the integration of the square of the wave function ($|\Psi|^2$) over the space and spin coordinates of all electrons, except one:

$$\rho(\mathbf{r}_1) = N \int \dots \int |\Psi(\mathbf{x}_1, \mathbf{x}_2, \dots, \mathbf{x}_N)|^2 d\sigma_1 d\mathbf{x}_2 \dots d\mathbf{x}_N, \quad (70)$$

where the coordinates \mathbf{x}_i for the i -th electron comprise both space and spin coordinates, i.e. \mathbf{r}_i and ω_i , respectively. $\rho(\mathbf{r})$ is a non-negative function of the three variables x, y, z , which represents the electron density of the electron cloud carrying N electrons, such that the integration of $\rho(\mathbf{r})$ over space gives the total number of electrons:

$$\int \rho(\mathbf{r}) d\mathbf{r} = N. \quad (71)$$

The first theorem of Hohenberg and Kohn states: "The external potential $v(\mathbf{r})$ is determined within an additive constant by the electron density $\rho(\mathbf{r})$." Therefore, $\rho(\mathbf{r})$ also determines the ground state wave function Ψ and all other electronic properties of the system. Indeed, suppose one has the electronic density of an unknown system. The number of electrons in the system is obtained by integrating the electronic density over space. By looking at values

of the function $\rho(\mathbf{r})$ at each point in space in order to find the locations of the cusps, one is able to indicate the positions of the nuclei. By examining how fast the electron density drops at the position of a nucleus, the charge of the nucleus can be determined (Kato's theorem) [35]. So far, one has thus enough information to write down the Hamiltonian and the corresponding Schrödinger equation, which determines the wave function of the system. Hence, the electron density $\rho(\mathbf{r})$ contains the same precise information about the system just as does the wave function Ψ .

The energy of the system can be expressed as a functional of the electron density ρ , as follows:

$$E[\rho] = V_{ne}[\rho] + T[\rho] + V_{ee}[\rho], \quad (72)$$

where $V_{ne}[\rho]$ is the nucleus-electron energy functional, $T[\rho]$ is the kinetic energy functional, and $V_{ee}[\rho]$ is the electron-electron interaction energy.

$V_{ne}[\rho]$ is given by:

$$V_{ne}[\rho] = \int \rho(\mathbf{r})v(\mathbf{r})d\mathbf{r}, \quad (73)$$

with $v(\mathbf{r})$ the external potential defined by eq. (6). The electron-electron interaction energy $V_{ee}[\rho]$ has two terms: the classical Coulomb repulsion term $J[\rho]$ and a term with a non-classical origin. The classical Coulomb repulsion term $J[\rho]$ is expressed as follows:

$$J[\rho] = \frac{1}{2} \iint \frac{1}{r_{12}} \rho(\mathbf{r}_1) \rho(\mathbf{r}_2) d\mathbf{r}_1 d\mathbf{r}_2. \quad (74)$$

The exact form of the non-classical contribution to $V_{ee}[\rho]$ is unknown and represents the main challenge of DFT.

The second theorem by Hohenberg and Kohn [36] is an analogue of the variation principle, which states that: "For a given number of electrons and an external potential $v(\mathbf{r})$, there exists a functional of ρ denoted by $E_v^{HK}[\rho]$, for which the following variation principle is satisfied:

$$E_v^{HK}[\rho] \geq E_v^{HK}[\rho_0] = E_0, \quad (75)$$

where ρ_0 stands for the ideal electronic density distribution for the ground state."

The Hohenberg–Kohn functional $E_v^{HK}[\rho]$ attains the minimum $E_v^{HK}[\rho] = E_0$ for the ideal (exact) density distribution. The ultimate goal of DFT is to find mathematically suitable forms of the Hohenberg–Kohn energy functional. A most basic problem is that there exists no exact formula for this functional. The best which can be achieved is to devise good enough approximations to the exact energy functional.

2.3.1 The Kohn-Sham theory

Kohn and Sham devised an approach for evaluating the kinetic energy functional, known as the Kohn-Sham method. They introduced a fictitious system of non-interacting electrons, which is referred to as the Kohn–Sham

system. The N electrons of this system are considered to be subject to an external potential $v_0(\mathbf{r})$, which replaces the interactions with nuclei. The external potential is constructed such that the corresponding electron density matches exactly the exact electron density. Let us assume that the mathematical form of this potential is known. In order to obtain the electronic density, one has only to solve the one-electron equation:

$$\left[-\frac{1}{2}\nabla^2 + v_0(\mathbf{r}) \right] \psi_i = \epsilon_i \psi_i, \quad (76)$$

where ψ_i represent spin-orbitals, referred to as Kohn-Sham spin-orbitals. The total ground-state wave function is a Slater determinant of the N lowest spin-orbitals:

$$\Psi_0 = \frac{1}{\sqrt{N!}} \det[\psi_1 \psi_2 \dots \psi_N]. \quad (77)$$

The exact electronic density distribution $\rho(\mathbf{r})$ is given by:

$$\rho(\mathbf{r}) = \sum_i^N \sum_{\sigma} |\psi_i(\mathbf{r}, \sigma)|^2. \quad (78)$$

The total energy of N -electron system is:

$$E_0[\rho] = T_0[\rho] + \int v_0(\mathbf{r}) \rho(\mathbf{r}) d\mathbf{r}, \quad (79)$$

where the kinetic energy T_0 is expressed as:

$$T_0[\rho] = -\frac{1}{2} \sum_i^N \langle \psi_i | \nabla^2 | \psi_i \rangle. \quad (80)$$

The general expression for the electronic ground-state energy of a real system contains the kinetic energy of the N electrons, their interactions with the

nuclei and the electron-electron interactions. In line with eq. (72), the total energy is thus written as:

$$E[\rho] = T_0 + \int v(\mathbf{r})\rho(\mathbf{r})d\mathbf{r} + J[\rho] + E_{XC}[\rho], \quad (81)$$

where

- T_0 represents the electronic kinetic energy of the fictitious Kohn-Sham system of non-interacting electrons;
- $\int v(\mathbf{r})\rho(\mathbf{r})d\mathbf{r}$ is the correct electron-nuclei interaction term;
- $J[\rho]$ stands for the self-interaction of the electron cloud with itself.

The integral $J[\rho]$ does not describe the electron-electron interaction completely, since it does not take the correlation of electronic motions into account. A Coulomb hole prevails in the electron density distribution around each electron, due to repulsion force between particles with the same charge. A Fermi or exchange hole also exists due to the anti-symmetry and exclusion principles, which prevent two electrons with the same spin to have the same location in space. The term which takes into account these exchange and correlation effects is the exchange–correlation energy functional $E_{XC}(\rho)$. This term also contains a correction to the kinetic energy, which arises from the difference in between the kinetic energy calculated for the true (i.e. interacting) electron system and for the non-interacting Kohn–Sham one.

At this stage, we need to establish a connection between the external potential v_0 and the exchange-correlation functional. The variation principle is applied by varying the spin-orbitals. Upon denoting $\delta\psi_i$ an infinitesimal change

in the spin orbitals, the variations in the successive contributions to the energy are:

$$\delta T_0 = -\frac{1}{2} \sum_i^N \langle \delta \psi_i | \nabla^2 | \psi_i \rangle, \quad (82)$$

$$\delta \int v \rho \, d\mathbf{r} = \int v \delta \rho \, d\mathbf{r} = \sum_i^N \langle \delta \psi_i | v \psi_i \rangle, \quad (83)$$

$$\delta J = \sum_{i,j}^N \langle \delta \psi_i(\mathbf{r}_2, \sigma_2) | \hat{J}_j(\mathbf{r}_2) \psi_i(\mathbf{r}_2, \sigma_2) \rangle_2, \quad (84)$$

$$\delta E_{XC} = \sum_i^N \langle \delta \psi_i | \frac{\delta E_{XC}}{\delta \rho} \psi_i \rangle. \quad (85)$$

In eq. (84) $\langle \dots | \dots \rangle_2$ means integration over the spatial coordinates and summation over the spin coordinates of electron 2. The Coulomb operator associated with orbital ψ_j is:

$$\hat{J}_j(\mathbf{r}_2) = \sum_{\sigma_1} \int \frac{\psi_j(\mathbf{r}_1, \sigma_1)^* \psi_j(\mathbf{r}_1, \sigma_1)}{|\mathbf{r}_1 - \mathbf{r}_2|} d\mathbf{r}_1. \quad (86)$$

The Kohn-Sham (KS) equation is derived upon applying the variation principle to the energy obtained as a functional of the electron density, subject to the constraint that spin orbitals remain orthonormal. This constraint is enforced by introducing a set of Lagrange multipliers ε_{ij} :

$$\delta E - \sum_{i,j}^N \varepsilon_{ij} \langle \delta \psi_i | \psi_j \rangle = 0. \quad (87)$$

Upon inserting equations (82-85) in eq. (87), the following expression is obtained:

$$\sum_i^N \langle \delta \psi_i | \left\{ \left[-\frac{1}{2} \nabla^2 + v + \sum_j^N \hat{J}_j + \frac{\delta E_{XC}}{\delta \rho} \right] \psi_i - \sum_{i,j}^N \varepsilon_{ij} \psi_j \right\} \rangle = 0. \quad (88)$$

Since the variations in spin-orbitals are performed independently, the only way to verify eq. (88) is that every individual ket $|\psi_i\rangle$ is equal to zero:

$$\left\{ -\frac{1}{2} \nabla^2 + v(\mathbf{r}) + v_{coul}(\mathbf{r}) + v_{XC}(\mathbf{r}) \right\} \psi_i = \sum_{i,j}^N \varepsilon_{ij} \psi_j, \quad (89)$$

along with:

$$v_{coul}(\mathbf{r}) = \sum_j^N \hat{J}_j(\mathbf{r}), \quad (90)$$

$$v_{XC}(\mathbf{r}) = \frac{\delta E_{XC}}{\delta \rho(\mathbf{r})}. \quad (91)$$

Since all operators in the curly brackets of eq. (89) are invariant with respect to an arbitrary unitary transformation of the spin orbitals, the non-diagonal Lagrange multipliers can be discarded and a one-electron equation, referred to as the Kohn-Scham equation, is obtained:

$$\left\{ -\frac{1}{2} \nabla^2 + v(\mathbf{r}) + v_{coul}(\mathbf{r}) + v_{XC}(\mathbf{r}) \right\} \psi_i = \varepsilon_i \psi_i. \quad (92)$$

The Kohn-Sham equations are solved iteratively, starting from zeroth-order approximations for orbitals, which are used for constructing a zeroth-order approximation to the density ρ , which is used in turn for constructing a zeroth-order approximation to the operators $v_{coul}(\mathbf{r})$ and $v_{XC}(\mathbf{r})$. Solving the Kohn-Sham equations gives new orbitals, from which the electron density and the

above mentioned operators can be recalculated. This procedure is repeated until self-consistency is achieved.

Density Functional Theory (DFT) is in principle exact. The main limitation to this theory is that the exact form of the exchange-correlation functional is unknown.

2.3.2 Exchange, correlation and hybrid functionals

Since the exact exchange-correlation functional is unknown, approximations must be introduced. It is customary to divide the exchange-correlation functional $E_{xc}[\rho]$ into two terms:

$$E_{xc}[\rho] = E_x[\rho] + E_c[\rho]. \quad (93)$$

The exchange term $E_x[\rho]$ takes into account the exchange energy arising from the anti-symmetry of the wave function with respect to the interchange of electron coordinates, whereas the correlation term $E_c[\rho]$ accounts for the correlation of the electronic motions.

The Kohn-Sham formalism can be generalized by splitting $\rho(\mathbf{r})$ into two parts, where one part corresponds to electrons with an α spin function and the other part corresponds to electrons possessing a β spin function:

$$\rho(\mathbf{r}) = \rho_\alpha(\mathbf{r}) + \rho_\beta(\mathbf{r}). \quad (94)$$

If these two contributions are not equal (i.e. if the system is spin polarized), a set of coupled Kohn-Sham equations for spin-up and spin-down electrons need to be solved using a potential which depends on the electron spin. This is the

same situation as one faces in the case of unrestricted Hartree-Fock theory, and which is referred to as unrestricted DFT.

2.3.2.1 Local density approximation

The Local Density Approximation (LDA) [37-40] is based on the assumption that the electron density can be locally treated as a uniform electron gas. Although the electronic density in molecules is clearly inhomogeneous, it is reasonable to assume that it is locally homogeneous within a small (infinitesimal) volume element. The contribution to the exchange-correlation energy E_{XC} from these volume elements can be calculated to a good approximation as a product of the volume element and of the exchange-correlation energy density, derived from homogeneous gas theory. The total exchange-correlation energy E_{XC} is then determined as a sum of the locally obtained contributions. The exchange energy for a uniform gas is given by Dirac formula:

$$E_x^{LDA}[\rho] = -C_x \int \rho^{4/3}(\mathbf{r}) d\mathbf{r}, \quad (95)$$

where $C_x = \frac{3}{4} \left(\frac{3}{\pi} \right)^{1/3}$.

The local density method which is employed when electron densities corresponding to opposite spins differ is referred to as the Local Spin Density Approximation (LSDA). Here the exchange energy functional is given by:

$$E_x^{LSDA}[\rho] = -2^{1/3} C_x \int [\rho_\alpha^{4/3} + \rho_\beta^{4/3}] d\mathbf{r}. \quad (96)$$

The correlation energy functional for the homogeneous electron gas has been determined using the Monte Carlo approach by Vosko, Wilk and Nusair, which has enabled them to construct an analytic interpolation formula suitable for DFT, which is known as the VWN functional [39, 41].

2.3.2.2 Gradient expansion approximation

All methods which go beyond the Local Spin Density Approximation (LSDA) assume that the exchange-correlation energy functional, E_{XC} , does not just locally depend on the electron density $\rho(\mathbf{r})$ at a given point, but also on the electron density $\rho(\mathbf{r})$ surrounding this point (non-locally). Hence, exchange-correlation energy functional E_{XC} depends on both the electron density $\rho(\mathbf{r})$ and its gradient $\nabla\rho(\mathbf{r})$. Such methods are known as Gradient Expansion Approximation (GEA) or Generalized Gradient Approximation (GGA). There exist many different gradient-corrected exchange functionals and gradient-corrected correlation functionals.

Well-known examples of gradient-corrected exchange functionals are the functionals by Becke (B88) [35, 36b] and by Gill (G96) [42]. Among the functionals which contain a gradient-corrected correlation part, the most popular ones are the Lee-Yang-Parr (LYP) [39, 43-46], the 1991 Perdew-Wang (PW91) and 1992 Perdew-Wang (PW92) [47-49] functionals.

Some functionals consider at the same time both the exchange and the correlation parts. Some of them are the Perdew-Yang 1991 exchange-correlation functional [50], Becke-Lee-Parr functional [51] and Becke-Perdew (BP86)

functional [39, 40b, 52]. The last one is a combination of the B88 gradient corrected exchange and P86 local correlation [52] functionals.

2.3.2.3 Hybrid methods

Hybrid approximations to the exchange-correlation functional are very popular, due to the fact that the results obtained with these are usually found to be in very good agreement with experiment. One of the most popular hybrid functional is the B3LYP exchange-correlation functional. The B3LYP exchange-correlation energy is obtained from the B88 exchange energy, the LYP correlation energy, the VWN correlation energy and the difference between the Hartree-Fock and LSDA exchange energy, according to:

$$E_{xc}^{B3LYP} = E_{xc}^{LSDA} + 0.20(E_x^{HF} - E_x^{LSDA}) + 0.72E_x^{B88} + 0.81E_c^{LYP} - 0.19E_c^{VWN}. \quad (97)$$

The parameters of eq. (97) were determined by Becke using a linear least square fit to a set of 56 atomization energies, 42 ionization potentials, 8 proton affinities, and 10 first-row total atomic energies [39, 53, 54].

The MPW1PW91 functional has been developed by Barone and Adamo [55]. This functional is a combination of the modified version of the PW91 exchange functional, the original PW91 correlation functional and a mixture of the exact and DFT exchange in a ratio of 1 to 4.

The MPW1K functional is a modification of the MPW1PW91 functional. It corresponds to a combination of the Hartree-Fock non-local exchange operator, local DFT exchange-correlation functionals and gradient-corrected density functional:

$$E_{xc}^{MPW1K} = E^{HF} + XE_x^{HF} + (1-X)(E_x^{LSDA} + E_x^{MPW1}) + E_c^{PW91}, \quad (98)$$

where the mixing ratio of the exact and DFT exchange energy terms is 0.428 : 0.572. E^{HF} denotes the non-exchange part of the HF operator, E_x^{HF} is the HF exchange energy, E_x^{LSDA} is the exchange energy part within the LSDA approximation, E_x^{MPW1} is the gradient corrected exchange functional, E_c^{PW91} is the Perdew-Wang correlation functional, and X is the fraction of Hartree-Fock exchange.

The PBE1PBE functional was constructed by Adamo [56]. This functional is a hybrid modification of a 1996 pure functional of Perdew, Burke and Ernzerhof [57, 58]. It uses 25% exchange and 75% correlation weighting, and is known in the literature as the PBE0 functional.

The B2PLYP functional is the double hybrid functional devised by Grimme [59], which combines exact HF exchange with a MP2-like correlation treatment employing Kohn-Sham orbitals and energies. The B2PLYPD functional includes in addition empirical corrections for dispersion interactions [60].

2.3.3 The self-interaction problem

Self-interaction of electrons is an important problem in DFT. In atoms and molecules an electron interact with other electrons by experiencing the Coulomb potential due to the presence of the other electrons, but cannot interact with itself.

In the expression for the total electronic energy (eq. (81)), the classical electrostatic repulsion term $J[\rho]$ and the exchange-correlation energy term $E_{xc}[\rho]$ cancel exactly if an exact exchange-correlation functional is used. There is thus no self-interaction error within an exact theoretical framework. When approximations are used, self-interaction errors are introduced. One consequence is that the electronic potential decays faster than $1/r$ in the asymptotic region ($r \rightarrow \infty$).

2.3.4 Computational implementation: LCAO ansatz in the Kohn-Sham equations

Just like for HF theory, the only way to make DFT computationally tractable for polyatomic systems is to introduce the LCAO formalism. Within the framework of a spin-unrestricted treatment, electrons with opposite spins are described by two different sets of orbitals. The set of orbitals $\{\psi_i^\alpha | i=1,2,\dots,n_\alpha\}$ corresponds to electrons with spin α , while the set $\{\psi_i^\beta | i=1,2,\dots,n_\beta\}$ corresponds to electrons with spin β . The partial densities are defined as follows:

$$\rho_\alpha = \sum_i^{n_\alpha} |\psi_i^\alpha|^2, \quad (99)$$

$$\rho_\beta = \sum_i^{n_\beta} |\psi_i^\beta|^2, \quad (100)$$

and the total density is thus:

$$\rho = \rho_\alpha + \rho_\beta. \quad (101)$$

At this point we rewrite the one-electron Kohn-Sham equations:

$$\left\{ -\frac{1}{2} \nabla^2 + v(\mathbf{r}) + v_{coul}(\mathbf{r}) + v_{xc}(\mathbf{r}) \right\} \psi_i = \varepsilon_i \psi_i, \quad (102)$$

into the more compact form:

$$\hat{f}^{KS} \psi_i = \varepsilon_i \psi_i, \quad (103)$$

where \hat{f}^{KS} represents the one-electron Kohn-Sham operator. The external potential $v(\mathbf{r})$ and $v_{coul}(\mathbf{r})$ are defined in eqs. (6) and (90), respectively.

$v_{xc}(\mathbf{r})$ is the exchange-correlation potential, obtained as the derivative of the selected exchange-correlation functional with respect to the density. In order to convert these integro-differential equations into a matrix form, a set of basis (atomic) functions $\{\phi_\mu | \mu = 1, 2, \dots, K\}$ has to be introduced. Molecular orbitals are thus expanded as follows:

$$\psi_i^\alpha = \sum_{\mu=1}^K c_{\mu}^\alpha \phi_\mu, \quad \psi_i^\beta = \sum_{\mu=1}^K c_{\mu}^\beta \phi_\mu, \quad i = 1, 2, \dots, K. \quad (104)$$

After substituting eq. (104) into eq. (103), the one-electron Kohn-Sham equations are multiplied from left by atomic basis functions and integrated over space. The result is a set of linear algebraic equations, which can be solved using standard diagonalization techniques:

$$\left. \begin{aligned} \sum_{\nu=1}^K (F_{\mu\nu}^\alpha - \varepsilon_i^\alpha S_{\mu\nu}) c_{\nu}^\alpha &= 0 \\ \sum_{\nu=1}^K (F_{\mu\nu}^\beta - \varepsilon_i^\beta S_{\mu\nu}) c_{\nu}^\beta &= 0 \end{aligned} \right\}, \quad (105)$$

where ε_i^α and ε_i^β represents the occupied orbitals energies and where $S_{\mu\nu}$ represents the elements of the overlap matrix. A set of Fock-type matrices are defined as follows:

$$F_{\mu\nu}^\alpha = H_{\mu\nu} + J_{\mu\nu} + V_{\mu\nu}^{xc,\alpha}, \quad (106)$$

$$F_{\mu\nu}^\beta = H_{\mu\nu} + J_{\mu\nu} + V_{\mu\nu}^{xc,\beta}. \quad (107)$$

Here $H_{\mu\nu}$ represents the Hamiltonian matrix of a system of non-interacting electrons and $J_{\mu\nu}$ represents the Coulomb matrix, which is:

$$J_{\mu\nu} = \sum_{\lambda}^K \sum_{\sigma}^K P_{\lambda\sigma} (\mu\nu|\lambda\sigma), \quad (108)$$

with $P_{\lambda\sigma} = P_{\lambda\sigma}^\alpha + P_{\lambda\sigma}^\beta$ the total electron density matrix.

Up to this point, there is no difference with the Hartree-Fock-Roothaan formalism. Differences only appear when considering the exchange-correlation term, the matrix elements of which read:

$$V_{\mu\nu}^{xc} = \langle \phi_\mu | v_{xc} | \phi_\nu \rangle, \quad (109)$$

with v_{xc} representing some approximation to the exchange-correlation potential.

The analogy is clear with the closed-shell Roothaan-Hall equations (when $c_{\mu\nu}^\alpha = c_{\mu\nu}^\beta$) and with the unrestricted open-shell equations of Pople-Nesbet (when $c_{\mu\nu}^\alpha \neq c_{\mu\nu}^\beta$). Once equations have been solved iteratively by means of a self-consistent field procedure, and the Kohn-Sham orbitals are obtained, one can determine the electronic density and the total electronic energy. The main difficulty is the evaluation of the integrals in the expressions for the energy,

which can only be carried out using a numerical procedure. Detailed descriptions of the integration grids and values for the different parameters can be found in [61-66].

2.4 Basis sets

Both with conventional wave function based approaches and with density functional theory, the basis set $\{\phi_\mu\}$ is almost universally chosen to consist of so-called Gaussian-type-orbitals (GTOs) of the form:

$$\phi^{GTO} = N x^l y^m z^n e^{-\alpha r^2}, \quad (110)$$

where α is the orbital exponent and $L=l+m+n$ is used to classify the GTOs as s-functions ($L=0$), p-functions ($L=1$), d-functions ($L=2$), etc. The GTO basis functions are computationally advantageous, since there exist very efficient algorithms for calculating exceedingly large numbers of four-center-two-electron integrals. GTOs unfortunately do not present a "cusp" at $r \rightarrow 0$ and decay too fast in the asymptotic region ($r \rightarrow \infty$). On the other hand, so-called Slater-type-orbitals (STOs) seem to be a more appropriate choice from a physical point of view, since they exhibit the correct cusp behavior at $r \rightarrow 0$ and the correct exponential decay in the asymptotic region ($r \rightarrow \infty$). STOs are of the form:

$$\phi^{STO} = N r^{n-1} e^{-\zeta r} Y_{lm}(\Theta, \phi), \quad (111)$$

where n is the principle quantum number, ζ is a orbital exponent and Y_{lm} are spherical harmonics. Although STOs are physically most suitable as atomic basis functions, the evaluation of four-center-two-electron integrals with such functions represents a too difficult and time consuming task from a

computational point of view, considering that there are no analytical expression for evaluating such integrals. On the other hand, these integrals are relatively easy to evaluate with GTOs, considering that the product of two Gaussian functions is also a Gaussian function. Therefore, one usually uses as basis functions fixed linear combinations of several GTOs, which are referred to as contracted Gaussian functions (CGFs):

$$\phi_{\mu}^{CGF} = \sum_{p=1}^L d_{p\mu} \phi_p^{GTO}. \quad (112)$$

The coefficients $d_{p\mu}$ are chosen in such a way that the CGF resembles as much as possible the relevant STO, in order to compensate the limitations of individual GTOs in the cusp and tail regions.

The simplest expansion of the molecular orbitals uses only one basis function (or one contracted function) for each occupied atomic orbital and these basis sets are therefore called *minimal* basis sets. One example of a *minimal* basis set is the STO-3G basis set, where three primitive GTO functions are combined into one CGF. In the case of carbon atoms, this basis set has only five functions, one for each 1s and 2s atomic orbitals and three atomic orbitals for the 2p shell (p_x , p_y and p_z). The following series of basis sets are the split-valence *double-zeta* basis sets. For each orbital contributing to the valence shell, there are two functions. The typical example is the 6-31G Gaussian basis set developed by Pople and co-workers [2]. The 6-31G acronym implies that the basis consists of inner shell functions, inner valence functions, and outer valence functions, which are contractions of 6, 3 and 1 primitive functions, respectively. Usually, such basis sets are augmented by functions of higher angular momenta than those occupied in atoms, which are called *polarization functions*. In this

way the 6-31G* basis [67, 68] has been created by adding d-type functions to heavy atoms (Li till F). The 6-31G** basis differs from the 6-31G* basis by the addition of one set of p-type GTO functions on each hydrogen.

Widely used basis sets are the correlation consistent basis sets (cc-pVXZ sets with X=D, T, Q, 5...) which have been developed by Dunning and co-workers [69]. The smallest set in this series is the correlation consistent polarized valence double-zeta basis set (cc-pVDZ). The addition of diffuse functions to the cc-pVXZ basis sets is denoted by the "aug" prefix. One diffuse function of each function type in use for a given atom is added [70, 71]. For example, the aug-cc-pVTZ basis incorporates one set of s, p, and d diffuse functions on hydrogen atoms, and one set of s, p, d, and f diffuse functions on heavy atoms (B through Ne and Al through Ar).

Energies computed using cc-pVXZ and aug-cc-pVXZ basis sets of improving quality (X=D, T, Q, 5,...) converge smoothly at the Hartree-Fock level [72] and at correlated levels [73], enabling extrapolations to the limit of an asymptotically complete basis set (X=∞). Hartree-Fock electronic energies E_∞ obtained using Dunning's series of cc-pVXZ and aug-cc-pVXZ basis sets can be extrapolated to the limit of an asymptotically complete basis set using Feller formula [72]:

$$E(l) = E_\infty + Ae^{-Bl}, \quad (113)$$

where the cardinal number l equals 2, 3, 4,... when X=D, T, Q,... respectively.

The electron correlation energies are extrapolated to an asymptotically complete basis set, by means of a three-point extension (referred to as Schwartz 6(lmn) [74]) of Schwartz's extrapolation formula [73]:

$$E(l) = E_{\infty} + \frac{B}{\left(l + \frac{1}{2}\right)^4} + \frac{C}{\left(l + \frac{1}{2}\right)^6}. \quad (114)$$

In the present thesis, use has been made of these extrapolation approaches along with correlation treatments of improving quality, in order to achieve the highest possible accuracy in the computation of the ionization energies, singlet-triplet energy gaps, electron attachments and dipole polarizabilities of polycyclic aromatic hydrocarbons.

2.5 Finite field method

In the sequel, the calculation of the static electronic polarizabilities of naphthalene, anthracene, and tetracene will be presented, using the Finite Field (FF) method [22, 75]. The present section provides a brief account of this method.

The FF method of Cohen and Roothaan [76] consists in numerical evaluations of derivatives (of first- or higher-order) of the electronic energy with respect to an external field. By adding a perturbation $\mathbf{F} \cdot \mathbf{r}_1$ accounting for the effect of the external electric field \mathbf{F} to the core one-electron operator defined by eq. (19), one gets:

$$\hat{h}(1) = -\frac{1}{2} \nabla_1^2 - \sum_{A=1} \frac{Z_A}{r_{1A}} + \mathbf{F} \cdot \mathbf{r}_1. \quad (115)$$

Upon inserting this perturbed core one-electron operator into the Fock operator of eq. (19), and solving consistently the resulting Hartree-Fock-Roothaan equations, relaxed Hartree-Fock orbitals and energies are obtained, which further serve as input for calculations coping with electron correlation, such as: Møller-

Plesset perturbation theory truncated at second-order (MP2), third-order (MP3), and fourth-order with single, double, and quadruple excitations (SDQ-MP4), as well as CCSD and CCSD(T) theory.

The FF method exploits an expansion of the energy in function of the external electric field \mathbf{F} , according to:

$$E(\mathbf{F})=E(\mathbf{0})-\sum_i \mu_i F_i -\frac{1}{2} \sum_{ij} \alpha_{ij} F_i F_j -\frac{1}{6} \sum_{ijk} \beta_{ijk} F_i F_j F_k -\dots. \quad (116)$$

Where μ is the permanent dipole moment, α is the polarizability tensor, and β is the first hyperpolarizability tensor. These properties relate to energy derivatives in function of the external electric field, as follows:

$$\mu_i = -\frac{dE}{dF_i}, \quad (117)$$

$$\alpha_{ij} = -\frac{d^2 E}{dF_i dF_j}, \quad (118)$$

$$\beta_{ijk} = -\frac{d^3 E}{dF_i dF_j dF_k}. \quad (119)$$

In practice, therefore, polarizabilities (and hyperpolarizabilities) can be estimated at a given level in correlation and using a specific basis set by numerically differentiating the energy in function of the applied external field.

2.6 Born-Oppenheimer molecular dynamics

In this section we describe the theory underlying the Born-Oppenheimer Molecular Dynamics (BOMD) [77-80] approach for computing classical atomic trajectories from forces obtained on a quantum mechanical ground, according to Hellmann-Feynman theorem [77]. BOMD simulations are employed in the sequel

in order to evaluate thermal corrections to the polarizabilities of naphthalene, anthracene and naphthacene (or tetracene).

Unlike traditional approaches for dynamics, the BOMD method avoids the explicit calculation of the whole potential energy surface. It consists in a sequence of local approximations to the true surface, which are calculated along the computed trajectory. The converged wave-function, which is optimized at each step of the trajectory, is used in order to yield a more accurate potential energy surface, which is then used in turn to evaluate accelerations, from the gradients and Hessians of the potential.

The method is based on the construction of a second-order model of the exact potential energy, which enables us to restrict the integration only to a small region around the expansion point. This small region is the so-called *trust region*, and only in this small region the model is a good enough approximation to the true potential energy surface. The calculated trajectory has to remain in the *trust region* for remaining reliable.

To derive the expressions for the model trajectory, one needs to consider first the classical equations of motion of an M -particle system in Cartesian coordinates:

$$\mathbf{m}\ddot{\mathbf{x}} = -\frac{dV(\mathbf{x})}{d\mathbf{x}}, \quad (120)$$

where \mathbf{x} denotes the $3M$ Cartesian component vector, $V(\mathbf{x})$ stands for the potential energy of the system, and \mathbf{m} is a $3M$ dimensional diagonal matrix containing the nuclear masses m_i of the system:

$$\mathbf{m} = \begin{pmatrix} m_1 & & \mathbf{0} \\ & \ddots & \\ \mathbf{0} & & m_{3N} \end{pmatrix}. \quad (121)$$

In a next step, the potential $V(\mathbf{x})$ is expanded for the *trust region* around a point \mathbf{x}^0 on the surface, up to second order in atomic displacements $\Delta\mathbf{x} = \mathbf{x} - \mathbf{x}^0$:

$$V_{\text{model}}(\mathbf{x}) = V^0 + \tilde{\mathbf{G}}\Delta\mathbf{x} + \frac{1}{2}\Delta\tilde{\mathbf{x}}\mathbf{H}\Delta\mathbf{x}. \quad (122)$$

In the above equation, V^0 , \mathbf{G} and \mathbf{H} represent the potential energy, gradient and Hessian of the potential, respectively. Upon inserting eq. (122) into eq. (120), the equations of motion become:

$$\mathbf{m}\Delta\ddot{\mathbf{x}} = -\mathbf{G} - \mathbf{H}\Delta\mathbf{x}. \quad (123)$$

Normal mode coordinates \mathbf{Q} are introduced in the usual way by diagonalizing the mass-weighted Hessian matrix:

$$\mathbf{Q} = \tilde{\mathbf{U}}\mathbf{m}^{1/2}\Delta\mathbf{x}, \quad (124)$$

$$\mathbf{g} = \tilde{\mathbf{U}}\mathbf{m}^{-1/2}\mathbf{G}, \quad (125)$$

$$\boldsymbol{\omega}^2 = \tilde{\mathbf{U}}\mathbf{m}^{-1/2}\mathbf{H}\mathbf{m}^{-1/2}\mathbf{U}. \quad (126)$$

Here \mathbf{g} and $\boldsymbol{\omega}^2$ represent the gradient and Hessian in normal coordinates, while \mathbf{U} denotes some unitary matrix. Diagonal matrix elements ω_i can be positive, negative or zero, which corresponds to real, imaginary or zero frequencies, respectively. Relation between conjugated momenta \mathbf{P} and Cartesian coordinate momenta \mathbf{p} is:

$$\mathbf{P} = \mathbf{U}\mathbf{m}^{-1/2}\mathbf{p}. \quad (127)$$

Using normal mode coordinates enables us to represent the equation of motion in $3M$ one-dimensional equations:

$$\ddot{Q}_i = -g_i - \omega_i^2 Q_i. \quad (128)$$

Taking into account the initial conditions:

$$Q_i = 0, \quad (129)$$

$$P_i = P_i^0, \quad (130)$$

one obtains, in the case of real frequencies ($\omega_i^2 > 0$), a solution of the form:

$$Q_i(t) = \frac{P_i^0}{\omega_i} \sin(\omega_i t) - \frac{g_i}{\omega_i^2} [1 - \cos(\omega_i t)], \quad (131)$$

$$P_i(t) = P_i^0 \cos(\omega_i t) - \frac{g_i}{\omega_i} \sin(\omega_i t). \quad (132)$$

In the special case of zero frequency ($\omega_i^2 = 0$), the solution has the form:

$$Q_i(t) = P_i^0 t - \frac{1}{2} g_i t^2, \quad (133)$$

$$P_i(t) = P_i^0 - g_i t. \quad (134)$$

At last, in the case of imaginary frequencies ($\omega_i^2 < 0$), the solution can be

expressed in terms of hyperbolic functions:

$$Q_i(t) = \frac{P_i^0}{|\omega_i|} \sinh(|\omega_i| t) + \frac{g_i}{|\omega_i|^2} [1 - \cosh(|\omega_i| t)], \quad (135)$$

$$P_i(t) = P_i^0 \cosh(|\omega_i| t) - \frac{g_i}{|\omega_i|} \sinh(|\omega_i| t). \quad (136)$$

Once $\mathbf{Q}(\mathbf{t})$ and $\mathbf{P}(\mathbf{t})$ have been obtained from the above expressions, it is easy to calculate the time evolution of Cartesian coordinates and momenta, using:

$$\mathbf{x}(t) = \mathbf{x}^0 + \mathbf{m}^{-1/2} \mathbf{U} \mathbf{Q}(t), \quad (137)$$

$$\mathbf{p}(t) = \mathbf{m}^{1/2} \mathbf{U} \mathbf{P}(t). \quad (138)$$

Once the gradient and Hessian of the potential are known, it is easy to calculate the trajectory on a second-order potential energy surface [eq. (122)]. The complete trajectory is obtained step by step. In a first step, we start by calculating the electronic energy, gradient and Hessian at an initial point in order to construct a local model surface. The integration [eq. (137)] is then carried out to the boundary of the *trust region*, enabling us to calculate a local trajectory. The same procedure is repeated in the next step, with the difference that the final point of the local trajectory from the previous *trust region* becomes a new initial point for the local trajectory in the next *trust region*. The process is repeated until the trajectory is completely calculated.

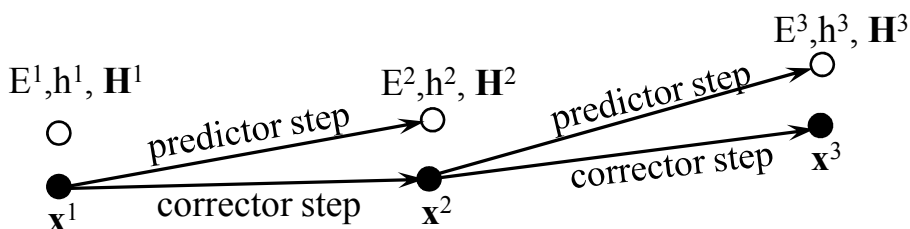


Figure 1. Hessian-based predictor–corrector algorithm [80] for integration of trajectories. A quadratic approximation to the surface at \mathbf{x}^1 is used in a predictor step to obtain \mathbf{x}^2 . Then the energies, gradients, and Hessians at \mathbf{x}^1 and \mathbf{x}^2 are fitted by a fifth-order polynomial so that a correction step could be taken on this fitted surface. The procedure is repeated for the following step starting with the quadratic approximation at \mathbf{x}^2 .

The quadratic approximation to the potential-energy surface [eq. (122)] is valid only for a given *trust* radius, which is relatively small. More accurate approaches have been devised, which allow taking larger steps. Within such approaches, the second-order method is used as a predictor step, which is followed by a corrector step (Figure 1). In order to get better local approximation to the potential-energy surface, one performs a fit of a higher-order surface to the energy, gradient, and Hessian, which have been calculated not only at the beginning but also at the end of the predictor step.

One type of local fitted surfaces employs a fifth-order polynomial fit [80]. During the fitting procedure, the Cartesian coordinates are rotated so that one component is parallel to the predictor step, \mathbf{x}_{\parallel} , while the others are perpendicular to the step, \mathbf{x}_{\perp} . For the parallel ($\Delta\mathbf{x}_{\parallel}$) and perpendicular ($\Delta\mathbf{x}_{\perp}$) displacements to the path direction, the energies, first and second derivatives parallel to the path are given by:

$$E^a = E^1 + \mathbf{g}_{\perp}^1 \prime \Delta\mathbf{x}_{\perp} + \frac{1}{2} \Delta\mathbf{x}_{\perp} \prime \mathbf{H}_{\perp,\perp}^1 \Delta\mathbf{x}_{\perp}, \quad (139)$$

$$\mathbf{g}^a = \mathbf{g}_{\parallel}^1 + \mathbf{H}_{\parallel,\perp}^1 \Delta\mathbf{x}_{\perp}, \quad (140)$$

$$h^a = \mathbf{H}_{\parallel,\parallel}^1, \quad (141)$$

$$E^b = E^2 + \mathbf{g}_{\perp}^2 \prime \Delta\mathbf{x}_{\perp} + \Delta\mathbf{x}_{\perp} \prime \mathbf{H}_{\perp,\perp}^2 \Delta\mathbf{x}_{\perp}, \quad (142)$$

$$\mathbf{g}^b = \mathbf{g}_{\parallel}^2 + \mathbf{H}_{\parallel,\perp}^2 \Delta\mathbf{x}_{\perp}, \quad (143)$$

$$h^b = \mathbf{H}_{\parallel,\parallel}^2, \quad (144)$$

where E^1 , \mathbf{g}^1 , and \mathbf{H}^1 are calculated at the beginning of the predictor step, while E^2 , \mathbf{g}^2 , and \mathbf{H}^2 are obtained at the end of the predictor step. A good approximation to the potential energy surface is constructed by fitting a fifth-order polynomial to E^a , \mathbf{g}^a , h^a , E^b , \mathbf{g}^b , and h^b :

$$\begin{aligned} V(\mathbf{x}) = & E^a(\Delta\mathbf{x}_\perp)y_1(\Delta\mathbf{x}_\parallel) + \mathbf{g}^a(\Delta\mathbf{x}_\perp)y_2(\Delta\mathbf{x}_\parallel) + \\ & + h^a(\Delta\mathbf{x}_\perp)y_3(\Delta\mathbf{x}_\parallel) + E^b(\Delta\mathbf{x}_\perp)y_4(\Delta\mathbf{x}_\parallel) + \\ & + \mathbf{g}^b(\Delta\mathbf{x}_\perp)y_5(\Delta\mathbf{x}_\parallel) + h^b(\Delta\mathbf{x}_\perp)y_6(\Delta\mathbf{x}_\parallel). \end{aligned} \quad (145)$$

The y functions are the appropriate fifth-order interpolating polynomials:

$$y_1(u) = 1 - 10u^3 + 15u^4 - 6u^5, \quad (146)$$

$$y_2(u) = s(u - 6u^3 + 8u^4 - 3u^5), \quad (147)$$

$$y_3(u) = s^2/2(u^2 - 3u^3 + 3u^4 - u^5), \quad (148)$$

$$y_4(u) = 10u^3 - 15u^4 + 6u^5, \quad (149)$$

$$y_5(u) = s(-4u^3 + 7u^4 - u^5), \quad (150)$$

$$y_6(u) = s^2/2(u^3 - 2u^4 + u^5), \quad (151)$$

where $u = \Delta x_\parallel / s$, and $s = |\mathbf{x}^2 - \mathbf{x}^1|$.

Using the Cartesian coordinates for the fitted surface, one faces the problem of the rotational invariance of the local potential-energy surface. The problem with translational and rotational invariance can be removed by projecting the mass-weighted gradient, $\mathbf{P}\mathbf{g}$, using the appropriate projector:

$$\mathbf{P} = \mathbf{I} - \sum_{i=1}^6 \mathbf{U}_i \mathbf{U}_i^t, \quad (152)$$

where \mathbf{U}_i ($i=1-6$) are the normalized vectors corresponding to overall translation and rotation in mass weighted coordinates.

2.6.1 Hellmann-Feynman theorem

The exact force corresponds to the first derivative of the energy. Since the energy in quantum mechanics is obtained as an expectation value of the Hamiltonian operator, for the real wave function the force is given by the expression:

$$\vec{\nabla} \langle \Psi | \hat{H} | \Psi \rangle = \langle \Psi | \vec{\nabla} \hat{H} | \Psi \rangle + 2 \langle \vec{\nabla} \Psi | \hat{H} | \Psi \rangle. \quad (153)$$

The first term on the right hand side of the above equation corresponds to the Hellmann-Feynman force, while the second term represents a correction to the Hellmann-Feynman force, which is known as the wave function response, Pulay force or incomplete basis set force. The second term can be expressed as follows:

$$\langle \vec{\nabla} \Psi | \hat{H} | \Psi \rangle = \langle \vec{\nabla} \Psi | \hat{H} - E | \Psi \rangle + E \langle \Psi | \vec{\nabla} \Psi \rangle, \quad (154)$$

where the second term on the right hand side of the latter equation usually vanishes.

If the system of interest is in the *stationary state* described by the normalized wave function Ψ then, according to Hellmann-Feynman theorem, the exact force is equal to the Hellmann-Feynman force. An important limitation to this theorem is that it is valid only for true stationary wave functions. To

prove this theorem, one has to differentiate the quantum mechanical energy

expression $E = \langle \Psi | H | \Psi \rangle$:

$$\begin{aligned} \frac{\partial E}{\partial x} &= \left\langle \frac{\partial \Psi}{\partial x} \left| \hat{H} \Psi \right. \right\rangle + \left\langle \Psi \left| \frac{\partial \hat{H}}{\partial x} \Psi \right. \right\rangle + \left\langle \Psi \left| \hat{H} \frac{\partial \Psi}{\partial x} \right. \right\rangle \\ &= E \left(\left\langle \frac{\partial \Psi}{\partial x} \left| \Psi \right. \right\rangle + \left\langle \Psi \left| \frac{\partial \Psi}{\partial x} \right. \right\rangle \right) + \left\langle \Psi \left| \frac{\partial \hat{H}}{\partial x} \Psi \right. \right\rangle. \end{aligned} \quad (155)$$

Upon differentiating the expression $\langle \Psi | \Psi \rangle = 1$ we find:

$$\left\langle \frac{\partial \Psi}{\partial x} \left| \Psi \right. \right\rangle + \left\langle \Psi \left| \frac{\partial \Psi}{\partial x} \right. \right\rangle = 0. \quad (156)$$

Using the above expression, and considering that \hat{H} is Hermitian, whereas Ψ represents its eigenfunction, we obtain the final form of Hellmann-Feynman theorem:

$$\frac{\partial E}{\partial x} = \left\langle \Psi \left| \frac{\partial \hat{H}}{\partial x} \Psi \right. \right\rangle. \quad (157)$$

In practice, most *ab initio* wave functions are obtained according to the variation principle, which generally does not yield the exact solution of the Schrödinger equation. Errors in the computation of forces arise due to approximate treatments of electronic correlation and the use of an incomplete basis set.

2.7 Translation symmetry: Bloch theorem, Bloch orbitals and Bloch functions

In the sequel, the scaling of spin contamination arising in applications of spin unrestricted treatments with respect to system size will be analyzed using

the formalism of crystalline orbitals for stereoangular polymers with one-dimensional periodicity (Figure 2). In this purpose we briefly review the band structure theory [81] of such systems.

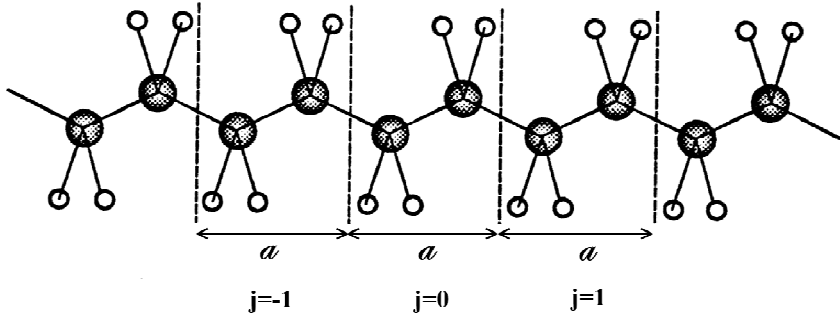


Figure 2. Model of an isolated and periodic (stereoregular) polymer chain, where j and a denote the unit cell index and the cell width, respectively.

For such a periodical system with one dimensional periodicity (along the z -axis), the periodic orbital electron densities satisfy:

$$\rho_n(\mathbf{r}) = |\varphi_n(\mathbf{r})|^2 = \rho_n(\mathbf{r} + ja\mathbf{e}_z) = \rho_n(\mathbf{r} + \mathbf{R}_j) = |\varphi_n(\mathbf{r} + \mathbf{R}_j)|^2, \quad (158)$$

where a is the length of the elementary unit cell of the periodic system in *direct space* (\mathbf{r}), and j is a cell index defining the position of the cell by a translation vector ($\mathbf{R}_j = ja\mathbf{e}_z$). Bloch's theorem [82] states the phase relation of the crystalline orbitals (Bloch orbitals) of periodic systems at periodically related points in the *direct space*:

$$\varphi_n(\mathbf{r} + \mathbf{R}_j) = e^{i\mathbf{k} \cdot \mathbf{R}_j} \varphi_n(\mathbf{r}) = e^{ikja} \varphi_n(\mathbf{r}), \quad (159)$$

where \mathbf{k} and k define a wave vector and the associated wave number, respectively (in this case: $\mathbf{k} = k\mathbf{e}_z$). Bloch's theorem is derived from the

commutation properties of the one-electron Hamiltonian operator and the translation operator $\mathbf{T}(\mathbf{R}_j)$ defined such as it translates any function $f(\mathbf{r})$ from \mathbf{r} to $\mathbf{r} + ja\mathbf{e}_z$:

$$T(\mathbf{R}_j)f(\mathbf{r}) = f(\mathbf{r} + ja\mathbf{e}_z) = f(\mathbf{r} + \mathbf{R}_j). \quad (160)$$

The one-electron potential function $V(\mathbf{r})$ and the orbital electron density $\rho_n(\mathbf{r})$ are eigenfunctions of the translation operator with an eigenvalue equal to 1, due to the periodic properties of the infinite lattice:

$$T(\mathbf{R}_j)V(\mathbf{r}) = V(\mathbf{r} + ja\mathbf{e}_z) = V(\mathbf{r} + \mathbf{R}_j) = 1V(\mathbf{r}), \quad (161)$$

$$T(\mathbf{R}_j)\rho_n(\mathbf{r}) = \rho_n(\mathbf{r} + ja\mathbf{e}_z) = \rho_n(\mathbf{r} + \mathbf{R}_j) = 1\rho_n(\mathbf{r}). \quad (162)$$

Due to the fact that the one-electron Hamiltonian operator and the translation operator commute, they must possess the same set of eigenfunctions. Formally, the eigenfunctions of the translation operator can be represented by the eigenvalue equation:

$$T(\mathbf{R}_j)\varphi_n(\mathbf{r}) = \varphi_n(\mathbf{r} + ja\mathbf{e}_z) = \lambda_j \varphi_n(\mathbf{r}). \quad (163)$$

Because of the periodic properties of the one-electron orbital densities in periodic systems:

$$\begin{aligned} \rho_n(\mathbf{r} + ja\mathbf{e}_z) &= T(\mathbf{R}_j)\rho_n(\mathbf{r}) = T(\mathbf{R}_j)|\varphi_n(\mathbf{r})|^2 = \\ &|\varphi_n(\mathbf{r} + ja\mathbf{e}_z)|^2 = \lambda_j^2 |\varphi_n(\mathbf{r})|^2 = |\varphi_n(\mathbf{r})|^2, \end{aligned} \quad (164)$$

it follows that the eigenvalue λ_j is a complex number of modulus equal to unity:

$$\lambda_j = e^{i\phi_j}. \quad (165)$$

It can be easily shown that:

$$\phi_j = \mathbf{k} \cdot \mathbf{R}_j = k j a . \quad (166)$$

Since a has the dimension of a length and j is an integer, in order for the exponent to remain dimensionless, k must have the dimension of an inverse length, i.e. k is a *wave number*. Correspondingly, \mathbf{R}_j is a vector belonging to the lattice in *direct space*, while \mathbf{k} is a wave vector belonging to the *reciprocal space*. The vector of a reciprocal lattice is denoted by \mathbf{G} , and (in z -direction) is defined as follows:

$$\mathbf{G} = G \mathbf{e}_z = l g \mathbf{e}_z , \quad (167)$$

where g is the length of the elementary unit cell in the reciprocal space, and l is an integer ($0, \pm 1, \pm 2, \dots$ etc). The values of k allowed within a single reference unit cell of the reciprocal lattice give non-redundant information. Therefore, in practice a calculation of the electronic structure of an extended periodic chain only needs to be performed over a range of k values equivalent to a single unit cell of the reciprocal lattice (i.e. corresponding to at most one translation $\mathbf{g} = g \mathbf{e}_z$ along the reciprocal lattice), and defining the *first Brillouin zone* ($-\pi/a \leq k \leq +\pi/a$) of the periodical system. This argument is based on the fact that Bloch orbitals which differ by a reciprocal lattice vector ($l g \mathbf{e}_z$) have the same eigenvalue for any translation operator:

$$T(\mathbf{R}_j) \varphi_n(k + l g, \mathbf{r}) = e^{i(k+l g)j a} \varphi_n(k + l g, \mathbf{r}) = e^{i k j a} \varphi_n(k + l g, \mathbf{r}) . \quad (168)$$

In the case of one-dimensional periodic systems, an alternative of Bloch's theorem is thus rather naturally obtained by factorizing the Bloch

orbitals into a periodic [$u_n(k, \mathbf{r} + \mathbf{R}_j) = u_n(k, \mathbf{r})$] contribution, referred to as a **Bloch function**, and a non-periodic free electron-like [e^{ikz}] contribution:

$$\varphi_n(k, \mathbf{r}) = e^{i\mathbf{k}\cdot\mathbf{r}} u_n(k, \mathbf{r}) = e^{ikz} u_n(k, \mathbf{r}). \quad (169)$$

As the Bloch orbitals to which they relate, Bloch functions are eigenfunctions of the translation operator with eigenvalues equal to e^{ikja} :

$$T(\mathbf{R}_j)u_n(k, \mathbf{r}) = e^{ikja} u_n(k, \mathbf{r}). \quad (170)$$

The proof that the above crystalline orbitals ($\phi_n(k, \mathbf{r}) = e^{ikja} u_n(k, \mathbf{r})$) satisfy the requirement of Bloch's theorem is easily given by showing that if $u_n(k, \mathbf{r})$ is periodic, one immediately finds:

$$\begin{aligned} T(\mathbf{R}_j)\varphi_n(k, \mathbf{r}) &= T(\mathbf{R}_j)[e^{ikz} u_n(k, \mathbf{r})] \\ &= e^{ik(z+ja)} u_n(k, \mathbf{r} + \mathbf{R}_j) \\ &= e^{ikja} e^{ikz} u_n(k, \mathbf{r}) \\ &= e^{ikja} \varphi_n(k, \mathbf{r}). \end{aligned} \quad (171)$$

When considering approximations such as the Linear Combination of Atomic Orbitals (LCAO) depiction, the Bloch functions are built up as symmetry-adapted linear combination of atomic orbitals (referred to as Bloch sums, γ_p) for the translation space group, as follows:

$$u_p(k, \mathbf{r}) = N^{-1/2} \sum_{j=1}^N e^{ikja} \gamma_p(\mathbf{r} - ja\mathbf{e}_z - \mathbf{R}_p), \quad (172)$$

where the [e^{ikja}] components are weight factors in the expansion, \mathbf{R}_p defines the position of the atomic center pertaining to orbital γ_p within the reference

unit cell, and the sum over j runs over all unit cells. The crystalline orbitals of periodic systems (i.e. Bloch orbitals) can thus be expressed as linear combinations of Bloch functions $[u_p(\mathbf{k}, \mathbf{r})]$, whose coefficients in the expansion are functions of a band index n and a wave number k :

$$\begin{aligned}\varphi_n(k, \mathbf{r}) &= \sum_{p=1}^K C_{pn}(k) u_p(k, \mathbf{r}) \\ &= N^{-1/2} \sum_{j=1}^N e^{ikja} \sum_{p=1}^K C_{pn}(k) \gamma_p(\mathbf{r} - ja\mathbf{e}_z - \mathbf{R}_p).\end{aligned}\tag{173}$$

Here the sum over p runs over the K atomic functions in the reference unit cell.

It is necessary to enforce space quantization in infinite systems using the cyclic boundary conditions over a super-cell, which contains, in a first approximation, a large but finite number (N) of unit cells. When there are many cells in the lattice, a very small error is introduced by making the assumption that the ends of the lattice can be brought round into a circle and joined. By introducing this assumption, the translation symmetry of a system is maintained and the influence of the end effects are eliminated. The circularity of the system implies:

$$\varphi_n(k, \mathbf{r} + Na\mathbf{e}_z) = \varphi_n(k, \mathbf{r}),\tag{174}$$

or equivalently in terms of Bloch functions:

$$u_p(k, \mathbf{r} + Na\mathbf{e}_z) e^{ik(z+Na)} = u_p(k, \mathbf{r}) e^{ikz}.\tag{175}$$

Thus, under the assumption that the periodic system is described as a super-cell containing N unit cells under the constraint of Born-Von Karman cyclic boundary condition, $N^{-1/2}$ in eqs. (172) and (173) is the normalization factor deriving from an orthonormal atomic orbital basis set. Since:

$$u_p(k, \mathbf{r} + Na\mathbf{e}_z) = u_p(k, \mathbf{r}), \quad (176)$$

it follows from eq. (175) that:

$$e^{ik(z+Na)} = e^{ikz}. \quad (177)$$

The above equality implies that:

$$e^{ikNa} = \cos(kNa) + i \cdot \sin(kNa) = 1, \quad (178)$$

which holds only if kNa takes values of the form $2\pi l$ where $l = 0, \pm 1, \pm 2, \dots$

For a super-cell containing N elementary unit cells under cyclic boundary constraints, there are therefore N permitted and non-redundant values of k within the first Brillouin zone ($k \leq |\pi/a|$):

$$k = \frac{2\pi l}{Na} = \frac{l}{N} g, \quad (179)$$

where $l = 0, \pm 1, \pm 2, \dots, \pm N/2$.

2.8 References

- [1] A. S. Szabo, N. S. Ostlund, *Modern Quantum Chemistry* (Mc Graw-Hill, New York, 1989).
- [2] W. J. Hehre, L. Radom, P. v. R. Scheyler, J. A. Pople, *Ab Initio molecular orbital theory*, (John Wiley, New York, 1986).
- [3] R. Mcweeny, *Methods of Molecular Quantum Mechanics*, Second Edition, (Academic Press, London, 1989).
- [4] J. Amlöf, *Notes on Hartree-Fock Theory and Related Topics* In Lecture Notes in Quantum Chemistry II, B.O. Roos (Ed.), (Springer- Verlag, Berlin 1994).

- [5] F. Jensen, *Introduction to Computational Chemistry* (Wiley, Chichester, 1999).
- [6] M. Born, J. R. Oppenheimer, *Ann. Physik*, **84**, 457 (1927).
- [7] D. R. Hartree, *Proc. Camb. Phil. Soc.* **24**, 89, 111, 426 (1928).
- [8] V. Fock, *Z. Phys.* **61**, 126 (1930).
- [9] T. A. Koopmans, *Physica (Amsterdam)* **1**, 104 (1933).
- [10] C. C. J. Roothaan, *Rev. Mod. Phys.* **23**, 69 (1951).
- [11] I. Shavitt, in *Modern theoretical Chemistry* (Ed. H. F. Schaefer III), (Plenum Press, New York, London, 1977) p.189.
- [12] C. W. Bauschlicher, Jr., S. R. Langhoff, and P. R. Taylor, *Adv. Chem. Phys.* **77**, 103 (1990).
- [13] P. O. Lowdin, *Advan, Chem. Phys.* **2**, 207 (1959).
- [14] C. Møller and M. S. Plesset, *Phys. Rev.* **46**, 618 (1934).
- [15] R. Krishnan and J.A. Pople, *Int. J. Quant. Chem.* **14**, 91 (1978).
- [16] R. Krishnan, J. S. Binkley, R. Seeger, J. A. Pople, *J Chem. Phys.* **72**, 650 (1980).
- [17] S. A. Kucharski, J. Noga and R. J. Bartlett, *J. Chem. Phys.* **90**, 7282 (1989).
- [18] D. Cremer and Z. He, *J. Phys. Chem.* **100**, 6173 (1996).
- [19] R. Krishnan, and J. A. Pople, *Int. J. Quant. Chem.* **14**, 91 (1978).
- [20] F. Coester, H. Kümmel, *Nucl. Phys.* **17**, 477 (1960).
- [21] F. Coester, *Nucl. Phys.* **7**, 421 (1958).

- [22] L. Piela, *Ideas of Quantum Chemistry*, (Elsevier B.V., Amsterdam, 2007).
- [23] G. D. Purvis III and R. J. Bartlett, *J. Chem. Phys.* **76**, 1910 (1982).
- [24] G. E. Scuseria, A. C. Scheiner, T. J. Lee, J. E. Rice, and H. F. Schaefer, *J. Chem. Phys.* **86**, 2881 (1987).
- [25] T. J. Lee and J. E. Rice, *Chem. Phys. Lett.* **150**, 406 (1988).
- [26] G. Scuseria, C. L. Jansen, H. F. Schaefer, *J. Chem. Phys.* **89**, 7382 (1988).
- [27] P. Piecuch, J. Paldus, *Int. J. Quantum. Chem.* **36**, 429 (1989).
- [28] J. F. Stanton, J. Gauss, J. D. Watts, and R. J. Bartlett, *J. Chem. Phys.* **94**, 4334 (1991).
- [29] J. Geertsen, S. Eriksen, and J. Oddershede, *Adv. Quantum Chem.* **22**, 168 (1991).
- [30] D. Jayatilaka and T. J. Lee, *Chem. Phys. Lett.* **199**, 211 (1992).
- [31] K. Raghavachari, G. W. Trucks, J. A. Pople and M. Head-Gordon, *Chem. Phys. Lett.* **157**, 479 (1989).
- [32] T. J. Lee and P.R. Taylor, *Int. J. Quantum Chem. Symp.* **23**, 199 (1989).
- [33] J. M. L. Martin, T. J. Lee, G. E. Scuseria, and P. R. Taylor, *J. Chem. Phys.* **97**, 6549 (1992).
- [34] A. Karton, E. Rabinovich, J.L.M. Martin, B. Ruscic, *J. Chem. Phys.* **125**, 144108 (2006).
- [35] T. Kato, *Commun. Pure Appl. Math.* **10**, 151 (1957).
- [36] P. Hohenberg and W. Kohn, *Phys. Rev.* **136**, B864. (1964).

- [37] R. G. Parr, W. Yang, *Density Functional Theory of Atoms and Molecules*, (Oxford University Press, Oxford, 1989).
- [38] J. C. Slater, *Phys. Rev.* **81**, 385 (1951).
- [39] T. H. Dunning, Jr. *J. Phys. Chem. A*, **104**, 9062 (2000); T. H. Dunning, Jr., K. A. Peterson, D. E. Woon, *Basis Sets: Correlation Consistent Sets in Encyclopedia of Computational Chemistry*, P.v.R. Schleyer, Editor, (John Wiley, New York, 1998).
- [40] (a) R. Gáspár, *Acta Phys. Acad. Sci. Hung.* **3**, 263 (1954); (b) A. D. Becke, *J. Chem. Phys.* **88**, 2547 (1988).
- [41] S. J. Vosko, L. Wilk, and M. Nusair, *Can. J. Phys.* **58**, 1200 (1980).
- [42] P. M. W. Gill, *Mol. Phys.* **89**, 433 (1996).
- [43] D. M. Ceperley, B. Alder, *J. Phys. Rev. Lett.* **45**, 566 (1980).
- [44] R. Colle, O. Salvetti, *Theor. Chim. Acta*, **37**, 329 (1975).
- [45] C. Lee, W. Yang, and R. G. Parr, *Phys. Rev. B* **37**, 785 (1988).
- [46] B. Miehlich, A. Savin, H. Stoll, H. Preuss, *Chem. Phys. Lett.* **157**, 200 (1989).
- [47] J. P. Perdew, in *Electronic Structure of Solids*, P. Ziesche and H. Eschrig (Eds.), (Akademic Verlag, Berlin, 1991).
- [48] J. P. Perdew, *Physica B*, **172**, 1 (1991).
- [49] J. P. Perdew and Y. Wang, *Phys. Rev. B*, **45**, 13244. (1992).
- [50] J. P. Perdew, J. A. Chevary, S. H. Vosko, K. A. Jackson, M. R. Pederson, D. J. Singh, and C. Fiolhais *Phys. Rev. B* **46**, 6671 (1992).

- [51] P. M. W. Gill, B. G. Johnson, J. A. Pople, and M. J. Frisch, *Int. J. Quantum Chem. Symp.* **26**, 319 (1992).
- [52] J. P. Perdew, *Phys. Rev. B*, **33**, 8822 (1986).
- [53] (a) J. Harris, and R. O. Jones, *J. Phys. F*, **4**, 1170 (1974); (b) O. Gunnarsson and B. I. Lundqvist, *Phys. Rev. B* **13**, 4274 (1976); (c) J. Harris, *Phys. Rev. A*, **29**, 1648 (1984); (d) A. D. Becke, *J. Chem. Phys.* **88**, 1053 (1988).
- [54] A. D. Becke, *J. Chem. Phys.* **98**, 1372 (1993).
- [55] C. Adamo and V. J. Barone, *Chem. Phys.* **108**, 664 (1998).
- [56] C. Adamo and V. Barone, *J. Chem. Phys.* **110**, 6158 (1999).
- [57] J. P. Perdew, K. Burke, and M. Ernzerhof, *Phys. Rev. Lett.* **77**, 3865 (1996).
- [58] J. P. Perdew, K. Burke, and M. Ernzerhof, *Phys. Rev. Lett.* **78**, 1396 (1997).
- [59] S. Grimme, *J. Chem. Phys.* **124**, 034108 (2006).
- [60] T. Schwabe and S. Grimme, *Phys. Chem. Chem. Phys.* **9**, 3397 (2007).
- [61] V. I. Lebedev, *Zh. Vychisl. Mat. Mat. Fiz.* **15**, 48 (1975); V. I. Lebedev, *Zh. vychisl. Mat. mat. Fiz.* **16**, 293 (1976); V. I. Lebedev, *Sibirsk. Mat. Zh.* **18**, 132 (1977); V. I. Lebedev, *Proc. Conf. Novosibirsk* (1978), edited by S. L. Sobolev (Nauka Sibirsk. Otdel., Novosibirsk, 1980).
- [62] S. I. Konyaev, *Mat. Zametki* **25**, 629 (1979).
- [63] P. M. W. Gill, B. G. Johnson, and J. A. Pople, *Chem. Phys. Lett.* **209**, 506 (1993).
- [64] C. W. Murray, N. C. Handy, and G. J. Laming, *Mol. Phys.* **78**, 997 (1993).

- [65] W. Koch, M. C. Holthausen, *A Chemist's Guide to Density Functional Theory*, 2nd Ed., (Wiley-VCH, Weinheim, 2001).
- [66] W. H. Press, S. A. Teukolsky, W. T. Vetterling, and B. P. Flannery, *Numerical Recipes in Fortran77: The Art of Scientific Computing*, 2nd ed., (Prentice Hall, Harlow, UK, 2001).
- [67] S. Huzinaga, *Comp. Phys. Reports*, **2**, 279 (1985).
- [68] P. C. Hariharan and J. A. Pople, *Theor. Chim. Acta*, **28**, 213 (1973).
- [69] T. H. Dunning, Jr., *J. Chem. Phys.* **90**, 1007 (1989), and references therein.
- [70] R. A. Kendall, T. H. Dunning, Jr., and R. J. Harrison, *J. Chem. Phys.* **96**, 6796 (1992).
- [71] D. E. Woon, T. H. Dunning, Jr., *J. Chem. Phys.* **98**, 1358 (1993).
- [72](a) D. Feller, *J. Chem. Phys.* **96**, 6104 (1992) Feller. (b) D. Feller, *J. Chem. Phys.* **98**, 7059 (1993).
- [73] C. Schwartz, *Estimating convergence rates of variational calculations*, in *Methods in Computational Physics 2*, Ed. B. J. Alder, (Academic Press, New York, 1963).
- [74] J. M. L. Martin, *Ab Initio Thermochemistry Beyond Chemical Accuracy for First- and Second-Row Compounds*, in NATO ASI Symposium volume *Energetics of Stable Molecules and Reactive Intermediates*, Ed. M. E. Mirrasda Piedade, and K. K. Irikura, (Kluwer: Dordrecht, The Netherlands, 1999).
- [75] S. P. A. Sauer, *Molecular Electromagnetism: A Computational Chemistry Approach*, (Oxford University Press Inc., New York, 2011).

- [76] H. D. Cohen and C. C. J. Roothaan, *J. Chem. Phys.* **43**, S34 (1965).
- [77] D. L. Thompson, *Modern methods for Multidimensional Dynamics Computations in Chemistry*, (World Scientific, Singapore, 1998) p. 143.
- [78] T. Helgaker, E. Uggerud, and H. J. A. Jensen, *Chem. Phys. Lett.* **173**, 145. (1990).
- [79] E. Uggerud and T. J. Helgaker, *J. Am. Chem. Soc.* **114**, 4265 (1992).
- [80] J. M. Millam, V. Bakken, W. Chen, W. L. Hase, H. B. Schlegel, *J. Chem. Phys.* **111** 3800 (1999).
- [81] J.-M. André, J. Delhalle, J.-L. Brédas, *Quantum Chemistry Aided Design of Organic Polymers: an Introduction to the Quantum Chemistry of Polymers and its Applications*, (World Scientific, Singapore 1992).
- [82] F. Bloch, *Z. Phys.* **52**, 555 (1928).

3 Half-metallicity and spin-contamination of the electronic ground state of graphene nanoribbons and related systems: an impossible compromise?

3.1 Context and scientific motivation

Half-metallicity, i.e. the coexistence of metallic nature for electrons with one spin orientation and insulating nature for the electrons of opposite spin, has been recently predicted for (*extended*) zig-zag graphene nanoribbons [1] (ZGNRs) of finite width (thus, with one-dimensional periodicity), on the ground of "first principle" calculations employing (spin-unrestricted) Density Functional Theory (DFT) [2] along with the local spin density approximation (LSDA) [3]. Peculiar states localize at the edges of the nanoribbon and form a twofold degenerate flat band at the Fermi energy (E_f) within one third of the first Brillouin zone (BZ) when the single graphite layer is terminated by zig-zag edges (i.e. polyacetylenic strands) on both sides [4]. Localized electronic states have been correspondingly observed in monoatomic graphitic step edges using scanning tunnelling microscopy and spectroscopy [5]. ZGNRs have compensated lattices in the sense that the number of carbon atoms belonging to each graphene sublattice is balanced. Therefore, according to Lieb's theorem for bipartite lattices [6] they have no total spin moment [7]. In view of the results of (spin-unrestricted) DFT calculations, edge states in these systems are thus believed to relate to antiferromagnetically ordered and spatially separated spin-orbitals, with opposite spin orientation across the ribbon, yielding a total spin (S) equal to zero [7, 8]. Reversing from condensed matter physics to the terminology employed in *molecular* quantum mechanics, ZGNRs are thus

considered to possess a (so-called) "singlet open-shell" electronic ground state characterized by symmetry-broken spin-densities, a view that spin-unrestricted DFT calculations with various functionals on large enough but finite polycyclic aromatic hydrocarbons [9] (PAHs) confirm. These functionals comprise the local spin density approximation [3], the gradient corrected functional of Perdew, Purke and Ernzerhof [10], the standard hybrid B3LYP (Becke-3-parameters-Lee-Yang-Parr [11]) functional and further screened hybrid exchange functionals.

The half-metallicity of ZGNRs [1, 8, 9] and of many related systems (edge-oxidized, edge-reconstructed or doped graphene nanoribbons [12], zigzag single-walled carbon or hybrid BN-C nanotubes of finite width [13], partially open armchair carbon nanotubes [14]) is still to date a pure theoretical conjecture, which has not been confirmed yet, neither experimentally nor by many body quantum mechanics. These predictions systematically find their roots into the results of (spin-unrestricted) DFT calculations and invariably the same constation that spatially separated spin-up and spin-down Kohn-Sham orbitals are subject to opposite energy shifts when an external electric field is applied across the nanoribbon, regardless of the band gap at zero field. Extended ZGNRs and finite *zig-zag graphene nanoislands* (ZGNIs) are thus considered nowadays to be highly promising materials with regards to *spintronics* (i.e. *spin transport electronics* [15]).

Several groups have been struggling for finding viable molecular illustrations of antiferromagnetism and half-metallicity among organic compounds. In particular (see the work by Hod *et al.*[9e]), PAHs with a non-zero band gap such as $C_{28}H_{14}$ (phenanthro[1,10,9,8-opqra]perylene, alias bisanthrene) or $C_{36}H_{16}$ (tetrabenzo[bc,ef,kl,no]coronene) have been recently predicted to be the *smallest* possible examples of ZGNIs with

antiferromagnetically ordered edge states subject to half-metallicity in the presence of a perpendicular external electric field. In line with these observations, it has also recently been conjectured [16] that n -acenes larger than pentacene or hexacene are “open-shell singlet” [i.e. *antiferromagnetic*] systems, resulting again most logically in half-metallicity in the macroscopic limit [17], $n \rightarrow \infty$. An electronic (singlet) instability was nevertheless diagnosed from the fact that in unrestricted calculations, the two outermost singly occupied α and β spin-orbitals deviate from the D_{2h} symmetry point group imposed by the nuclear frame, due to a *symmetry-breaking* in the form of a localization of the two frontier electrons on the two zig-zag edges. At the UB3LYP/6-31G* level of theory, [n]cyclacenes were similarly found to have a spin-polarized open-shell wave function in their singlet ground state when n is greater than 5 [18]. Unsurprisingly therefore, when reporting the synthesis of large acenes (heptacene, octacene, and nonacene), many synthetic chemists are speculating at the moment on the antiferromagnetic nature of these and large related PAHs (see e.g. ref. [19]). In sharp contrast with these views, a symmetry-restricted depiction is still most commonly employed for unravelling the site-dependence of electron transport properties of polycyclic aromatic hydrocarbons in molecular junctions, from the topological characteristics and atomic orbital coefficients of frontier orbitals [20].

From a theoretical viewpoint, large n -acenes, ZGNIs and ZGNRs are notoriously difficult, i.e. strongly correlated compounds. A recent study of n -acenes containing up to $n=8$ benzenoid rings by means of the variational two-electron reduced density matrix (2-RDM) approach [21] along with a basis set of double zeta quality demonstrates for instance from the evolution of natural

occupation numbers the smooth emergence of bi- and polyradical (i.e. multireference) character with increasing system size. At another extreme, recent GW calculations on zig zag graphene nanoribbons of width 2.4–0.4 nm [22] based on symmetry-broken LSDA spin-densities indicate quasi-particle band gaps, in the range of 0.5–3.0 eV, which are at first glance large enough to impede any spontaneous spin-flip. The existing literature regarding the electronic structure of these systems and their electric or magnetic properties is thus undeniably extremely confusing and badly needs further benchmark theoretical analyses and computational verifications.

A main conceptual difficulty for many chemists and physicists is that symmetry-breakings of spin-densities in the singlet eigenstates of spin-free Hamiltonians violate well-established principles and basic theorems of quantum mechanics or quantum chemistry (*point group theory, spin quantization*). A *singlet* ground state in (large but finite) molecules with an even number ($2N$) of electrons implies in particular that canonical orbitals transform according to irreducible representations of the molecular symmetry point group [23] and most strictly forbids any difference in between α and β spin-densities. Even in the presence of an external electric field, there must thus be an equal number of spin-up (α) and spin-down (β) electrons ($N_\alpha=N_\beta=N$) when $S=0$. Regardless of the extent of the multi-reference character (i.e. bi- or polyradicalism) of the electronic wave function, each α spin-orbital contribution has then a β partner with the same space function, and the spin-density is identically zero at every point in space. A typical example is H_2 in its $^1\Sigma_g^+$ electronic ground state [24–26], which by virtue of the antisymmetry principle has to relate to a 2-electron

spin function of the form $(1/2)^{1/2}[\alpha(1)\beta(2) - \beta(1)\alpha(2)]$, and this up to the dissociation limit. Also, in the absence of energy degeneracies, spin-orbitals are symmetry-adapted, exactly paired, and the charge density is totally symmetric under the molecular point group. In other words, when $S=0$, departures of spin- or charge-densities from the symmetry dictated by the Full Hamiltonian and by the nuclear framework are *artefactual* [27].

Physical symmetry breakings pertain to those cases where the molecular symmetry dictated by clamped nuclei configurations under the Born-Oppenheimer approximation does break [27]. There are numerous molecular systems exhibiting multiple minima of low symmetry on their potential energy surface, which interconvert through transition states of higher symmetry. Typical examples are the Jahn-Teller distortions induced by energy degeneracies under non-abelian symmetry point groups [25, 28]. However, even in this case, only electric charges can localize if the wave function remains a *singlet*. At this stage, it is thus useful to remember that there is nowadays a large consensus on the fact that n -acenes exhibit a D_{2h} symmetry point group [16], whatever their size, and this up to the macroscopic limit ($n \rightarrow \infty$).

If an unrestricted Self-Consistent Field (SCF) calculation upon a *singlet* wave function enforces different localizations for orbitals with opposite spin and an energy lowering into a so-called "singlet open-shell" ground state [16, 18], a spin-contamination by (magnetically active) triplet, quintet... etc. states arises, and the result of the calculation is trivially "*unphysical*", due to an incomplete or too approximate treatment of electron correlation [26, 29]. Spin-orbit coupling interactions are at first glance intrinsically far too weak to provide any support to the idea of "*spontaneous*" symmetry breakings in carbonaceous materials:

their estimated effect on the band gap of graphene does not exceed 24 μeV [30]. Electronic instabilities are the consequence of the non-analyticity of variational SCF procedures in symmetry breaking situations [31]. Self-consistent field Hamiltonian operators are not dilation analytic upon symmetry lowering, because of a non-physical “overcounting” and amplification of the effect of the symmetry breaking during the SCF procedure. When using unrestricted wave functions as zero-order solutions, one must then pay more tribute in the treatment of electronic correlation in order to compensate for the unphysical starting point, and recover the correct (charge- and spin-) symmetries. Note that, in their discussion of the spin-polarization of edge states of graphene islands of finite (nano-metric) dimension, Rudberg *et al.* [9b] already grasped that the half-metallic nature of the ZGNRs structures [1] may be an artefact of the employed DFT approaches.

In continuation of large-scale many-body wave function theoretical determinations of the ionization and electron attachments energies of benzene and *n*-acenes [32] within or close to chemical accuracy [1 kcal/mol, i.e. 43 meV], our group has published recently a focal point analysis of the electronic ground state and singlet-triplet energy gap of these compounds [33]. This study irrefutably demonstrates that high-level and large scale treatments of electronic correlation are necessary for compensating giant symmetry-breakings in unrestricted single-reference treatments of the electronic wave function of *n*-acenes. Symmetry-breakings are more likely to occur when limiting the size of the basis set, or when increasing the fraction of HF exchange in hybrid functionals. We noted as an extreme example that even benzene and naphthalene can be subject to *spurious* symmetry breakings of α and β spin-

densities when treating these compounds at the uncorrelated Hartree-Fock level in conjunction with a minimal STO-3G basis set (Slater-type orbital employing linear contractions of 3 primitive Gaussians per atomic function [33a]). Upon studying the performance of post-SCF restricted and unrestricted approaches, it was found that in all reported cases the energy difference between the lowest singlet closed-shell and so-called "singlet open-shell" states of benzene and acenes reverse at the MP2 level, and identically cancel when approaching the full-CI (configuration interaction) limit. The composition of multi-configurational wave functions, the topologies of natural orbitals in symmetry-unrestricted complete active space self consistent field (CASSCF) calculations, the T1 diagnostics [34] of Coupled Cluster theory and further energy-based criteria [35] also demonstrate that acenes up to (at least) undecacene [33b] exhibit a 1A_g singlet closed-shell single-reference electronic ground state [33]. In line with the trends emerging from natural occupation numbers [21], and obviously because of the imposed symmetry restrictions on spin-densities, extrapolations of our results indicate nonetheless a vanishing singlet-triplet energy gap and, thus, a *metallic (multi-reference) regime* in the limit of an infinite periodic chain. This should not be mistaken for a *half-metallic* regime [1, 8, 9, 12, 13, 14, 17], implying that for one set of symmetry-broken orbitals of a given spin the band gap opens when an external electric field is applied, whereas the other spin-band system remains (or becomes) metallic.

The purposes of the present work are three-fold:

(1) Assuming that an antiferromagnetic depiction prevails for an electronic singlet ground state with a total spin $S=0$, and, thus, that each unit cell in a finite ZGNI or extended ZGNR is subject to a measurable (and thus finite) symmetry-breaking in spin-densities, as in the original *Nature's* article by Son *et*

a/ [1], and all publications [8,9,12,13,14,17] on this topic thereafter, we first wish to analytically investigate the scaling properties of the spin contamination of a symmetry-broken electronic wave function, as a function of the number of unit cells in the system, using the formalism [36] of crystalline orbitals for extended systems with periodicity in one-dimension (Figure 1). It will be shown in particular that, in such a situation and in sharp contrast with the expected value (0) for the S^2 operator in a singlet ($S=0$) ground state, the spin contamination in an unrestricted HF or DFT treatment has to diverge with increasing system size, which implies a complete loss of control upon spin-related properties in the macroscopic limit.

(2) Considering that symmetry-breakings of spin-densities can be enforced *at will* on any compound by *imposing too strong limitations on the employed wave function*, we will then resort to unrestricted Hartree-Fock (UHF) calculations to show that from its valence electronic structure even naphthalene can exhibit features that are reminiscent of the half-metallicity of large but finite *Zig-zag Graphene NanoIslands* (ZGNIs) with a D_{2h} symmetry point group [37] in spin-unrestricted treatments. This conclusion will be tested against more robust calculations employing basis sets and many-body treatments of improving quality, in order to prove by analogy with larger systems and contradiction (*reductio ad absurdum*) of all available theoretical and experimental evidences for this compound that the half-metallicity of ZGNIs, ZGNRs, *n*-acenes and related systems will be quenched by an exact treatment of electron correlation in quantum mechanical calculations converging to the full-CI limit.

(3) At last, upon enforcing from the onset of the *n*-acene and ZGNI series the appearance of spin-polarized edge states with a *deliberately too approximate* treatment of electron correlation, we will verify the scaling properties of the

spin-contamination as a function of the length of the ribbon, and verify on computational grounds that half-metallicity in finite ZGNIs and extended ZGNRs is nothing else but a measure of the extent of an artefactual symmetry-breaking of spin-densities in spin-unrestricted one-determinantal (HF or DFT) calculations.

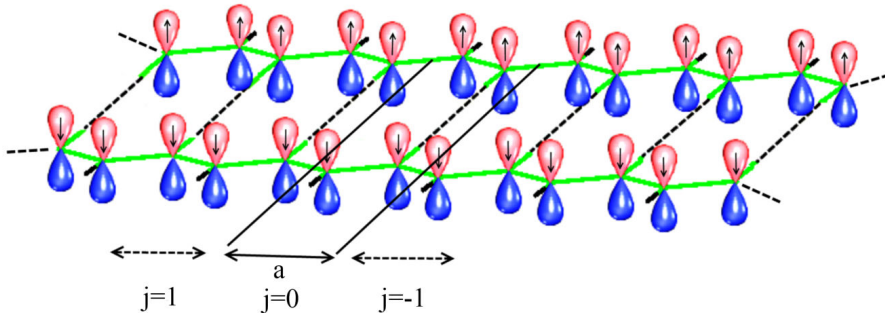


Figure 1. CO-LCAO analysis of symmetry-breakings in extended ZGNRs and related systems with periodicity in one dimension.

3.2 Crystalline orbital analysis of spin-contamination in extended periodic systems

Any spin-unrestricted wavefunction (e.g. unrestricted HF, unrestricted B3LYP, LSDA, ...) for a given spin state may be subject to contamination by higher-spin states, resulting in an expectation value for the S^2 operator that exceeds the exact $[S_z(S_z+1)]$ value, because the contaminants have larger values of S . In particular, it can be shown that, for any single-determinantal spin-unrestricted wave function, the $\langle S^2 \rangle$ expectation value is of the form [24, 26]:

$$\langle S^2 \rangle_{UX} = S_z(S_z + 1) + N_\beta - \sum_{ij=1}^{MO} \langle \phi_i^\alpha | \phi_j^\beta \rangle^2, \quad (1)$$

where UX may stand for UHF (unrestricted Hartree-Fock), LSDA (Local Spin Density Approximation), UB3LYP (unrestricted B3LYP), or *any* single-determinantal spin-unrestricted DFT expansion that may yield spin-polarized edge states in a graphene nanoribbon. Note from the above equation that if the α and β orbitals are identical in the singlet ($S_z=0$) ground state, there is no spin contamination, and the unrestricted wave function is identical to the restricted one.

For an hypothetical singlet antiferromagnetic ground state in n -acenes or finite graphene nanoislands, the error in spin-contamination provides therefore a measure of the extent of the symmetry breaking resulting from spin-polarized edge states:

$$\langle S^2 \rangle_{UX} - \langle S^2 \rangle_{exact} = N_\beta - \sum_{i=1}^{N_\alpha} \sum_{j=1}^{N_\beta} \langle \phi_i^\alpha | \phi_j^\beta \rangle \langle \phi_j^\beta | \phi_i^\alpha \rangle. \quad (2)$$

In order to evaluate the scaling properties of this error as a function of system size, we assume first an expansion of spin-unrestricted molecular orbitals as a linear combination of K atomic functions $\gamma_p(\vec{r})$:

$$\phi_i^\alpha(\vec{r}) = \sum_{p=1}^K C_{pi}^\alpha \gamma_p(\vec{r}), \quad (3)$$

$$\phi_j^\beta(\vec{r}) = \sum_{q=1}^K C_{qj}^\beta \gamma_q(\vec{r}), \quad (4)$$

under the usual orthonormality constraints for space functions relating to the same spin, i.e.,

$$\mathbf{C}^{\alpha\dagger} \mathbf{S} \mathbf{C}^\alpha = \mathbf{1}, \quad (5)$$

$$\mathbf{C}^{\beta\dagger} \mathbf{S} \mathbf{C}^{\beta} = \mathbf{1}, \quad (6)$$

where

$$S_{pq} = \langle \gamma_p | \gamma_q \rangle = \delta_{pq}. \quad (7)$$

Suppose:

$$\phi_j^{\beta}(\vec{r}) = \phi_j^{\alpha}(\vec{r}) + \delta_j(\vec{r}), \quad (8)$$

$$\phi_j^{\beta}(\vec{r}) = \sum_{q=1}^K (C_{qj}^{\alpha} + \Delta_{qj}) \gamma_q(\vec{r}). \quad (9)$$

Considering that $N_{\alpha}=N_{\beta}=N$, and upon taking the orthonormality of orbitals relating to the same spin function into account, we find:

$$\langle S^2 \rangle_{UX} - \langle S^2 \rangle_{exact} = \Delta_1 \langle S^2 \rangle + \Delta_2 \langle S^2 \rangle, \quad (10)$$

along with:

$$\Delta_1 \langle S^2 \rangle = - \sum_{i=1}^N \left[\left(\langle \phi_i^{\alpha} | \delta_i \rangle + \langle \delta_i | \phi_i^{\alpha} \rangle \right) \right], \quad (11)$$

$$\begin{aligned} \Delta_2 \langle S^2 \rangle &= - \sum_{i=1}^N \sum_{j=1}^N \langle \phi_i^{\alpha} | \delta_j \rangle \langle \delta_j | \phi_i^{\alpha} \rangle \\ &= - \sum_{i=1}^N \sum_{j=1}^N \left| \langle \phi_i^{\alpha} | \delta_j \rangle \right|^2 \leq 0. \end{aligned} \quad (12)$$

Both contributions to the spin contamination identically cancel in the absence of any symmetry-breaking (i.e. $\delta_i(\vec{r}) = 0$ for $i=1,2, \dots, N$), and differ from zero otherwise. Whereas the second-order contribution Δ_2 in terms of the symmetry-breaking is obviously zero or negative, further analysis demonstrates that the first-order term, Δ_1 , is necessarily zero or positive:

$$\begin{aligned}
\Delta_1 \langle S^2 \rangle &= -2 \sum_{i=1}^N \left[\operatorname{Re} \left(\langle \phi_i^\alpha | \delta_i \rangle \right) \right] \\
&= -2 \sum_{i=1}^N \left[\operatorname{Re} \left(\langle \phi_i^\alpha | \phi_i^\beta \rangle - 1 \right) \right] \geq 0,
\end{aligned} \tag{13}$$

since

$$\operatorname{Re} \left(\langle \phi_i^\alpha | \phi_i^\beta \rangle \right) \leq 1. \tag{14}$$

For instance, in an unrestricted single-determinantal treatment of H_2 , using a minimal basis set, $\Delta_1=+2$ whereas $\Delta_2=-1$ in the dissociation limit ($R_{H-H} \rightarrow \infty$), resulting in a triplet contamination ($\Delta_1 + \Delta_2=1$) that represents 50% of the wave function [24]. If the electronic ground state is a singlet, spin-contamination can only arise through admixture of states of higher spin-multiplicity (triplet, quintet, ...), and the spin contamination therefore can only be positive or equal to zero. It is thus clear that the two contributions can never exactly compensate (except if $\delta_i(\vec{r}) = 0 \quad \forall \quad i=1,2, \dots N$):

$$\Delta_1 \langle S^2 \rangle \geq -\Delta_2 \langle S^2 \rangle. \tag{15}$$

We now proceed with an adaptation of equation (11) and (12) to extended systems with periodicity in one dimension along with the LCAO ansatz (Figure 1), and consider spin-unrestricted crystalline-orbitals (CO) of the form [36]:

$$\phi_n^\alpha(k, \vec{r}) = N_0^{-1/2} \sum_{j=1}^{N_0} e^{ikja} \sum_{p=1}^K C_{pn}^\alpha(k) \gamma_p^j(\vec{r}), \tag{16}$$

$$\phi_n^\beta(k, \vec{r}) = N_0^{-1/2} \sum_{j=1}^{N_0} e^{ikja} \sum_{p=1}^K C_{pn}^\beta(k) \gamma_p^j(\vec{r}), \tag{17}$$

together with

$$\gamma_p^j(\vec{r}) = \gamma_p(\vec{r} - ja\vec{e}_z - \vec{R}_p). \quad (18)$$

In these equations, N_0 is the number of unit cells of width a of an extended periodic system with periodicity in one-dimension along the z -axis, under the usual (Born – Von Karman) constraint of cyclic boundary conditions [38]. j , n and k stand for the cell index, band index and wave number (electron momentum), respectively. As usual, and in straightforward analogy with equations (3) and (4), we assume K atomic functions per cell, and that crystalline orbitals are orthonormal with regards to band indices, since they are eigenfunctions of effective one-electron hamiltonian [hermitian] operators (Fock operator, Kohn-Sham hamiltonian, ... etc).

In straightforward analogy with equation (8), we define crystalline spin-orbital differences as:

$$\begin{aligned} \delta_n(k, \vec{r}) &= \phi_n^\beta(k, \vec{r}) - \phi_n^\alpha(k, \vec{r}) \\ &= N_0^{-1/2} \sum_{j=1}^{N_0} e^{ikja} \sum_{p=1}^K \Delta_{pn}(k) \gamma_p^j(\vec{r}). \end{aligned} \quad (19)$$

$\phi_n^\alpha(k, \vec{r})$, $\phi_n^\beta(k, \vec{r})$, and $\delta_n(k, \vec{r})$ are obviously periodic functions that can be constructed as linear combinations of symmetry adapted functions, referred [39] to as Bloch functions, $u_p(k, \vec{r})$:

$$\phi_n^\alpha(k, \vec{r}) = \sum_{p=1}^K C_{pn}^\alpha(k) u_p(k, \vec{r}), \quad (20)$$

$$\phi_n^\beta(k, \vec{r}) = \sum_{p=1}^K C_{pn}^\beta(k) u_p(k, \vec{r}), \quad (21)$$

$$\delta_n(k, \vec{r}) = \sum_{p=1}^K \Delta_{pn}(k) u_p(k, \vec{r}), \quad (22)$$

along with:

$$u_p(k, \vec{r}) = N_0^{-1/2} \sum_{j=1}^{N_0} e^{ikja} \gamma_p^j(\vec{r}). \quad (23)$$

Bloch functions are eigenfunctions of the translation operators $T(\vec{R}_j) = T(ja\vec{e}_z)$ characterizing the periodic lattice with eigenvalues equal to e^{ikja} . These functions can be obtained from a function without any particular symmetry by means of the projection operator [40]:

$$O_k = N_0^{-1} \sum_{j=1}^{N_0} e^{ikja}, \quad (24)$$

which has most important properties:

$$O_k O_{k'}^\dagger = \delta(k, k') O_k, \quad (25)$$

and:

$$O_k^\dagger = O_k. \quad (26)$$

(See ref. [41] for a generalization of translation operators to many-electron wave functions). Therefore:

$$\langle \phi_n^\alpha(k) | \phi_n^\alpha(k') \rangle = \langle \phi_n^\beta(k) | \phi_n^\beta(k') \rangle = \delta_{nn'} \delta(k, k'). \quad (27)$$

More generally, the properties of Bloch functions regarding translation symmetry imply a block-diagonalization in k . It is thus clear that any functions with different k labels cannot couple. Another important and well-known consequence of translation symmetry is periodicity of the electronic structure in

the reciprocal (k) space [42], whose elementary unit cell defines the first Brillouin zone (BZ), ranging from $-\pi/a$ to $+\pi/a$. For the forthcoming discussion, it is essential to remind that if the super-cell contains N_0 unit cells, there will be only N_0 possible discrete values of k in the first Brillouin zone. Each of these values corresponds to a particular irreducible representation of the translational symmetry point group, containing K spin-up and K spin-down Bloch functions characterized by their band index $n=1, 2, 3, \dots, K$.

In the macroscopic limit of an infinite system with finite densities, one most customarily makes use of the equivalence:

$$\lim_{N_0 \rightarrow \infty} \frac{1}{N_0} \sum_{j=1}^{N_0} \Leftrightarrow \frac{a}{2\pi} \int_{-\pi/a}^{+\pi/a} dk. \quad (28)$$

Expanding the first-order contribution to spin contamination in terms of crystalline spin-orbitals, and carrying out lattice summations, we get:

$$\begin{aligned} \Delta_1 \langle S^2 \rangle &= - \sum_n \sum_k^{BZ} \left[\left(\langle \phi_n^\alpha(k) | \delta_n(k) \rangle + \langle \delta_n(k) | \phi_n^\alpha(k) \rangle \right) \right] \\ &= \frac{-1}{N_0} \sum_n \sum_k^{BZ} \sum_{j,j'=1}^{N_0} e^{ik(j'-j)a} \\ &\quad \times \sum_{pq=1}^K \left(C_{pn}^{\alpha*}(k) \Delta_{qn}(k) S_{pq}^{jj'} + C_{pn}^\alpha(k) \Delta_{qn}^*(k) S_{pq}^{jj'^*} \right), \end{aligned} \quad (29)$$

along with

$$S_{pq}^{jj'} = \langle \gamma_p^j | \gamma_q^{j'} \rangle. \quad (30)$$

Since

$$S_{pq}^{jj'} = S_{pq}^{0j''}, \quad j'' = j' - j, \quad (31)$$

and

$$\sum_{j,j'=1}^{N_0} \Leftrightarrow N_0 \sum_{j''=1}^{N_0}, \quad (32)$$

upon exploiting translation symmetry, equation (29) can be reduced to:

$$\Delta_1 \langle S^2 \rangle = - \sum_n \sum_k^{BZ} \Gamma_n(k), \quad (33)$$

along with:

$$\begin{aligned} \Gamma_n(k) &= \sum_{j''=1}^{N_0} e^{ikj''a} \\ &\times \sum_{pq=1}^K \left(C_{pn}^{\alpha*}(k) \Delta_{qn}(k) S_{pq}^{0j''} + C_{pn}^{\alpha}(k) \Delta_{qn}^*(k) S_{pq}^{0j''*} \right). \end{aligned} \quad (34)$$

Even in the macroscopic limit $N_0 \rightarrow \infty$, $\Gamma_n(k)$ will obviously remain a finite bounded function, since successive terms in the lattice summation decay exponentially with j'' [43], as the overlap between the atomic functions $\gamma_p^0(\vec{r}) = \gamma_p(\vec{r} - \vec{R}_p)$ and $\gamma_q^{j''}(\vec{r}) = \gamma_q(\vec{r} - j''a\vec{e}_z - \vec{R}_q)$. Since there are only N_0 possible discrete values of k in the first BZ, it is clear that this first contribution to the spin-contamination scales proportionally to the number of unit cells in the periodic system. In the macroscopic limit, using the equivalence (28), this yields:

$$\lim_{N_0 \rightarrow \infty} \Delta_1 \langle S^2 \rangle = - N_0^{+1} \frac{a}{2\pi} \int_{-\pi/a}^{+\pi/a} \left(\sum_n \Gamma_n(k) \right) dk. \quad (35)$$

Similarly, for the “second-order” contribution to spin-contamination in terms of the spin-polarization of orbitals, we find:

$$\begin{aligned}
\Delta_2 \langle S^2 \rangle &= - \sum_{n,n',k,k'} \sum_{BZ} \langle \phi_n^\alpha(k) | \delta_{n'}(k') \rangle \langle \delta_{n'}(k') | \phi_n^\alpha(k) \rangle \\
&= - \sum_{n,n'} \sum_k \sum_{BZ} \langle \phi_n^\alpha(k) | \delta_{n'}(k) \rangle \langle \delta_{n'}(k) | \phi_n^\alpha(k) \rangle \\
&= \frac{-1}{N_0^2} \sum_{n,n'} \sum_k \sum_{j_1, j_2=1}^{N_0} \sum_{j_3, j_4=1}^{N_0} e^{ik(j_2+j_4-j_1-j_3)a} \times \\
&\quad \sum_{pqrs=1}^K C_{pn}^{\alpha*}(k) \Delta_{qn'}(k) \Delta_{rn'}^*(k) C_{sn}^\alpha(k) S_{pq}^{j_1 j_2} S_{rs}^{j_3 j_4}.
\end{aligned} \tag{36}$$

Again, because of the periodicity of the lattice, we have:

$$\begin{aligned}
S_{pq}^{j_1 j_2} &= S_{pq}^{0 j'}, \\
S_{rs}^{j_3 j_4} &= S_{rs}^{j'' 0} = S_s^{0 j''*},
\end{aligned} \tag{37}$$

with $j' = j_2 - j_1$ and $j'' = j_3 - j_4$, along with the equivalences:

$$\sum_{j_1, j_2=1}^{N_0} \Leftrightarrow N_0 \sum_{j'=1}^{N_0}, \quad \sum_{j_3, j_4=1}^{N_0} \Leftrightarrow N_0 \sum_{j''=1}^{N_0}. \tag{38}$$

Therefore, because of translation symmetry, the second-order contribution to spin-contamination reduces to:

$$\begin{aligned}
\Delta_2 \langle S^2 \rangle &= - \sum_{n,n'} \sum_k \sum_{j', j''=1}^{N_0} e^{ik(j'-j'')a} \\
&\quad \times \sum_{pqrs=1}^K C_{pn}^{\alpha*}(k) \Delta_{qn'}(k) \Delta_{rn'}^*(k) C_{sn}^\alpha(k) S_{pq}^{0 j'} S_{rs}^{0 j''*} \\
&= - \sum_{n,n'} \sum_k \sum_{j', j''=1}^{N_0} e^{ik(j'-j'')a} \\
&\quad \times \sum_{pqrs=1}^K C_{pn}^{\alpha*}(k) \Delta_{qn'}(k) S_{pq}^{0 j'} C_{rn}^\alpha(k) \Delta_{sn'}^*(k) S_{rs}^{0 j''*}.
\end{aligned} \tag{39}$$

Note already that the sole surviving summation over k implies a proportionality factor equal to N_0^{+1} , since there are N_0 possible values of k in the first Brillouin zone. Again, each term in the lattice summations over j' and j'' decays exponentially as the charge distributions $\gamma_p^{0*}(\vec{r}')\gamma_q^{j'}(\vec{r}')$ and $\gamma_r^{0*}(\vec{r}')\gamma_s^{j''}(\vec{r}')$, and these summations therefore both have to converge to a finite value in the macroscopic limit $N_0 \rightarrow \infty$. Defining:

$$\lambda_{n,n'}(k) = \sum_{j'=1}^{N_0} e^{ikj'a} \sum_{pq=1}^K C_{pn}^{\alpha*}(k) \Delta_{qn'}(k) S_{pq}^{0j'} , \quad (40)$$

and correspondingly:

$$\lambda_{n,n'}^*(k) = \sum_{j''=1}^{N_0} e^{-ikj''a} \sum_{rs=1}^K C_{rn}^{\alpha}(k) \Delta_{sn'}^*(k) \left(S_{rs}^{0j''} \right)^* , \quad (41)$$

we therefore find that, in the macroscopic limit:

$$\lim_{N_0 \rightarrow \infty} \Delta_2 \langle S^2 \rangle = -N_0^{+1} \frac{a}{2\pi} \int_{-\pi/a}^{+\pi/a} \left(\sum_{n,n'} |\lambda_{n,n'}(k)|^2 \right) dk . \quad (42)$$

Since the first-order and second-order contribution are positive and negative, respectively, and cannot exactly compensate (except if they both identically and separately vanish), a most important result is that for any unrestricted single-determinantal treatment (UHF, LSDA, UB3LYP, ...) which results into a net transversal spin-polarization (Figure 1), the spin-contamination of the electronic ground state of n -acenes and extended graphene nanoribbons of finite width and periodicity into one dimension has to scale proportionally to system size, and to diverge therefore to an infinite positive value in the macroscopic limit of an extended acene or graphene nanoribbon. This conclusion

is obviously in most striking contradiction with the implications [8] of Lieb's theorem [7] for compensated bipartite lattices and with what is normally expected for a singlet and so-called antiferromagnetic ground state, whose total spin has to be equal to zero,

$$\lim_{N_0 \rightarrow \infty} \left\langle S^2 \right\rangle_{UX} - \left\langle S^2 \right\rangle_{exact} = -N_0^{+1} \frac{a}{2\pi} \int_{-\pi/a}^{+\pi/a} \sum_n \left[\Gamma_n(k) + \sum_{n'} \left| \lambda_{n,n'}(k) \right|^2 \right] dk = +K N_0^{+1}. \quad (43)$$

In the above equation, K is identically 0 in the absence of symmetry-breaking (i.e. $\delta_n(k, \vec{r}) = 0 \quad \forall n = 1, 2, \dots, K; \forall k \in BZ$); otherwise K is equal to a positive and bounded constant that depends upon the structural characteristics of the target nanoribbon and employed one-determinantal approach (UHF, LSDA, UB3LYP, ...).

3.3 Methodology and computational details

For the sake of consistency in the analysis, all computations that are reported in the present work have been made on field-free geometries that were optimized at the level of Restricted Hartree-Fock theory [24] or Restricted Density Functional Theory, under the constraint of the topologically required D_{2h} symmetry point group.

Admittedly, Hartree-Fock theory may certainly not be regarded as highly fashionable nowadays. If use is *deliberately* made of unrestricted Hartree-Fock (UHF) approach, this is to *enforce* a symmetry-breaking of spin-densities at the onset of the n -acene series (naphthalene) and in the absence of any external perturbation, in order to study throughout the series the consequences of such

symmetry-breakings when an external electric field is progressively switched on, using the well-established Finite Field approach [44]. We shall first consider Finite Field calculations on naphthalene at the Hartree-Fock level, using basis sets of improving quality (STO-3G, 6-31G, 6-31G**) [24]. We then evaluate for this compound the influence of the external field on symmetry-broken (i.e. unrestricted) and symmetry-restricted spin-densities at varying orders in electron correlation, according to single-point calculations employing the same HF/STO-3G geometry and STO-3G basis set, at the level of Møller-Plesset theory [45] truncated at second-order (MP2) [46,47], third-order (MP3) [47], and fourth order with single, double and quadruple terms (MP4SDQ) [48], as well as Coupled Cluster Theory along with Single, Double or Single, Double and perturbative Triple excitations, shortly CCSD or CCSD(T) [49].

The correlation energy is a measure of how much the movement of one electron is influenced by the presence of all other electrons. *Fermi correlation* is the outcome of the antisymmetry principle for electrons with the same spin, and is already accounted for at the level of Hartree-Fock theory [24]. Electrons with opposite spin can correlate in two possible ways, due to the Coulomb force. It is most customary to distinguish the *dynamic correlation* resulting in a deformation of orbitals compared to an uncorrelated system, due to repulsions between electrons, from the *static correlation* associated with an admixture of electronically low-lying excited states in the ground state wave function, resulting in fractional orbital occupation numbers. Note that this distinction is essentially methodological: systems with large band gaps and dominated by dynamic correlation can be reliably described using single-reference approaches, whereas multi-reference techniques such as CASSCF (Complete Active Space SCF theory [50]) are required for systems characterized by near energy

degeneracies between the ground and excited electronic states. Note also that both types of correlation are obviously recovered in the full-CI (Configuration Interaction) limit [24], which amounts to a CASSCF treatment with a complete active space in the selected basis set. In other words, static correlation is indirectly recovered when proceeding towards the full-CI limit through the interplay of single-reference treatments (HF, MP2, MP3, MP4SDQ, CCSD, CCSD(T), CCSDT, CCSDT(Q) ...) of improving quality. At this stage, it is useful to remind that naphthalene has a relatively large band gap and sizeable electronic excitation energies. The vertical singlet-triplet energy gap of naphthalene amounts for instance to 3.31 eV [33]. There is therefore a very large consensus on the fact that naphthalene is a closed-shell non-magnetic system that can be very reliably described by single-reference approaches [see e.g. ref. [16b]].

In a next step, the UHF/6-31G** approach is retained for studying the relationships prevailing between the half-metallic spin-polarization of edge states in unrestricted treatments of PAH systems of increasing size and the underlying spin-contamination, as a measure of the extent of the symmetry-breaking. The selected target systems (Figure 2) comprise (1) the n -acene [$2 \times n$] series, from naphthalene up to decacene in the case of spin-unrestricted DFT, and (2) finite rectangular graphene nanoislands such as perylene [4×2], bisanthene [4×3], tetrabenzo[bc,ef,kl,no]coronene ([4×4], and larger related compounds ([4×5], [4×6]). We here employ the notation by Hod *et al* [9e] for discriminating these ribbons according to the number of hydrogen atoms passivating the edges, such that an [$X \times Y$] finite ribbon has X hydrogen atoms on its armchair edge and Y atoms on its zigzag edge. Comparison is also made with spin-unrestricted DFT calculations upon the n -acene [$2 \times n$] series, along with the 6-31G basis, and a variety of functionals, comprising the gradient

corrected Becke-Lee-Yang-Parr (BLYP) functional, the hybrid Becke-3-parameters-Lee-Yang-Parr (B3LYP) [51] functional, and the Modified 1-parameter Perdew-Wang functional for kinetic (MPW1K [52], as well as the double hybrid dispersion corrected B2PLYPD [53] functional.

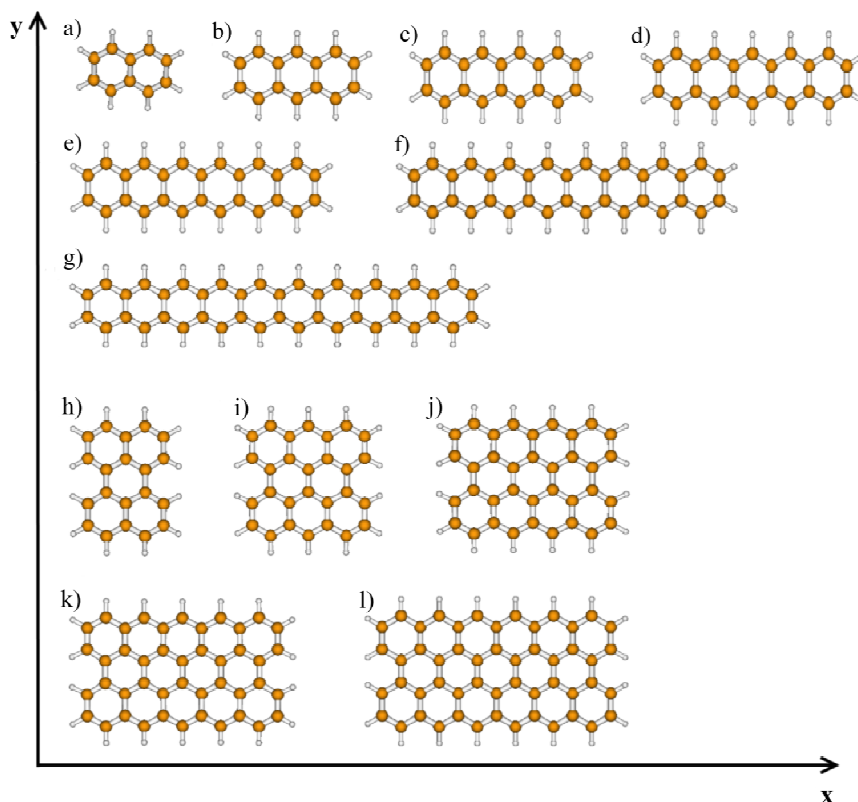


Figure 2. The n -acene $[2 \times n]$ nanoribbon series: (a) naphthalene, (b) anthracene, (c) tetracene (or naphthacene); (d) pentacene; (e) hexacene; (f) octacene; (g) decacene. The n -acene $[4 \times n]$ nanoribbon series: (h) perylene $[4 \times 2]$; (i) bisanthene $[4 \times 3]$, (j) tetrabenzo[bc,ef,kl,no]coronene $[4 \times 4]$, (k) $[4 \times 5]$, (l) $[4 \times 6]$.

The MPW1K functional is a modification version of the MPW1PW91 (modified Perdew-Wang 991 Perdew Wang) functional [54] with an increase fraction of HF versus DFT exchange (0.428:0.572 instead of 0.25:0.75). This functional has

been specifically designed for handling situations where HF exchange dominates because of enhanced electron delocalization, as for instance in transition states on chemical reaction pathways. All calculations presented in this work have been carried out using the GAUSSIAN09 package of programs [55]. No symmetry constraint was enforced when a field was applied along the y axis in the standard orientation (Figure 2) defined according to the usual conventions [56] for a molecule exhibiting a D_{2h} point group [37], i.e. perpendicularly to the zig-zag edges.

3.4 Naphthalene: the smallest half-metallic graphene nanoisland?

Vibrational analysis at the UHF (Unrestricted Hartree-Fock) level along with STO-3G, 6-31G and 6-31G** basis sets confirms that the global energy minimum form of naphthalene is perfectly consistent with a D_{2h} symmetry point group [37], and that striking deviations of canonical spin-orbitals from this symmetry-point group in the absence of an external electric field (Figure 3) are thus purely artefactual. At the UHF/STO-3G level, a check upon atomic orbital coefficients using a homemade program confirms that at fields (F) smaller than ~ 0.1 a.u. ($1 \text{ a.u.} = E_h e^{-1} a_0^{-1} = 5.142 \cdot 10^{11} \text{ V m}^{-1}$) these spin orbitals transform according to irreducible representations of the C_{2v} point group [37] (at larger fields, the effective symmetry for spin-densities further reduces to the C_s point group) [37]. Note in particular the striking resemblance of our UHF/STO-3G contour plots for the frontier spin-orbitals (HOMO, LUMO) of naphthalene (Figure 3) with comparable plots of Kohn-Sham orbitals for the edge states of extended ZGNRs [1] and large but finite PAHs [9e] in unrestricted DFT treatments. If we go on reasoning by contradiction (*reductio ad absurdum*), it makes sense therefore to state that, at the UHF/STO-3G level, naphthalene is the *smallest*

possible example of an *anti-ferromagnetic* zig-zag graphene nanoisland exhibiting spin-polarized edge states.

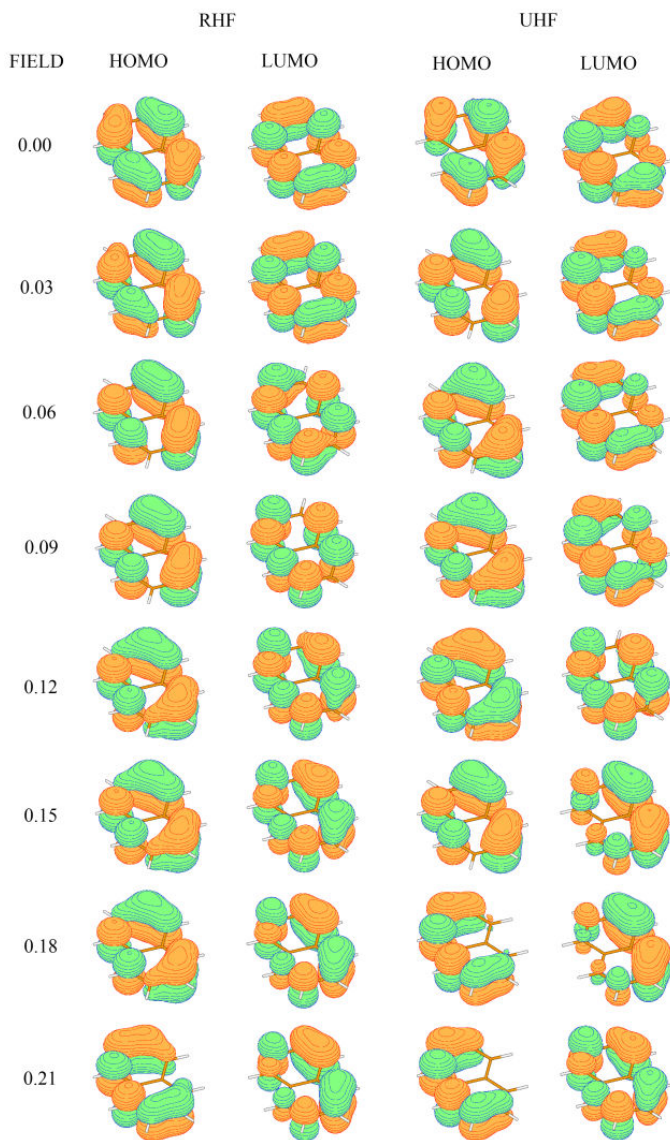


Figure 3. Evolution of the frontier spin-orbitals (HOMO, LUMO) of naphthalene in function of the applied external electric field (in a.u.) at the RHF/STO-3G level and UHF/STO-3G levels.

The fact that naphthalene is notoriously known as a single reference closed-shell *diamagnetic* system with a sizeable singlet-triplet energy gap (about 76 kcal/mol [33]) most obviously demonstrates the inconvenience of such a statement. Remind also that in DFT any PAH compound (e.g. tetracene, alias naphthacene [33]) can be converted into an “open-shell singlet” spin-polarized biradical by increasing the fraction of non local HF exchange.

In the absence of an external field, symmetry-broken α and β spin-orbitals have identical energies. Due to the different space localization of α and β spin-densities in an unrestricted treatment, energy degeneracies between spin band systems are released when applying an external field in the plane and across the longitudinal axis of the molecule (Figure 4). Energy splittings due to the symmetry breaking are particularly striking for the π -levels, and barely noticeable for the σ -levels. Again in straightforward analogy with extended ZGNRs [1] and large but finite PAHs with the proper D_{2h} symmetry point group [9e], opposite shifts in the energies of the spatially separated and ferromagnetically-ordered spin-edge states are observed in the π -band system, both among occupied and unoccupied levels, when applying an external electric field of increasing strength across the nanoribbon. At the UHF/STO-3G level (Figure 5), we correspondingly observe an opening of the HOMO-LUMO energy gap in a given [e. g. α] spin band system, at field intensities lower than ~ 0.0225 a.u., whereas a decrease of this energy gap is seen in the opposite [say β] spin band system. If we continue to employ the terminology proposed by Son *et al* for extended ZGNRs [1], or by Hod *et al* for finite ZGNIs [9e], we may argue therefore that at the UHF/STO-3G level and at very low electric

fields, naphthalene is the *smallest* possible example of a zig-zag graphene nanoisland exhibiting “half-metallic” spin-polarization properties, in the sense that it becomes easier to promote electrons with an α spin from the valence to the unoccupied π -band systems, whereas β electrons become more difficult to excite.

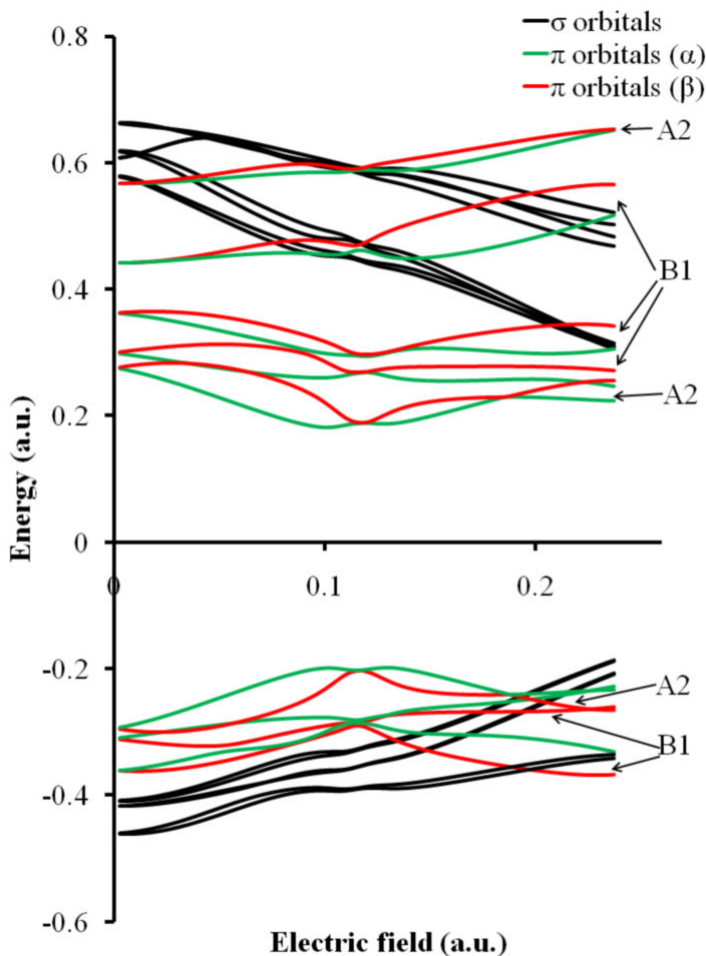


Figure 4. Evolution of the UHF/STO-3G energies of valence and unoccupied molecular spin-orbitals of naphthalene belonging to the π and σ band systems as a function of the applied electric field. Symmetry labels for π -orbitals are consistent with the effective C_{2v} symmetry point group when symmetry is reduced by the external field.

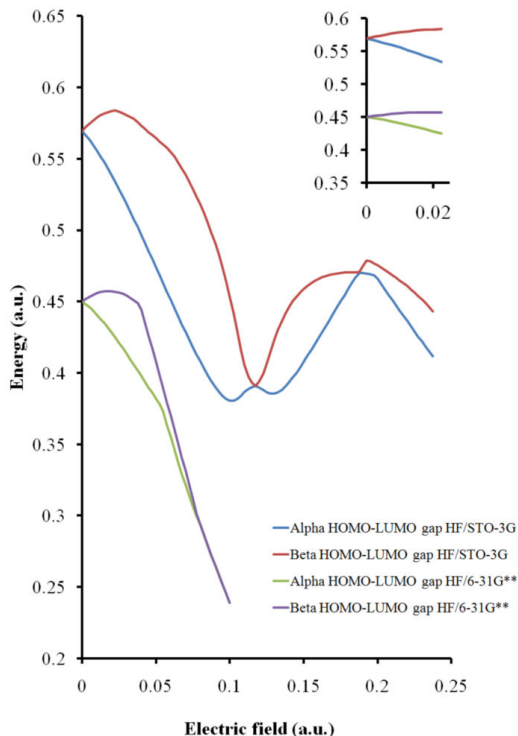


Figure 5. Evolution at the UHF/STO-3G level and UHF/6-31G** levels of the electronic (HOMO-LUMO) energy gap in the α and β -spin band systems of naphthalene, in function of the applied external field (in a.u.). Results at the lowest fields ($F < 0.02$ a.u.) are shown in an inset.

Pursuing towards larger field intensities (Figure 4), we observe overall a destabilization of the occupied π and σ levels, and conversely a stabilization of the unoccupied π and σ levels of naphthalene, resulting (Figure 5) in a decrease of the HOMO-LUMO gaps both in the spin α and spin β -band systems – again in very straightforward analogy with the UDFT results obtained by Hod *et al.* (Figure 6) [9e] using various functionals (LSDA, PBE, HSE06) upon much larger ZGNIs ([4×14], [6×10], [8×7]).

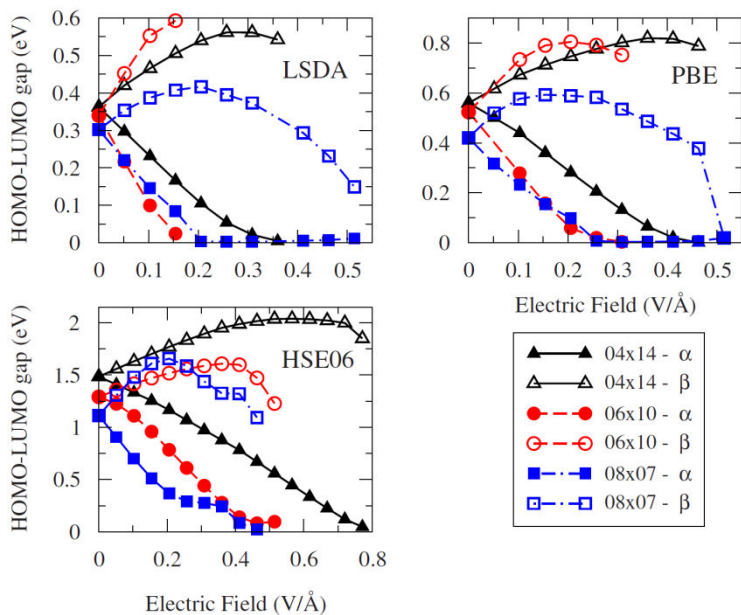


Figure 6. Evolution of UDFT frontier energy levels in the α and β -spin band systems of ZGNIs ([4 \times 14], [6 \times 10], [8 \times 7]) in function of the applied external field. Figure is taken from ref. [9e].

Note incidentally that at the UHF/STO-3G level (Figure 4), these trends reverse in the π -band system of naphthalene at field strengths larger than 0.1175 a.u., in line with an avoided crossing between the HOMO and LUMO, due to a reversal of the polarization of π -levels (Figure 3) as a result of push-pull interactions with electrons in the σ band system. This behaviour is precisely reminiscent of that observed for the frontier orbitals of model hydrogen chains subject to longitudinal electric fields [57]. Upon strengthening further the field, various crossings in energies are observed between σ - and π -levels, and at fields larger than 0.20 a.u., the highest occupied molecular orbital corresponds to the outermost σ -level derived from the $9A_g$ orbital [40] in the D_{2h} symmetry

point group.

In Figure 3, we also compare contour plots of the frontier molecular orbitals of naphthalene at the restricted Hartree-Fock(RHF)/STO-3G and UHF/STO-3G levels. The strongest differences in orbital topologies and spreads are observed at zero field, and effectively measure the extent of the symmetry-breaking associated with the HF singlet instability [26,29]. In the absence of a field, at the RHF/STO-3G level, these orbitals transform according to the A_u (HOMO) and B_{1g} (LUMO) irreducible representations of the D_{2h} symmetry point group, as they should [58], whereas the extent of the symmetry breaking is the greatest at the UHF/STO-3G level. Due to the release of symmetry in the environment, these differences tend to disappear when an electric field is progressively switched on, an observation which is in line with the energy curves displayed in Figure 4. The α and β spin band systems almost converge to the same symmetry-restricted solution at a field around 0.115 a.u., before diverging again.

In Figure 7a, we display in function of the field the evolution of the expectation value for the S^2 operator. The spin contamination is at its maximum at zero field. In line with the symmetry breakings that can be detected from the contour plots and energy curves given in Figures 3 and 4, the $\langle S^2 \rangle$ value smoothly decreases upon increasing fields, to almost vanish at $F=0.115$ a.u. (a value at which the symmetry-breaking between α and β spin-orbitals becomes barely noticeable), prior to increasing again up to another maximum at $F=0.195$ a.u., presumably because of an electronic transition to an excited state. Indeed, according to symmetry-restricted (RHF and ROHF) calculations at the CCSD(T)/6-31G level, the (vertical) singlet-triplet energy gap vanishes or even

reverses in favour of the lowest triplet state at fields larger than 0.1 a.u. (Figure 7b).

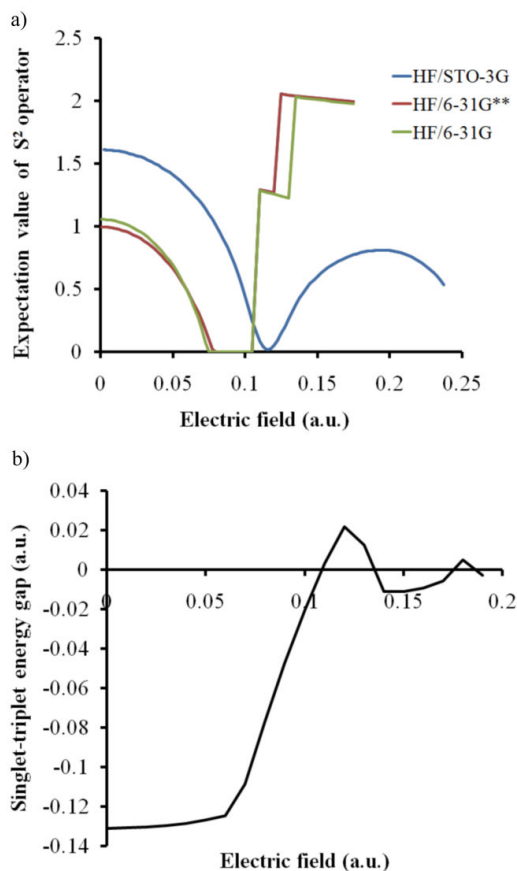


Figure 7. Evolution of (a) the UHF expectation value of the S^2 operator and (b) CCSD(T)/6-31G singlet-triplet excitation energy of naphthalene in function of the applied external electric field (in a.u.).

Very similar considerations prevail at the HF level when considering larger basis sets. Inspection of the HF/6-31G** results displayed in Figure 8 shows that improving the basis set obviously helps to limit the extent of the symmetry-breaking in α and β - spin-densities and orbital energies, as well as the avoided

crossing between the HOMO and LUMO. Note correspondingly that at zero field, symmetry-breakings occur at the UHF level, irrespective of the employed basis set: see in Figure 9 the evolution of the difference between the RHF and UHF energies obtained in conjunction with basis sets of increasing size, among which Dunning's correlation consistent polarized valence basis sets of triple-, quadruple- and pentuple-zeta quality [59], along with the corresponding estimate in the limit of an asymptotically complete basis set (cc-pV ∞ Z), according to an extrapolation employing Feller's formula [60]. Also, both at the UHF/6-31G and UHF/6-31G** levels, fields comprised between ~ 0.08 and ~ 0.1 a.u. prevent any symmetry-breaking in spin-densities, resulting in a $\langle S^2 \rangle$ value equal to zero (Figure 7). Energy degeneracies between the α and β -spin band systems correspondingly disappear (Figure 8).

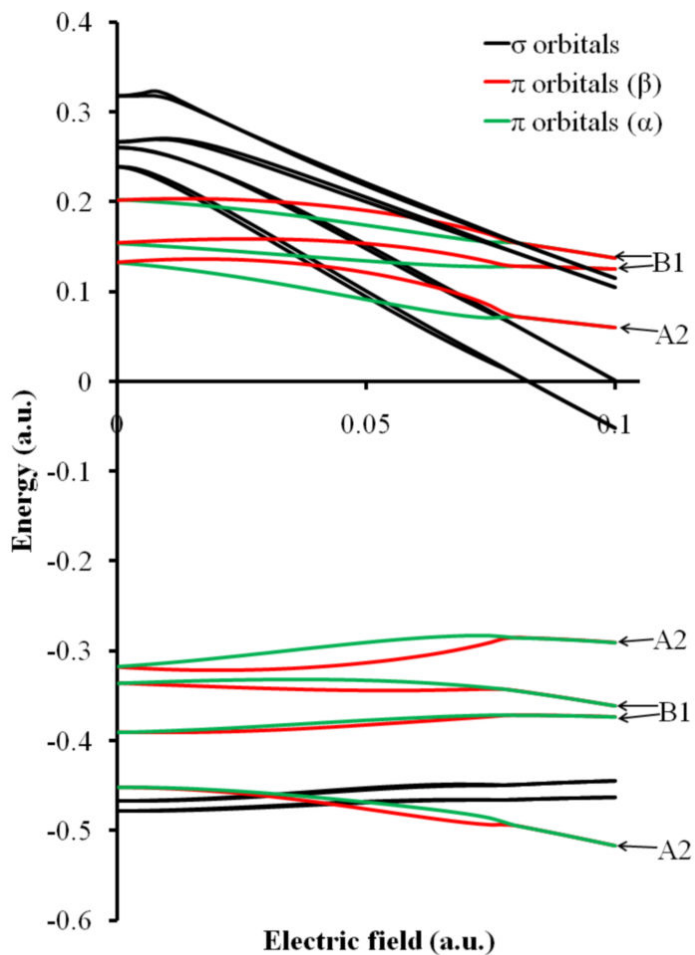


Figure 8. Evolution of the UHF/6-31G** energies of the molecular spin-orbitals of naphthalene as a function of the applied electric field. Symmetry labels for π -orbitals are consistent with the effective C_{2v} point group when symmetry is reduced by the external field. Results obtained at the UHF/6-31G level are almost the same.

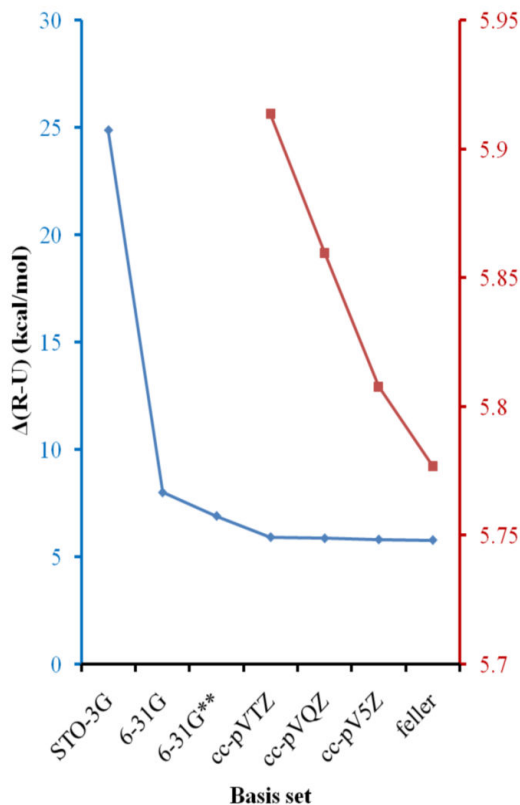


Figure 9. Evolution of the energy difference (in kcal/mol) between the RHF and UHF wave functions of naphthalene upon using basis sets of increasing size and converging to the limit of an asymptotically complete basis set. The red and blue axes correspond to results displayed in red and blue, respectively.

Turning on electronic correlation with the interplay of Many-Body Quantum Mechanics [24,50] enlightens the methodological origin of the anti-ferromagnetic and “half-metallic” spin-polarization properties of naphthalene at any UHF level, and by straightforward extension of finite ZGNIs or of extended ZGNRs subject to a spin-polarization of edge states in unrestricted HF or DFT treatments. In Tables 1, 2 and 3, we provide the evolution of the energy differences between the spin-unpolarized singlet closed-shell and symmetry-broken “singlet open-shell” states of naphthalene, according to various restricted

(R) and unrestricted (U) treatments of electron correlation in the singlet ground state, along with basis sets of improving quality (STO-3G, 6-31G, and 6-31G**) and electric fields of increasing strength.

Table 1. Energy difference (in kcal/mol) between the “closed shell” RHF/STO-3G and “open-shell” UHF/STO-3G solutions for the singlet electronic ground state of naphthalene in function of the applied external electric field (in a.u.).

Level	HF	MP2	MP3	MP4SDQ	CCSD	CCSD(T)
Electric	$\Delta E(U-R)$	$\Delta E(U-R)$	$\Delta E(U-R)$	$\Delta E(U-R)$	$\Delta E(U-R)$	$\Delta E(U-R)$
0.00	-24.87	55.29	51.71	43.12	10.03	7.74
0.01	-24.54	55.19	51.56	42.95	9.93	7.65
0.02	-23.56	54.86	51.09	42.45	9.64	7.37
0.03	-21.95	54.23	50.34	41.56	9.14	6.92
0.04	-19.75	53.21	48.95	40.21	8.46	6.29
0.05	-17.01	51.61	47.12	38.27	7.58	5.51
0.06	-13.83	49.16	44.26	35.57	6.54	4.60
0.07	-10.34	45.46	40.30	31.87	5.34	3.61
0.08	-6.75	39.86	34.65	26.79	4.03	2.58
0.09	-3.41	31.27	26.44	19.81	2.64	1.59
0.10	-0.93	18.10	14.67	10.45	1.25	0.72
0.11	-0.03	3.32	2.54	1.64	0.18	0.10
0.12	-0.01	2.02	1.55	0.92	0.07	0.04
0.13	0.00	0.00	0.00	0.00	0.00	0.00
0.14	0.00	0.00	0.00	0.00	0.00	0.00

Table 2. Energy difference (in kcal/mol) between the “closed shell” RHF/6-31G and “open-shell” UHF/6-31G solutions for the singlet electronic ground state of naphthalene in function of the applied external electric field (in a.u.).

Level	HF	MP2	MP3	MP4SDQ	CCSD	CCSD(T)
Electric	$\Delta E(U-R)$	$\Delta E(U-R)$	$\Delta E(U-R)$	$\Delta E(U-R)$	$\Delta E(U-R)$	$\Delta E(U-R)$
0.00	-7.99	39.29	28.59	23.07	4.21	3.58
0.01	-7.75	38.89	28.27	22.78	4.12	3.49
0.02	-7.02	37.63	27.29	21.90	3.87	3.25
0.03	-5.88	35.37	25.54	20.34	3.45	2.87
0.04	-4.40	31.82	22.80	17.96	2.88	2.36
0.05	-2.74	26.50	18.76	14.54	2.17	1.76
0.06	-1.17	18.59	12.91	9.78	1.35	1.10
0.07	-0.12	6.59	4.41	3.24	0.42	0.35
0.08	0.00	0.00	0.00	0.00	0.00	0.00
0.09	0.00	0.00	0.00	0.00	0.00	0.00
0.10	0.00	0.00	0.00	0.00	0.00	0.00

Table 3. Energy difference (in kcal/mol) between the “closed shell” RHF/6-31G** and “open-shell” UHF/6-31G** solutions for the singlet electronic ground state of naphthalene in function of the applied external electric field (in a.u.).

Level	HF	MP2	MP3	MP4SDQ	CCSD	CCSD(T)
Electric	$\Delta E(U-R)$	$\Delta E(U-R)$	$\Delta E(U-R)$	$\Delta E(U-R)$	$\Delta E(U-R)$	$\Delta E(U-R)$
0.00	-6.90	39.79	26.38	19.64	4.01	3.97
0.01	-6.70	39.37	26.09	19.39	3.93	3.89
0.02	-6.09	38.08	25.20	18.64	3.72	3.65
0.03	-5.14	35.79	23.60	17.32	3.36	3.27
0.04	-3.92	32.26	21.17	15.34	2.87	2.75
0.05	-2.55	27.14	17.65	12.57	2.25	2.13
0.06	-1.23	19.87	12.73	8.85	1.51	1.42
0.07	-0.26	9.78	6.10	4.10	0.68	0.64
0.08	0.00	0.00	0.00	0.00	0.00	0.00
0.09	0.00	0.00	0.00	0.00	0.00	0.00
0.10	0.00	0.00	0.00	0.00	0.00	0.00

Whatever the basis set, Fermi correlation at the UHF level most systematically overemphasizes the biradical character of the wave function, resulting in a “singlet open-shell” state which is located several tenths kcal/mol below the proper singlet closed-shell state. Besides, whatever the employed basis set and applied external field, in the event of a symmetry breaking at the UHF level, the energy order always reverses in favour of the restricted wave functions with spin-unpolarized orbitals when including dynamic electron correlation at the UMP2 and higher levels. At last, whatever the basis set and applied external field, the spin-unrestricted and symmetry-restricted solutions obviously converge smoothly towards the same value in the full-CI limit, through the interplay of the well-established hierarchy of MP3, MP4SDQ, CCSD and CCSD(T) levels. Convergence of energies to the full-CI limit (or to, at least, the CCSD(T) approximation of this limit), is obviously faster when starting from the spin-symmetric RHF solution (Tables 4, 5, 6)

Table 4. Evolution of the energies of naphthalene with improving single-reference treatments of electron correlation in conjunction with the STO-3G basis set. Energies and electric field intensities are in a.u.

Field	0.00			0.03			0.06		
	RHF	UHF		RHF	UHF		RHF	UHF	
HF	-378.68685	-378.726485		-378.718765	-378.753748		-378.81532	-378.837361	
MP2	-379.266821	-379.17871		-379.297267	-379.21084		-379.38943	-379.311093	
MP3	-379.341423	379.259025		-379.371143	-379.290922		-379.46077	-379.390237	
MP4SDQ	-379.360535	-379.291826		-379.389648	-379.323416		-379.47807	-379.421382	
CCSD	-379.37648	-379.360491		-379.40491	-379.390339		-379.49157	-379.481158	
CCSD(T)	-379.392163	-379.379823		-379.421031	-379.410009		-379.50893	-379.501601	

Table 5. Evolution of the energies of naphthalene with improving single-reference treatment of electron correlation in conjunction with the 6-31G basis set. Energies and electric field intensities are in a.u.

Field	0.00			0.03			0.06		
	RHF	UHF		RHF	UHF		RHF	UHF	
HF	-383.22153	-383.23427		-383.268326	-383.277691		-383.411188	-383.413057	
MP2	-384.076636	-384.01403		-384.123418	-384.067055		-384.266093	-384.236474	
MP3	-384.112223	-384.06666		-384.158171	-384.117477		-384.298614	-384.278045	
MP4SDQ	-384.131019	-384.09425		-384.176842	-384.144432		-384.317151	-384.301562	
CCSD	-384.137701	-384.13100		-384.183145	-384.17765		-384.322548	-384.320398	
CCSD(T)	-384.175068	-384.16937		-384.220916	-384.216345		-384.361517	-384.359768	

Table 6. Evolution of the energies of naphthalene with improving single-reference treatment of electron correlation in conjunction with the 6-31G** basis set. Energies and electric field intensities are in a.u.

Field	0.00		0.03		0.06	
	RHF	UHF	RHF	UHF	RHF	UHF
HF	-383.368619	-383.37962	-383.416092	-383.424285	-383.56085	-383.562806
MP2	-384.67492	-384.61152	-384.722749	-384.665717	-384.868352	-384.83668
MP3	-384.715778	-384.67374	-384.762894	-384.725277	-384.906575	-384.886281
MP4SDQ	-384.723028	-384.69174	-384.770128	-384.742524	-384.913964	-384.899854
CCSD	-384.724443	-384.71806	-384.77138	-384.766019	-384.914818	-384.912407
CCSD(T)	-384.78852	-384.78219	-384.835744	-384.830535	-384.980084	-384.977823

These observations numerically illustrate the statement that symmetry-breakings and half-metallic spin-polarizations in spin-unrestricted calculations upon singlet states are necessarily the outcome of a too approximate treatment of *symmetry-restoring* electron correlation. Since α and β spin-densities in a closed-shell system ($\langle S^2 \rangle = 0$) have obviously to delocalize symmetrically on both edges of the molecule in the full-CI limit (see e.g. the CASSCF contour plots of natural spin-orbital densities in ref. [25]), it is also clear that the external field can only have exactly the same influence upon the α and β spin-band systems, and, thus, that the idea [9e] of intrinsic half-metallicity in finite systems such as bisanthene or tetrabenzob[bc,ef,kl,no]coronene is physically unsound.

3.5 Spin-contamination and half-metallicity as a function of system size.

The UHF/6-31G** results displayed in Figures 10 and 11 for the n -acene ($n=2-11$) and $[4 \times n]$ ZGNI series demonstrate that artifactual symmetry-breakings in spin-densities and half-metallic splits of spin-up and spin-down orbital energies in the presence of a transversal electric field are clearly enhanced when proceeding to larger PAH compounds, by virtue of a progressive (but imperfect) closure of the band gap between occupied and unoccupied levels. Indeed, in symmetry breaking situations, the equation that governs the convergence of expansion coefficients of (electronic) wave functions in an arbitrary orbital basis and in any iterative SCF procedure is of the form [31]:

$$\left(\varepsilon_{\mu} - \varepsilon_n\right) C_{\mu n}^{(q)} + \sum_{k=1}^N \sum_{\nu} \left[\langle \mu \nu || n k \rangle + \langle \mu k || n \nu \rangle \right] C_{\nu k}^{(q)} = D_{\mu n}^{(q)} \quad , \quad (44)$$

with $\langle \alpha\beta || ij \rangle$ and ε_α the standard notation [24] for anti-symmetrized bielectron integrals and orbital energies, respectively. In the above equation, q denotes the order of the change in the orbitals and in the associated energies, according to a one-electron perturbation expansion with respect to an infinitesimally small geometrical variation (or complex rotation). For small nuclear displacements, the first-order driving term $D_{\mu n}^{(1)}$ simply relates to minus the gradient of the electron-nuclei attraction potential in the direction of the symmetry-breaking transformation. Since Hamiltonian operators are necessarily Hermitian, $C_{\mu n}^{(q)}$ is equal to $(-C_{n\nu}^{(q)})$ in any SCF (HF, DFT, or even CASSCF) procedure, and only occupied – non-occupied elements of the $\mathbf{C}^{(q)}$ matrix effectively contribute to the SCF energy [31a].

Therefore, because of the energy-dependence of the first term on the left hand side of the above equation, it is clear that the convergence of orbital expansion coefficients in SCF calculations becomes particularly problematic in the event of near energy degeneracies between occupied and unoccupied levels. If the band gap vanishes, tiny distortions in orbital symmetries induced for instance by infinitesimally small nuclear displacements (or numerical errors) may then amplify during the SCF iterations and ultimately result into an asymptotically diverging energy lowering, *unless* these artefactual symmetry breakings prevent in turn a full closure of the band gap, because of an artificial stabilization of the outermost occupied orbitals.

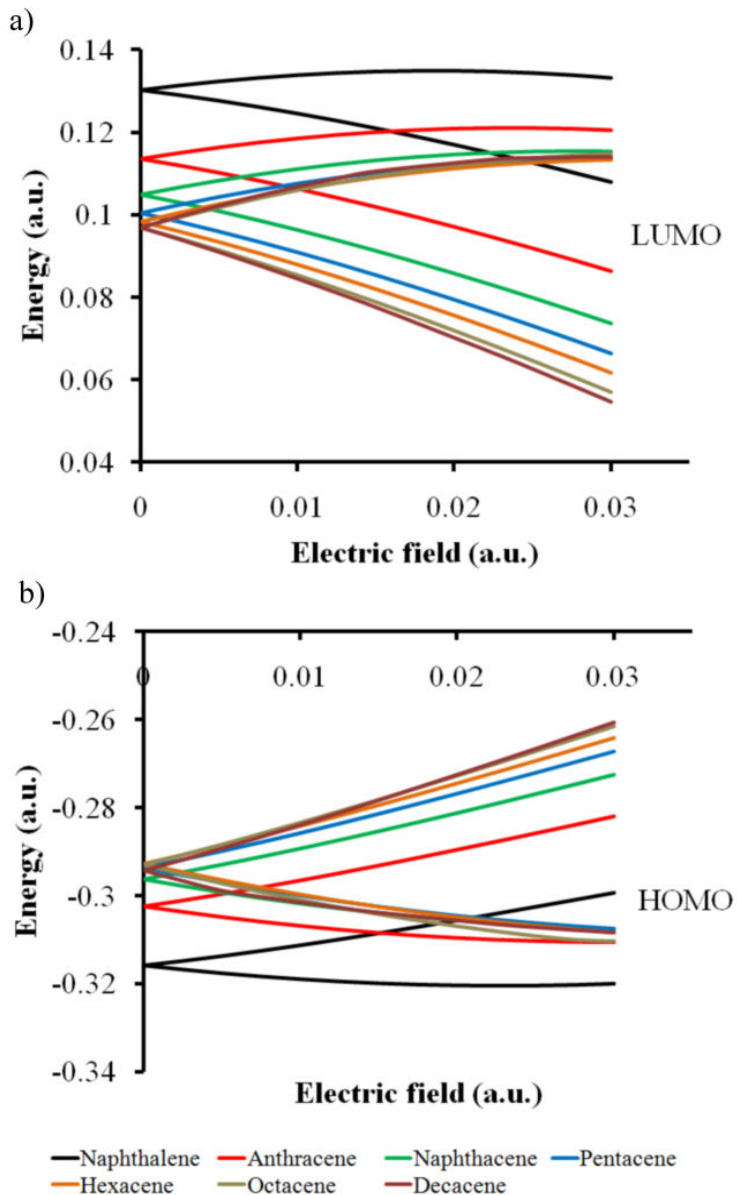


Figure 10. Half-metallic energy split of the frontier orbitals of n -acenes ($[2 \times n]$ ribbons, $n=2-10$) in function of the applied transversal field (UHF/6-31G** results, energies and field values are both in a.u.).

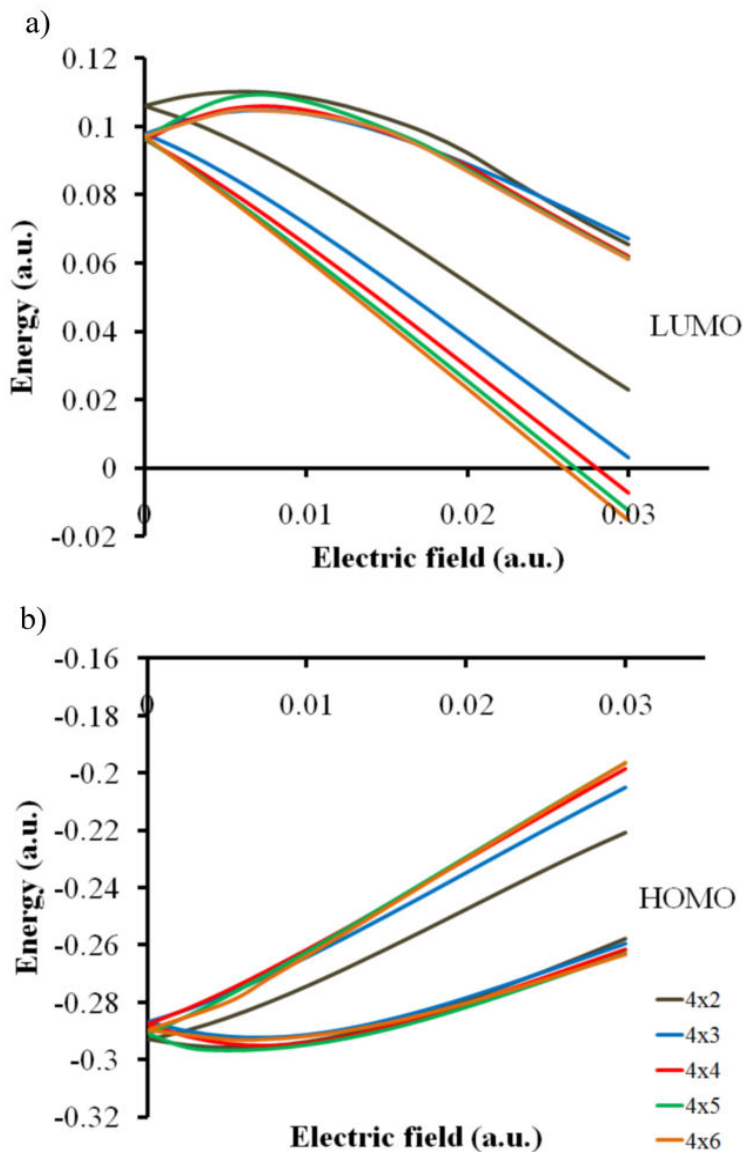


Figure 11. Half-metallic energy split of the frontier orbitals of rectangular $[4 \times n]$ ($n=2-6$) graphene nanoribbons, $n=2-6$) in function of the applied transversal field (UHF/6-31G** results, energies and field values are both in a.u.).

Precisely in line with these latter remarks, we note that in the n -acene $[2 \times n]$ and $[4 \times n]$ ZGNI series, the HOMO-LUMO band gap decreases up to $n \sim 8$

and $n \sim 4$ (Figure 12), respectively, prior to slightly increasing again at larger values of n . Although the dependence of the band gap upon n is much stronger in the n -acene series, the half-metallic energy split of frontier orbitals at this level and at a given electric field will rather clearly saturate at much larger values in the $[4 \times n]$ ZGNI series, in the limit $n \rightarrow \infty$ (Figure 10 versus Figure 11), and this most obviously because of the larger average distance between spin-polarized edge states.

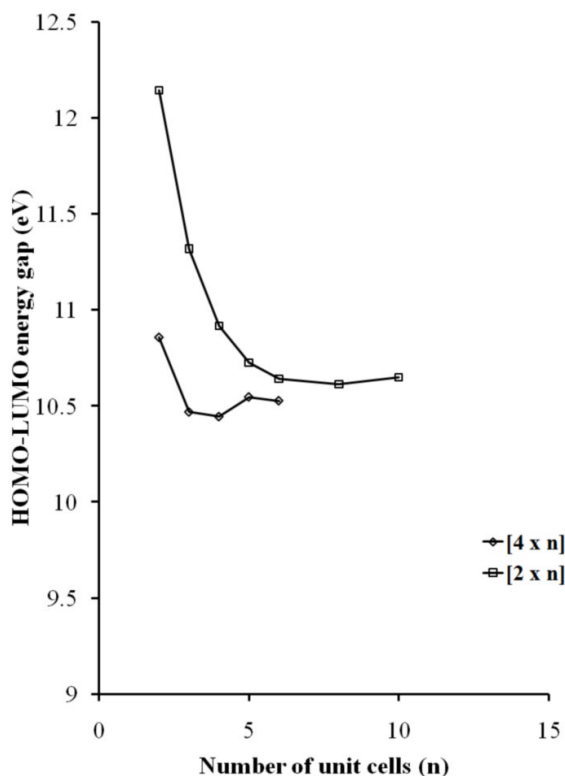


Figure 12. Evolution of the HOMO-LUMO energy gap (in eV) as a function of the length of the ribbon (n) in the n -acenes $[2 \times n]$ and rectangular ZGNI $[4 \times n]$ series (UHF/6-31G** results).

To quantify more precisely this behaviour, we define and compute for

each target system (Figure 12) an Half-Metallicity Index (HMI) (in atomic units, 1 a.u. = 1 e a₀ = 8.479 10⁻³⁰ J m V⁻¹), as follows:

$$\text{HMI} = \left| \left(\frac{\partial \varepsilon_{\alpha}}{\partial F} \right)_{F=0} - \left(\frac{\partial \varepsilon_{\beta}}{\partial F} \right)_{F=0} \right|, \quad (45)$$

where ε_{α} and ε_{β} represent the energies (in atomic units, 1 a.u = 1 E_h = 4.3597482 10⁻¹⁸ J) of the highest occupied molecular orbitals with spin-up and spin-down, respectively. This index increases almost [$R^2=0.9995$] logarithmically as a function of n (HMI = $A \ln(n) + b$) both in the n -acene [$2 \times n$] and [$4 \times n$] ZGNI series, until $n=10$ and 6, respectively (Figure 13a). The pre-logarithmic factors in these two series give a $A_{[4 \times n]}/A_{[2 \times n]}$ ratio of 3.06, which most favourably compares with an average ratio of 3.04 on the interdistance in between carbon atoms on opposite zig-zag edges. The HMI appears therefore to be above all a measure of the symmetry-breaking (and thus average of the distance) between spin-polarized densities that are in practice fully localized on opposite zig-zag edges. In the n -acene series, the HMI becomes simply proportional to $\langle S^2 \rangle$ at large values of n (Figure 13b). If a non-vanishing HMI value was not due to a methodological artefact, more detailed analysis could be probably useful to quantitatively unravel its dependence upon the width of the nanoribbon.

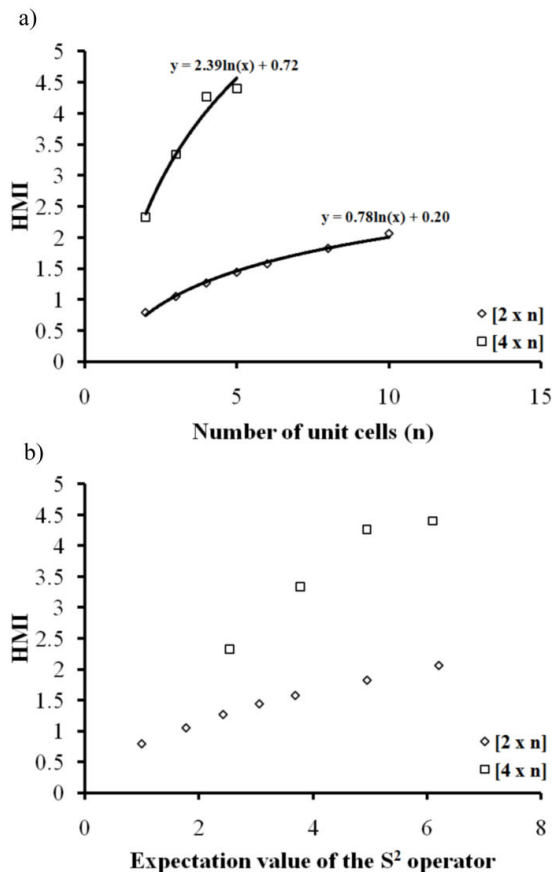


Figure 13. Evolution of the Half-Metallicity Index (HMI, equation 45) as a function (a) of the length of the ribbon (n) and (b) spin-contamination in the n -acenes $[2 \times n]$ and rectangular ZGNI $[4 \times n]$ series (UHF/6-31G** results).

Last but not least, and as was to be expected from the CO-LCAO analysis of section 3.2, we find (Figure 14) that, both in the n -acene $[2 \times n]$ and $[4 \times n]$ ZGNI series, $\langle S^2 \rangle$ increases linearly with the number of unit cells (n) in the system at the UHF level of theory. Again, the ratio (1.84) of the slopes in these two linear regressions rather straightforwardly reflect the increased interdistance between artefactually symmetry-broken edge states.

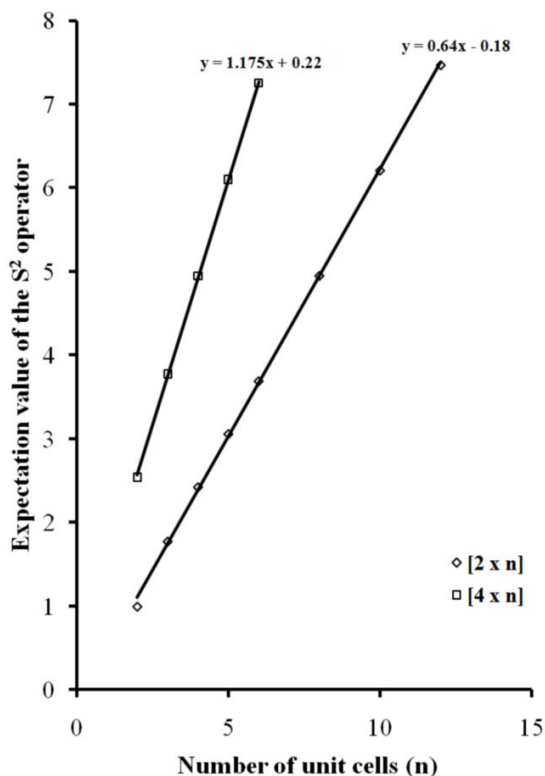


Figure 14. Evolution of the spin-contamination as a function of the length of the ribbon (n) in the n -acenes $[2 \times n]$ and rectangular ZGNI $[4 \times n]$ series (UHF/6-31G** results).

Furthermore, we find (Figure 15) from our UDFT calculations on model n -acenes ($n=1-11$) that, with all selected functionals, $\langle S^2 \rangle$ becomes also linearly dependent upon the number of unit cells (n) in the system, when this number becomes large enough. At the UHF/6-31G level, the onset of the symmetry breaking in spin-densities lies at the origin of the n -acenes series (benzene, naphthalene), and the scaling in size of the spin contamination is therefore perfectly linear. The onset of the symmetry-breaking lies at the level of naphthacene ($n=4$), hexacene ($n=6$) and octacene ($n=8$) with the MPW1K,

B3LYP and BLYP functionals, respectively. A singlet instability and spin-polarization into a “singlet open-shell” wave function is also observed when $n \geq 4$ with the SCF wave function employed in the B2PLYPD model.

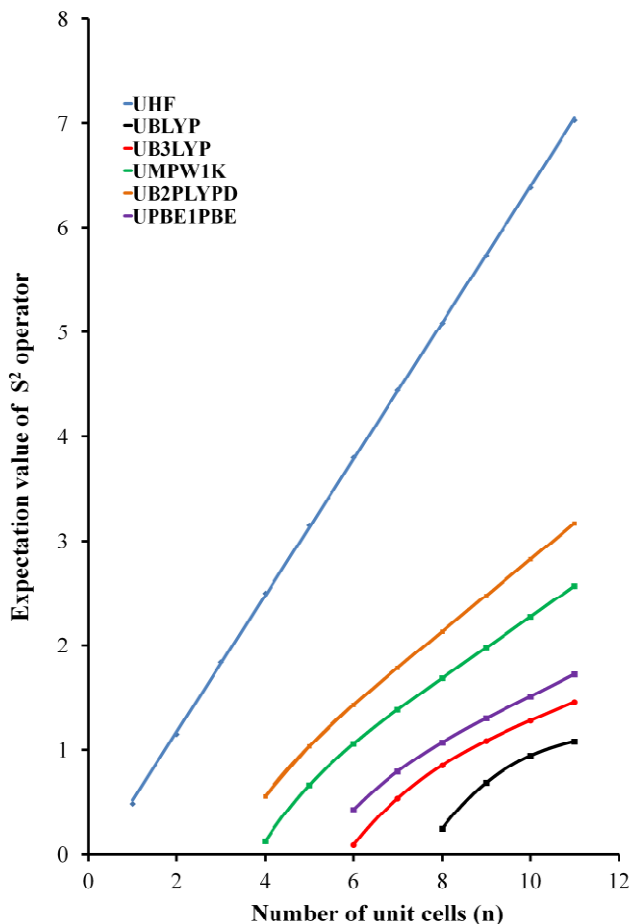


Figure 15. Evolution of the spin-contamination as a function of the length of the ribbon (n) in the n -acenes $[2 \times n]$ series (results obtained using various exchange-correlation functionals along with the 6-31G basis, upon RB3LYP/cc-pVTZ geometries).

Note that, for all systems, at the B2PLYPD/6-31G level, the energy-order reverses in favor of the singlet closed-shell electronic ground state when the

second-order (MP2-like) correlation energy is added to the obtained SCF (HF-like) energy. These fits numerically confirm that, whenever a non-vanishing symmetry-breaking in spin-densities is detected in each unit cell, due to a too approximate treatment of electron correlation, $\langle S^2 \rangle$ has to diverge proportionally to system size in the macroscopic limit. Therefore, unless one wants to call Lieb's theorem [7] into question and its implications [8] for compensated bipartite lattices, as well as more fundamental quantum mechanical postulates (antisymmetry principle, group theory, spin quantization), we are thus forced to conclude that antiferromagnetism and half-metallicity in perfectly regular graphene nanoribbons and related systems exhibiting a singlet electronic ground state are mathematically impossible in the framework of non-relativistic many-body quantum mechanics at 0K, therefore in the absence of complications such as thermal excitations or magnetic perturbations.

3.6 Further considerations on spontaneous spin flips and symmetry breakings.

Prior to closing this case, and sort out much confusion in the literature regarding the physical relevance of artefactual spin-symmetry-breakings in unrestricted DFT calculations, one may wonder whether spontaneous spin flips may not ultimately be induced by thermal excitations to higher spin states or intrinsic magnetic perturbations. In order to answer this question, recent estimates [33] of the singlet-triplet energy gaps are supplied for all target species in Table VII, at the confines of the current computational possibilities. To our knowledge these data have not been superseded yet by data of higher accuracy. Our best (FPA-QZ) estimates of the vertical singlet-triplet energy gaps

of n -acenes ($[2 \times n]$ nanoribbons, $n=2-11$) are based on dual extrapolations to the CCSD(T) level in conjunction with an asymptotically complete basis set (cc-pV ∞ Z), by virtue of the principles of a Focal Point Analysis (see our works in refs. [33a] and b for methodological details). Similar estimates to the same methodological level are supplied for the $[4 \times n]$ nanoribbons, based on linear regressions between the available FPA-QZ results in the n -acene ($[2 \times n]$) series and B3LYP/cc-pVDZ values for the HOMO-LUMO band gap or singlet-triplet energy gaps. Whereas the expected accuracy on the FPA-QZ results is of the order of 1 to 2 kcal/mol, a lower accuracy is expected for results inferred for the $[4 \times n]$ series, because of the trend of B3LYP in underestimating band gaps and in overestimating the stability of the triplet state of large conjugated species, due to the well-known self-interaction error, which the proposed linear regressions may not entirely cure. In the present state of the available methodologies and computer means, accuracies better than ~ 1 or ~ 2 kcal/mol are clearly beyond reach for the singlet-triplet energy gap of a model nanoribbon as large as the $[4 \times 6]$ nanoribbon. Focal Point Analyses aiming at sub-chemical accuracy (~ 0.1 kcal/mol) imply in particular further calculations of minor contributions due to core correlation, scalar relativistic effects, and diagonal Born-Oppenheimer corrections on reliable enough correlated (CCSD) grounds. Such calculations are simply intractable at present for compounds larger than tetracene ($[2 \times 4]$ species, see ref. [33b] and references therein).

In spite of these uncertainties, our best (FPA-QZ) estimates for singlet-triplet energy gaps are in general much larger than thermal fluctuations (kT ~ 0.58 kcal/mol at 298K) or magnetic perturbations due to C-13 nuclei which are bound to be randomly present in matter. Taking into account an average interdistance of ~ 150 Å between such nuclei, the resulting magnetic anisotropic

dipole-dipole interactions between unpaired electrons [D] should be indeed of the order of a few Mhz at most (~ 0.1 to $\sim 0.02 \cdot 10^{-6}$ kcal/mol), considering the results by Lon Knight *et al* in refs. [61] and [62] (see in particular Figure 10 in the latter reference). Spontaneous symmetry-breaking in the absence of external magnetic fields due to thermal fluctuations or coupling to magnetic nuclei seem therefore most unlikely for large but finite systems. This is particularly true for the bisanthrene ([4×3]) compound ($VE_{S-T}=25$ kcal/mol), which has been described by Scuseria and his co-workers in ref. [9e] as the *smallest* example of a *half-metallic* nanographene island, upon simply considering the behavior of symmetry-broken spin-densities when external electric fields are applied.

A further important conclusion that can be drawn upon examining Table 7 is that releasing spin-symmetries in unrestricted (UHF or UB3LYP treatments) yields unrealistically large band gaps, in comparison with the restricted values and FPA-QZ estimates for the singlet-triplet energy gaps. At this stage, it is thus worth reminding that, whereas a vanishing singlet-triplet energy gap may be expected for *n*-acenes in the macroscopic limit ($n \rightarrow \infty$) [33], recent GW calculations on zig zag graphene nanoribbons of width 2.4–0.4 nm [22] indicate very large quasi-particle band gaps, in the range of 0.5–3.0 eV. These too large values are most certainly the outcome of a symmetry-breaking in the underlying LSDA spin-densities, and make us further believe that there exist today no consistent (i.e. accurate) enough study of antiferromagnetism and half-metallicity in graphene nano-islands and nanoribbons.

Table 7. Evaluation of the HOMO-LUMO band gaps and singlet-triplet excitation energies of the selected model nanoribbons, at various theoretical levels (all results are in kcal/mol).

nanoribbon (2*n or 4*n)	HOMO-LUMO band gap (UHF/6-31G**)	HOMO-LUMO band gap (RHF/6-31G**)	HOMO-LUMO band gap (UB3LYP/cc-pVDZ)	HOMO-LUMO band gap (RB3LYP/cc-pVDZ)	VE _{S-T} (B3LYP/cc-pVDZ)	VE _{S-T} (FPA-QZ)
[2x2]	280.02	239.34	111.47	111.47	73.25	76.03 ^a
[2x3]	260.98	198.64	83.04	83.04	49.89	56.87 ^a
[2x4]	251.72	170.45	64.18	64.18	34.25	40.74 ^a
[2x5]	247.31	149.97	50.99	50.99	23.32	31.66 ^a
[2x6]	245.38	134.50	42.23	41.36	15.40	23.21 ^a
[2x7]	244.71	122.65	40.77	34.21	9.62	18.48 ^a
[2x8]	244.73	113.02	39.87	28.59	5.12	13.81 ^b
[2x9]	245.10	105.17	39.41	24.15	1.62	11.15 ^b
[2x10]	245.55	98.94	39.23	20.69	-0.99	8.49 ^b
[2x11]	245.88	93.74	39.33	17.88	-3.04	7.73 ^b
[4x2]	250.36	178.09	70.48	70.48	42.21	48.39 ^c , 45.92 ^d
[4x3]	241.38	132.50	42.59	42.59	17.25	25.53 ^c , 25.02 ^d
[4x4]	240.83	99.21	38.41	25.41	1.31	10.92 ^c , 12.15 ^d
[4x5]	243.19	75.71	39.08	15.67	-7.82	2.56 ^c , 4.85 ^d
[4x6]	242.74	60.87	40.14	10.79	-12.19	-1.44 ^c , 1.19 ^d

a) See ref. 33a.

b) See ref. 33b.

c) Extrapolated values, obtained by means of a linear regression of the available FPA-QZ results for the 2*n nanoribbons (n-acenes) onto the B3LYP/cc-pVDZ estimates for the vertical singlet-triplet energy gap (VES-T): FPA-QZ = 0.916*B3LYP + 9.7242; R² = 0.999.d) Extrapolated values, obtained by means of a linear regression of the available FPA-QZ results for the 2*n nanoribbons (n-acenes) onto the RB3LYP/cc-pVDZ estimates for the HOMO-LUMO band gap: FPA-QZ = 0.7494 *B3LYP - 6.8938; R² = 0.9987.

3.7 Conclusions and outlook for the future

To summarize, we have applied the formalism of crystalline orbitals for extended systems with periodicity in one dimension in order to demonstrate that any antiferromagnetic and half-metallic spin-polarization of edge states in graphene nanoribbons (including n -acenes) of finite width would imply a spin contamination $\langle S^2 \rangle$ that increases proportionally to the length of the ribbon. The proof is general and valid for any approximate spin-unrestricted one-determinantal (i.e. HF or DFT) treatment of electron correlation in these systems. A diverging $\langle S^2 \rangle$ value implies obviously a complete loss of control upon spin- and related electric or magnetic properties in the macroscopic limit, in sharp and clear contradiction with the expected value ($\langle S^2 \rangle = 0$) for the awaited [8] singlet ($S=0$) electronic ground state, according to the implications of Lieb's theorem [7] for compensated bipartite lattices.

In support to this finding, we have applied the *most approximate* UHF/STO-3G methodology along with the finite field approach on naphthalene in its field-free equilibrium geometry in order to *enforce the largest possible symmetry breakings* in spin densities at the very beginning of the n -acene series and demonstrate that, when using spin-unrestricted wave functions, any polycyclic aromatic hydrocarbon can be turned *at will* into a half-metallic system, depending on the selected basis set and retained fraction of HF exchange (or on the quality of the employed exchange-correlation functional). On the other hand, symmetry breakings and 'half-metallicity' in the form of

opposite shifts of α and β one-electron levels upon applying a transversal electric field are no longer observed for naphthalene as soon as electron correlation is included in a many-body (perturbation or coupled cluster) treatment. Also, whatever the employed basis set and applied external field, both spin-unrestricted and symmetry-broken solutions clearly converge to the closed-shell non-magnetic singlet ($\langle S^2 \rangle = 0$) ground state, in the full-CI limit. At the UHF level, improving the basis set most significantly reduces the extent of the "half-metallic" behaviour of symmetry-broken spin-densities in naphthalene, but without totally removing these features. Due to a release of symmetry in the environment, the external electric field tends to attenuate the extent of the symmetry breaking. Even in this case, a RHF wave function remains clearly a better starting point [31] for further electron correlation calculations. Note that symmetry-breakings in spin-densities and spin contamination in spin-unrestricted calculations can also occur in systems with no symmetry point group, but are in this case more difficult to detect. In any case, the most basic principles of symmetry point group theory should never be violated for *singlet* states, even in the context of Density Functional Theory [64].

At last, upon enforcing from the onset of the n -acene [$2 \times n$] and [$4 \times n$] ZGNI series the appearance of spin-polarized edge states, again with a *deliberately too approximate* (UHF/6-31G**) treatment of electron correlation, we have computationally verified that, whatever its extent, a finite (i.e. observable) symmetry breaking in each unit cell of a nanoribbon of finite width results into a spin contamination $\langle S^2 \rangle$ that increases proportionally with its

length (i.e., with n). The same scaling properties of the $\langle S^2 \rangle$ value in function of system size have been also verified from UDFT calculations at the n -acene $[2 \times n]$ series, using variety of exchange-correlation functionals in conjunction with the 6-31G basis set. We have correspondingly verified on the same computational grounds that half-metallicity in finite ZGNIs (and by extension extended ZGNRs) is therefore nothing else but a measure of the extent of an artefactual symmetry-breaking of spin-densities.

To conclude, we believe that our analysis using crystalline orbitals and our model calculations are altogether robust (and provocative) enough for calling into question the idea that graphene nanoislands and nanoribbons of finite width (including n -acenes) are anti-ferromagnetic and half-metallic systems, in the absence of complications such as thermal excitations, structural defects or magnetic perturbations, since these views imply sharp contradictions not only with the implications of Lieb's theorem for compensated bipartite lattices, but also with most basic principles and general theorems of (non-relativistic) quantum mechanics (antisymmetry principle, group theory, spin quantization). At this stage, it is worth mentioning that, to our knowledge, no direct experimental proof of edge magnetism in pristine graphene has been reported so far [8b]. Magnetism in graphene is most commonly ascribed to structural defects or impurities [64]. The greatest care is therefore advocated with conclusions that systematically find their root in artefactually broken spin-symmetry densities, due to a too limited treatment of electron correlation. Indeed, finite field calculations upon naphthalene using deliberately symmetry-broken UHF spin-densities as starting input in post-SCF calculations of improving quality demonstrates that antiferromagnetism and half-metallicity in zig zag

graphene nanoribbons or islands with a non vanishing energy gap will necessarily be quenched by an exact treatment of electron correlation ($\langle S^2 \rangle = 0$), at the confines of *non-relativistic* quantum mechanics: *electron correlation restores symmetry breakings* [33a].

At these confines, zig zag graphene nanoislands of large but finite dimension *cannot* exhibit intrinsic half-metallicity at 0K in their *singlet closed-shell* ground state, thus in the absence of magnetic fields, structural defects (vacancies, adatoms), or complications like thermally induced spin-flips, since they possess an even number of electrons. Contrary to recent affirmations [12b], doping for instance an extended ZGNR by an equal number of boron and nitrogen atoms in order to induce asymmetric charge distributions should therefore normally not result into any genuine or enhanced half-metallicity, since the system remains *singlet closed-shell*, and exhibits a larger band gap than the undoped ZGNR.

All studies so far of the half-metallicity of graphene nanoribbons and related systems make use of spin-Unrestricted Density Functional Theory. In extended systems with translation symmetry in one dimension and with a vanishing band gap, a physical symmetry breaking of spin-densities due to a spin-dependent potential or thermally induced spin flips may nonetheless still result into an intrinsic half-metallic transport behaviour. Further studies employing *many-body relativistic quantum mechanics* are therefore very much required for verifying whether extremely weak spin-orbit coupling interactions, of the order of a few tenths μeV only [30], or anisotropic magnetic dipole-dipole interactions between unpaired electrons, could nevertheless be strong enough to induce a physical and effectively measurable spin-polarization of edge states in

large enough, perfectly planar and undistorted ZGNRs, with vanishingly small excitation energies, in the absence of any external magnetic perturbation or complications like thermal excitations [33]. When the required methodologies will become affordable, it will be worth verifying on the ground of calculations reaching at least spectroscopic accuracy ($\sim 1 \text{ cm}^{-1}$) whether couplings to magnetically active and randomly distributed C_{13} nuclei or thermal fluctuations can overpower the Coulombic couplings of highly delocalized electrons in the edge states. It will then also be necessary to consider the outcome of thermal fluctuations, which are known to result into wave-like out-of-plane distortions of the nanoribbons, and may certainly in turn influence their band gap [33b] and propensity to undergo spin-flips.

Note in particular that it has not been confirmed yet from robust enough band structure calculations coping with both static and dynamic correlation that the band gap of infinite acenes and ZGNR systems effectively vanishes within a few tenths of a kcal/mol, especially when releasing symmetry constraints upon the wave function. Even then, one should wonder whether there will ever be a non-relativistic unrestricted quantum mechanical treatment of correlation that is in practice robust enough for restoring the correct symmetries of spin-densities in the singlet (closed-shell) non-magnetic states of these systems, and for handling therefore these singlet states on equal grounds with (effectively) spin-polarized magnetic (open-shell triplet, quintet, septet, ...) states.

3.8 References

- [1] Y.-W. Son, M. L. Cohen, S.G. Louie, *Nature*, **444**, 347 (2006).
- [2] R. G. Parr, W. Yang, *Density Functional Theory of Atoms and Molecules* (Oxford University Press, New York, 1989); R. M. Dreizler, E. K. U. Gross, *Density Functional Theory* (Springer-Verlag, Berlin Heidelberg, New York, 1990); W. Koch, M. Holthausen, *A Chemist's Guide to Density Functional Theory, Second Ed.* (Wiley-VCH, Weinheim, 2001).
- [3] J. P. Perdew, A. Zunger, *Phys. Rev. B*, **23**, 5048 (1981).
- [4] M. Fujita, K. Wakabayashi, K. Nakada, K. Kusakabe, *J. Phys. Soc. Jpn.* **65**, 1920 (1996); K. Nakada, M. Fujita, G. Dresselhaus, M.S. Dresselhaus, *Phys. Rev. B*, **54**, 17954 (1996); K. Wakabayashi, M. Fujita, H. Ajiki, M. Sigrist, *Phys. Rev. B*, **59**, 8271 (1999); Y. Miyamoto, K. Nakada, M. Fujita, *Phys. Rev. B*, **59**, 9858 (1999).
- [5] Y. Kobayashi, K.-I. Fukui, T. Enoki, K. Kusakabe, Y. Kaburagi, *Phys. Rev. B*, **71**, 193406 (2005); T. Enoki, Y. Kobayashi, *J. Mat. Chem.*, **15**, 3999 (2005); Y. Niimi, T. Matsui, H. Kambara, K. Tagami, M. Tsukada, H. Fukuyama, *Phys. Rev. B*, **73**, 085421 (2006).
- [6] S. Okada, A. Oshiyama, *Phys. Rev. Lett.*, **87**, 146803 (2001); H. Lee, Y.-W. Son, N. Park, S. Han, J. Yu, *Phys. Rev. B*, **72**, 174431 (2005).
- [7] E. H. Lieb, *Phys. Rev. Lett.* **62**, 1201 (1989).
- [8] (a) J. Fernandez-Rossier and J. J. Palacios, *Phys. Rev. Lett.* **99**, 177204 (2007); (b) O. V. Yazyev, *Rep. Phys. Rep.* **73**, 056501 (2010).
- [9] (a) D. Jiang, B. G. Sumpter, S. Dai, *J. Chem. Phys.* **127**, 124703 (2007); (b) E. Rudberg, P. Salek, Y. Luo, *Nano Lett.*, **7**, 2211 (2007); (c) P. G. Silvestorv, K. B. Efetov, *Phys. Rev. Lett.*, **98**, 016802 (2007); (d) P. Shemella, Y. Zhang,

- M. Mailman, P. M. Ajaya, S. K. Nayak, Appl. Phys. Lett., **91**, 042101 (2007);
(e) O. Hod, V. Barone, G. E. Scuseria, Phys. Rev. B, **77**, 035411 (2008).
- [10] J. P. Perdew, K. Burke, M. Ernzerhof, Phys. Rev. Lett., **77**, 3865 (1996);
ibid, **78**, 1396 (1997).
- [11] C. Lee, W. Yang, and R. G. Parr, Phys. Rev. B, **37**, 785 (1998); A. D.
Becke, J. Chem. Phys. **98**, 5648 (1993).
- [12] (a) O. Hod, V. Barone, J.E. Peralta, G.E. Scuseria, Nano Letters, **7**, 2295
(2007); (b) S. Dutta, A. K. Manna, S.K. Pati, Phys. Rev. Lett. **102**, 096601
(2009); (c) S. Duppa, S. K. Patti, Carbon, **48**, 4409 (2010).
- [13] A. Mañanes, F. Duque, A. Ayuela, M. J. López, J. A. Alonso, Phys. Rev. B,
78, 035432 (2008); B. Huang, C. Si, H. Lee, L. Zhao, J. Wu, B.-L. Gu, W.
H. Duan, Appl. Phys. Lett. **97**, 043115 (2010); S. Tang, Z. Cao, Comp.
Mat. Sciences, **50**, 1917 (2011).
- [14] B. Huang, Y.-W. Son, G. Kim, W. Duan, J. Ihm, J. Am. Chem. Soc. **131**,
17919 (2009).
- [15] S. A. Wolf, D. D. Awschalom, R. A. Buhrman, J. M. Daughton, S. von
Molnár, M. L. Roukes, A. Y. Chtchelkanova, D. M. Treger, Science, **294**,
1488 (2001).
- [16] (a) M. Bendikov, H. M. Duong, K. Starkey, K. N. Houk, E. A. Carter, and F.
Wudl, J. Am. Chem. Soc., **126**, 7416 (2004); (b) *ibid*, **126**, 10493 (2004);
(c) J. Hachmann, J. J. Dorando, M. Avilés, G. K.-L. Chan, *J. Chem. Phys.*,
127, 134309 (2007); (d) Z. Qu, D. Zhang, C. Liu, and Y. Jiang, J. Phys.
Chem. A, **113**, 7909 (2009); (e) M. C. dos Santos, Phys. Rev. B, **74**,
045426 (2006); (f) D. E. Jiang, S. Dai, J. Phys. Chem. A, **112**, 332 (2008);
(g) D. E. Jiang, S. Dai, Chem. Phys. Lett. **466**, 72 (2008); (h) T. Ishida, J.
Aihara, Phys. Chem. Chem. Phys. **11**, 7197 (2009).

- [17] D.E. Jiang, X.Q. Chen, W. Luo, W. A. Shelton, *Chem. Phys. Lett.* **483**, 120 (2009).
- [18] Z. Chen, D. E. Jiang, X. Lu, H. F. Bettinger, S. Dai, P.v.R Schleyer, K. N. Houk, *Organic Lett.* **9**, 5449 (2007).
- [19] C. Tönshoff, H. F. Bettinger, *Angew. Chem. Int.* **49**, 4125 (2010).
- [20] K. Yoshizawa, T. Tada, A. Staykov, *J. Am. Chem. Soc.* **130**, 9406 (2008); P.W. Fowler, B.T. Pickup, T.Z. Todorova, W. Myrvold, *J. Chem. Phys.* **131**, 244110 (2009).
- [21] G. Gidofalvi and D. Mazziotti, *J. Chem. Phys.* **129**, 134108 (2008).
- [22] L. Yang, C.-H. Park, Y.-W. Son, M.L. Cohen, S. G. Louie, *Phys. Rev. Lett.* **99**, 186801 (2007).
- [23] R.K. Nesbet, *Rev. Mod. Phys.* **33**, 28 (1961); P.-O. Löwdin, *Rev. Mod. Phys.* **35**, 496 (1963).
- [24] A. S. Szabo, N. S. Ostlund, *Modern Quantum Chemistry* (Mc Graw-Hill, New York, 1989).
- [25] I.R Levine, *Quantum Chemistry* (Prentice Hall; 5th edition, 1999).
- [26] F. Jensen, *Introduction to Computational Chemistry* (Wiley, Chichester, 1999).
- [27] E.R. Davidson, W.T. Borden, *J. Phys. Chem.* **87**, 4783 (1983).
- [28] R. Manne, *Mol. Phys.* **24**, 935 (1972).
- [29] C.J. Cramer, *Essentials of Computational Chemistry, second ed.* (Wiley & Sons, Chichester (UK), 2004).
- [30] M. Gmitra, S. Konschuh, C. Ertler, C. Ambrosch-Draxl, J. Fabian, *Phys. Rev. B*, **80**, 235431(2009).
- [31] (a) L. S. Cederbaum, F Tarantelli, P. Winkler, *J. Phys. B*, **23**, L747 (1990); (b) L. S. Cederbaum, P. Winkler, *Theor. Chim. Acta*, **88**, 257 (1994).

- [32] M. S. Deleuze, L. Claes, E. S. Kryachko, J. -P. François, J. Chem. Phys. **119**, 3106 (2003); B. Hajgató, M. S. Deleuze, D. J. Tozer, F. De Proft, J. Chem. Phys. **129**, 084308 (2008).
- [33] (a) B. Hajgató, D. Szieberth, P. Geerlings, F. De Proft, M.S. Deleuze, J. Chem. Phys. **131**, 224321 (2009); (b) B. Hajgató, M. Huzak, M. S. Deleuze, J. Phys. Chem. A, **116**, 9282 (2011).
- [34] T. J. Lee, P. R. Taylor, Int. J. Quantum Chem. **36(S23)**, 199 (1989).
- [35] A. Karton, E. Rabinovich, J.M.L. Martin, B. Ruscic, J. Chem. Phys. **125**, 144108 (2006).
- [36] J. M. André, L. Gouverneur, and G. Leroy, Int. J. Quantum Chem. **1**, 427, 451 (1967); J. M. André and G. Leroy, Theor. Chim. Acta **9**, 123 (1967); J. Ladik, Adv. Quantum Chem. **7**, 397 (1973); J. Ladik, *Electronic Structure of Polymers and Molecular Crystals*, edited by J. M. André and J. Ladik (Plenum, New York, 1975); J. Ladik, *Quantum Theory of Polymers*, edited by J. M. André, J. Delhalle, and J. Ladik (Reidel, New York, 1975); J. Ladik, Adv. Quantum Chem. **12**, 65 (1980); M. Kertesz, Adv. Quantum Chem. **15**, 161 (1982); J. Ladik and J. M. André, *Quantum Chemistry of Polymers: Solid State Aspects* (Reidel, Dordrecht, 1984); J. Ladik, *Quantum Theory of Polymers as Solids* (Plenum, New York, 1988); J. M. André, J. Delhalle, and J. L. Brédas, *Quantum Chemistry Aided Design of Organic Polymers* (World Scientific, London, 1991); J. J. Ladik, Phys. Rep. **313**, 171 (1999); J. G. Fripiat, J. Delhalle and F. E. Harris, in *Computation in Modern Science and Engineering*, edited by T.E. Simos and G. Maroulis (American Institute of Physics, Melville, NY, 2007), Vol. 2, Pt. A, pp 179-182; I. Flamant, J. G. Fripiat, J. Delhalle, F. E. Harris, Theor. Chem. Acta, **104**, 350 (2000); J. G. Fripiat, J. Delhalle, F. E. Harris, Chem. Phys. Lett. **422**, 11 (2006); J. G.

- Fripiat, J. Delhalle, I. Flamant, F. E. Harris, J. Chem. Phys. **132**, 044108 (2010).
- [37] J.P. Lowe, K. A. Peterson, *Quantum Chemistry* (Elsevier, Amsterdam, 2005); P. W. Atkins, R. S. Friedmann, *Molecular Quantum Mechanics* (Oxford University Press, 2005); G. C. Schatz, M. A. Ratner, *Quantum Mechanics in Chemistry* (Dover Publications, Mineola, New York, 2002); or any text book on group theory.
- [38] M. Born and T. Karman, Phys. Z. **13**, 297 (1912).
- [39] F. Bloch, Z. Phys. **52**, 555 (1928).
- [40] P.-O. Löwdin, Adv. Phys. **5**, 1 (1956).
- [41] J.-L Calais, B. T. Pickup, M. S. Deleuze, J. Delhalle, Eur. J. Phys. **16**, 179 (1995).
- [42] R. H. Bube, in *Electronic Properties of Crystalline Solids-An Introduction to Fundamentals* (Academic, New York, 1974).
- [43] H. J. Monkhorst and K. Kertesz, Phys. Rev. B **24**, 3015 (1981); J. Delhalle and J. L. Calais, J. Chem. Phys. **85**, 5286 (1986); M. Deleuze, J. Delhalle, B. T. Pickup, J.-L. Calais, Phys. Rev. B, **46**, 15668 (1992); M. Deleuze, J. Delhalle, B. T. Pickup, J.-L Calais, Adv. Quantum Chem. **26** 35 (1995); M. Deleuze, M. K. Scheller, L. S. Cederbaum, J. Chem. Phys. **103**, 3578 (1995).
- [44] C. J. Jameson, P. W. Fowler, J. Chem. Phys. **85**, 3432 (1986); P. G. Jasien, G. Fitzgerald, J. Chem. Phys. **93**, 2554 (1990); F. Sim, D. R. Salahub, S. Chin, Int. J. Quantum Chem. **43**, 463 (1992); J. Guan, P. Duffy, J. T. Carter, D. P. Chong, K. C. Casida, M. E. Casida, M. Wrinn, J. Chem. Phys. **98**, 4753 (1993); D. A. Dixon, N. Matsuzawa, J. Phys. Chem. **98**, 3967 (1994); N. Matsuzawa, D. A. Dixon, J. Phys. Chem. **98**, 2545 (1994); J.

- Guan, M. E. Casida, A. M. Köster, D. R. Salahub, *Phys. Rev. B*, **52**, 2184 (1995); S. A. C. McDowell, R. D. Amos, N. C. Handy, *Chem. Phys. Lett.* **235**, 1 (1995); N. Matsuzawa, M. Ata, D. A. Dixon, *J. Phys. Chem.* **99**, 7698 (1995).
- [45] C. Møller, M. S. Plesset, *Phys Rev.* **46**, 618 (1934).
- [46] M. Head-Gordon, J. A. Pople, M. J. Frisch, *Chem. Phys. Lett.* **153**, 503 (1988).
- [47] R. Krishnan, J. A. Pople, *Int. J. Quantum Chem.* **14**, 91 (1978).
- [48] G. D. Purvis III, R. J. Bartlett, *J. Chem. Phys.* **76**, 1910 (1982).
- [49] K. Raghavachari, G. W. Trucks, J. A. Pople, M. Head-Gordon, *Chem. Phys. Lett.* **157**, 479 (1989); R. J. Bartlett, J. D. Watts, S. A. Kucharski, J. Noga, *Chem. Phys. Lett.* **165**, 513 (1990); J. F. Stanton, *Chem. Phys. Lett.* **281**, 130 (1997).
- [50] T. Helgaker, P. Jørgensen, J. Olsen, *Molecular Electronic-Structure Theory* (John Wiley and Sons, Chichester, 2000).
- [51] C. Lee, W. Yang, and R. G. Parr, *Phys. Rev. B* **37**, 785 (1998); A. D. Becke, *J. Chem. Phys.* **98**, 5648 (1993).
- [52] B. J. Lynch, P. L. Fast, M. Harris, D. G. Truhlar, *J. Phys. Chem. A*, **104**, 4811 (2000); B. J. Lynch, D. G. Truhlar, *J. Phys. Chem. A*, **105**, 2936 (2001).
- [53] S. Grimme, *J. Chem. Phys.* **124**, 034108 (2006).
- [54] C. Adamo and V. J. Barone, *Chem. Phys.* **108**, 664 (1998).
- [55] Gaussian 09, Revision B.01, M. J. Frisch, G. W. Trucks, H. B. Schlegel, G. E. Scuseria, M. A. Robb, J. R. Cheeseman, G. Scalmani, V. Barone, B. Mennucci, G. A. Petersson, H. Nakatsuji, M. Caricato, X. Li, H. P. Hratchian, A. F. Izmaylov, J. Bloino, G. Zheng, J. L. Sonnenberg, M. Hada, M. Ehara,

- K. Toyota, R. Fukuda, J. Hasegawa, M. Ishida, T. Nakajima, Y. Honda, O. Kitao, H. Nakai, T. Vreven, J. A. Montgomery, Jr., J. E. Peralta, F. Ogliaro, M. Bearpark, J. J. Heyd, E. Brothers, K. N. Kudin, V. N. Staroverov, R. Kobayashi, J. Normand, K. Raghavachari, A. Rendell, J. C. Burant, S. S. Iyengar, J. Tomasi, M. Cossi, N. Rega, J. M. Millam, M. Klene, J. E. Knox, J. B. Cross, V. Bakken, C. Adamo, J. Jaramillo, R. Gomperts, R. E. Stratmann, O. Yazyev, A. J. Austin, R. Cammi, C. Pomelli, J. W. Ochterski, R. L. Martin, K. Morokuma, V. G. Zakrzewski, G. A. Voth, P. Salvador, J. J. Dannenberg, S. Dapprich, A. D. Daniels, Ö. Farkas, J. B. Foresman, J. V. Ortiz, J. Cioslowski, and D. J. Fox, Gaussian, Inc., Wallingford CT, 2009.
- [56] H. H. Jaffé, M. Orchin, *Symmetry in Chemistry* (John Wiley & Sons, New York, 1965).
- [57] M. S. Deleuze, J. Delhalle, B.T. Pickup, *Theor. Chim. Acta*, **82**, 309 (1992).
- [58] M.S. Deleuze, A. B. Trofimov, L.S. Cederbaum, *J. Chem. Phys.* **115**, 5859 (2001).
- [59] T. H. Dunning, Jr., *J. Chem. Phys.* **90**, 1007 (1989).
- [60] D. Feller, *J. Chem. Phys.* **96**, 6104 (1992); D. Feller, *J. Chem. Phys.*, **98**, 7059 (1993).
- [61] L. B. Knight, Jr., B. A. Bell, D. P. Cobranchi, E. R. Davidson, *J. Chem. Phys.* **111**, 3145 (1999).
- [62] L. B. Knight, Jr., W. E. Rice, L. Moore, E. R. Daviudson, R. S. Dailey, *J. Chem.. Phys.* **109**, 1409 (1998).
- [62] Spin-contamination is not well-defined in DFT methods [see e.g. J.A. Pople, P.M.W. Gill and N.C. Handy, *Int. J. Quantum Chem.* **56**, 303 (1995)], except if the real interacting function is a spin singlet ($S=0$). For singlet states, charge- and spin-densities must therefore exhibit the full symmetry

- of the molecular point group [J. P. Perdew, A. Ruzinsky, L.A. Constantin, J. Sin, G. I. Csonka, J. Chem. Theor. Comput. **5**, 902 (2009)].
- [64] O. V. Yazyev, L. Helm, Phys. Rev. B, **75**, 125408 (2007).

4 Focal point analysis of the singlet-triplet energy gap of octacene and larger acenes

4.1 Introduction

Compounds like tetracene and pentacene have received considerable attention because their planar and rigid structure as well as their low band gap make them particularly well-suited for the making of nicely organized two-dimensional organic thin films with large charge carrier mobilities [1]. In contrast, experimental studies of the electronic structure and excitation properties of heptacene, octacene and larger acenes have been long hampered by the quickly increasing reactivity in the acene series [2]. Synthesis [3] of heptacene in a polymethylmethacrylate matrix at 298K and subsequent analysis of the electronic structure at 10 K in solid noble gas have only been achieved very recently [4]. By using cryogenic matrix-isolation technique and a protection group strategy, C. Tönshoff and H.F. Bettinger succeeded a few years ago to complete the synthesis of octacene and nonacene [5]. Although pentacene has often been reported to be the best available organic p-type semiconductor, larger acenes could be even more useful [6] for material applications [7], in particular when using bulky substituents for kinetically moderating their reactivity.

From a theoretical viewpoint, large acenes are also notoriously difficult, i.e. strongly correlated compounds, and the nature of their electronic ground state has been subject to much debate. Whereas spin-unrestricted Density Functional Theory calculations indicate that heptacene and larger acenes should possess an antiferromagnetic (AFM) singlet ground state [8], extrapolation of

experimental triplet energies from oligoacenes up to hexacene suggests that the electronic ground state of nonacene should be a triplet one [9]. Antiferromagnetism along with an electronic (singlet) instability was diagnosed [8] from the fact that according to unrestricted calculations employing Density Functional Theory (DFT) the two outermost singly occupied spin orbitals do not transform according to irreducible representations of the D_{2h} symmetry point group imposed by the nuclear frame, but undergo an overwhelmingly strong symmetry breaking, in the form of a spatial separation and localization of the two frontier electrons with spin-up and spin-down on the opposite polyacetylenic strands, resulting in strongly polarized spin-densities for a total spin equal to zero. In support to these theoretical data, the presence of strong absorption bands at too short wave lengths (418 and 377 nm) in the VIS/NIR absorption spectrum of octacene and nonacene confirms that these compounds cannot have a triplet state as their ground state [5].

However, in the present state of our knowledge, this certainly does not mean that octacene and nonacene exhibit an AFM singlet ground state, unless one wants to call into question the most basic laws and principles of non-relativistic quantum mechanics (group theory, spin-quantization). Indeed, according to the Pauli anti-symmetry principle for electronic wavefunctions, in an exact quantum mechanical depiction, it is mathematically impossible for a system with an even number of electrons, an equal number of spin-up and spin-down electrons ($N_{\alpha}=N_{\beta}$) and a total spin $S=0$ to exhibit any difference in between spin-up and spin-down densities, and this even if the two frontier electrons behave as biradicals, as was suggested for acenes larger than pentacene or hexacene [8, 10].

In line with previous works on the ionization and electron attachment energies of these systems [11], our original scope was to reach chemical accuracy on the computed vertical and adiabatic transition energies [1 kcal/mol; i.e. 43 meV], by virtue of an extrapolation of results to the level of Coupled Cluster theory [12] incorporating Single, Double and perturbative Triple excitations [CCSD(T)], in conjunction with an asymptotically Complete Basis Set (CBS), and by taking further complications into account such as zero-point vibrations. The most consistent and unquestionable picture that emerges upon considering the composition of multi-configurational wave functions, the topologies of natural orbitals in symmetry-unrestricted CASSCF calculations, the T1 diagnostics [13] of Coupled Cluster theory and further energy-based criteria devised by J.M.L. Martin and his co-workers [14] from the computation of atomization energies, is that acenes up to heptacene exhibit a 1A_g singlet closed-shell electronic ground state which is dominantly of single-reference character [15].

In line with the trends emerging from natural occupation numbers [16], extrapolations of all our results so far indicate nonetheless a vanishing singlet-triplet energy gap within an accuracy of ~ 3 kcal/mol (~ 0.12 eV) and, thus, a *metallic regime* in the limit of an infinite periodic chain. In continuation to our work in ref. [15], the present study aims first at investigating at the CCSD(T)/CBS level the singlet-triplet energy differences of acenes ranging from octacene to undecacene, and check from the obtained results whether a metallic regime still holds in the stereoregular polymer limit. The magnitude of smaller corrections terms pertaining to core correlation, scalar relativistic effects [17] and diagonal Born-Oppenheimer corrections [18] will be separately ascertained. Of relevance for the present work are recent calculations of excited states of

octacene [19] with the proper symmetries at the CC2 level or using the combined DFT/MRCI approach devised by Grimme [20] – an approach which contains nonetheless semi-empirical parameters in order to screen the Coulomb integrals.

4.2 Methodology

As has been explained in section 3.3, static correlation is indirectly recovered when proceeding towards the FCI limit through the interplay of single-reference treatments (HF, MP2, MP3, MP4SDQ, CCSD, CCSD(T), ...) of improving quality. Note also that for open-shell states, the UCCSD(T) approach is known to be very resilient to complications arising from static correlation, and to sustain most favorably the comparison with Complete Active Space Self-Consistent Field (CASSCF) calculations in most challenging situations (see e.g. Figure 11.10 describing the H₂O dissociation curve in ref. [21]). In line with our analysis in ref. [15], all computations that are presented in this work have been performed on geometries that were optimized by means of Density Functional Theory (DFT) [22] along with the Becke three-parameter Lee-Yang-Parr (B3LYP) functional [23] and the cc-pVTZ basis set [24]. The same approach and basis sets were used to compute harmonic vibrational energies and zero-point energies. A main reason for using the cc-pVTZ basis set at this stage is that it was shown to yield almost negligible intramolecular basis set superposition errors [25].

The Focal Point Analyses [FPA] that we present in the sequel are comparable to strategies pursuing chemical [1 kcal/mol] or even sub-chemical [0.1 kcal/mol] accuracies in benchmark studies of conformational energy differences or torsional barriers [26], the barrier to linearity in water [27], reaction and activation energies [28], ionization energies [29], heats of

formation [30], binding energies of π -complexes [31], polarizabilities [32], etc., which also combine (perturbative) MPn and (iterative) CC treatments. Focal Point Analyses exploit the idea of a dual extrapolation towards the highest attainable level in electron correlation (ideally, the full-CI limit, in practice in this case the CCSD(T) level), and in the limit of an asymptotically complete basis set (CBS).

Single point energy calculations have been performed at the level of Hartree-Fock theory (HF), of Møller-Plesset theory truncated at second-order (MP2), third-order (MP3), and fourth-order with single, double, and quadruple terms (SDQ-MP4), as well as at the CCSD and CCSD(T) levels of coupled cluster theory in conjunction with basis sets of improving quality, under the frozen core approximation at all correlated levels, using Dunning's correlation consistent polarized valence (cc-pVXZ) basis sets of double (X=D), triple (X=T), quadruple (X=Q) and pentuple (X=5) zeta quality [24].

Total HF energies and correlation energies at the MP2, MP3, and MP4SDQ levels have been separately extrapolated to the limit of an asymptotically CBS from results obtained using the latter basis sets, in conjunction with Feller's three-point extrapolation formula [33], and a three-point extension [34] of Schwartz extrapolation formula [35], respectively. In straightforward analogy with our recent work [15] on the first seven terms ($n=1-7$) in the acene series, CBS results for the Δ HF singlet-triplet (ST) energy differences or +MP2, +MP3, +MP4(SDQ) energy corrections to the Δ HF, Δ MP2 and Δ MP3 energy differences are referred in the sequel to as F-QZ or S-QZ (shortly F/S-QZ) results, since in the employed Feller or Schwartz extrapolation procedures use is made of data obtained using cc-pVDZ, cc-pVTZ, and cc-pVQZ basis sets. We note that the largest employed cc-pVQZ basis sets for decacene and undecacene contain up to

3030 and 3310 atomic basis functions. Further results referred to as F/S-AQZ and F/S-5Z results derive from 3-point extrapolations employing the aug-cc-pVXZ (X=D,T,Q) and cc-pVXZ (X=T,Q,5) basis sets, respectively.

Further extrapolations were performed towards the CCSD(T) level of theory in the limit of an asymptotically complete basis set, using the principles of a Focal Point Analysis (FPA). In such an approach, the faster convergence of the higher-order correlation corrections to the calculated energy differences is exploited in well-suited extrapolations of results obtained using CCSD(T) theory. To be more specific, reliable estimations of CCSD(T) energy differences in the limit of an infinitely large basis set have been made by adding to the MP2/CBS [more precisely referred to as S_{MP2-QZ}] result +MP4(SDQ)/cc-pVTZ and +CCSD(T)/cc-pVDZ corrections to the ST energy difference. In line with the notations we adopted in ref. [15], this CCSD(T)/CBS estimate of the ST energy gap will thus be referred as a FPA-QZ result:

$$\begin{aligned} \text{FPA-QZ} = & S_{MP2-QZ} + (E_{MP4/cc-pVTZ} - E_{MP2/cc-pVTZ}) \\ & + (E_{CCSD(T)/cc-pVDZ} - E_{MP4/cc-pVDZ}). \end{aligned} \quad (1)$$

As in ref. [15], the outcome of further basis set extensions in the FPA has been carefully studied beyond the latter level, and more accurate estimations of the ST energy gaps of the largest terms in the n -acene series are provided by matching through linear regressions results obtained using different FPA protocols, at the confines of the current computational possibilities:

$$\begin{aligned} \text{FPA-AQZ} = & S_{MP2-AQZ} + (E_{MP4/aug-cc-pVTZ} - E_{MP2/aug-cc-pVTZ}) \\ & + (E_{CCSD(T)/aug-cc-pVDZ} - E_{MP4/aug-cc-pVDZ}), \end{aligned} \quad (2)$$

$$\begin{aligned} \text{FPA-5Z} = & S_{MP2-5Z} + (E_{MP4/cc-pVTZ} - E_{MP2/cc-pVTZ}) \\ & + (E_{CCSD(T)/cc-pVDZ} - E_{MP4/cc-pVDZ}), \end{aligned} \quad (3)$$

$$\begin{aligned} \text{FPA-5Z2} = S_{\text{MP2-5Z}} + (E_{\text{MP4/cc-pVQZ}} - E_{\text{MP2/cc-pVQZ}}) \\ + (E_{\text{CCSD(T)/cc-pVTZ}} - E_{\text{MP4/cc-pVTZ}}), \end{aligned} \quad (4)$$

$$\begin{aligned} \text{FPA-5Z3} = S_{\text{MP2-5Z}} + (S_{\text{MP4-QZ}} - E_{\text{MP2-QZ}}) \\ + (E_{\text{CCSD(T)/cc-pVTZ}} - E_{\text{MP4/cc-pVTZ}}). \end{aligned} \quad (5)$$

In eq. (2), energies referred to as $S_{\text{MP2-AQZ}}$ results are obtained as the sum of the HF energy extrapolated at the HF/aug-cc-pV ∞ Z (F-AQZ) level, and of the MP2 electron correlation energy extrapolated in the limit of the same asymptotically CBS, according to a three-point Schwartz extrapolation employing MP2 results obtained using the augmented Dunning's correlation basis sets (aug-cc-pVXZ) [36] of double (X=D), triple (X=T) and quadruple (X=Q) zeta quality. Similarly, in equations (3-5), energies referred to as $S_{\text{MP2-5Z}}$ results are obtained as the sum of the HF energy extrapolated at the HF/cc-pV ∞ Z (F-5Z) level, and of the MP2 electron correlation energy extrapolated to the same limit, according to Feller or Schwartz extrapolations employing HF and MP2 energies obtained using the cc-pVTZ, cc-pVQZ and cc-pV5Z basis sets.

Most calculations, comprising geometry optimizations, vibrational analyses, as well as the single-point MP2, MP3, and MP4 energy calculations have been carried out using the GAUSSIAN09 program package [37]. All CCSD and CCSD(T) single-point energy calculations on closed- and open-shell systems have been performed using the MOLPRO2010.1 package of programs [38]. Whereas the UHF reference wave functions for the triplet states are subject to spin-contamination, which subsequent treatments of electron correlation at finite order (MP2, MP3, MP4) may not entirely cure, all our Coupled Cluster calculations are based on ROHF wave functions, and partially spin-adapted coupled cluster treatments, which involves the deletion of most of the terms that cause spin-contamination in the Coupled Cluster expansion. Therefore, our

CCSD and CCSD(T) calculations and the subsequent FPAs enable an essentially correct treatment of spin.

Scalar relativistic contributions to the singlet-triplet energy gaps have been estimated using GAUSSIAN09 according to energy calculations employing DFT along with the B3LYP exchange-correlation functional, the second-order Douglas-Kroll transformed Hamiltonian [39], and the finite nucleus, spin-free, Foldy-Wouthusen recontraction of the correlation consistent polarized valence double ζ [cc-pVDZ(fi/sf/fw)] basis set [40]. Core correlation corrections were evaluated with MOLPRO at the CCSD level, using the correlation consistent polarized core/valence double ζ (cc-pCVDZ) basis of Woon and Dunning [41]. At last, the outcome of Diagonal Born-Oppenheimer Corrections (DBOCs) [18] to adiabatic energies has been evaluated at the HF-SCF level, along with the cc-pVDZ and aug-cc-pVDZ basis sets, using the analytic approach by Handy *et al* [18a], which has been implemented in the CFOUR program package [42]. At the moment, the only other possible alternative for evaluating DBOCs with the latter package of programs is the CCSD approach, which remains intractable for computations on large open-shell systems like acenes in their triplet excited states. Recent calculations of the atomization energies of benzene, naphthalene, anthracene and tetracene indicate that a proper treatment of electron correlation should reduce the HF-SCF values for DBOCs by 25-30% [43]. Note that, in the latter study, DBOCs could not be generated at the level of second-order Møller-Plesset theory for anthracene and tetracene, which makes us believe that highly precise values for these corrections in systems as large as those we wish to address here will remain beyond reach for quite a while.

4.3 Results and discussion

In the present work, compared with ref. [15], the FPA analysis of both the singlet-triplet vertical (VE_{S-T}) and "well-to-well" (WWE_{S-T}) energy gaps was improved up to the FPA-5Z3 level for benzene, naphthalene, anthracene, and naphthacene. For larger acenes the FPA-5Z, FPA-5Z2, and FPA-5Z3 results that are provided in the sequel were extrapolated according to linear regressions upon the FPA-QZ results obtained for these four compounds. Similarly, FPA-AQZ values for the ST energy gap were computed for benzene, naphthalene, and anthracene, and reemployed in linear regressions in order to evaluate at the FPA-AQZ level the singlet-triplet energy gap of larger acenes from FPA-QZ results. In order to establish such regressions, additional data had to be generated for these compounds at intermediate levels (e.g. CCSD(T)/cc-pVDZ, MP4(SDQ)/(aug)-cc-pVTZ, S_{MP4-QZ} , S_{MP4-5Z}). For the completeness of the analysis, these additional data are provided in an appendix to this chapter, since they nicely confirm the convergence within chemical accuracy [1 kcal/mol] of each successive contribution to the ST energy gap, with respect to further improvements of the basis set.

Prior to considering the results of single-reference calculations on systems as large and reactive as octacene, nonacene, decacene and undacene, it is certainly useful to assess for these four systems the extent of static correlation, compared with smaller terms in the acene series. The T1 diagnostics of Coupled Cluster theory (< 0.012) and $\%TAE[(T)]$, as well as the percentages of the total atomization energy accounted for by parenthetical connected triple excitations indicate (Table 1) that all investigated compounds are largely dominated by dynamical correlation, and can thus be reliably and accurately described

according to high-level single-reference Coupled Cluster approaches converging to the full-CI limit.

Table 1. T1 diagnostics (CCSD/cc-pVDZ level of theory), and contributions (in %) from perturbative triple (T) excitations to Total Atomization Energies (TAEs), calculations based on the B3LYP/cc-pVTZ geometries for the singlet closed-shell electronic ground state).

	T1	%TAE[(T)] ^a	%TAE[(T)] ^b	%TAE[(T)] ^c	%TAE[(T)] ^d
Benzene	0.0098	1.39	1.47	1.83	1.90
Naphthalene	0.0103	1.56	1.66	2.03	
Anthracene	0.0106	1.66	1.77	2.15	
Naphthacene	0.0109	1.73	1.84	2.22	
Pentacene	0.0112	1.78	1.89		
Hexacene	0.0114	1.82	1.94		
Heptacene	0.0115	1.85	1.97		
Octacene	0.0116	1.87	2.00		
Nonacene	0.0117	1.89	2.02		
Decacene	0.0117	1.91	2.04	~2.42 ^e	~2.49 ^f
Undecacene	0.0117	1.92	2.06	~2.44 ^e	~2.51 ^f

a) Upon a comparison of CCSD/cc-pVDZ, CCSD(T)/cc-pVDZ and CCSD(T)/cc-pV ∞ Z (FPA-QZ) results for TAEs.

b) Upon a comparison of CCSD/cc-pVDZ with CCSD(T)/cc-pVDZ results for TAEs.

c) Upon a comparison of CCSD/cc-pVTZ with CCSD(T)/cc-pVTZ results for TAEs.

d) Upon a comparison of CCSD/cc-pVQZ with CCSD(T)/cc-pVQZ results for TAEs.

e) Estimate obtained by adding the difference between results obtained for naphthacene using the cc-pVQZ and cc-pVTZ basis sets to the result obtained using the cc-pVTZ basis set for decacene.

f) Estimate obtained by adding the difference between results obtained for naphthacene using the cc-pVQZ and cc-pVTZ basis sets to the result obtained using the cc-pVTZ basis set for undecacene.

According to the analysis by Karton and co-workers [14] of atomization energies within chemical accuracy, one of the most stringent tests of many-body quantum mechanical theories, %TAE[(T)] values below 2% indicate systems dominated by dynamical correlation, %TAE[(T)] values in between 2% and 4%–5% and in between 4%–5% and ~10% indicate mild and moderate nondynamical correlation, whereas values in excess of 10% are indicative of severe, nondynamical correlation. Also, T1 diagnostic values above 0.02 were

originally retained by Lee and Taylor [13] as indicative of significant non-dynamical correlation and as foretelling therefore a significant decrease of the reliability of CCSD-based results. Although the data reported in Table 1 undoubtedly reflect a smooth increase of the multi-reference character of the ground state electronic wave function upon enlarging the basis set and with increasing system size, they are still far from reaching the recommended warning thresholds. We thus conclude from Table 1 that our approach must enable highly quantitative insights into the singlet-triplet energy gap of acenes, and this up to undecacene.

Details of the focal point analysis of the vertical singlet-triplet energy gaps of octacene, nonacene, decacene and undecacene are displayed in Tables 2-5.

Table 2. Focal point analysis of the vertical singlet-triplet gaps of octacene (all results are given in kcal/mol).

OCTACENE				
# basis	cc-pVDZ	cc-pVTZ	cc-pVQZ	F/S-QZ
Δ HF	-16.22	-16.75	-16.86	-16.87 ^a
+MP2	57.56	59.98	60.88	61.52 ^b
+MP3	-17.00	-19.55		
+MP4(SDQ)	-8.99	-10.11		
+CCSD	-2.60			
+CCSD(T)	1.43			
Δ CCSD(T)	14.18			

a) F-QZ; b) S_{MP2} -QZ

Table 3. Focal point analysis of the vertical singlet-triplet gaps of nonacene (all results are given in kcal/mol).

NONACENE				
	cc-pVDZ	cc-pVTZ	cc-pVQZ	cc-pV ∞ Z
# basis	642	1448	2750	(F/S-QZ)
Δ HF	-22.73	-23.34	-23.45	-23.47 ^a
+MP2	66.86	69.84	70.88	71.60 ^b
+MP3	-20.39	-23.41		
+MP4(SDQ)	-10.85	-12.23		
+CCSD	-3.63			
+CCSD(T)	2.27			
Δ CCSD(T)	11.53			

a)F-QZ; b) S_{MP2}-QZ**Table 4.** Focal point analysis of the vertical singlet-triplet gaps of decacene (all results are given in kcal/mol).

DECACENE				
	cc-pVDZ	cc-pVTZ	cc-pVQZ	cc-pV ∞ Z
# basis	708	1596	3030	(F/S-QZ)
Δ HF	-28.25	-28.94	-29.07	-29.10 ^a
+MP2	77.74	81.47	82.69	83.52 ^b
+MP3	-24.40	-28.00		
+MP4(SDQ)	-13.17	-14.87		
+CCSD	-5.66			
+CCSD(T)	2.59			
Δ CCSD(T)	8.86			

a)F-QZ; b) S_{MP2}-QZ**Table 5.** Focal point analysis of the vertical singlet-triplet gaps of undecacene (all results are given in kcal/mol).

UNDECACENE				
	cc-pVDZ	cc-pVTZ	cc-pVQZ	cc-pV ∞ Z
# basis	774	1744	3310	(F/S-QZ)
Δ HF	-32.45	-33.24	-33.40	-33.43 ^a
+MP2	88.99	93.72	95.18	96.17 ^b
+MP3	-28.46	-32.77		
+MP4(SDQ)	-15.62	-17.68		
+CCSD	-7.94			
+CCSD(T)	3.20 ^c			
Δ CCSD(T)	7.73			

a)F-QZ; b) S_{MP2}-QZ; c) Extrapolated.

In these tables, the HF values for the singlet-triplet energies are reported as Δ_{HF} results. Values reported in the following rows under the +MP2, +MP3, +MP4, +CCSD, and +CCSD(T) entries correspond to the corrections obtained at the MP2, MP3, MP4, CCSD, and CCSD(T) levels, compared to the HF, MP2, MP3, MP4, and CCSD levels, respectively. As was reported already for hexacene and heptacene [15], we note that, whatever the employed basis set, the triplet state lies markedly below the singlet one at the HF level, whereas electron correlation yields a reversal in their energy order, and this whatever the order attained in the correlation potential. In other words, due to the neglect of dynamical correlation, HF theory incorrectly predicts the triplet state to be the electronic ground state of large acenes. For all systems, the second order (+MP2) terms are positive and strongly dominate the correlation corrections, and their convergence towards the CBS limit is much slower than that observed for the Δ_{HF} term. In line with the expected closure of the fundamental band gap, electron correlation amplifies with increasing system size, whereas the convergence of correlation corrections with respect to improving basis sets slightly degrades. We note that for decacene or undecacene, extrapolation to the $S_{\text{MP2-QZ}}$ level is required for ensuring a convergence of the $\Delta_{\text{MP2}} S_0\text{-}T_1$ excitation energy within chemical accuracy (1 kcal/mol). For all systems, the +MP2 corrections are mitigated by the +MP3, +MP4SDQ and +CCSD corrections, which are all negative and sharply decrease with the order attained in correlation. At last, perturbative triple excitations result into minor positive corrections to the vertical ST gaps of large acenes, ranging from 0.21 kcal/mol for pentacene up to 2.59 kcal/mol for decacene. In view of the convergence of these corrections compared with that observed up to the MP2 level, we expect a cc-pVTZ basis set to be large enough for determining the +MP3 and +MP4SDQ

corrections within or close to chemical accuracy (1 kcal/mol). Also, the +CCSD and +CCSD(T) corrections should be amenable within the same accuracy with a basis set of cc-pVDZ quality. Due to limitations in CPU time, it was not possible to determine explicitly the +CCSD(T)/cc-pVDZ corrections required for undecacene. The values that are reported for these corrections in Table 5 are therefore the results of an extrapolation (see Table 6) employing +CCSD(T) values obtained with the 6-31G and cc-pVDZ basis sets from lower terms in the acene series. In this extrapolation, we evaluate for each terms of the acene series the variation ($\Delta[+CCSD(T)/\{cc-pVDZ \leftarrow 6-31G\}]$) induced in the +CCSD(T) correction upon replacing the 6-31G basis set by the cc-pVDZ one, which appears to monotonously decrease with system size for systems larger than naphthacene (tetracene). In view of this evolution, the $\Delta[+CCSD(T)/\{cc-pVDZ \leftarrow 6-31G\}]$ correction is expected to lie at around -0.49 kcal/mol for decacene. Combined with a +CCSD(T)/6-31G correction of 3.69 kcal/mol, this results therefore for this compound into an extrapolated +CCSD(T)/cc-pVDZ correction of 3.20 kcal/mol to the vertical S_0-T_1 excitation energy.

Table 6. Extrapolation of +CCSD(T) and Δ CCSD(T) results for undecacene.

Vertical	benzene	naphthalene	anthracene	4cene	5cene	6cene	7cene	8cene	9cene	10cene	11cene
Δ CCSD/cc-pVDZ	105.45	79.69	57.73	42.26	31.79	23.31	17.70	12.75	9.26	6.27	4.53
+CCSD(T)/cc-pVDZ	0.00	-2.66	-0.33	-1.07	0.20	0.22	1.16	1.43	2.27	2.59	3.20^b
Δ CCSD(T)/cc-pVDZ	105.45	77.03	57.40	41.19	31.99	23.53	18.86	14.18	11.53	8.86	7.73^c
6-31G											
Δ CCSD/6-31G	105.98	80.37	58.81	43.62	33.34	25.10	19.69	14.98	11.70	8.93	7.37
+CCSD(T)/6-31G	-0.96	-2.83	-0.66	-1.20	0.08	0.18	1.22	1.57	2.56	2.98	3.69
Δ CCSD(T)/6-31G	105.02	77.54	58.15	42.42	33.42	25.28	20.91	16.55	14.26	11.91	11.06
Δ [+CCSD(T) {/cc-pVDZ \leftarrow 6-31G}] ^a	0.96	0.17	0.33	0.13	0.12	0.04	-0.06	-0.14	-0.29	-0.39	-0.49^d
Adiabatic											
benzene											
Δ CCSD/cc-pVDZ	89.49	65.73	46.59	33.21	23.90	16.52	11.51	7.19	4.27	1.70	0.01
+CCSD(T)/cc-pVDZ	0.44	-1.11	0.51	-0.16	1.05	1.08	2.03	2.32	3.21	3.58	4.31^b
Δ CCSD(T)/cc-pVDZ	89.93	64.62	47.10	33.05	24.95	17.60	13.54	9.51	7.48	5.28	4.32^c
6-31G											
Δ CCSD/6-31G	88.91	65.92	47.40	34.39	25.35	18.27	13.47	9.42	6.73	4.41	2.92
+CCSD(T)/6-31G	0.07	-1.28	0.19	-0.30	0.92	1.04	2.10	2.46	3.49	3.96	4.79
Δ CCSD(T)/6-31G	88.98	64.64	47.59	34.09	26.27	19.31	15.57	11.88	10.22	8.37	7.71
Δ [+CCSD(T) {/cc-pVDZ \leftarrow 6-31G}] ^a	0.37	0.17	0.32	0.14	0.13	0.04	-0.07	-0.14	-0.28	-0.38	-0.48^d

a) Variation induced upon the +CCSD(T) correction upon replacing the 6-31G basis set by the cc-pVDZ one.

b) Extrapolated value, obtained by adding the above Δ [+CCSD(T){/cc-pVDZ \leftarrow 6-31G}] variation to the +CCSD(T)/6-31G correction.

c) Extrapolated value, obtained by adding to the Δ CCSD/cc-pVDZ result the above extrapolated +CCSD(T)/cc-pVDZ correction.

d) Extrapolated variation, obtained upon comparing the results obtained for 9cene and 10cene.

Results obtained so far for the ST energy gap of *n*-acenes (*n*=1-11) according to various FPA protocols are summarized in Table 7.

Table 7. Estimates of the vertical singlet-triplet gaps of benzene and *n*-acenes (*n*=2-11; all results are given in kcal/mol). "Well to well" S_0 - T_1 excitation energies (WWE_{S-T}) results are in parenthesis. Best estimates in boldface.

	FPA-QZ	Maximal Error (FPA-QZ)	FPA-AQZ	FPA-5Z	FPA-5Z2	FPA-5Z3
Benzene	103.91 (91.97)	-0.42 (-0.82)	104.19 (-)	103.68 (91.79)	104.38 (92.23)	103.90 (91.73)
Naphthalene	76.03 (65.93)	-0.59 (-0.77)	76.17 (-)	75.90 (65.83)	76.26 (66.17)	76.02 (65.83)
Anthracene	56.87 (48.32)	-0.23 (-0.34)	56.79 (-)	56.87 (48.35)	57.09 (48.55)	56.77 (48.21)
Naphthacene	40.74 (33.88)	-0.47 (-0.58)	40.56 ^a (-)	40.74 (33.91)	40.78 (33.99)	40.36 (33.49)
Pentacene	31.66 (25.54)	-0.43 (-0.57)	31.42 ^a (-)	31.72 ^b (25.62) ^e	31.67 ^c (25.68) ^f	31.34 ^d (25.27) ^g
Hexacene	23.21 (17.98)	-0.55 (-0.68)	22.90 ^a (-)	23.30 ^b (18.10) ^d	23.16 ^c (18.11) ^e	22.84 ^d (17.71) ^g
Heptacene	18.48 (13.68)	-0.64 (-0.77)	18.14 ^a (-)	18.60 ^b (13.81) ^d	18.41 ^c (13.80) ^e	18.09 ^d (13.40) ^g
Octacene	13.81 (9.49)	-0.84 (-0.98)	13.43 ^a (-)	13.94 ^b (9.64) ^d	13.71 ^c (9.60) ^f	13.40 ^d (9.20) ^g
Nonacene	11.15 (7.29)	-1.00 (-1.14)	10.74 ^a (-)	11.29 ^b (7.45) ^d	11.03 ^c (7.40) ^f	10.72 ^d (7.00) ^g
Decacene	8.49 (4.94)	-1.31 (-1.42)	8.07 ^a (-)	8.64 ^b (5.10) ^d	8.36 ^c (5.03) ^f	8.05 ^d (4.64) ^g
Undecacene	7.73 (4.32)	-1.88 (-2.06)	7.12 ^a (-)	7.71 ^b (4.12) ^d	7.41 ^c (4.05) ^f	7.10 ^d (3.65) ^g

a) Extrapolated results; $FPA-AQZ=1.0076FPA-QZ-0.4861$.

b) Extrapolated results; $FPA-5Z=0.9961FPA-QZ+0.1866$.

c) Extrapolated results; $FPA-5Z2=1.0062FPA-QZ-0.1847$.

d) Extrapolated results; $FPA-5Z3=1.0052FPA-QZ-0.4854$.

e) Extrapolated results; $FPA-5Z=0.9960FPA-QZ+0.1878$.

f) Extrapolated results; $FPA-5Z2=1.0021FPA-QZ+0.0880$.

g) Extrapolated results; $FPA-5Z3=1.0016FPA-QZ-0.3037$.

Differences in between results obtained up to the FPA-5Z3 model for the smallest terms of the acene series are far below 1 kcal/mol, which allows quantitative extrapolations to the FPA-5Z3 level of results obtained using protocols of lower quality for the longest terms of the series, by virtue of linear regression of extremely high quality ($r^2=1.0000$). Note in particular that the

incorporation of diffuse functions in the basis sets does obviously not significantly affect the extrapolated CBS values for the S_0 - T_1 excitation energies. FPA-QZ and FPA-AQZ results obtained for benzene, naphthalene and anthracene (Table 7) do not differ indeed by more than 0.3 kcal/mol. Discrepancies between the different FPA results for the vertical (adiabatic) S_0 - T_1 excitation energies of n -acenes do not exceed 0.38 (0.41), 0.46 (0.40), 0.51 (0.41), 0.54 (0.44), 0.57 (0.45), 0.59 (0.46), 0.60 (0.47) kcal/mol, when $n=5-11$, respectively, indicating convergence of our treatment of electron correlation within chemical (1 kcal/mol) accuracy, with the FPA-5Z3 values representing our best estimates for the vertical (VE_{S-T}) and well-to-well (WWE_{S-T}) singlet-triplet energy gaps of n -acenes.

The interested reader is referred further to Table 8 for statistical correlations between our FPA-QZ estimates with the results of lower level calculations until decacene. Clearly, the outcome of a dual extrapolation to the CCSD(T)/CBS limit by virtue of a Focal Point Analysis can be reliably predicted from linear regressions employing MP4SDQ/cc-pVDZ, CCSD/cc-pVDZ or CCSD(T)/cc-pVDZ as row inputs.

Some care is needed however, because it is well-known that at a correlated level, the influence of the basis set increases with system size, especially when working with large conjugated systems, due to the closure of the band gap [11]. Individual estimates for (maximal) errors in dual extrapolations of vertical and well-to-well singlet-triplet energy gaps towards the CCSD(T)/CBS limit, according to the principles of the FPA-QZ analysis, are therefore also reported separately for each compounds in Table 7. These estimates are based on comparisons with extrapolated results obtained by simply and rather roughly adjusting the +MP3+MP4(SDQ)/cc-pVTZ, and +CCSD

+CCSD(T)/cc-pVDZ corrections to the CBS limit according to linear ratios between the +MP2/CBS, +MP2/cc-pVTZ and +MP2/cc-pVDZ values. ST-energy gaps obtained with this approach are systematically lower than the FPA-QZ values.

Table 8. Correlation between FPA-QZ and lower level methods for vertical S_0 - T_1 energy gaps of Benzene and n -Acenes [$n=2-11$] (“Well to well” (WWE_{S-T}) results are in parenthesis).

Method	A	B	R ²
MP2/cc-pVDZ	1.0717 (1.1435)	-25.498 (-32.409)	0.8981 (0.8377)
MP3/cc-pVDZ	1.0349 (1.1106)	-10.057 (-12.442)	0.9842 (0.9752)
MP4SDQ/cc-pVDZ	0.9746 (1.0222)	-0.7734 (-1.1131)	0.9981 (0.9971)
CCSD/cc-pVDZ	0.9548 (0.9861)	1.5590 (2.3074)	0.9990 (0.9991)
CCSD(T)/cc-pVDZ	0.9885 (1.0264)	-0.1199 (-0.2302)	1.0000 (1.0000)

Therefore, due to the increasing influence of the basis set, expected overestimations of the vertical (adiabatic) singlet-triplet energy gap with the FPA-QZ approach increases from 0.23 (0.34) kcal/mol for anthracene up to 1.88 (2.06) kcal/mol for undecacene. Considering that higher-order corrections in correlation are known to converge faster with the basis set than lower-order ones, these error estimates are most certainly largely overestimated, especially for decacene and nonacene.

The reader is referred to Table 9 for a comparison of our best FPA-5Z3 theoretical estimates with available experimental values. In this table, we provide theoretical values for adiabatic transition energies obtained by adding B3LYP/cc-pVTZ estimates for changes induced by the transition upon zero-point vibrational energies ($\Delta ZPVEs$) to the WWE_{S-T} energy differences.

Table 9. Calculated and experimental singlet-triplet energy gaps of benzene and *n*-acenes, along with zero-point vibrational energy (ΔZPE) and geometry relaxation (GRXE) contributions. All results are given in kcal/mol.

	VE_{S-T} CCSD(T)/ cc-pV ∞ Z ^a	WWE_{S-T} CCSD(T)/ cc-pV ∞ Z ^a	GRXE WWE_{S-T} VE_{S-T}	ΔZPE B3LYP/ cc-pVTZ	$\langle T S^2 T \rangle$ B3LYP/ cc-pVTZ	AE_{S-T} CCSD(T)/ cc-pV ∞ Z ^{a,b}	Experimental
BENZENE	100.36 ^c	91.73	-8.63	-5.20	2.0494	86.53	84.34 ^d
NAPHTHALENE	76.02	65.83	-10.19	-3.31	2.0237	62.52	60.90 ^e , 61.00 ^f
ANTHRACENE	56.77	48.21	-8.56	-2.29	2.0207	45.92	42.60 ^g , 43.10 ^h
NAPHTHACENE	40.36	33.49	-6.87	-1.78	2.0259	31.72	29.45 ⁱ
PENTACENE	31.34	25.27	-6.07	-1.42	2.0289	23.85	19.83 \pm 0.70 ^j
HEXACENE	22.84	17.71	-5.13	-1.21	2.0322	16.50	12.43 \pm 1.20 ^k
HEPTACENE	18.09	13.40	-4.69	-1.07	2.0351	12.33	
OCTACENE	13.40	9.20	-4.20	-0.99	2.0379	8.21	
NONACENE	10.72	7.00	-3.72	-0.95	2.0403	6.05	
DECACENE	8.05	4.64	-3.41	-0.97	2.0425	3.67	
UNDECACENE	7.10	3.65	-3.45	-1.07	2.0444	2.58	
Infinite size	1.42 ^l	0.15 ^m				-1.06 ⁿ	
Infinite size	1.86 ^o	0.18 ^p				-1.06 ^q	

a) FPA-5Z3 estimate (see text for details).

b) Upon adding ΔZPE corrections to WWE_{S-T} CCSD(T)/cc-pV ∞ Z data.

c) Symmetry-corrected result, the non-corrected one is 103.90.

d) In Ar or Methane matrix at 4K, for details see Ref. [19] and references therein.

e) In ether-isopentane-alcohol or related (solid) solvents (EPA+) at 77K, for details see Ref. [19] and references therein.

f) From Ref. [20]. (No experimental details were provided).

g) In ether-isopentane-alcohol or related (solid) solvents (EPA+) at 77K, for details see Ref. [19] and references therein.

h) From Ref. [44]. Gas phase photodetachment photoelectron spectroscopy, refers to the difference between Vertical Anion to Singlet and Vertical Anion to Triplet state.

i) Poly-methylmethacrylate matrix at room temperature, for details see Ref. [19] and references therein.

j) In naphthalene matrix at room temperature, for details see Ref. [45].

k) In silicone oil at room temperature, for details see Ref. [46].

- l) Using the formula $1.4237 + 134.57e^{-0.30147n}$ $R^2 = 0.9997$ (benzene-decacene).
m) Using the formula $0.15499 + 127.03e^{-0.32797n}$ $R^2 = 0.9999$ (benzene-decacene).
n) Using the formula $-1.0627 + 120.44e^{-0.31841n}$ $R^2 = 0.9999$ (benzene-decacene).
o) Using the formula $1.8554 + 134.49e^{-0.30445n}$ $R^2 = 0.9997$ (benzene-undecacene).
p) Using the formula $0.17983 + 127.02e^{-0.32819n}$ $R^2 = 0.9999$ (benzene-undecacene).
q) Using the formula $-1.0551 + 120.44e^{-0.31847n}$ $R^2 = 0.9999$ (benzene-undecacene).

Geometrical relaxation energies (GRXEs) are also evaluated according to the FPA-5Z3 protocol by comparing the vertical and well-to-well singlet-triplet energy gaps. In line with the increased delocalization of the molecular orbitals, geometrical relaxation energies and $\Delta ZPVE$ corrections smoothly decrease with increasing system size, when $n=1-10$, due to the increasing delocalization of the orbitals that are involved in the transition. A reversal in these trends is nonetheless observed around $n=10$, which may either relate to the onset of a localization of the S_0-T_1 excitation onto an excitonic wave, or be the result of an increasing spin-contamination of the B3LYP/cc-pVTZ wave function of the triplet excited state, in the form of slight deviations from the expected value (2) for the S^2 operator in this state. The main factor limiting the accuracy of our calculations in vacuum is most probably not the solution of the electronic Schrödinger equation, but that of the *nuclear* Schrödinger equation [47]. Besides, large-amplitude motions induced by thermal excitations are also known to significantly influence the electronic excitation spectrum of large conjugated systems [48]. As was pointed out already [15], our best estimates for the ST energy gaps of benzene and acenes at 0K in vacuum systematically overestimate the available experimental values by ~ 3 to ~ 4 kcal/mol. Most of these values were obtained from measurements in solutions and glassy matrices and are therefore subject to complications due to intermolecular interactions and packing effects. Bathochromic shifts of the order of several kcal/mol are far from being uncommon when polycyclic aromatic hydrocarbons become exposed to such interactions, as for instance in zeolites [49]. Further geometrical complications are also quite likely in the case of photoelectron detachment experiments on mass-selected anions, as was for instance the case with anthracene.

To our knowledge, there are no spectroscopic data available for the lowest triplet excited state for acenes larger than hexacene, which prevents us from doing any straightforward comparison with experimental S_0-T_1 excitation energies. Extrapolation of our FPA-5Z3 data for benzene and n -acenes ranging from naphthalene ($n=2$) to undecacene ($n=11$) according to a least-square fitting function of the form $a+be^{-c}$ indicates a vanishing S_0-T_1 energy gap in the limit $n \rightarrow \infty$. The accuracy in this limit is of the order of ~ 1.5 kcal/mol (0.06 eV), considering the differences observed between the vertical (VE_{S-T}), well-to-well (WWE_{S-T}) and adiabatic (AE_{S-T}) estimates, which ought to converge to the same value when $n \rightarrow \infty$, in the absence of complications such as localizations of the electronic transitions into excitonic waves and local disruptions thereby of translation symmetry.

Residual differences from these least square fits do not exceed 1.3 kcal/mol. It is worth noticing therefore that extending our FPA analysis at the FPA-5Z3 level until undecacene has enabled us therefore to considerably reduce the uncertainty upon the S_0-T_1 energy gap of an infinite periodic acene chain, which will most certainly display all features that characterize a truly metallic system, including the possibility of undergoing easily spin-flip transitions. This view corroborates the absence of Peierls distortions in the polymer limit [8e], i.e. the absence of any alternation between outer bond lengths in this limit [8b,8d], and the closure of the fundamental gap therefore (see Fig. 2 in Ref. 50). It is certainly useful to note at this stage that our final CCSD(T)/cc-pV ∞ Z (FPA-5Z3) estimates (1.4 to 1.8 kcal/mol) of the vertical ST gap in the polymer limit is all in all rather close to that (3.33 kcal/mol) proposed by Hatchman *et al* [8c], based on an extrapolation of CASCI/cc-pVDZ data obtained for compounds ranging from naphthalene up to hexacene.

Since each further excitation which is included in the Coupled-Cluster equations is one order of magnitude closer to the FCI energy, we do not expect quadruple and higher excitations to result into corrections exceeding ~ 0.1 kcal/mol (octacene) to ~ 0.4 kcal/mol (undecacene). Theoretical studies aiming at sub-chemical (~ 0.1 kcal/mol) or even spectroscopic (a few cm^{-1}) accuracy recommend the computations of further small correction terms, like those due to core correlation, scalar relativistic effects, and Diagonal Born-Oppenheimer Corrections (DBOCs). Prior to closing this discussion, the reader is therefore referred to Table 10 for an evaluation of these contributions to the vertical and/or adiabatic singlet-triplet energy gaps of benzene and larger acenes up to undecacene. All these individual corrections remain individually smaller than the requested accuracy (1 kcal/mol). For vertical transition energies, core correlation corrections are almost totally insignificant, whereas scalar relativistic corrections oscillate in between -0.31 (pentacene) and -0.58 kcal/mol (benzene) or -0.38 kcal/mol (undecacene). For adiabatic transition energies, scalar relativistic corrections evolve smoothly from 0.57 kcal/mol (benzene) to -0.31 kcal/mol (undecacene). If core correlation corrections to adiabatic singlet-triplet energy gaps appear to be quite significant for the smallest terms of the series (up to 0.48 kcal/mol, in the case of benzene), their influence decay rapidly with increasing system size, in line with the lesser importance of structural relaxation for the longest terms of the series. At last, UHF geometries are not very reliable for triplet states of large conjugated systems, due to strong electronic instabilities, and result therefore in most doubtful DBOC corrections, that evolve erratically with increasing system.

Table 10. Evaluation the extent of scalar relativistic (REL), core correlation (CC) and diagonal Born-Oppenheimer (DBOC) corrections to the vertical (ΔE^V) and/or adiabatic (ΔE^A) singlet-triplet energy gap of benzene and *n*-acenes ($n=2-11$).

	$\Delta E^V(\text{REL})$ B3LYP/ DZ ^a	$\Delta E^A(\text{REL})$ B3LYP/ DZ ^b	$\Delta E^V(\text{CC})$ CCSD/ DZ ^c	$\Delta E^A(\text{CC})$ CCSD/ DZ ^d	$\Delta E^A(\text{DBOC})$ HF/ cc-pVDZ ^e	$\Delta E^A(\text{DBOC})$ HF/aug- cc-pVDZ ^e
BENZENE	- ^f	0.57	0.01	0.48	0.09	0.10
NAPHTHALENE	-0.58	0.52	0.02	0.35	0.11	0.12
ANTHRACENE	-0.40	0.49	0.00	0.25	0.36	0.51
NAPHTHACENE	-0.33	0.38	0.00	0.18	0.88	-
PENTACENE	-0.31	0.26	-0.01	0.12	0.59	-
HEXACENE	-0.31	0.15	-0.01	0.08	0.40	-
HEPTACENE	-0.32	0.05	-0.01	0.05	0.33	-
OCTACENE	-0.33	-0.05	-0.02	0.02	0.42	-
NONACENE	-0.35	-0.15	-	-	0.66	-
DECACENE	-0.37	-0.24	-	-	1.54	-
UNDECACENE	-0.38	-0.31	-	-	₉	-

a) $\Delta E^V(\text{REL}) = \{E[\text{T},\text{B3LYP},\text{DKH2},\text{cc-pVDZ}(\text{fi/sf/fw})] - E[\text{S},\text{B3LYP},\text{DKH2},\text{cc-pVDZ}(\text{fi/sf/fw})]\} - \{E[\text{T},\text{B3LYP},\text{NONREL},\text{cc-pVDZ}] - E[\text{S},\text{B3LYP},\text{NONREL},\text{cc-pVDZ}]\}$, using B3LYP/cc-pVTZ optimized geometries for the initial singlet ground state.

b) $\Delta E^A(\text{REL}) = \{E[\text{T},\text{B3LYP},\text{DKH2},\text{cc-pVDZ}(\text{fi/sf/fw})] - E[\text{S},\text{B3LYP},\text{DKH2},\text{cc-pVDZ}(\text{fi/sf/fw})]\} - \{E[\text{T},\text{B3LYP},\text{NONREL},\text{cc-pVDZ}] - E[\text{S},\text{B3LYP},\text{NONREL},\text{cc-pVDZ}]\}$, using the B3LYP/cc-pVTZ optimized geometries for the initial singlet ground state and final triplet excited state.

c) $\Delta E^V(\text{CC}) = \{E[\text{T},\text{CCSD},\text{FULL},\text{cc-pCVDZ}] - E[\text{S},\text{CCSD},\text{FULL},\text{cc-pCVDZ}]\} - \{E[\text{T},\text{CCSD},\text{frozen-core},\text{cc-pVDZ}] - E[\text{S},\text{CCSD},\text{frozen-core},\text{cc-pVDZ}]\}$, using the B3LYP/cc-pVTZ optimized geometries for the initial singlet ground state.

d) $\Delta E^A(\text{CC}) = \{E[\text{T},\text{CCSD},\text{FULL},\text{cc-pCVDZ}] - E[\text{S},\text{CCSD},\text{FULL},\text{cc-pCVDZ}]\} - \{E[\text{T},\text{CCSD},\text{frozen-core},\text{cc-pVDZ}] - E[\text{S},\text{CCSD},\text{frozen-core},\text{cc-pVDZ}]\}$, using the B3LYP/cc-pVTZ optimized geometries for the initial singlet ground state and final triplet excited state.

e) DBOC corrections obtained using HF/cc-pVDZ geometries for the initial singlet ground state and final triplet excited state.

- f) An aberrant value of 12.59 kcal/mol was obtained, presumably because of the symmetry breaking in the electronic wave function for the triplet excited state of benzene which is inherent to a calculation under the constraint of a D_{6h} point group, and the non point-like description of nuclei.
- g) Unconverged geometry.

Whereas UB3LYP always gives a geometry of D_{2h} symmetry, in their first triplet excited state, benzene and n -acenes exhibit correspondingly at the UHF level an erratic and most doubtful symmetry point group: D_{2h} ($n=1$), C_s ($n=2$), C_{2v} ($n=3$), D_{2h} ($n=4-10$), corresponding to geometries with far too pronounced and unrealistic bond length alternations. Also, the lower symmetry of the nuclear framework prevented us to compute DBOCs for the triplet state of undecacene. Developments of appropriate schemes employing Density Functional Theory seem therefore very much needed for assessing the extent of DBOCs in large conjugated systems, especially when considering open-shell excited states. For a complete treatment of relativistic effects, spin-orbit coupling interactions should also be considered.

4.4 Conclusions and further challenges to theoreticians

The vertical singlet-triplet excitation energies of n -acenes ranging from octacene to undecacene have been quantitatively determined from an extrapolation of the results of single-reference many-body calculations to the confines of nonrelativistic quantum mechanics for solving the electronic Schrödinger equation in clamped-nuclei configurations, upon considering that the T1 diagnostics of Coupled Cluster theory and further energy-based criteria indicate that a single-reference depiction prevails for the electronic singlet ground state. The present study is based on various Focal Point Analyses (FPAs) that exploit the overall smooth and regular convergence of electronic energy differences with regards to the size of the basis set and level of correlation attained in calculations employing the HF, MP2, MP3, MP4SDQ, CCSD, and CCSD(T) approaches along with increasingly complete Dunning's correlation consistent polarized valence basis sets (up to 3310 basis functions for undecacene). Such

analyses allow us to perform extrapolations to the CCSD(T) level in conjunction with asymptotically complete basis sets, up to the so called FPA-5Z3 level [Eq. (5)], which amounts specifically to an extrapolation to the CCSD(T)/cc-pV ∞ Z level, based on three-point Feller's and Schwartz's extrapolations of HF total energies and MP2 correlation energies obtained using Dunning's cc-pVXZ basis sets ($X=\{D,T,Q,5\}$), in combination with +MP3/cc-pV ∞ Z, +MP4SDQ/cc-pV ∞ Z, +CCSD/cc-pVTZ, and +CCSD(T)/cc-pVTZ corrections. Discrepancies between the different FPA results for the vertical and adiabatic S_0-T_1 excitation energies of all n -acenes investigated so far ($n=1-11$) do not exceed 0.6 kcal/mol (0.026 eV). This observation along with our analysis of multi-reference effects makes us believe that, regardless of possible complications pertaining to nuclear motions or relativistic effects, we have managed to grasp the lowest excitation energies of acenes up to undecacene in vacuum within or close to chemical accuracy (1 kcal/mol, i.e. 43.4 meV). In line with data by Hatchmann *et al* [8c], further extrapolations with respect to system size indicate within an accuracy of ~ 1.5 kcal/mol (~ 0.06 eV) that both the lowest vertical and adiabatic ST excitation energies tend to vanish in the polymer limit ($n \rightarrow \infty$). In view of the trends that emerge from our calculations, it seems quite likely that finite acenes approaching the polymer limit would still possess a singlet electronic ground state, with a total spin equal to zero. We wish nonetheless to emphasize that by no means this latter conclusion implies that the singlet electronic ground state of large acenes converging to the polymer limit would exhibit antiferromagnetically ordered edge states, which would most obviously result into a diverging and basically uncontrollable spin-contamination, due to giant and artefactual symmetry-breakings in spin-densities [15].

There are still at this stage some challenging and most puzzling issues regarding the electronic structure and related properties of large n -acenes, that certainly deserve further investigations and discussions. For instance, according to Tönshoff and Bettinger [5], the optical absorption threshold of octacene and nonacene is located at 377 nm (3.29 eV, i.e. 75.84 kcal/mol) and 418 nm (2.97 eV, i.e. 68.40 kcal/mol), respectively. Zade and Bendikov report correspondingly [51] optical and electrochemical HOMO-LUMO gaps of 1.35 and 1.38 eV (i.e. 31.13 kcal/mol and 31.82 kcal/mol, respectively) – thus far above all calculated S_0 - T_1 energy gaps so far. Assuming that no other optical transitions fall below the observed and so-called p-bands, extrapolation of available experimental UV-Vis data through an exponential fit gives an optical gap of 1.18 ± 0.06 eV, i.e. 27.21 ± 1.39 kcal/mol, in the limit of an infinite periodic acene chain [5], whereas the FPA-5Z3 analysis led us to conclude that the S_0 - T_1 energy gap identically vanishes in this limit, with an uncertainty of the order of 1.5 kcal/mol (0.06 eV). Considering that preliminary B3LYP/cc-pVTZ calculations upon model twisted or curved structures (see Figure 1 and the analysis therein) indicate that large out-of-plane distortions may certainly result into a very substantial decrease of the HOMO-LUMO gap of nonacene, it is quite possible that this huge difference between the theoretical S_0 - T_1 and optical S_0 - S_1 band gaps is the result of structural distortions left by the photogeneration of octacene and nonacene in a rigid solid argon matrix from twisted diketone precursors. Note in particular that Bettinger *et al* [4b,5] discarded weak structures in the optical absorption spectrum of pentacene, hexacene, heptacene, octacene and nonacene [4b,5], at excitation energies below the HOMO-LUMO optical threshold, which were precisely thought to be the result of deviations from the expected planarity, due to constraints imposed by the matrix host (in their works, Bettinger and co-

workers locate the HOMO-LUMO gap at the maximum in absorption of the optically brightest band).

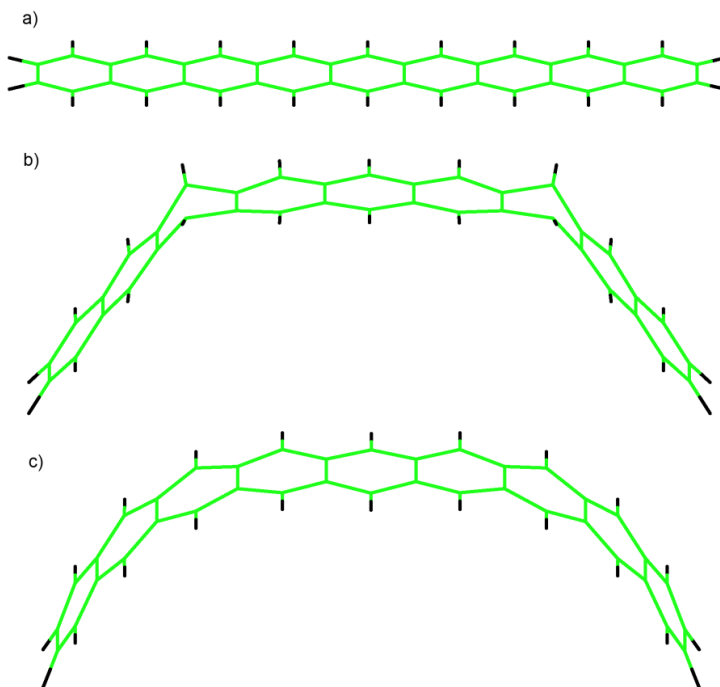


Figure 1. Preliminary (B3LYP/cc-pVTZ) study of the outcome of out-of-plane distortions left by the photogeneration of nonacene in a rigid solid argon matrix from twisted diketone precursors. Whereas a planar structure produces a HOMO-LUMO gap of 1.05 eV, a twisted (b) and a curved (c) structure exhibit HOMO-LUMO gaps equal to 0.79 and 0.45 eV, respectively. These two latter structures lie at 139.89 and 39.94 kcal/mol above the planar structure, respectively. In line with the three-dimensional molecular architecture of the photoprecursor 6 in ref. [5], the twisted and curved structures were optimized upon freezing all dihedral angles in the third and seventh rings to their values prior to removing the two diketone bridges in this precursor, and upon imposing an out-of-plane displacements of 5.30 Å and 5.16 Å in between the end and central carbon atoms, respectively.

This huge difference between the theoretical S_0 - T_1 and optical S_0 - S_1 band gaps in the polymer limit may also be the outcome of the energy costs required for spin-flip processes in finite systems. Indeed, CC2/cc-pVTZ calculations on octacene ($n=2,3,4,5,6,8$) locate for instance the optical absorption threshold (S_0 - S_1 energy gap) at 1.43 eV [28], which by comparison with our FPA-5Z3 value (0.58 eV) for the S_0 - T_1 gap indicates a T_1 - S_1 energy difference around 0.85 eV (i.e. 6855 cm^{-1} or 19.60 kcal/mol). This observation is quantitatively in line with the T_1 - S_1 energy differences reported by Nijegorodov [52] for n -acenes ($n=1,6$), which regularly decrease from 11660 cm^{-1} down to 8000 cm^{-1} when n increases from 3 to 6. Nevertheless, by analogy with dissociating H_2 , or considering that bielectronic interactions scale in general like n^{-1} in homogeneous oligomer series [53] (with n the number of monomer units in the chain), one would intuitively expect that the T_1 - S_1 energy difference identically vanishes at infinite system size, unless electronic excitations localize into excitonic waves. A further complication in the analysis may arise because of the role played by double electronic excitations. Indeed, according to recent ADC(2)-x and DFT/MRCI data (see ref. [54] and references therein), the first doubly excited state becomes the lowest singlet excited state of n -acenes larger than pentacene or hexacene. Note correspondingly the presence of a very low-lying shake-up $\pi^{-2}\pi^{*+1}$ state in the ADC(3) ionization spectrum of pentacene [55]. Further benchmark many-body quantum mechanical studies of energy demands for spin-flip and double electronic excitation processes would therefore certainly be most necessary for unravelling (or predicting) the electrochemical, magnetic and optical properties of large n -acenes.

4.5 References

- [1] (a) C. D. Dimitrakopoulos, S. Purishotoman, J. Kymissis, A. Callegari, and M. J. Shaw, *Science* **283**, 822 (1999); (b) S. Verlaak, S. Steudel, P. Heremans, D. Janssen, and M. S. Deleuze, *Phys. Rev. B*, **68**, 195409 (2003); (c) M. Bendikov, F. Wudl, D. F. Perepichka, *Chem. Rev.* **104**, 4891 (2004); (d) J. E. Anthony, *Chem. Rev.* **106**, 5028 (2006); (e) F. Würtner, R. Schmidt, *ChemPhysChem*, **7**, 793 (2006).
- [2] W. Schmidt, D. Biermann, *J. Am. Chem. Soc.* **102**, 3163 (1980).
- [3] R. Mondal, B. K. Shah, D. C. Neckers, *J. Am. Chem. Soc.* **128**, 9612 (2006).
- [4] (a) H. F. Bettinger, R. Mondal, D. C. Neckers, *Chem. Commun.*(Cambridge, U. K.), 5209 (2007); (b) R. Mondal, C. Tönshoff, D. Khon, D. C. Neckers, H. F. Bettinger, *J. Am. Chem. Soc.* **131**, 14281 (2009).
- [5] C. Tönshoff, H. F. Bettinger, *Angew. Chem.* **49**, 4125 (2010).
- [6] J. E. Anthony, *Angew. Chem. Int. Ed.* **47**, 452 (2008).
- [7] (a) M. M. Payne, S. R. Parkin, J. E. Anthony, *J. Am. Chem. Soc.* **127**, 8028 (2005); (b) D. Chun, Y. Cheng, F. Wudl, *Angew. Chem. Int. Ed.* **47**, 8380 (2008); (c) I. Kaurr, N. N. Stein, R. P. Kopreski, G. P. Miller, *J. Am. Chem. Soc.* **131**, 3424 (2009).
- [8] (a) M. Bendikov, H. M. Duong, K. Starkey, K. N. Houk, E. A. Carter, F. Wudl, *J. Am. Chem. Soc.* **126**, 7416 (2004); **126**, 10493 (Erratum) (2004); (b) M.C. Dos Santos, *Phys. Rev. B* **74**, 045426 (2006); (c) J. Hachmann, J. J. Dorando, M. Avilès, G. K.-L. Chan, *J. Chem. Phys.* **127**, 134309 (2007); (d) D. Jiang, S. Dai, *J. Phys. Chem. A*, **112**, 332 (2008); (e) D.-E. Jiang, S. Dai, *Chem. Phys. Lett.*, **466**, 72 (2008); (f) Z. Qu, D.

- Zhang, C. Liu, Y. Jiang, *J. Phys. Chem. A*, **113**, 7909 (2009); X. Gao, J.-L. Hodgson, D. E. Jiang, S. B. Nagase, G. P. Miller, Z. Chen, *Org. Lett.* **13**, 3316 (2011);
- [9] (a) H. Angliker, E. Rommel, J. Wirz, *Chem. Phys. Lett.* **87**, 208 (1982); (b) N. Nijegorodov, V. Ramanchandran, D. P. Winkoun, *Spectrochim. Acta*, **53**, 1813 (1997).
- [10] (a) J. Poater, J. M. Bofill, P. Alemany, M. Solà, *J. Phys. Chem. A*. **109**, 10629 (2005); (b) T. Ishida and J. Aihara, *Phys. Chem. Chem. Phys.* **11**, 7197 (2009).
- [11] (a) M. S. Deleuze, L. Claes, E. S. Kryachko, and J.-P. François, *J. Chem. Phys.* **119**, 3106 (2003); (b) B. Hajgató, M. S. Deleuze, D. J. Tozer, and F. De Proft, *J. Chem. Phys.* **129**, 084308 (2008).
- [12] (a) G. D. Purvis, and R. J. Bartlett, *J. Chem. Phys.* **76**, 1910 (1982); (b) G. E. Scuseria, C. L. Janssen, and H. F. Schaefer, III. *J. Chem. Phys.* **89**, 7382 (1988); (c) K. Raghavachari, G. W. Trucks, M. Head-Gordon, and J. A. Pople, *Chem. Phys. Lett.* **157**, 479 (1989); (d) R. J. Bartlett, *J. Phys. Chem.* **93**, 1697 (1989).
- [13] T. J. Lee, P. R. Taylor, *Int. J. Quantum Chem., Quantum Chem. Symp.* **23**, 199 (1989).
- [14] A. Karton, E. Rabinovitch, J. M. L. Martin, B. Ruscic, *J. Chem. Phys.* **125**, 144108 (2006).
- [15] B. Hajgato, D. Szieberth, P. Geerlings, F. De Proft, M. S. Deleuze, *J. Chem. Phys.* **131**, 224321 (2009).
- [16] G. Gidofalvi and D. Mazziotti, *J. Chem. Phys.*, **129**, 134108 (2008).
- [17] (a) R. D. Cowan, M Griffin, *J. Opt. Soc. Am.* **66**, 1010 (1976); (b) R. L. Martin, *J. Phys. Chem.* **87**, 750(1983).

- [18] (a) N. C. Handy, Y. Yamaguchi, H. F. Schaefer III, *J. Chem. Phys.* **84**, 4481(1986); (b) N. C. Handy, *Chem. Phys. Lett.* **252**, 425 (1996); (c) W. Kutzelnigg, *Mol. Phys.* **90**, 909 (1997); (d) D. W. Schwenke, *J. Phys Chem. A*, **105**, 2352(2001); (e) E. F. Valeev, C. D. Sherrill, *J. Chem. Phys.* **118**, 3921(2003); (f) A. Tajti, P. G. Szalay, A. G. Csaszar, M. Kallay, J. Gauss, E. F. Vallev, B. A. Flowers, J. Vasquez, J. F. Stanton, *J. Chem. Phys.* **121**, 11599 (2004); (g) J. Gauss, A. Tajti, M. Kallay, J. F. Stanton, P. G. Szalay, *J. Chem. Phys.* **125**, 144111 (2006).
- [19] (a) S. Grimme, M. Parac, *Chem. Phys. Chem.* **4**, 292 (2003); (b) C.M. Marian and N. Gilka, *J. Chem. Theory and Comput.* **4**, 1501 (2008).
- [20] S. Grimme, M. Waletzke, *J. Chem. Phys.* **111**, 5645 (1999).
- [21] F. Janssen, "Introduction to Computational Chemistry", (Wiley, Chichester, 1999).
- [22] R. Dreizler, E. Gross, *Density Functional Theory* (Plenum Press, New York, 1995).
- [23] (a) C. Lee, W. Yang, and R. G. Parr, *Phys. Rev. B* **37**, 785 (1998); (b) A. D. Becke, *J. Chem. Phys.* **98**, 5648 (1993).
- [24] T. H. Dunning, Jr., *J. Chem. Phys.* **90**, 1007 (1989).
- [25] (a) R. M. Balabin, *J. Chem. Phys.* **129**, 164101 (2008); (b) R. M. Balabin, *Mol. Phys.* **943**, 2011 (2011).
- [26] (a) N. L. Allinger, J. T. Ferman, W. D. Akken and H. F. Schaefer III, *J. Chem. Phys.* **106**, 5143 (1997); (b) A. G. Császár, W. D. Allen, H. F. Schaefer III, **108**, 9751 (1998); (c) A. Salam, M. S. Deleuze, *J. Chem. Phys.*, **116**, 1296 (2002); (d) E. Czinski, A. G. Császár, *Chem. Eur. J.*, **9**, 1008 (2003); (e) E. Czinki, A. G. Császár, *Chem. Eur. J.* **9**, 1008 (2003); (f) S. P. Kwasniewski, L. Claes, J.-P. François and M. S. Deleuze, *J. Chem.*

- Phys. **118**, 7823 (2003); (g) K. Kahn; T. C. Bruice, *Theor. Chem. Acc.* **111**, 18 (2004); (h) A. G. Császár, V. Szalay, M. L. Senent, *J. Chem. Phys.*, **120**, 1203 (2004); (i) K. Kahn, T. C. Bruice, *Chem. Phys. Chem.* **6**, 487 (2005); (j) K. Kahn, I. Kahn, *J. Comp. Chem.* **29**, 900 (2008); (k) J. Demaison, J. Liévin, A. G. Császár, C. Guttle, *J. Phys. Chem. A*, **112**, 4427 (2008); (l) O. S. Bokareva, V. A. Bataev, *Int. J. Quantum Chem.* **108**, 2719 (2008); (m) T. Szidarovszky, G. Czakó, A. G. Császár, *Mol. Phys.* **107**, 761 (2009); (n) J. J. Wilke, M. C. Lind, H. F. Schaefer III, A. G. Császár, and A. D. Allen, *J. Chem. Theor. Comp.*, **5**, 1511 (2009); (o) R. M. Balabin, *Chem. Phys. Lett.* **479**, 195 (2009); (p) E. V. Rastotseva, V. A. Bataev, I. A. Godunov, *J. Mol. Struct. (THEOCHEM)* **905**, 86 (2009); (q) G. A. Çiftçioğlu, C. Trindle, I. Yavuz, *Mol. Phys.* **108**, 2601 (2010); (r) R. M. Balabin, *Comp. Theor. Chem.* **965**, 15 (2011).
- [27] G. Tarczay, A. G. Császár, W. Klopper, V. Szalay, *J. Chem. Phys.* **110**, 11971 (1999).
- [28] (a) S. J. Klippenstein, A. L. L. East, W. D. Allen, *J. Chem. Phys.* **105**, 118 (1996); (b) E. F. Valeev, W. D. Allen, H. F. Schaefer III, A. G. Császár, A. L. L. East, *J. Phys. Chem. A*, **105**, 2716 (2001); (c) N.D. Petraco, W. D. Allen, H. F. Schaefer III, *J. Chem. Phys.* **116**, 10229 (2002); (d) S. E. Wheeler, W. D. Allen, H. F. Schaefer III, *J. Chem. Phys.* **121**, 8800 (2004); (e) R. M. Balabin, *J. Chem. Phys.*, **131**, 154307(2009); (f) , R. M Balabin.; *J. Phys. Chem. A*, **114**, 3698 (2010); (g) J. C. Hargis, E. Vöhringer-Martinez, H. L. Woodcock, A. Toro-Labbé, H. F. Schaefer III, *J. Phys. Chem. A*, **115**, 2650 (2011).
- [29] K.-C. Lau, C.Y. Ng, *J. Chem. Phys.* **122**, 224310 (2005).
- [30] (a) A. L. L. East, W. D. Allen, *J. Chem. Phys.* **99**, 4638 (1993); (b) A. G.

- Császár, M. L. Leininger, V. Szalay, *J. Chem. Phys.* **118**, 10631 (2003); (c) M. S. Schuurman, S. R. Muir, W. D. Allen, H. F. Schaefer III, *J. Chem. Phys.* **120**, 11586 (2004).
- [31] J. C. Sancho-García, *Chem. Phys. Lett.* **468**, 138 (2009).
- [32] R. Monten, B. Hajgató, and M. S. Deleuze, *Mol. Phys.* **109**, 2317 (2011).
- [33] D. Feller, *J. Chem. Phys.* **96**, 6104 (1992); **98**, 7059 (1993).
- [34] J. M. L. Martin, in *Energetics of Stable Molecules and Reactive Intermediates*, NATO ASI Symposium Series, edited by M. E. Mirrasda Piedade and K. K. Irikura (Kluwer, Dordrecht, 1999).
- [35] C. Schwartz, in *Methods in Computational Physics*, edited by B. J. Alder (Academic, New York, 1963).
- [36] R. A. Kendall, T. H. Dunning, Jr., and R. J. Harrison, *J. Chem. Phys.* **96**, 6796 (1992).
- [37] Gaussian 09, Revision A.1, M. J. Frisch, G. W. Trucks, H. B. Schlegel, G. E. Scuseria, M. A. Robb, J. R. Cheeseman, G. Scalmani, V. Barone, B. Mennucci, G. A. Petersson, H. Nakatsuji, M. Caricato, X. Li, H. P. Hratchian, A. F. Izmaylov, J. Bloino, G. Zheng, J. L. Sonnenberg, M. Hada, M. Ehara, K. Toyota, R. Fukuda, J. Hasegawa, M. Ishida, T. Nakajima, Y. Honda, O. Kitao, H. Nakai, T. Vreven, J. A. Montgomery, Jr., J. E. Peralta, F. Ogliaro, M. Bearpark, J. J. Heyd, E. Brothers, K. N. Kudin, V. N. Staroverov, R. Kobayashi, J. Normand, K. Raghavachari, A. Rendell, J. C. Burant, S. S. Iyengar, J. Tomasi, M. Cossi, N. Rega, J. M. Millam, M. Klene, J. E. Knox, J. B. Cross, V. Bakken, C. Adamo, J. Jaramillo, R. Gomperts, R. E. Stratmann, O. Yazyev, A. J. Austin, R. Cammi, C. Pomelli, J. W. Ochterski, R. L. Martin, K. Morokuma, V. G. Zakrzewski, G. A. Voth, P. Salvador, J. J. Dannenberg, S. Dapprich, A. D. Daniels, Ö. Farkas, J. B. Foresman, J. V. Ortiz, J.

- Cioslowski, and D. J. Fox, Gaussian, Inc., Wallingford CT, 2009.
- [38] (a) MOLPRO is a package of ab initio programs written by H.-J. Werner and P. J. Knowles, with contributions from R. D. Amos, A. Bernhardsson, A. Berning, P. Celani, D. L. Cooper, M. J. O. Deegan, A. J. Dobbyn, F. Eckert, C. Hampel, G. Hetzer, T. Korona, R. Lindh, A. W. Lloyd, S. J. McNicholas, F. R. Manby, W. Meyer, M. E. Mura, A. Nicklass, P. Palmieri, R. Pitzer, G. Rauhut, M. Schütz, H. Stoll, A. J. Stone, R. Tarroni, and T. Thorsteinsson; (b) For integral evaluation see: R. Lindh, U. Ryu, and B. Liu, *J. Chem. Phys.* **95**, 5889 (1991); (c) For partially Spin Restricted Open-Shell Coupled Cluster see: P. J. Knowles, C. Hampel, and H.-J. Werner, *ibid.* **99**, 5219 (1993); **112**, 3106(E) (2000); (d) For perturbative triples: J. D. Watts, J. Gauss, and R. J. Bartlett, *ibid.* **98**, 8718 (1993).
- [39] (a) M. Douglas, N. M. Kroll, *Ann. Phys. (N. Y.)*, **82**, 89 (1974); (b) B. A. Hess, *Phys. Rev. A*, **32**, 756 (1985); (c) B. A. Hess, *Phys. Rev. A*, **33**, 3742 (1986); (d) G. Jansen, B. A. Hess, *Phys. Rev. A*, **39**, 6016 (1986).
- [40] (a) K. G. Dyall, *J. Chem. Phys.* **100**, 2118 (1994); (b) L. Visscher, K. G. Dyall, *At. Data Nucl. Data Tables*, **67**, 207 (1997); (c) K. G. Dyall, *J. Chem. Phys.* **106**, 9618 (1997); (d) K. G. Dyall, T. Enevoldsen, *J. Chem. Phys.* **111**, 10000 (1999).
- [41] D. E. Woon, T. H. Dunning, Jr. *J. Chem. Phys.* **103**, 4572 (1995).
- [42] CFOUR, a quantum chemical program package written by J.F. Stanton, J. Gauss, M. E. Harding, P. G. Szalay with contributions from A. A. Auer, R. J. Bartlett, U. Benedikt, C. Berger, D. E. Bernholdt, Y. J. Bomble, O. Christiansen, M. Heckert, O. Heun, C. Huber, T.-C. Jagau, D. Jonsson, J. Jusélius, K. Klein, W. J. Lauderdale, D. A. Matthews, T. Metzroth, D. P. O'Neill, D. R. Price, E. Prochnow, K. Ruud, F. Schiffmann, S. Stopkowicz, A.

- Tajti, J. Vázquez, F. Wang, J. D. Watts and the integral packages MOLECULE (J. Almlöf and P.R. Taylor), PROPS (P. R. Taylor), ABACUS (T. Helgaker, H. J. Aa. Jensen, P. Jørgensen, and J. Olsen), and ECP routines by A. V. Mitin and C. van Wüllen. For the current version, see <http://www.cfour.de>.
- [43] A.Tajti, P. G. Szalay, J. Gauss, *J. Chem. Phys.* **127**, 014102 (2007).
- [44] T. Helgacker, P. Jørgensen, J. Olsen, *Molecular Electronic Structure Theory*, (Wiley, Chichester, 2000)
- [45] J. Burgos, M. Pope, Ch. E. Swenberg, R. R. Alfano, *Phys. Status Solidi*, **83**, 249 (1977).
- [46] H. Angliker, E. Rommel, J. Wirz, *Chem. Phys. Lett.* **87**, 208 (1982).
- [47] A. Karton, B. Ruscic, and J. M. L. Martin, *J. Mol. Struct.: THEOCHEM*, **811**, 345 (2007).
- [48] S. P. Kwasniewski, J.-P. François, M. S. Deleuze, *J. Phys. Chem. A*, **107**, 5168 (2003).
- [49] (a) F. Márquez, C. M. Zicovich-Wilson, A. Corma, E. Palomares, and H. García, *J. Phys. Chem. B*, **105**, 9973 (2001); (b) F. Márquez, H. García, E. Palomares, L. Fernandez, and A. Corma, *J. Am. Chem. Soc.* **122**, 6520 (2000).
- [50] C. Raghu, Y. A. Pati, and S. Ramaseha, *Phys. Rev. B* **65**, 155204 (2002).
- [51] S. Zade, M. Bendikov, *Ang. Chem. Int. Ed.* **49**, 412 (2010).
- [52] N. Nijegorodov, V. Ramachandran, D. P. Winkoun, *Spectrochimica Acta A*, **53**, 1813 (1997).
- [53] (a) M. Deleuze, J. Delhalle, B. T. Pickup, J.-L. Calais, *Phys. Rev. B*, **46**, 15668 (1992); (b) M. Deleuze, J. Delhalle, B. T. Pickup, J.-L. Calais, *Adv. Quantum Chem.* **26**, 35 (1997); (c) M. Deleuze, M. K. Scheller, *L.S.*

Cederbaum, J. Chem. Phys. **103**, 3578 (1995); (d) M. S. Deleuze, Int. J. Quantum Chem., **93**, 191 (2003).

[54] S. Knippenberg, J. H. Startcke, M. Wormit, A. Dreuw, Mol. Phys. **108**, 2801 (2010).

[55] M. S. Deleuze, A. B. Trofimov, L. S. Cederbaum, J. Chem. Phys. **115**, 5859 (2001).

4.6 Appendix

Table A1. Focal point analysis of the vertical singlet-triplet gaps of benzene (all energies and corrections are given in kcal/mol). The Δ values are the singlet-triplet energy gaps at a given level. The +MP2, +MP3, +MP4, +CCSD, and +CCSD(T) entries correspond to the corrections obtained at the MP2, MP3, MP4, CCSD, and CCSD(T) levels, compared with the HF, MP2, MP3, MP4, and CCSD levels, respectively. "Well to well" S0-T1 excitation energies (WWES-T) results are in parenthesis.

BENZENE

# basis	cc-pVDZ	cc-pVTZ	cc-pVQZ	cc-pV5Z	aug-cc- pVDZ	aug-cc- pVTZ	aug-cc- pVQZ	cc-pV ω Z (F/S-QZ)	aug-cc- pV ω Z (F/S-AQZ)	cc-pV ω Z (F/S-5Z)
Δ HF	78.99 (63.13)	77.79 (63.09)	77.57 (63.06)	77.48 (63.07)	78.30 (-)	77.61 (-)	77.48 (-)	77.52 ^a (63.04) ^a	77.46 ^b (-)	77.44 ^c (63.08) ^c
+MP2	46.84 (47.77)	48.08 (50.40)	48.51 (51.29)	48.62 (51.52)	46.86 (-)	47.83 (-)	48.39 (-)	48.82 ^d (51.90) ^d	48.83 ^e (-)	48.68 ^f (51.68) ^f
+MP3	-12.60 (-13.89)	-14.17 (-15.38)	-14.65 (-15.88)		-12.87 (-)	-14.25 (-)	-14.70 (-)	-14.97 ^g (-16.21) ^g	-15.01 ^h (-)	
+MP4(SDQ)	-4.88 (-4.72)	-5.37 (-5.23)	-5.58 (-5.46)		-5.51 (-)	-5.58 (-)	-5.66 (-)	-5.73 ⁱ (-5.62) ⁱ	-5.73 ^j (-)	
+CCSD	-2.90 (-2.79)	-1.87 (-1.83)	-1.55 (-)		-2.43 (-)	-1.67 (-)	-1.46 (-)	-1.34 ^k (-)	-1.33 ^l (-)	
+CCSD(T)	0.01 (0.43)	0.36 (0.63)	0.40 (-)		0.16 (-)	0.38 (-)	0.40 (-)	0.42 ^m (-)	0.41 ⁿ (-)	
Δ CCSD(T)	105.45 (89.93)	104.82 (91.67)	104.70 (-)		104.50 (-)	104.32 (-)	104.32 (-)			104.46 (-)

a) F-QZ; b) F-AQZ; c) F-5Z; d) S_{MP2}-QZ; e) S_{MP2}-AQZ; f) S_{MP2}-5Z; g) S_{MP3}-QZ; h) S_{MP3}-AQZ; i) S_{MP4}(SDQ)-QZ; j) S_{MP4}(sdq)-AQZ; k) S_{CCSD}-QZ; l) S_{CCSD}(T)-QZ; m) S_{CCSD}(T)-AQZ; n) S_{CCSD}(T)-AQZ.

Table A2. Focal point analysis of the vertical singlet-triplet gaps of naphthalene. "Well to well" S_0 - T_1 excitation energies (WWE_{S-T}) results are in parenthesis (all results are given in kcal/mol).

NAPHTHALENE													
# basis	cc-pVDZ	cc-pVTZ	cc-pVQZ	cc-pV5Z	aug-cc- pVDZ	aug-cc- pVTZ	aug-cc- pVQZ	cc- pV ∞ Z	aug-cc- pV ∞ Z	cc- F/S-QZ	aug-cc- F/S-AQZ	cc- pV ∞ Z	cc- F/S-5Z
Δ HF	69.27 (50.69)	68.18 (50.57)	67.88 (50.45)	67.71 (50.40)	68.13 (-)	67.74 (-)	67.67 (-)	67.76 ^a (50.38) ^a	67.65 ^b (-)	67.76 ^a (50.38) ^a	67.65 ^b (-)	67.62 ^c (50.38) ^c	67.62 ^c (50.38) ^c
+MP2	21.91 (32.04)	22.83 (34.04)	23.24 (34.72)	23.40 (34.92)	22.36 (-)	22.913 (-)	23.28 (-)	23.54 ^d (35.18) ^d	23.56 ^e (-)	23.54 ^d (35.18) ^d	23.56 ^e (-)	23.56 ^f (35.09) ^f	23.56 ^f (35.09) ^f
+MP3	-7.50 (-11.81)	-8.34 (-12.92)	-8.59 (-13.26)	-8.59 (-13.26)	-7.64 (-)	-8.35 (-)	-8.35 (-)	-8.76 ^g (-13.48) ^g	-8.76 ^g (-13.48) ^g	-8.76 ^g (-13.48) ^g	-8.76 ^g (-13.48) ^g	-8.76 ^g (-13.48) ^g	-8.76 ^g (-13.48) ^g
+MP4(SDQ)	-3.97 (-4.64)	-4.25 (-5.04)	-4.36 (-5.21)	-4.36 (-5.21)	-4.25 (-)	-4.32 (-)	-4.32 (-)	-4.44 ^h (-5.33) ^h	-4.44 ^h (-5.33) ^h	-4.44 ^h (-5.33) ^h	-4.44 ^h (-5.33) ^h	-4.44 ^h (-5.33) ^h	-4.44 ^h (-5.33) ^h
+CCSD	-0.03 (-0.55)	0.60 (0.19)	0.60 (0.19)	0.60 (0.19)	0.19 (-)	0.19 (-)	0.19 (-)	0.19 (-)	0.19 (-)	0.19 (-)	0.19 (-)	0.19 (-)	0.19 (-)
+CCSD(T)	-2.66 (-1.12)	-2.56 (-1.02)	-2.56 (-1.02)	-2.56 (-1.02)	-2.56 (-)	-2.56 (-)	-2.56 (-)	-2.56 (-)	-2.56 (-)	-2.56 (-)	-2.56 (-)	-2.56 (-)	-2.56 (-)
Δ CCSD(T)	77.03 (64.62)	76.46 (65.82)	76.46 (65.82)	76.46 (65.82)	76.22 (-)	76.22 (-)	76.22 (-)	76.22 (-)	76.22 (-)	76.22 (-)	76.22 (-)	76.22 (-)	76.22 (-)

a) F-QZ; b) F-AQZ; c) F-5Z; d) S_{MP2} -QZ; e) S_{MP2} -AQZ; f) S_{MP2} -5Z; g) S_{MP3} -QZ; h) S_{MP4SDQ} -QZ.

Table A3. Focal point analysis of the vertical singlet-triplet gaps of anthracene. "Well to well" S_0-T_1 excitation energies (WWE_{S-T}) results are in parenthesis (all results are given in kcal/mol).

ANTHRACENE

# basis	cc-pVDZ	cc-pVTZ	cc- pVQZ	cc-pV5Z	aug-cc- pVDZ	aug-cc- pVTZ	aug-cc- pVQZ	cc-pV ω Z	aug-cc- pV ω Z	cc-pV ω Z
	246	560	1070	1824	412	874	1580	F/S-QZ	F/S-AQZ	F/S-5Z
Δ HF	44.68 (30.83)	44.02 (30.91)	43.83 (30.82)	43.74 (30.79)	44.05 (-)	43.79 (-)	43.73 (-)	43.76 ^a (30.75) ^a	43.71 ^b (-)	43.70 ^c (30.77) ^c
+MP2	18.63 (25.67)	19.26 (27.26)	19.66 (27.89)	19.85 (28.14)	18.99 (-)	19.44 (-)	19.75 (-)	19.98 ^d (28.35) ^d	20.00 ^e (-)	20.04 ^f (28.36) ^f
+MP3	-4.23 (-7.68)	-5.02 (-8.74)	-5.29 (-9.08)	-4.54 (-)	-4.54 (-)	-5.13 (-)	-5.13 (-)	-5.53 ^g (-9.31) ^g	-5.53 ^g (-)	-5.53 ^g (-9.31) ^g
+MP4(SDQ)	-2.39 (-3.13)	-2.56 (-3.44)	-2.66 (-3.60)	-2.64 (-)	-2.64 (-)	-2.67 (-)	-2.67 (-)	-2.74 ^h (-3.72) ^h	-2.74 ^h (-)	-2.74 ^h (-3.72) ^h
+CCSD	1.05 (0.89)	1.49 (1.42)	1.23 (-)	1.23 (-)	1.23 (-)	1.23 (-)	1.23 (-)	1.23 (-)	1.23 (-)	1.23 (-)
+CCSD(T)	-0.33 (0.52)	-0.18 (0.67)	-0.36 (-)	-0.36 (-)	-0.36 (-)	-0.36 (-)	-0.36 (-)	-0.36 (-)	-0.36 (-)	-0.36 (-)
Δ CCSD(T)	57.40 (47.10)	57.00 (48.09)	56.73 (-)	56.73 (-)	56.73 (-)	56.73 (-)	56.73 (-)	56.73 (-)	56.73 (-)	56.73 (-)

a) F-QZ; b) F-AQZ; c) F-5Z; d) S_{MP2} -QZ; e) S_{MP2} -AQZ; f) S_{MP2} -5Z; g) S_{MP3} -QZ; h) S_{MP4SDQ} -QZ.

Table A4. Focal point analysis of the vertical singlet-triplet gaps of naphthacene. "Well to well" S_0 - T_1 excitation energies (WWE_{S-T}) results are in parenthesis (all results are given in kcal/mol).

NAPHTHACENE						
	cc- pVDZ	cc- pVTZ	cc- pVQZ	cc- pV5Z	cc-pV ∞ Z	cc-pV ∞ Z
# basis	312	708	1350	2298	(F/S-QZ)	(F/S-5Z)
Δ HF	25.05 (13.09)	24.53 (13.20)	24.40 (13.15)	24.36 (13.12)	24.36 ^a (13.09) ^a	24.33 ^b (13.10) ^b
+MP2	29.35 (35.76)	30.30 (37.39)	30.79 (38.05)	30.99 (38.31)	31.16 ^c (38.54) ^c	31.19 ^d (38.56) ^d
+MP3	-7.74 (-10.32)	-8.96 (-11.81)			-9.63 ^e (-12.59) ^e	
+MP4(SDQ)	-4.13 (-4.77)	-4.49 (-5.23)			-4.83 ^f (-5.65) ^f	
+CCSD	-0.27 (-0.56)	0.31 (0.17)				
+CCSD(T)	-1.06 (-0.16)	-1.01 (-0.09)				
Δ CCSD(T)	41.19 (33.05)	40.67 (33.63)				

a) F-QZ; b) F-5Z; c) S_{MP2} -QZ; d) S_{MP2} -5Z; e) S_{MP3} -QZ; f) S_{MP4SDQ} -QZ.

Table A5. Focal point analysis of the vertical singlet-triplet gaps of pentacene. "Well to well" S_0 - T_1 excitation energies (WWE_{S-T}) results are in parenthesis (all results are given in kcal/mol).

PENTACENE				
	cc-pVDZ	cc-pVTZ	cc-pVQZ	cc-pV ∞ Z
# basis	378	856	1630	(F/S-QZ)
Δ HF	11.50 (0.46)	11.02 (0.49)	10.91 (0.44)	10.88 ^a (0.39) ^a
+MP2	34.11 (42.53)	35.36 (44.40)	35.94 (45.13)	36.37 ^b (45.66) ^b
+MP3	-9.07 (-12.44)	-10.54 (-14.28)		
+MP4(SDQ)	-4.83 (-5.96)	-5.34 (-6.60)		
+CCSD	0.08 (-0.69)			
+CCSD(T)	0.21 (1.06)			
Δ CCSD(T)	31.99 (24.95)			

a) F-QZ; b) S_{MP2} -QZ.

Table A6. Focal point analysis of the vertical singlet-triplet gaps of hexacene. "Well to well" S_0 - T_1 excitation energies (WWE_{S-T}) results are in parenthesis (all results are given in kcal/mol).

HEXACENE				
	cc-pVDZ	cc-pVTZ	cc-pVQZ	cc-pV ∞ Z
# basis	444	1004	1910	(F/S-QZ)
Δ HF	0.18 (-9.92)	-0.28 (-9.96)	-0.37 (-10.01)	-0.39 ^a (-10.05) ^a
+MP2	40.59 (49.29)	42.08 (51.38)	42.74 (52.19)	43.22 ^b (52.77) ^b
+MP3	-11.05 (14.55)	-12.78 (-16.69)		
+MP4(SDQ)	-5.69 (-6.90)	-6.35 (-7.72)		
+CCSD	-0.72 (-1.41)			
+CCSD(T)	0.23 (1.08)			
Δ CCSD(T)	23.53 (17.60)			

a) F-QZ; b) S_{MP2} -QZ.

Table A7. Focal point analysis of the vertical singlet-triplet gaps of heptacene. "Well to well" S_0 - T_1 excitation energies (WWE_{S-T}) results are in parenthesis (all results are given in kcal/mol).

HEPTACENE				
	cc-pVDZ	cc-pVTZ	cc-pVQZ	cc-pV ∞ Z
# basis	510	1152	2190	(F/S-QZ)
Δ HF	-8.69 (-18.39)	-9.17 (-18.54)	-9.26 (-18.60)	-9.28 ^a (-18.63) ^a
+MP2	49.20 (58.50)	51.10 (60.93)	51.86 (61.83)	52.41 ^b (62.47) ^b
+MP3	-14.04 (-17.70)	-16.15 (-20.26)		
+MP4(SDQ)	-7.37 (-8.62)	-8.25 (-9.65)		
+CCSD	-1.41 (-2.28)			
+CCSD(T)	1.16 (2.03)			
Δ CCSD(T)	18.86 (13.54)			

a) F-QZ; b) S_{MP2} -QZ.

5 Benchmark theoretical study of the ionization energies, electron affinities and singlet-triplet energy gaps of azulene, phenanthrene, pyrene, chrysene and perylene

5.1 Introduction

In continuation of benchmark theoretical studies of the electronic properties of benzene and *n*-acenes [1-4], we aim at investigating at the confines of non-relativistic quantum mechanics the ionization energies, electron affinities, and singlet-triplet energy gaps of azulene, phenanthrene, pyrene, chrysene and perylene, using the well-established principles of a Focal Point Analysis (FPA) [5] in order to reach or approach chemical accuracy (1 kcal/mol, i.e. 0.043 eV) on the computed energy differences. Our main motivation for this work stems from the observation that large discrepancies exist among the reported experimental values. For instance, discrepancies as large as 0.62 eV have been observed when comparing the available experimental data for the electron affinity of perylene [6-8]. Also, the three latest experimental determinations of the EAs of phenanthrene [9-11] exhibit deviations around 0.3 eV. Similarly, recently obtained experimental values for the ionization energy of chrysene [12, 13] and perylene [12] exhibit discrepancies around 0.41 eV and 0.2 eV, respectively. Experimental data for the singlet-triplet energy gap of these five compounds are rather scarce [14-18]. To date, no benchmark theoretical study of their electronic properties has been reported yet. Such studies appear to be very much needed for reliable enough insights into the available experimental data. Indeed, the reported theoretical values for the electron affinity, ionization energy and excitation energies of the target systems

are the results of calculations employing empirical (Hückel) or semi-empirical Hamiltonians, Density Functional Theory (DFT) [19] or Time Dependent DFT (TDDFT) [20]. Accuracies around 0.1-0.2 eV [21, 22] have been claimed when employing DFT in order to evaluate the electron affinities of large PAHs as energy differences in between the neutral and anionic states. However, when dealing with large conjugated systems, it is well known [23, 24] that applications of standard exchange-correlation functionals result in much larger uncertainties and errors, because of the too fast decay of the electronic potential at large distances resulting from an incomplete compensation of the self-interaction error.

The singlet-triplet energy gap (E_{ST}) is a most important electronic property concerning the areas where photo-luminescent processes take place. For instance, singlet-triplet gaps can be used to evaluate the strength of electron-electron correlation in luminescent polymers [25]. The singlet-triplet energy gaps of phenanthrene, pyrene and chrysene have been measured from phosphorescence spectra decades ago, and discussed in a paper by Siebrand [14] (1967) and in the book by Bircks [26]. The singlet-triplet energy gap of chrysene has been determined more recently from photodetachment-photoelectron spectra (PD-PES) at wavelengths of 266 nm and 355 nm [17]. Experimental values for the singlet-triplet energy gap of azulene have been also recently obtained by means of the pulse radiolysis technique [15] and flash kinetic spectrometry [16]. At last, the singlet-triplet energy gap of perylene has been measured [18] by means of the so-called solvent perturbation technique, using chloranil in carbon tetrachloride solution, along with oxygen under high pressure.

Electron affinities (EAs) and ionization energies (IEs) are also most important electronic properties [22]. Detailed knowledge about EAs and IEs is needed in studies of the toxicity and carcinogenicity of PAHs on the ground of computer modeling employing Quantitative Structure-Activity Relationship (QSAR) theories [27]. Indeed, most important descriptors of biological and chemical activity are the energies of the Highest Occupied Molecular Orbital (HOMO) and of the Lowest Unoccupied Molecular Orbital (LUMO), which relate to vertical ionization energies (VIEs) and vertical electron affinities (VEAs), according to Koopmans' theorem [28, 29]. EAs are also important in the modeling of rate constants in gas-phase oxidation reactions in diesel combustion [30], and IEs are one of the key features in designing electro-optically active materials [31]. Most of the available experimental data for the electron affinities of the compounds of interest have been obtained by means of Electron Capture Detection (ECD) [10, 11, 32, 33] and Laser Photoelectron Spectroscopy (LPES) [7, 17, 34-36], whereas experimental data for ionization energies are essentially the results of experiments employing photoionization mass spectrometry (PI) [37], ion/molecule equilibrium constant determination (EQ) [12], photoelectron spectroscopy (PE) [12, 38], and laser spectroscopy (LS) [12, 39]. On theoretical side, most estimates of IEs and EAs so far are the results of calculations employing DFT [19, 40-42]. *Ab initio* multireference configuration interaction approach with single and double excitations, and time-dependent density functional theory along with the Becke-Lee-Yang-Parr functional (TDDFT/BLYP) have also been used for predicting the ionization spectra of PAHs [19, 20]. Our group has published detailed studies [43] of the valence one-electron and shake-up ionization spectra of azulene, phenanthrene, pyrene, chrysene, and perylene using the third-order outer-valence Green's function (OVGF [44, 45])

and algebraic-diagrammatic construction [ADC(3)] schemes, as well as basis sets of improving quality (6-31G, 6-31G*, cc-pVDZ). Discrepancies around 0.3 to 0.4 eV were observed for the five target compounds when comparing the OVGf/cc-pVDZ values for one-electron binding energies with high resolution experimental (He I UPS) data.

In the present work, vertical electron affinities, ionization energies or electronic excitation energies are determined as energy differences between the total electronic energies of the neutral molecules and of the anions, cations or excited species, respectively, upon the geometries of the initial (neutral) electronic ground state. The corresponding "well-to-well" estimates are obtained by adding to the vertical values the stabilization energies of the anions, cations or excited species due to geometry relaxation from the vertically ionized or excited states. Adiabatic estimates are ultimately inferred by adding zero-point vibrational energy corrections.

Focal Point Analyses combining size-consistent (size-extensive) approaches such as Møller-Plesset Perturbation theory and Coupled-Cluster theory in conjunction with basis sets of improving quality have been extensively exploited in highly accurate studies [5] of conformational energy differences or torsional barriers, reaction and activation energies, heats of formation, binding energies of π -complexes, ... or static dipole polarizabilities. The FPA approach supplemented by extrapolations to an asymptotically complete basis cc-pV ∞ Z set has been found in particular to provide exceedingly accurate insights into negative electron affinities [2], corresponding to meta-stable anions with a life time estimated to be around 10^{-14} s [46], provided diffuse functions are deliberately removed from the employed correlation consistent cc-pVXZ (X=D,T,Q, ∞) basis sets, in order to enforce a localization of the impinging

electron in the molecular region. FPAs exploit the idea of a dual extrapolation towards the highest attainable level in electronic correlation [ideally, the full-CI (configuration interaction) limit [29], in practice Coupled Cluster theory [47] with single, double and perturbative triple excitations, CCSD(T)], and to the limit of an asymptotically Complete Basis Set (CBS).

5.2 Computational details

All calculations including geometry optimization, vibrational analysis, and single point energy determinations have been carried out using the Gaussian09 [48] program package. Geometry optimization and vibrational analysis have been performed using DFT [49] in conjunction with the Becke three-parameter Lee-Yang-Parr (B3LYP) functional [50] and the cc-pVTZ basis set [51]. The tightest optimization convergence criteria have been enforced at all stages of the calculations, using the Gaussian09 keyword `opt=verytight`. An ultra-fine pruned integration grid consisting of 99 radial shells per atom and 590 angular points per shell has also been requested for the DFT calculations, resulting in about 7000 points per atom. Single point energy calculations have been performed, in conjunction with various basis sets, upon the optimized B3LYP/cc-pVTZ geometries, at the level of Hartree-Fock (HF) theory [29], Møller-Plesset theory [52] truncated at second-order (MP2) [53], third-order (MP3) [54], and fourth-order with single, double, and quadruple excitations (SDQ-MP4) [55], and at the CCSD and CCSD(T) [47] levels of theory. For the sake of simplicity, the SDQ-MP4 approach will be throughout this study referred to as the MP4 level. The employed basis sets were the Dunning's correlation consistent cc-pVXZ basis sets [51] ($X=\{D,T,Q\}$).

Here also use has been made of the Feller's three-point extrapolation formula [56] for evaluating the total HF energy in the limit of an asymptotically complete (cc-pV ∞ Z) basis set. Electron correlation energies at the MP2 level were correspondingly obtained using the Schwarz [57] three-point extrapolation formula. The total energy obtained at the MP2 level in the limit of the asymptotically complete cc-pV ∞ Z basis set from a three-point extrapolation employing $l=2,3,4$ will be referred to as the S_{MP2} -QZ result. This value is obtained by adding to the Feller's extrapolated HF energy [$E^{HF}(\infty)$], the result of the Schwartz extrapolation of the MP2 correlation energy [$E^{corr}(\infty)$]. Further extrapolation has been performed toward the CCSD(T) level of theory in the limit of an asymptotically CBS using the principles of a FPA, by means of the extrapolation formula:

$$\begin{aligned} \text{FPA-QZ} = & S_{MP2}\text{-QZ} + (E_{MP4/cc-pVTZ} - E_{MP2/cc-pVTZ}) + \\ & + (E_{CCSD(T)/cc-pVDZ} - E_{MP4/cc-pVDZ}). \end{aligned} \quad (1)$$

The latter formula stems from the observation [1-5] that higher-order correlation contributions are usually much smaller, and converge much faster than the lower-order ones, upon improving the basis set.

Vertical singlet-triplet energy gaps, electron affinities and ionization energies are the results of calculations which have been performed on the geometries of the neutrals. Vertical and "well-to-well" energy differences have been estimated at the CCSD(T) level in the limit of an infinitely large cc-pV ∞ Z basis set, according to the above equation, by adding to the S_{MP2} -QZ result almost converged and small high-level correlation corrections, obtained at the MP4/cc-pVTZ and CCSD(T)/cc-pVDZ levels of theory. The outcome of relaxation effects (Geometry Relaxation Energy (GRXE)) has

therefore also been most generally evaluated at the CCSD(T)/cc-pV ∞ Z level by considering the difference in-between the FPA estimates for vertical and “well-to-well” transition energies, except in two particular cases, namely the determination of the electronic affinity and ionization energy of chrysene. Rather unfortunately, the coupled cluster iterations upon the anion and cation of this compound indeed failed to properly converge when employing the cc-pVTZ and cc-pVQZ basis sets. In order to supply anyway reliable enough estimates for the missing pieces of information, comparison has been systematically made throughout the study with B3LYP/cc-pVTZ values for GRXEs. The CCSD(T)/cc-pV ∞ Z and B3LYP/cc-pVTZ estimates of GRXEs were found to be practically equal, within 0.01 eV accuracy, and B3LYP/cc-pVTZ relaxation energies have therefore been used to determine the “well-to-well” electron attachment and ionization energies of chrysene, which correspond to energy differences between minima on the relevant potential energy surface. Adiabatic values were ultimately obtained for all studied electronic transitions by adding B3LYP/cc-pVTZ estimates for zero-point vibrational energy corrections to the FPA estimates of the relevant “well-to-well” transition energies.

5.3 Results and discussion

5.3.1 The electronic ground state

Prior to any other consideration, it was necessary to verify whether a single-reference wavefunction for the electronic neutral ground state is suitable for further many-body calculations on the selected PAHs. This check has been made by using the T1 diagnostics [58] of CCSD theory and energy-

based criteria devised by Karton *et al* [59] (Table 1). For all studied compounds, the T1 values are lower than 0.0121 at the CCSD/cc-pVDZ level of theory. Also, the percentage of the total atomization energy accounted for by the parenthetical triple excitations %TAE[(T)] is lower than 1.16 % for all studied compounds. According to stringent tests of many-body quantum mechanical theories [59], and since all %TAE[(T)] values are below 2 %, we can safely draw the conclusion that all targets are essentially dominated by dynamical correlation and should be reliably described by single-reference treatments.

Table 1. T1 diagnostics (CCSD/cc-pVDZ level of theory), and contributions (in %) from perturbative triple (T) excitations to Total Atomization Energies (TAEs, calculations based on the B3LYP/cc-pVTZ geometries for the singlet closed-shell electronic ground state).

	T1	%TAE[(T)] ^a	%TAE[(T)] ^b	%TAE[(T)] ^c
Azulene	0.0121	0.91	0.94	1.16
Phenanthrene	0.0104	0.83	0.86	1.08
Pyrene	0.0106	0.89	0.92	1.15
Chrysene	0.0105	0.86	0.89	
Perylene	0.0107	0.92	0.95	

a) Upon a comparison of CCSD/cc-pVDZ, CCSD(T)/cc-pVDZ and CCSD(T)/cc-pV ∞ Z (FPA_QZ) results for TAEs.

b) Upon a comparison of CCSD/cc-pVDZ with CCSD(T)/cc-pVDZ results for TAEs.

c) Upon a comparison of CCSD/cc-pVTZ with CCSD(T)/cc-pVTZ results for TAEs.

In all the FPAs that are reported in the sequel, the HF estimates for the E_{ST} s, IEs and EAs are given as HF energy differences (Δ HF results), and the successive improvements in the treatment of electronic correlation are denoted by +MP2, +MP3, +MP4, +CCSD, and +CCSD(T). These improvements correspond to the corrections obtained at the MP2, MP3, MP4, CCSD, and CCSD(T) levels, compared to the HF, MP2, MP3, MP4, and CCSD results, respectively. The CCSD(T)/cc-pVDZ values for the E_{ST} , IE and EA are

given as $\Delta\text{CCSD(T)}$ entries.

5.3.2 Singlet-triplet energy gap

All detailed intermediate results involved in the FPAs of the vertical singlet-triplet energy gaps (VE_{ST}) of azulene, phenanthrene, pyrene, chrysene, and perylene are given as main entries in Tables 2-6, along with their "well-to-well" (WWE_{ST}) counterparts, which are given in brackets. The corresponding triplet excited states are: 3B_2 for azulene and phenanthrene, ${}^3B_{1u}$ for pyrene and perylene, and 3B_u for chrysene. Upon inspecting these tables, it is clear that the ΔHF values for both the vertical and the "well-to-well" singlet-triplet energy gaps converge rather rapidly to finite values with respect to successive improvements of the basis set. Whatever the level attained in correlation and the size of the basis set, the lowest singlet (closed shell) state of all considered compounds is located below in energy than the first triplet state. The +MP2 corrections are systematically positive and largely dominate the correlation corrections, especially for systems like phenanthrene (Table 3) and perylene (Table 6). On the other hand, the +MP3, +MP4 and +CCSD corrections are all negative. The corrections corresponding to triple perturbative excitations are positive and very small. Convergence of the +MP2 corrections upon improvements of the basis set is smooth for all systems and enables safe extrapolations to the limit of an asymptotically complete (i.e. infinitely large) basis set. In view of the convergence of results upon improving the basis set and upon increasing the level attained in correlation, and experience acquired with comparable FPAs [1-4] upon *n*-acenes, highly reliable estimates for the vertical (VE_{ST}) and "well-to-well" (WWE_{ST}) singlet-triplet gap can be obtained for azulene,

pyrene and chrysene, within an estimated accuracy of a few hundredths eV, upon extrapolating the CCSD(T) results to the limit of an asymptotically complete cc-pV ∞ Z basis set, using equation (1) along with Feller's and Schwarz three-point extrapolation formula. Adiabatic singlet-triplet energy gaps (AE_{ST}) have been correspondingly determined by adding to the WWE_{ST} values obtained in this limit the B3LYP/cc-pVTZ estimates for zero-point vibrational energy (ZPVE) (Table 7). Geometry relaxation energies (GRXE) are displayed as third entry in Table 7. These latter contributions have been estimated in the limit of a CCSD(T)/cc-pV ∞ Z treatment as the energy differences in between the vertical and "well-to-well" singlet-triplet energy gaps. The reader is referred further to Table 7 for a comparison of our best FPA-QZ estimates with experimental results.

Table 2. Focal point analysis of the vertical singlet-triplet gap of azulene. "Well to well" S_0 - T_1 excitation energies (WWE_{S-T}) are in parenthesis (all results are given in eV).

Azulene				
No. basis	cc-pVDZ 180	cc-pVTZ 412	cc-pVQZ 790	cc-pV ∞ Z
Δ HF	1.46 (0.72)	1.44 (0.73)	1.43 (0.73)	1.43 ^a (0.73) ^a
+MP2	1.61 (2.25)	1.63 (2.35)	1.64 (2.37)	1.64 ^b (2.39) ^b
+MP3	-0.54 (-0.77)	-0.67 (-0.85)		
+MP4(SDQ)	-0.18 (-0.25)	-0.12 (-0.28)		
+CCSD	-0.18 (-0.30)			
+CCSD(T)	0.14 (0.20)			
Δ CCSD(T)	2.30 (1.84)			

a) Obtained using Feller's three-point extrapolation formula.

b) S_{MP2} -QZ result.

Table 3. Focal point analysis of the vertical singlet-triplet gap of phenanthrene. "Well to well" S_0 - T_1 excitation energies (WWE $_{S-T}$) are in parenthesis (all results are given in eV).

Phenanthrene				
	cc-pVDZ	cc-pVTZ	cc-pVQZ	cc-pV ∞ Z
No. Basis	246	560	1070	
Δ HF	2.31 (1.63)	2.28 (1.63)	2.28 (1.63)	2.28 ^a (1.63) ^a
+MP2	3.37 (3.49)	3.48 (3.64)	3.52 (3.69)	3.54 ^b (3.73) ^b
+MP3	-1.03 (-1.12)	-1.16 (-1.25)		
+MP4(SDQ)	-0.47 (-0.47)	-0.52 (-0.51)		
+CCSD	-0.69 (-0.66)			
+CCSD(T)	0.08 (0.13)			
Δ CCSD(T)	3.57 (2.99)			

a) Obtained using Feller's three-point extrapolation formula.

b) S_{MP2} -QZ result.**Table 4.** Focal point analysis of the vertical singlet-triplet gap of pyrene. "Well to well" S_0 - T_1 excitation energies (WWE $_{S-T}$) are in parenthesis (all results are given in eV).

Pyrene				
	cc-pVDZ	cc-pVTZ	cc-pVQZ	cc-pV ∞ Z
No. basis	274	620	1180	
Δ HF	2.08 (1.41)	2.06 (1.43)	2.06 (1.43)	2.06 ^a (1.43) ^a
+MP2	1.45 (1.80)	1.49 (1.89)	1.52 (1.92)	1.53 ^b (1.94) ^b
+MP3	-0.39 (-0.55)	-0.44 (-0.62)		
+MP4(SDQ)	-0.21 (-0.23)	-0.23 (-0.26)		
+CCSD	-0.23 (-0.23)			
+CCSD(T)	0.00 (0.07)			
Δ CCSD(T)	2.71 (2.27)			

a) Obtained using Feller's three-point extrapolation formula.

b) S_{MP2} -QZ result.

Table 5. Focal point analysis of the vertical singlet-triplet gap of chrysene. "Well to well" S_0 - T_1 excitation energies (WWE_{S-T}) are in parenthesis (all results are given in eV).

Chrysene				
No. basis	cc-pVDZ	cc-pVTZ	cc-pVQZ	cc-pV ∞ Z
Δ HF	2.58 (1.65)	2.55 (1.66)	2.55 (1.66)	2.55 ^a (1.67) ^a
+MP2	1.80 (3.65)	1.85 (3.83)	1.88 (3.87)	1.90 ^b (3.91) ^b
+MP3	-0.59 (-1.27)	-0.66 (-1.41)		
+MP4(SDQ)	-0.25 (-0.54)	-0.28 (-0.59)		
+CCSD	-0.29 (-0.75)			
+CCSD(T)	0.02 (0.10)			
Δ CCSD(T)	3.27 (2.86)			

a) Obtained using Feller's three-point extrapolation formula.

b) S_{MP2} -QZ result.**Table 6.** Focal point analysis of the vertical singlet-triplet gap of perylene. "Well to well" S_0 - T_1 excitation energies (WWE_{S-T}) are in parenthesis (all results are given in eV).

Perylene				
No. Basis	cc-pVDZ	cc-pVTZ	cc-pVQZ	cc-pV ∞ Z
Δ HF	1.21 (0.59)	1.18 (0.59)	1.17 (0.58)	1.17 ^a (0.58) ^a
+MP2	2.66 (2.95)	2.75 (3.06)	2.78 (3.10)	2.80 ^b (3.13) ^b
+MP3	-0.77 (-0.89)	-0.86 (-1.00)		
+MP4(SDQ)	-0.38 (-0.40)	-0.42 (-0.44)		
+CCSD	-0.56 (-0.55)			
+CCSD(T)	0.03 (0.09)			
Δ CCSD(T)	2.19 (1.79)			

a) Obtained using Feller's three-point extrapolation formula.

b) S_{MP2} -QZ result.

Table 7. Calculated and experimental singlet-triplet energy gaps, along with the zero-point vibrational energy (ΔZPE) and geometry relaxation (GRXE) contributions. All results are given in eV.

	<u>VES-I</u>	<u>WWES-I</u>	<u>GRXE</u>	<u>ΔZPE</u>	<u>AES-I</u>	
	CCSD(T)/ cc-pV ∞ Z ^a	CCSD(T)/ cc-pV ∞ Z ^a	CCSD(T)/ cc-pV ∞ Z	B3LYP/ cc-pVTZ	CCSD(T)/ cc-pV ∞ Z ^b	
Azulene	2.24	1.89	-0.35	-0.11	1.79	Experimental 1.739 \pm 0.009 ^c 1.677 ^d
Phenanthrene	3.54	3.06	-0.48	-0.14	2.92	2.68 ^e
Pyrene	2.70	2.34	-0.36	-0.12	2.22	2.10 ^e
Chrysene	3.24	2.93	-0.31	-0.14	2.79	2.64 \pm 0.01 ^f
Perylene	2.14	1.81	-0.34	-0.10	1.71	1.55 ^g

a) FPA-QZ estimate (see text for details).

b) Upon adding ΔZPE corrections to $WWE_{S,T}$ CCSD(T)/cc-pV ∞ Z data.

c) Obtained by means of the Pulse Radiolysis Technique, for details see Ref. [16].

d) Obtained from the measurements of the rates of energy transfer by means of the flash kinetic spectrometry, for details see Ref. [15].

e) Measurement has been carried out in a mixture of ether, isopentane, and alcohol at 77 K where it forms a glass, or in another related solvent (EPA+), for details see Ref. [14], and references therein.

f) Determined from PD-PES spectra, for detail see Ref. [17].

g) Measured using so-called solvent perturbation technique using oxygen under high pressure, for details see text and Ref. [18].

The best agreement between experiment and theory is observed with azulene, with a discrepancy of 0.046 eV only. The experimental result for azulene has been obtained by means of the pulse radiolysis technique [16] applied on non-polar benzene solutions of anthracene ($6-8 \times 10^{-2} \text{ mol L}^{-1}$) containing azulene ($4-10 \times 10^{-4} \text{ mol L}^{-1}$). Differences between our best adiabatic estimates and experimental data for the other compounds are 0.24 eV (phenanthrene), 0.12 eV (pyrene), 0.12 eV (chrysene), and 0.16 eV (perylene). These rather large differences between theory and experiment are certainly due to the fact that experimental values were obtained from measurements in polar solutions and glassy matrices, which may give rise to complications associated with intermolecular interactions. Indeed, the experimental values for the singlet-triplet energy gaps of phenanthrene and pyrene are the results of measurements in a mixture of ether, isopentane, and alcohol at 77 K where it forms a glass. Similarly, the experimental data [18] for perylene have been obtained from measurements employing the solvent perturbation technique, using chloranil in carbon tetrachloride solution along with oxygen under high pressure at room temperature. The oxygen forms a contact charge-transfer complex with the hydrocarbon and the absorption spectrum corresponds therefore to the superposition of the $S_0 \rightarrow T_1$ transition, on the charge-transfer band. At last, note that the experimental value for chrysene was determined from Photodetachment-Photoelectron Spectroscopy (PD-PES) spectra at wavelengths of 266 nm and 355 nm [17] and is subject therefore to geometrical complications arising from the removal of an electron from the *anion*.

5.3.3 Electron affinities

The anions of azulene, phenanthrene, pyrene, chrysene, and perylene anions possess a ${}^2B_{1g}$, 2A_2 , 2A_u , 2B_g , and ${}^2B_{1g}$ electronic ground state, respectively. The results of the focal point analysis of the vertical electron affinities (VEAs) and corresponding “well-to-well” values of these five compounds are given in Tables 8-12. Again, ΔHF results converge smoothly to a finite value with respect to successive improvements of the basis set. In the case of azulene (Table 8), phenanthrene (Table 9) and perylene (Table 12), the +MP2 corrections are negative while higher order corrections up to the CCSD(T) level are positive.

Table 8. Focal point analysis of the vertical electron affinity of azulene. “Well to well” electron affinities (WWEA) are in parenthesis (all results are given in eV).

Azulene				
No. Basis	cc-pVDZ 180	cc-pVTZ 412	cc-pVQZ 790	cc-pV ∞ Z
ΔHF	-0.19 (0.05)	-0.07 (0.14)	0.00 (0.20)	0.04 ^a (0.24) ^a
+MP2	-0.77 (-0.73)	-0.56 (-0.56)	-0.49 (-0.50)	-0.44 ^b (-0.45) ^b
+MP3	0.43 (0.44)	0.43 (0.44)		
+MP4(SDQ)	0.22 (0.22)	0.25 (0.24)		
+CCSD	0.23 (0.21)			
+CCSD(T)	-0.11 (-0.11)			
$\Delta CCSD(T)$	-0.19 (0.08)			

a) Obtained using Feller’s three-point extrapolation formula.

b) S_{MP2-QZ} result.

Table 9. Focal point analysis of the vertical electron affinity of phenanthrene. "Well to well" electron affinities (WWEA) are in parenthesis (all results are given in eV).

Phenanthrene				
No. Basis	cc-pVDZ	cc-pVTZ	cc-pVQZ	cc-pV ∞ Z
Δ HF	-1.37 (-1.13)	-1.25 (-1.06)	-1.19 (-1.01)	-1.15 ^a (-0.97) ^a
+MP2	-0.49 (-0.53)	-0.27 (-0.35)	-0.19 (-0.29)	-0.14 ^b (-0.24) ^b
+MP3	0.36 (0.40)	0.36 (0.41)		
+MP4(SDQ)	0.25 (0.26)	0.26 (0.27)		
+CCSD	0.24 (0.26)			
+CCSD(T)	0.00 (0.01)			
Δ CCSD(T)	-1.02 (-0.73)			

a) Obtained using Feller's three-point extrapolation formula.

b) S_{MP2} -QZ result.**Table 10.** Focal point analysis of the vertical electron affinity of pyrene. "Well to well" electron affinities (WWEA) are in parenthesis (all results are given in eV).

Pyrene				
No. Basis	cc-pVDZ	cc-pVTZ	cc-pVQZ	cc-pV ∞ Z
Δ HF	-0.79 (-0.65)	-0.70 (-0.61)	-0.66 (-0.56)	-0.63 ^a (-0.53) ^a
+MP2	-0.05 (-0.03)	0.19 (0.17)	0.27 (0.24)	0.32 ^b (0.29) ^b
+MP3	0.01 (0.20)	0.16 (0.18)		
+MP4(SDQ)	0.32 (0.17)	0.16 (0.17)		
+CCSD	0.10 (0.11)			
+CCSD(T)	0.00 (0.02)			
Δ CCSD(T)	-0.41 (-0.19)			

a) Obtained using Feller's three-point extrapolation formula.

b) S_{MP2} -QZ result.

Table 11. Focal point analysis of the vertical electron affinity of chrysene. "Well to well" electron affinities (WWEA) are in parenthesis (all results are given in eV).

Chrysene				
No. Basis	cc-pVDZ	cc-pVTZ	cc-pVQZ	cc-pV ∞ Z
Δ HF	-1.13 (-0.78)	-1.03 (-0.73)	-0.97 (-0.68)	-0.94 ^a (-0.65) ^a
+MP2	0.25 (-1.31)	0.51 (-1.17)	0.59 (-1.11)	0.64 ^b (-1.07) ^b
+MP3	0.09 (0.66)	0.06 (0.70)		
+MP4(SDQ)	0.12 (0.39)	0.13 (0.42)		
+CCSD	0.04 (- ^c)			
+CCSD(T)	0.03 (- ^c)			
Δ CCSD(T)	-0.59 (- ^c)			

a) Obtained using Feller's three-point extrapolation formula.

b) S_{MP2}-QZ result.

c) Unconverged.

Table 12. Focal point analysis of the vertical electron affinity of perylene. "Well to well" electron affinities (WWEA) are in parenthesis (all results are given in eV).

Perylene				
No. Basis	cc-pVDZ	cc-pVTZ	cc-pVQZ	cc-pV ∞ Z
Δ HF	-0.05 (0.07)	0.04 (0.12)	0.09 (0.17)	0.13 ^a (0.20) ^a
+MP2	-1.32 (-1.33)	-1.11 (-1.16)	-1.03 (-1.09)	-0.98 ^b (-1.05) ^b
+MP3	0.60 (0.62)	0.63 (0.65)		
+MP4(SDQ)	0.36 (0.37)	0.39 (0.40)		
+CCSD	0.47 (0.50)			
+CCSD(T)	-0.01 (0.01)			
Δ CCSD(T)	0.06 (0.24)			

a) Obtained using Feller's three-point extrapolation formula.

b) S_{MP2}-QZ result.

For these three compounds the +MP2 corrections tend to decrease in absolute value when going to the limit of an asymptotically complete basis set. For chrysene (Table 11) the “well-to-well” +MP2 corrections are also all negative, whereas the vertical +MP2 corrections are all positive. For pyrene (Table 10), the +MP2 correction reverses from a negative to a positive value as the basis set improves. Starting from the MP3 level, the correlation energy systematically increases the VEA and adiabatic electron affinity (AEA) upon including higher order correlation terms. For pyrene and chrysene (Tables 10 and 11), the influence of the high-order correlation energy terms on our theoretical estimates of the electron affinity is particularly noticeable. The actual electron affinity of those two PAHs is positive, due to the contributions of higher order electron correlation corrections and the contributions of the ΔZPE , which are all positive. According to the FPAs and extrapolations of results to the CCSD(T)/cc-pV ∞ Z level, our best estimates for the VEAs of azulene, phenanthrene, pyrene, chrysene, and perylene are 0.4036 eV, -0.4246 eV, 0.1241 eV, -0.0451 eV, and 0.6288 eV, respectively. The vertical electron affinity of chrysene at the HF level is negative and it remains negative even after incorporating correlation corrections up to the CCSD(T) level, in the limit of an asymptotically complete cc-pV ∞ Z basis set.

AEAs are calculated by adding to the “well-to-well” electron affinities (WWEA) the ΔZPE correction calculated at the B3LYP/cc-pVTZ level of theory. In the case of chrysene, the WWEA could not be obtained at the CCSD(T)/cc-pV ∞ Z level, because the coupled cluster iterations failed to converge to the correct state when employing the cc-pVTZ and cc-pVQZ basis sets, and structural relaxation energies had therefore to be supplied at the B3LYP/cc-pVTZ and CCSD(T)/cc-pVDZ levels of theory. From a comparison (Table 13)

of GRXEs obtained for the electron affinities of all other compounds at these two levels as well as the CCSD(T)/cc-pV ∞ Z level of theory, we expect that the error arising from this restriction in our treatment should not exceed 0.01 eV. Adiabatic estimates, together with the corresponding vertical and 'well-to-well' estimates, GRXE, Δ ZPE corrections and experimentally obtained values are given in Table 13. Our best estimates for the AEAs obtained by means of the FPA are 0.7075 eV, -0.0795 eV, 0.3999 eV, 0.2446, and 0.8709 eV for azulene, phenanthrene, pyrene, chrysene and perylene, respectively. These compare very favourably, within an average accuracy of 0.05 eV (1.25 kcal/mol), with the most recent experimental values that were reported for the electron affinities of these five compounds: 0.690 ± 0.040 eV [35], -0.01 ± 0.04 eV [9], 0.406 ± 0.010 eV [36], 0.32 ± 0.01 eV [17], and 0.973 ± 0.005 eV [8], respectively. A discrepancy of 0.07 eV is noticed for phenanthrene. Note that in this case, the experimental value has been obtained from an extrapolation to vacuum of data obtained for water clusters [17], and should be apprehended therefore with the greatest care. Besides, for molecules with very low electron affinities (< 0.1 eV), as is the case of phenanthrene, electron scattering is a most difficult problem [60]. In such situations, the experimental values which are obtained by means of Electron Capture Detection (ECD) must be regarded as upper limits of the true adiabatic EAs.

Table 13. Calculated and experimental electron affinities, along with the zero-point vibrational energy (ΔZPE) and geometry relaxation (GRXE) contributions. All results are given in eV.

	VEA		WWEA		GRXE		GRXE		ΔZPE		AEA		Experimental
	CCSD(T)/ cc-pV ∞ Z ^a	0.40	CCSD(T)/ cc-pV ∞ Z ^a	0.58	CCSD(T)/ cc-pV ∞ Z	0.17	B3LYP/ cc-pVTZ	0.15	B3LYP/ cc-pVTZ	0.13	CCSD(T)/ cc-pV ∞ Z ^b	0.71	
Azulene													0.80 \pm 0.10 ^f 0.690 \pm 0.040 ^g 0.790 \pm 0.008 ^h
Phenanthrene	-0.42		-0.26		0.17		0.16		0.18		-0.08		-0.01 \pm 0.04 ⁱ <0.269 \pm 0.035 ^j
Pyrene	0.12		0.24		0.12		0.11		0.16		0.40		0.39 ^k 0.406 \pm 0.010 ^l
Chrysene	-0.05		- ^c		0.11 ^d		0.11		0.18		0.24 ^e		0.32 \pm 0.01 ^m 0.3970 \pm 0.0080 ⁿ
Perylene	0.63		0.72		0.09		0.09		0.15		0.87		0.973 \pm 0.005 ^o 0.993 \pm 0.043 ^p

a) FPA-QZ estimate (see text for details).

b) Upon adding ΔZPE corrections to WWEA CCSD(T)/cc-pV ∞ Z data.

c) Unconverged.

d) CCSD(T)/cc-pVDZ result.

e) Using the B3LYP/cc-pVTZ estimate for the GRXE.

f) Obtained by means of Laser Photoelectron Spectroscopy (LPES), for details see Ref. [34].

g) Obtained with the Electron Capture Detection (ECD), for details see Ref. [32].

h) Obtained by means of LPES, for details see Ref. [35].

i) By an extrapolation method using the water cluster data, for details see Ref. [9].

j) Obtained using ECD, for details see Ref. [10].

k) Obtained using ECD, for details see Ref. [33].

l) Obtained by means of LPES, for details see Ref. [36].

m) Obtained by means of LPES, for details see Ref. [17].

n) Obtained using ECD, for details see Ref. [11].

o) Obtained by means of LPES, for details see Ref. [7].

p) Obtained by means of Ion/molecule reaction equilibrium method, for details see Ref. [8].

This observation is in line with a recent determination of the EA of phenanthrene using the ECD approach, giving an upper limit of 0.269 ± 0.035 [10], thus 0.35 eV above our benchmark value for the adiabatic EA. The rather large disagreements (0.0754 eV and 0.1021 eV) between theory and LPES data in the case of chrysene and perylene are also worth some further examination. The experimental EA of these two compounds were simply directly inferred from the laser photoelectron detachment energies of the *anions* [7, 17]. Very obviously, however, these may not exactly compare with the adiabatic electron affinities of the *neutrals*, due to the different geometry implications of the transitions of interest, especially if one considers that the experimentally studied photodetachment processes are vertical transitions.

5.3.4 Ionization energies

The cations of azulene, phenanthrene, pyrene, chrysene, and perylene were found to possess a 2A_2 , 2B_1 , ${}^2B_{1g}$, 2A_u , 2A_u electronic state, respectively. Details of the Focal Point Analyses of the associated vertical and well-to-well ionization energies are supplied in Tables 14-18, respectively. Again, the ΔHF results and the +MP2 corrections converge smoothly with the cardinal number (X) characterizing the cc-pVXZ basis set, and can thus be extrapolated reliably to an asymptotically complete cc-pV ∞ Z basis set. The estimates obtained on the ground of the FPAs [eq. (1)] by extrapolation of results obtained at the CCSD(T) level to the limit of an asymptotically complete cc-pV ∞ Z basis set are supplied in Table 19. Upon inspecting Tables 14-18, it appears that the +MP2 contributions are systematically positive, and that they largely dominate the correlation corrections.

Table 14. Focal point analysis of the vertical ionization energy of azulene. "Well to well" ionization energies (WWIE) are in parenthesis (all results are given in eV).

Azulene				
	cc-pVDZ	cc-pVTZ	cc-pVQZ	cc-pV ∞ Z
No. Basis	180	412	790	
Δ HF	5.62 (5.45)	5.63 (5.47)	5.65 (5.49)	5.66 ^a (5.50) ^a
+MP2	2.64 (2.64)	2.97 (2.98)	3.07 (3.08)	3.13 ^b (3.14) ^b
+MP3	-0.72 (-0.72)	-0.83 (-0.84)		
+MP4(SDQ)	-0.22 (-0.22)	-0.26 (-0.26)		
+CCSD	-0.26 (-0.25)			
+CCSD(T)	0.14 (0.15)			
Δ CCSD(T)	7.22 (7.05)			

a) Obtained using Feller's three-point extrapolation formula.

b) S_{MP2}-QZ result.**Table 15.** Focal point analysis of the vertical ionization energy of phenanthrene. "Well to well" ionization energies (WWIE) are in parenthesis (all results are given in eV).

Phenanthrene				
	cc-pVDZ	cc-pVTZ	cc-pVQZ	cc-pV ∞ Z
No. basis	246	560	1070	
Δ HF	6.54 (6.36)	6.53 (6.36)	6.54 (6.37)	6.55 ^a (6.38) ^a
+MP2	2.46 (2.50)	2.80 (2.84)	2.89 (2.94)	2.96 ^b (3.01) ^b
+MP3	-0.64 (-0.66)	-0.76 (-0.78)		
+MP4(SDQ)	-0.26 (-0.25)	-0.30 (-0.30)		
+CCSD	-0.34 (-0.34)			
+CCSD(T)	0.03 (0.03)			
Δ CCSD(T)	7.79 (7.64)			

a) Obtained using Feller's three-point extrapolation formula.

b) S_{MP2}-QZ result.

Table 16. Focal point analysis of the vertical ionization energy of pyrene. "Well to well" ionization energies (WWIE) are in parenthesis (all results are given in eV).

Pyrene				
No. Basis	cc-pVDZ	cc-pVTZ	cc-pVQZ	cc-pV ∞ Z
Δ HF	6.01 (5.88)	6.00 (5.89)	6.02 (5.90)	6.03 ^a (5.92) ^a
+MP2	1.98 (2.03)	2.28 (2.33)	2.36 (2.42)	2.42 ^b (2.48) ^b
+MP3	-0.46 (-0.47)	-0.61 (-0.57)		
+MP4(SDQ)	-0.15 (-0.16)	-0.12 (-0.19)		
+CCSD	-0.18 (-0.19)			
+CCSD(T)	0.03 (0.03)			
Δ CCSD(T)	7.23 (7.13)			

a) Obtained using Feller's three-point extrapolation formula.

b) S_{MP2}-QZ result.**Table 17:** Focal point analysis of the vertical ionization energy of chrysene. "Well to well" ionization energies (WWIE) are in parenthesis (all results are given in eV).

Chrysene				
No. basis	cc-pVDZ	cc-pVTZ	cc-pVQZ	cc-pV ∞ Z
Δ HF	6.39 (6.00)	6.38 (5.99)	6.40 (6.01)	6.41 ^a (6.02) ^a
+MP2	1.56 (3.33)	1.82 (3.72)	1.90 (3.83)	1.96 ^b (3.91) ^b
+MP3	-0.33 (-0.95)	-0.41 (-1.11)		
+MP4(SDQ)	-0.09 (-0.39)	-0.11 (-0.45)		
+CCSD	-0.14 (^c)			
+CCSD(T)	0.02 (^c)			
Δ CCSD(T)	7.40 (^c)			

a) Obtained using Feller's three-point extrapolation formula.

b) S_{MP2}-QZ result.

c) Unconverged.

Table 18. Focal point analysis of the vertical ionization energy of perylene. "Well to well" ionization energies (WWIE) are in parenthesis (all results are given in eV).

Perylene				
No. basis	cc-pVDZ	cc-pVTZ	cc-pVQZ	cc-pV ∞ Z
Δ HF	5.29 (5.18)	5.28 (5.17)	5.29 (5.18)	5.31 ^a (5.19) ^a
+MP2	3.44 (3.48)	3.82 (3.87)	3.94 (3.99)	4.01 ^b (4.07) ^b
+MP3	-0.94 (-0.95)	-1.11 (-1.12)		
+MP4(SDQ)	-0.38 (-0.39)	-0.44 (-0.45)		
+CCSD	-0.61 (-0.62)			
+CCSD(T)	0.04 (0.04)			
Δ CCSD(T)	6.83 (6.75)			

a) Obtained using Feller's three-point extrapolation formula.

b) S_{MP2}-QZ result.

Also, these contributions tend to increase upon improving the basis set. For all compounds of interest, corrections at the +MP3, +MP4, and +CCSD levels are on the contrary always negative, and tend therefore to compensate the +MP2 contribution. Estimates of VIEs obtained by means of the FPA amount to 7.5836 eV, 8.1348 eV, 7.5722 eV, 7.7416 eV, and 7.1991 eV for azulene, phenanthrene, pyrene, chrysene and perylene, respectively.

The adiabatic ionization energies (AIE) have been obtained by adding to the FPA estimates of WWIEs the B3LYP/cc-pVTZ estimates for zero-point vibrational energy correction. Estimates of the adiabatic and vertical IE at the CCSD(T)/cc-pV ∞ Z level, "well-to-well" values, GREXs and Δ ZPE corrections are provided in Table 19, where they can be compared with the experimentally obtained results. Our best FPA estimates of the adiabatic ionization energies of azulene, phenanthrene, pyrene, chrysene and perylene

are equal to 7.4283 eV, 8.0129 eV, 7.4755 eV, 7.6527 eV, and 7.1487 eV, respectively. The experimental IE values were obtained from measurements employing gas-phase ion-equilibrium constant determination [13], photoionization mass spectrometry [37], photoelectron spectroscopy [12, 38] and laser spectroscopy [12, 39]. The experimentally obtained ionization energies amount to 7.38 ± 0.03 eV [12] for azulene, 7.903 eV [38] for phenanthrene, 7.4256 ± 0.0006 eV [39] for pyrene, 7.60 ± 0.03 eV [12] for chrysene and 6.960 ± 0.001 eV [12] for perylene. Discrepancies between our best FPA estimates for adiabatic ionization energies and experimental values are thus 0.0438 eV for azulene, 0.0499 eV for pyrene, and 0.0517 eV for chrysene. Discrepancies deceptively increase to 0.107 eV in the case of phenanthrene and even to 0.199 eV in the case of perylene. These larger discrepancies may be indicative of stronger correlation effects, which a CCSD(T) treatment may fail to apprehend within chemical accuracy. Indeed, details of the focal point analysis of the vertical and well-to-well ionization energy of perylene (Table 18) clearly demonstrate the very strongly correlated nature of this compound. Indeed, the individual +MP2, +MP3, +MP4 and +CCSD corrections are in absolute values much larger than usual, and their convergence with the basis set appears also to be much slower.

Table 19. Calculated and experimental ionization energies, along with the zero-point vibrational energy (ΔZPE) and geometry relaxation (GRXE) contributions. All results are given in eV.

	VIE		WWIE		GRXE		GRXE		ΔZPE		AIE	
	CCSD(T)/ cc-pV ∞ Z ^a	7.58	CCSD(T)/ cc-pV ∞ Z ^a	7.44	CCSD(T)/ cc-pV ∞ Z	-0.14	B3LYP/ cc-pVTZ	-0.13	B3LYP/ cc-pVTZ	-0.01	CCSD(T)/ cc-pV ∞ Z ^b	7.43
Azulene												7.38 \pm 0.03 ^e 7.32 \pm 0.05 ^f 7.43 \pm 0.04 ^g
Phenanthrene	8.13		8.01		-0.13		-0.11		0.00		8.01	7.903 ^h 7.87 \pm 0.02 ⁱ 7.8914 \pm 0.0006 ^j
Pyrene	7.57		7.49		-0.09		-0.08		-0.01		7.48	0.4256 \pm 0.0006 ^j 7.4 ^k 7.50 \pm 0.05 ^l
Chrysene	7.73		- ^c		- ^c		-0.08		0.00		7.65 ^d	7.60 \pm 0.03 ^m 8.0 \pm 0.2 ⁿ 7.59 \pm 0.05 ^l
Perylene	7.20		7.12		-0.08		-0.07		0.03		7.15	6.960 \pm 0.001 ^o 6.90 \pm 0.01 ^m 7.00 \pm 0.01 ^m

a) FPA-QZ estimate (see text for details).

b) Upon adding ΔZPE corrections to WWIE CCSD(T)/cc-pV ∞ Z data.

c) Unconverged.

d) Using the B3LYP/cc-pVTZ estimate for the GRXE.

e) Determined by means of photo-ionization mass spectrometry, for details see Ref. [37].

f) Determined by means of ion/molecule equilibrium constant determination, for details see Ref. [12].

g) Obtained by means of photoelectron spectroscopy, for details see Ref. [61].

h) Obtained by means of photoelectron spectroscopy, for details see Ref. [38].

i) Obtained from the time-resolve photo-ionization efficiently curve, for details see Ref. [62].

j) Obtained by means of two laser resonant photo-ionization mass spectroscopy, for details see Ref. [39].

k) Obtained by means of photoelectron spectroscopy, for details see Ref. [63].

l) Determined using gas-phase ion-equilibrium measurements, for details see Ref. [13].

- m) Obtained by means of photoelectron spectroscopy, for details see Ref. [12].
- n) Obtained by means of electron impact techniques, for details see Ref. [12].
- o) Obtained by means of laser spectroscopy, for details see Ref. [12].

For chrysene, because of convergency problem in the coupled cluster iterations for the cation, the GREX contribution to "well-to-well" ionization energy could only be determined on the grounds of B3LYP/cc-pVTZ calculations (Table 19). Comparison of B3LYP/cc-pVTZ and CCSD(T)/cc-pV ∞ Z estimates for the GRXEs associated with the ionization energies of all other target PAHs indicate that the error made in estimating the GREX for the ionization energy of chrysene at the B3LYP/cc-pVTZ level is around 0.01 eV.

5.4 Conclusions

The vertical, well-to-well and adiabatic singlet-triplet energy gaps, electron affinities and ionization energies of azulene, phenanthrene, pyrene, chrysene and perylene have been quantitatively evaluated, at benchmark theoretical levels within the limits of non-relativistic quantum mechanics. The principles of a Focal Point Analysis have been systematically applied on energy differences calculated at the level of Hartree-Fock [HF] theory, second- [MP2], third- [MP3], and fourth-order [SDQ-MP4] Møller-Plesset perturbation theory, as well as coupled cluster theory including single, double and perturbative triple excitations [CCSD(T)], in conjunction with correlation consistent cc-pVXZ basis sets of improving quality (X=D,T,Q), in order to evaluate vertical and well-to-well transition energies at the CCSD(T) level in the limit of an asymptotically complete (X= ∞) basis set. Adiabatic transition energies were ultimately obtained by adding to the well-to-well CCSD(T)/cc-pV ∞ Z energy differences B3LYP/cc-pVTZ estimates for the zero-point vibrational corrections.

Our best estimates for the vertical singlet-triplet energy gaps of azulene, phenanthrene, pyrene, chrysene, perylene amount to 2.24 eV, 3.54 eV, 2.70 eV, 3.24 eV, 2.14 eV, respectively. The best adiabatic estimates obtained by adding

the zero-point vibration energies and geometry relaxation energy contribution to the vertical estimates, are, in the same order, 1.79 eV, 2.92 eV, 2.22 eV, 2.79 eV, and 1.71 eV. In view of the complexity and strongly correlated nature of the selected molecular targets, these results support favorably the comparison with experiment, with discrepancies ranging from 0.046 eV (azulene) up to 0.24 eV (phenanthrene). We noted that most experimental data are the results of measurements which have been performed in solid matrices or solvents, and are thus subject to complications arising from the molecular environment (intermolecular forces and polarization effects, packing effects).

Our best estimates for the vertical electron affinities of azulene, phenanthrene, pyrene, chrysene and perylene amount to 0.40 eV, -0.42 eV, 0.12 eV, -0.05 eV, and 0.63 eV, respectively. Upon taking into account geometry relaxation effects and zero point vibrational energy, we obtain adiabatic electron affinities that are equal to 0.71 eV, -0.08 eV, 0.40 eV, 0.24 eV, and 0.87 eV, respectively. Our theoretical results sustain again most favorably the comparison with experiment, with discrepancies ranging from only 0.006 eV and 0.017 eV for pyrene and azulene, up to 0.075 and 0.1 eV in the case of chrysene and perylene, respectively. We noted that the latter two experimental values were obtained using laser photodetachment electron spectroscopy, and are therefore subject to geometrical complications arising with the sudden (vertical) removal of an electron from the anion.

Our best FPA estimates for the vertical ionization energies of azulene, phenanthrene, pyrene, chrysene and perylene amount to 7.58 eV, 8.13 eV, 7.57 eV, 7.73 eV, and 7.20 eV, respectively. Adiabatic estimates obtained upon incorporating geometry relaxation energies and zero point vibrational contributions are, in the same order, equal to 7.43 eV, 8.01 eV, 7.48 eV, 7.65

eV, and 7.15 eV, respectively. Discrepancies between theory and experiment range from 0.04 eV, 0.05 eV and 0.05 eV, for azulene, pyrene and chrysene, up to 0.11 and 0.19 eV for phenanthrene and perylene. The latter very large discrepancy is probably ascribable to the more strongly correlated nature of perylene, which a single-reference CCSD(T) treatment may fail to apprehend within chemical accuracy. Also, one should examine more closely the outcome of steric hindrances and vibronic coupling interactions within the bay regions of compounds like phenanthrene and chrysene.

5.5 References

- [1] M. S. Deleuze, L. Claes, E. S. Kryachko, J.-P. Francois, *J. Phys. Chem.* **119**, 3106 (2003).
- [2] B. Hajgató, M. S. Deleuze, D. J. Tozer, F. De Proft, *J. Chem. Phys.* **129**, 084308 (2008).
- [3] B. Hajgató, D. Szieberth, P. Geerlings, F. De Proft, M. S. Deleuze, *J. Chem. Phys.* **131**, 224321 (2009).
- [4] B. Hajgató, M. Huzak, M. S. Deleuze, *J. Phys Chem. A.* **115**, 9282 (2011).
- [5] A. L. L. East, W. D. Allen, *J. Chem. Phys.* **99**, 4638 (1993); S. J. Klippenstein, A. L. L. East, W. D. Allen, *J. Chem. Phys.* **105**, 118 (1996); N. L. Allinger, J. T. Fermann, W. D. Allen, H. F. Schaefer III, *J. Chem. Phys.* **106**, 5143 (1997); A. G. Császár, W. D. Allen, H. F. Schaefer III, *J. Chem. Phys.* **108**, 9751 (1998); G. Tarczay, A. G. Császár, W. Klopper, V. Szalay, *J. Chem. Phys.* **110** 11971(1999); E. F. Valeev, W. D. Allen, H. F. Schaefer III, A. G. Császár, A. L. L. East, *J. Phys. Chem. A*, **105**, 2716 215

- (2001); A. Salam, M. S. Deleuze, *J. Chem. Phys.* **116**, 1296 (2002); N. D. Petraco, W. D. Allen, H. F. Schaefer III, *J. Chem. Phys.* **116**, 10229 (2002); S. P. Kwasniewski, L. Claes, J.-P. François, M. S. Deleuze, *J. Chem. Phys.* **118**, 7823 (2003); E. Czinski, A. G. Császár, *Chem. Eur. J.* **9**, 1008 (2003); A. G. Császár, M. L. Leininger, V. Szalay, *J. Chem. Phys.* **118**, 10631 (2003); K. Kahn; T. C. Bruice, *Theor. Chem. Acc.* **111**, 18 (2004); S. E. Wheeler, W. D. Allen, H. F. Schaefer III, *J. Chem. Phys.* **121**, 8800 (2004); A. G. Császár, V. Szalay, M. L. Senent, *J. Chem. Phys.* **120**, 1203 (2004); M. S. Schuurman, S. R. Muir, W. D. Allen, H. F. Schaefer III, *J. Chem. Phys.* **120**, 11586 (2004); K. Kahn, T. C. Bruice, *Chem. Phys. Chem.* **6**, 487 (2005); K.-C. Lay, C. Y. Ng, *J. Chem. Phys.* **122**, 224310 (2005); K. Kahn, I. Kahn, *J. Comp. Chem.* **29**, 900 (2008); J. Demaison, J. Liévin, A. G. Császár, C. Guttle, *J. Phys. Chem. A*, **112**, 4427 (2008); O. S. Bokareva, V. A. Bataev, *Int. J. Quantum Chem.* **108**, 2719 (2008); T. Szidarovszky, G. Czakó, A. G. Császár, *Mol. Phys.* **107**, 761 (2009); J. J. Wilke, M. C. Lind, H. F. Schaefer III, A. G. Császár, and A. D. Allen, *J. Chem. Theor. Comp.* **5**, 1511 (2009); R. M. Balabin, *Chem. Phys. Lett.* **479**, 195 (2009); E. V. Rastotseva, V. A. Bataev, I. A. Godunov, *J. Mol. Struct (THEOCHEM)* **905**, 86 (2009); R. Monten, B. Hajgató, M. S. Deleuze, *Mol. Phys.* **109**, 2317 (2011).
- [6] G. D. Chen, R. G. Cooks, *J. Mass. Spectrom.* **30**, 1167 (1995.)
- [7] J. Scheidt, R. Weinkauff, *Chem. Phys. Lett.* **274**, 18 (1997).
- [8] L. Crocker, T. B. Wang, P. Kebarle, *J. Am. Chem. Soc.* **115**, 7818 (1993).
- [9] M. Tschurl, U. Boesl, S. Gilb, *J. Chem. Phys.* **125**, 194310 (2006).
- [10] L. Wojnarovits, G. Foldiak, *J. Chromatogr. Sci.* **206**, 511 (1981).
- [11] R. S. Becker, E. Chen, *J. Chem. Phys.* **45**, 2403 (1966).

- [12] P. J. Linstrom, W. G. Mallard, Eds., NIST Chemistry WebBook, NIST Standard Reference Database Number 69, National Institute of Standards and Technology, Gaithersburg MD, 20899, <http://webbook.nist.gov>, (retrieved January 18, 2012).
- [13] M. Mautner (Meot-Ner), J. Phys. Chem. **84**, 2716 (1980).
- [14] W. Siebrand, J. Chem. Phys. **47**, 2411 (1967) (and references therein).
- [15] W. G. Herkstroeter, J. Am. Chem. Soc. **97** (15), 4161 (1975).
- [16] A. A. Gorman, I. Hamblett, R. J. Harrison, J. Am. Chem. Soc. **106** (23), 6952 (1984).
- [17] M. Tschurl, U. Boesl, Int. J. Mass. Spectrom. **249**, 364 (2006).
- [18] J. B. Birks, M. A. Slifkin, Nature [London] **191**, 761 (1961).
- [19] A. Modelli, L. Mussoni, D. Fabbri, J. Phys. Chem. A **110**, 6482 (2006).
- [20] S. Hirata, T. J. Lee, M. Head-Gordon, J. Chem. Phys. **111**, 8904 (1999).
- [21] J. C. Rienstra-Kiracofe, C. J. Barden, S. T. Brown, H. F. Schaefer III, J. Phys. Chem. A **105**, 524 (2001); F. De Proft, P. Geerlings, J. Chem. Phys. **106**, 3270 (1997); A. Modelli, L. Mussoni, D. Fabbri, J. Phys. Chem. A **110**, 6482 (2006).
- [22] J. C. Rienstra-Kiracofe, G. S. Tschumper, H. F. Schaefer III, S. Nandi, G. B. Ellison, Chem. Rev. Washington DC **102**, 231 (2002).
- [23] Z. L. Cai, K. Sendt, J. R. Reimers, J. Chem. Phys. **117**, 5543 (2002).
- [24] J. R. Reimers, Z.-L. Cai, A. Bilic, and A. S. Hush, Ann. N.Y. Acad. Sci. **110**, 235 (2003); J. R. Reimers, Z. L. Cai, A. Bilic, N. S. Hush, Ann. NY Acad. Sci. **1006**, 235 (2003).
- [25] A. P. Monkman, H. D. Burrows, L. J. Hartwell, L.E. Horsburgh, I. Hamblett, S. Navaratnam, Phys. Rev. Lett. **86**, 1358 (2001).
- [26] J. B. Birks, *Organic Molecular Photophysics*, Vol 2 (Wiley, London, 1975).

- [27] G. D. Veith, O. G. Mekenyan, G. T. Ankley, J. D. Call, *Chemosphenen*. **30**, 2129 (1995).
- [28] T. Koopmans, *Physica* **1**, 104 (1934).
- [29] A. Szabo, N. S. Ostlund, *Modern Quantum Chemistry* (McGraw-Hill, New York, 1982).
- [30] M. M. Rhead, S. A. Hardy, *Fuel* **82**, 385 (2003); P. J. Tancell, M. M. Rhead, R. D. Pemberton, J. Braven, *Environ. Sci. Technol.* **29**, 2871 (1995).
- [31] J. Ivanco, T. Haber, R. Resel, F. P. Netzer, M. G. Ramsey, *Thin Solid Films* **514**, 156 (2006).
- [32] E. C. M. Chen, E. S. Chen, M. S. Milligan, W. E. Wentworth, J.R. Wiley, *J. Phys. Chem.* **96**, 2385 (1992).
- [33] W. E. Wentworth, R. S. Becker, *J. Am. Chem. Soc.* **84**, 4263 (1962).
- [34] N. Ando, M. Mitsui, A. Nakajima, *J. Chem. Phys.* **128**, 154318 (2008).
- [35] J. Schiedt, W. J. Knott, K. Le Barbu, E. W. Schlag, R. Weinkauff, *J. Chem. Phys.* **113**, 9470 (2000).
- [36] N. Ando, S. Kokubo, M. Mitsui, A. Nakajima, *Chem. Phys. Lett.* **389**, 279 (2004).
- [37] H.-W. Jochims, H. Rasekh, E. Rühl, H. Baumgärtel, S. Leach, *Chem. Phys.* **168**, 159 (1992).
- [38] N. Thantu, P. M. Weber, *Chem. Phys. Lett.* **214**, 276 (1993).
- [39] J. W. Hager, S. C. Wallace, *Anal. Chem.* **60**, 5 (1988).
- [40] L. D. Betowski, M. Enlow, L. Riddick, D. H. Aue, *J. Phys. Chem. A*, **110**, 12927 (2006).
- [41] J. L. Weisman, T. J. Lee, M. Head-Gordon, *Spectrochim. Acta, Part A*, **57**, 931 (2001).

- [42] N. Treitel, R. Shenhar, I. Aprahamian, T. Sheradsky, M. Rabinovitz, *Phys. Chem. Chem. Phys.* **6**, 1113 (2004).
- [43] M. S. Deleuze, *J. Chem. Phys.* **116**, 7012 (2002).
- [44] L. S. Cederbaum, W. Domcke, *Adv. Chem. Phys.* **36**, 205, (1977), and references therein.
- [45] L. S. Cederbaum, *J. Phys. B*, **8**, 290 (1975).
- [46] K. D. Jordan, P. D. Burrow, *Chem. Rev.* **87**, 557 (1987).
- [47] G. D. Purvis; R. J. Bartlett, *J. Chem. Phys.* **76**, 1910 (1982); G. E. Scuseria, C. L. Janssen, H. F. Schaefer III., *J. Chem. Phys.* **89**, 7382 (1988); K. Raghavachari, G. W. Trucks, M. Head-Gordon, J. A. Pople, *Chem. Phys. Lett.* **157**, 479 (1989); R. J. Bartlett, *J. Phys. Chem.* **93**, 1697 (1989).
- [48] Gaussian 09, Revision A.1, M. J. Frisch, G. W. Trucks, H. B. Schlegel, G. E. Scuseria, M. A. Robb, J. R. Cheeseman, G. Scalmani, V. Barone, B. Mennucci, G. A. Petersson, H. Nakatsuji, M. Caricato, X. Li, H. P. Hratchian, A. F. Izmaylov, J. Bloino, G. Zheng, J. L. Sonnenberg, M. Hada, M. Ehara, K. Toyota, R. Fukuda, J. Hasegawa, M. Ishida, T. Nakajima, Y. Honda, O. Kitao, H. Nakai, T. Vreven, J. A. Montgomery, Jr., J. E. Peralta, F. Ogliaro, M. Bearpark, J. J. Heyd, E. Brothers, K. N. Kudin, V. N. Staroverov, R. Kobayashi, J. Normand, K. Raghavachari, A. Rendell, J. C. Burant, S. S. Iyengar, J. Tomasi, M. Cossi, N. Rega, J. M. Millam, M. Klene, J. E. Knox, J. B. Cross, V. Bakken, C. Adamo, J. Jaramillo, R. Gomperts, R. E. Stratmann, O. Yazyev, A. J. Austin, R. Cammi, C. Pomelli, J. W. Ochterski, R. L. Martin, K. Morokuma, V. G. Zakrzewski, G. A. Voth, P. Salvador, J. J. Dannenberg, S. Dapprich, A. D. Daniels, Ö. Farkas, J. B. Foresman, J. V. Ortiz, J. Cioslowski, and D. J. Fox, Gaussian, Inc., Wallingford CT, 2009.

- [49] R. Dreizler, E. Gross, *Density Functional Theory* (Plenum Press, New York, 1995).
- [50] C. Lee, W. Yang, R. G. Parr, *Phys. Rev. B*, **37**, 785 (1988); A.D. Becke, *J. Chem. Phys.* **98**, 5648 (1993).
- [51] T. H. Dunning Jr., *J. Chem. Phys.* **90**, 1007 (1989).
- [52] C. Møller, M.S. Plesset, *Phys. Rev.* **46**, 618 (1934).
- [53] M. Head-Gordon, J. A. Pople, and M. J. Frisch, *Chem. Phys. Lett.* **153**, 503 (1988).
- [54] J. A. Pople, R. Seeger, and R. Krishnan, *Int. J. Quant. Chem. Symp.* **11**, 149 (1977).
- [55] R. Krishnan, and J. A. Pople, *Int. J. Quant. Chem.* **14**, 91 (1978).
- [56] D. Feller, *J. Chem. Phys.* **96**, 6104 (1992); D. Feller, *J. Chem. Phys.* **98**, 7059 (1993).
- [57] C. Schwartz, *Methods in Computational Physics* Vol. 2 edited by Alder B Academic (New York, 1963).
- [58] T. J. Lee, P. R. Taylor, *Int. J. Quantum. Chem., Quantum. Chem. Symp.* **23**, 199 (1989).
- [59] A. Karton, E. Rabinovich, J.L.M. Martin, B. Ruscic, *J. Chem. Phys.* **125**, 144108 (2006).
- [60] E. C. M. Chen, W. E. Wentworth, *Mol. Cryst. Liq. Cryst.* **171**, 271 (1989).
- [61] R. Boschi, E. Clar, W. Schmidt, *J. Chem. Phys.* **60**, 4406 (1974).
- [62] Y. Gotkis, M. Oleinikova, M. Naor, C. Lifshitz, *J. Phys. Chem.* **97**, 12282 (1993).
- [63] E. Clar, J. M. Robertson, R. Schlogl, W. Schmidt, *J. Am. Chem. Soc.* **103**, 1320 (1981).

6 Benchmark theoretical study of the electric polarizabilities of naphthalene, anthracene and tetracene

6.1 Introduction

The static electric dipole polarizabilities of molecules are very important properties which play an important role in many physical phenomena, such as dielectric polarization, intermolecular dispersion forces and Stark effect [1]. Polarizabilities are also used as predictors of the biodegradation rates [2] of widespread pollutants such as alkylated polycyclic aromatic hydrocarbons. Static electric dipole polarizabilities measure the change at first order in the molecular dipole moment when an external homogenous and frequency-independent electric field is applied:

$$\mu_i(\vec{F}) = \mu_i(\vec{0}) + \sum_j \alpha_{ij} F_j + \dots \quad (1)$$

The polarizability tensor [α_{ij} $\{i=x,y,z; j=x,y,z\}$] is therefore cast in terms of second-order energy derivatives with respect to the external static electric field [3], in line with the expansion:

$$E(\vec{F}) = E(\vec{0}) - \sum_i \mu_i F_i - \frac{1}{2} \sum_{ij} \alpha_{ij} F_i F_j - \dots \quad (2)$$

A main rotational invariant is the isotropic polarizability, defined as:

$$\bar{\alpha} = \frac{1}{3} (\alpha_{xx} + \alpha_{yy} + \alpha_{zz}) \quad (3)$$

The electric polarizabilities of naphthalene, anthracene and tetracene have been subject of numerous studies. On theoretical side, most results have been obtained using Hartree-Fock (HF) theory [4,5], Density Functional Theory (DFT)

[5, 6, 7, 8, 9] in conjunction with different functionals and basis sets, second-order Møller–Plesset perturbation theory [5, 6], or semi-empirical methods [10]. Of particular relevance is a recent work by Hammond *et al.*, [11] which describes calculations of the polarizabilities of naphthalene, anthracene and tetracene using coupled-cluster singles and doubles linear response (CCSD-LR) theory [12] in conjunction with the Sadlej pVTZ basis set [13]. On the experimental side, the polarizabilities of naphthalene and anthracene have been measured using a variety of techniques, such as Laser Stark-effect spectroscopy [14, 15], Kerr-effect experiments [16, 17], crystal refraction [18], Electric field NMR [19], and Cotton-Moutton-effect [20]. From a quantitative viewpoint the current situation is far from being satisfactory, considering the extent of the discrepancies observed among experimental values for the isotropic polarizabilities of naphthalene [14,16,18,21] and anthracene [15,17,19,20] (up to 23 and 60 a.u., respectively, with $1 \text{ a.u.} = 1 \text{ e}^2 \text{ a}_0^2 \text{ E}_h^{-1} = 1.648778 \cdot 10^{-41} \text{ C}^2 \text{ m}^2 \text{ J}^{-1}$), or the extent of the discrepancies observed between the latest DFT and CCSD-LR theoretical determinations of the polarizabilities of anthracene, up to 22 a.u. [see Table VII in ref. [11] for details]. For all these reasons, systematic studies of the dependence of the polarizabilities of oligoacenes on the level attained in electron correlation and on quality of the basis set are most desirable.

Three decades ago, agreement between experimentally derived and theoretically predicted polarizabilities was a major issue [22]. Since then, various aspects of the theoretical determination of polarizabilities have been examined in depth in comprehensive reviews [23]. It is now well-established that energies and related response properties are very sensitive to electron correlation and to the employed basis set [24]. Unfortunately, large scale treatments of electron correlation remain in most situations far too prohibitive

for straightforward applications upon compounds of great practical relevance, as for instance large conjugated systems in non-linear optics [25]. In such situations, one of the most affordable options for reaching the so-called chemical accuracy on energies [1 kcal/mol; i.e. 0.043 eV] consists in exploiting separately the faster convergence with respect to the basis set of the highest-order correlation corrections to energies, by virtue of the principles of a Focal Point Analysis [26]. The reader is referred in particular to benchmark theoretical studies, within or close to chemical accuracy (1 kcal/mol, i.e. 0.043 eV), of the ionization energies [27], electron attachment energies [28] or singlet-triplet energy gaps [29] of *n*-acenes, which are notoriously difficult, i.e. strongly correlated compounds. The fact that the latter properties could be computed within or close to chemical accuracy within the framework of a closed-shell symmetry-restricted depiction for the electronic ground state has led us to call into question [30] the view [31] that zig-zag graphene nanoribbons are antiferromagnetic systems subject to a half-metallic spin-polarization of edge states in the presence of a transversal electric field.

Considering the lack of accurate enough data for these systems, and the extent of discrepancies between the currently available theoretical and experimental values, the scope of the present work is to investigate at similar benchmark levels the electric polarizabilities of naphthalene, anthracene and tetracene. In this purpose we aim first at determining how these properties converge to the CCSD(T)/CBS level [i.e. Coupled Cluster Theory along with Single, Double and perturbative Triple electronic excitations [32], in conjunction with an asymptotically complete basis set (CBS)] when resorting to well-established hierarchies of basis sets and size-consistent many-body wave function approaches, along with the Finite Field (FF) approach [33]. The

principles of a Focal Point Analysis are thereafter applied in order to evaluate the static dipole electric polarizabilities up to the CCSD(T)/CBS level, by combining pairwise energies obtained using successive treatments of electron correlation and basis sets of improving quality. In line with a comparable and highly quantitative study [34] of the polarizabilities of Ne, CO, N₂, F₂, HF, H₂O, HCN, and C₂H₂ (acetylene), we supply at last vibrationally averaged results for the isotropic polarizabilities of all target systems at 298K, which are obtained by combining our best FPA estimates with thermal corrections derived from classical trajectory simulations, using Born-Oppenheimer Molecular Dynamics (BOMD) [35].

6.2 Computational details

Relating linear molecular properties to second-order derivatives of the energy allows all standard post-SCF quantum chemical techniques for calculating energies at a correlated level to be used, and thus bypasses the need for more elaborate, specific analytical approaches, as for instance Polarization Propagator [36] or Coupled Perturbed Electron Propagator [37] theories. However, in order to minimize non-linear effects, which are most commonly enhanced when electron correlation is included, one has to limit the extent of the external perturbation, and the energy differences to compute are therefore rather small. On the other hand, the field has still to be large enough in order to induce energy differences that are substantially larger than the uncertainties due to the employed approximations and numerical errors. Typically, upon taking 0.0003 a.u. ($1 \text{ a.u.} = E_h e^{-1} a_0^{-1} = 5.142 \cdot 10^{11} \text{ V m}^{-1}$) as the basic step size on the electric field, polarizabilities can be computed within an accuracy of 1 a.u. ($1 \text{ a.u.} = 1 e^2 a_0^2 E_h^{-1} = 1.648778 \cdot 10^{-41} \text{ C}^2 \text{ m}^2 \text{ J}^{-1}$) when evaluating numerically

energy differences within 10^{-6} a.u. uncertainty ($1 \text{ a.u.} = 1 E_h = 4.3597482 \cdot 10^{-18}$ J).

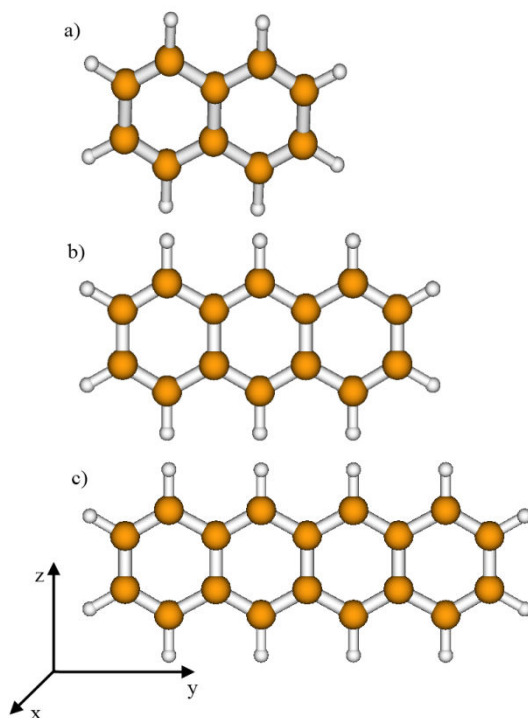


Figure 1. Molecular orientation retained for (a) naphthalene, (b) anthracene and (c) tetracene.

All calculations that are presented in the sequel are based on molecular geometries which have been optimized by means of DFT [38] in conjunction with the Becke three-parameter-Lee-Yang-Parr (B3LYP) functional [39] and the cc-pVTZ basis set [40], using the Gaussian09 program package [41]. The tightest optimization convergence criteria were enforced at all stages of the optimization process. All calculations have been performed upon the standard molecular orientation defined (Figure 1) from the main symmetry elements of the molecular target, according to the conventions described in the book by Jaffé

and Orchin [42], so that all off-diagonal components of the polarizability tensor identically vanish. Naphthalene, anthracene and tetracene were placed in the yz plane, with the y -axis set parallel to the long molecular axis, while the z -axis was parallel to the short molecular axis and the x -axis was perpendicular to the molecular plane. Finite Field calculations have been performed, in conjunction with various basis sets, upon the optimized B3LYP/cc-pVTZ geometries, at the level of Hartree-Fock (HF) theory [43], Møller-Plesset theory [44] truncated at second-order (MP2) [45], third-order (MP3) [46], and fourth-order with single, double, and quadruple excitations (SDQ-MP4) [47], and at the CCSD [48] and CCSD(T) [32] levels of theory using MOLPRO 2010.1 [49]. The diagonal components of the polarizability tensor were determined according to equation (2) from second-order derivatives of the energy with respect to the relevant components of the field, using a second-order polynomial least squares fit over energies obtained after embedding the target of interest in homogenous electric fields of strength equal to ± 0.9 , ± 0.3 and $0.0 \cdot 10^{-3}$ a.u. in the x -, y - and z -directions.

The employed basis sets are the Dunning's correlation consistent cc-pVXZ basis sets [40, 50] ($X=\{D,T,Q,5\}$) and aug-cc-pVXZ basis sets [51] ($X=\{D,T,Q\}$). These basis sets allow extrapolations of electronic energies in clamped nuclei configurations to the limit of an asymptotically complete basis set. Specifically, Feller's three-point extrapolation formula [52] has been used for extrapolating HF energies to this limit, while MP2 electron correlation energies are extrapolated separately, according to the so-called 6(lmn) extension [53] of Schwartz's [54] formula.

The total energies estimated at the MP2 level in the limit of the asymptotically complete (aug)-cc-pV ∞ Z basis sets have thus been obtained

by adding the extrapolated HF energies [$E^{HF}(\infty)$] to the extrapolated value obtained for the MP2 correlation energy [$E^{corr}(\infty)$]. MP2 energies obtained from three-point extrapolations employing $l=2,3,4$ and $l=3,4,5$ along with the cc-pVXZ basis sets will be referred to as S_{MP2-QZ} and S_{MP2-5Z} results, respectively. Similarly, the $S_{MP2-augQZ}$ label will refer to results obtained from three-point extrapolations employing $l=2,3,4$ along with the aug-cc-pVXZ basis sets. In line with the principles of a FPA, total energies are then estimated at the CCSD(T) level of theory in the limit of an asymptotically complete (aug)-cc-pV ∞ Z basis set, according to the following protocols:

$$\begin{aligned} \text{FPA-QZ} = S_{MP2-QZ} + (E_{MP4/cc-pVTZ} - E_{MP2/cc-pVTZ}) + \\ + (E_{\text{CCSD(T)}/cc-pVDZ} - E_{MP4/cc-pVDZ}), \end{aligned} \quad (4)$$

$$\begin{aligned} \text{FPA-AQZ} = S_{MP2-augQZ} + (E_{MP4/aug-cc-pVTZ} - E_{MP2/aug-cc-pVTZ}) + \\ + (E_{\text{CCSD(T)}/aug-cc-pVDZ} - E_{MP4/aug-cc-pVDZ}), \end{aligned} \quad (5)$$

$$\begin{aligned} \text{FPA-5Z} = S_{MP2-5Z} + (E_{MP4/cc-pVQZ} - E_{MP2/cc-pVQZ}) + \\ + (E_{\text{CCSD(T)}/cc-pVTZ} - E_{MP4/cc-pVTZ}). \end{aligned} \quad (6)$$

We note that the same protocols have been used recently in quantitative studies of the singlet-triplet excitation energies of oligoacenes [29].

In the case of tetracene, due to the prohibitive cost of these calculations, it was not possible to consider MP3 and higher order calculations in conjunction with the cc-pVQZ or larger basis sets. Further extrapolation protocols applying the principles of a FPA have therefore been retained in this particular case for

evaluating energies at the MP3, MP4 and CCSD levels in the limit of an asymptotically complete cc-pV ∞ Z basis set:

$$E_{\text{MP3/cc-pV}\infty\text{Z}} = S_{\text{MP2-QZ}} + (E_{\text{MP3/cc-pVTZ}} - E_{\text{MP2/cc-pVTZ}}), \quad (7)$$

$$E_{\text{MP4/cc-pV}\infty\text{Z}} = S_{\text{MP2-QZ}} + (E_{\text{MP4/cc-pVTZ}} - E_{\text{MP2/cc-pVTZ}}), \quad (8)$$

$$E_{\text{CCSD/cc-pV}\infty\text{Z}} = S_{\text{MP2-QZ}} + (E_{\text{MP4/cc-pVTZ}} - E_{\text{MP2/cc-pVTZ}}) + \\ + (E_{\text{CCSD/cc-pVDZ}} - E_{\text{MP4/cc-pVDZ}}). \quad (9)$$

For naphthalene and anthracene, use has also been made of the extrapolation formula:

$$E_{\text{CCSD/cc-pV}\infty\text{Z}} = S_{\text{MP2-5Z}} + (E_{\text{MP4/cc-pVQZ}} - E_{\text{MP2/cc-pVQZ}}) + \\ + (E_{\text{CCSD/cc-pVTZ}} - E_{\text{MP4/cc-pVTZ}}). \quad (10)$$

All correlated wave function calculations presented in this work have been performed under the frozen core approximation.

BOMD simulations were run along with Density Functional Theory in conjunction with the dispersion corrected ω B97XD exchange-correlation functional [55] and the cc-pVDZ or aug-cc-pVDZ basis sets, in order to evaluate thermal corrections to the polarizabilities of naphthalene, anthracene, and tetracene. BOMD calculations were run according to the principles of classical trajectory simulations [56], using the implementation [57] of the approach [35] which is available in the Gaussian 09 package of programs. In all BOMD simulations, the Bulirsch-Stoer method was used for the integration scheme [58, 59], along with an integration time step of 0.2 fs, and using a fifth-order polynomial fit in the integration-correction scheme. The trajectory step size was set to 0.250 a.u, and atomic coordinates were dumped at time intervals of approximately 1 fs. Thermalization to standard room temperature (298K) was ensured by setting the initial rotational energy from a thermal distribution assuming a symmetric top. The time average was made on isotropic

polarizabilities computed at each point of the calculated BOMD trajectories. Runtimes comprised between 1.025 and 1.321 μs , corresponding to time averages over 2000 thermally distorted structures. The BOMD simulations were performed for a microcanonical (NVE) ensemble and the equilibration time was set to 0.1 μs . Thermalization was checked by monitoring the time-dependence of the kinetic energies, potential energies and isotropic polarizabilities obtained at each point of the computed trajectories.

6.3 Results and discussion

6.3.1 Convergence of molecular polarizabilities towards the CCSD(T)/CBS level

Static electric dipole polarizabilities obtained at the HF, MP2, MP3, MPQ(SDQ), CCSD and CCSD(T) levels of theory in conjunction with cc-pVXZ basis sets of improving quality ($X=D,T,Q,5$) and extrapolated up to the limit of an asymptotically complete (cc-pV ∞ Z) basis set are displayed in Figures 2-4 for naphthalene, anthracene and tetracene, respectively. Upon examining these figures, it is systematically apparent that, whatever the treatment retained for electron correlation, all components of the polarizability tensor increase and converge smoothly to the CBS limit when X evolves from D to ∞ . Very clearly also, it appears that the differences in the polarizability values, due to the use of different basis sets, are much larger than the differences which can be observed when resorting to different treatments of electron correlation.

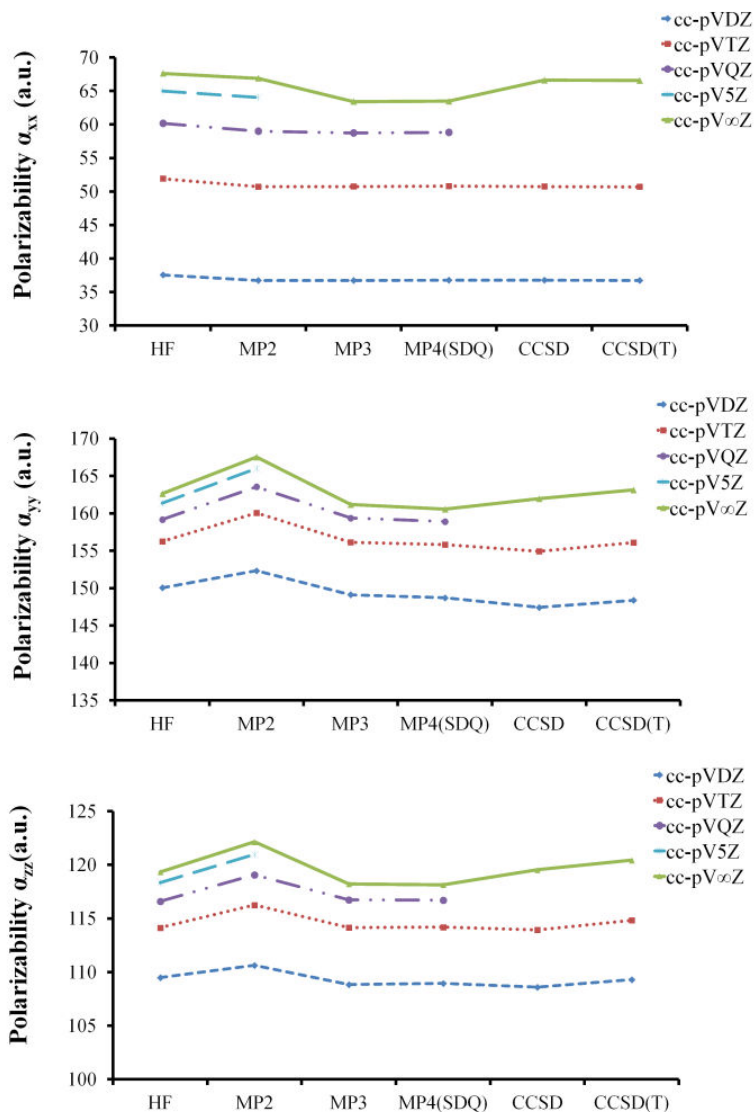


Figure 2. Evolution of the static electric dipole polarizability tensor of naphthalene as a function of the theoretical level attained in the treatment of electron correlation using basis sets of improving quality. HF/cc-pV ∞ Z and MP2/cc-pV ∞ Z results were obtained by applying the Feller's and Schwartz's three point extrapolation formula on energies obtained using the cc-pVXZ ($X=T,Q,5$) basis sets. The MP3/cc-pV ∞ Z and MP4/cc-pV ∞ Z data are also the results of three point extrapolations, but using the cc-pVXZ ($X=D,T,Q$) basis sets. The CCSD/cc-pV ∞ Z and CCSD(T)/cc-pV ∞ Z (FPA-5Z) values are at last the result of FPA extrapolations of energies, according to equations 10 and 6, respectively.

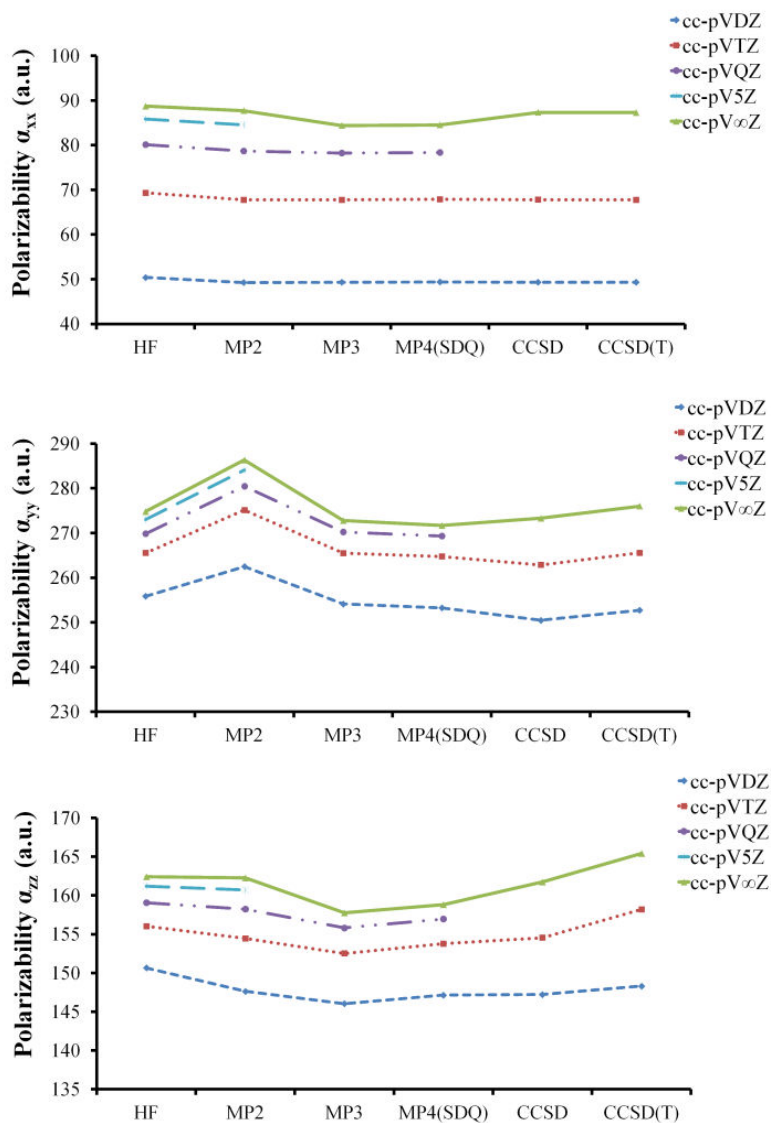


Figure 3. Evolution of the static electric dipole polarizability tensor of anthracene as a function of the theoretical level attained in the treatment of electron correlation using basis sets of improving quality. HF/cc-pV ∞ Z and MP2/cc-pV ∞ Z results were obtained by applying the Feller's and Schwartz's three point extrapolation formula on energies obtained using the cc-pVXZ ($X=T,Q,5$) basis sets. The MP3/cc-pV ∞ Z and MP4/cc-pV ∞ Z data are also the results of three point extrapolations, but using the cc-pVXZ ($X=D,T,Q$) basis sets. The CCSD/cc-pV ∞ Z and CCSD(T)/cc-pV ∞ Z (FPA-5Z) values are at last the result of FPA extrapolations of energies, according to equations 10 and 6, respectively.

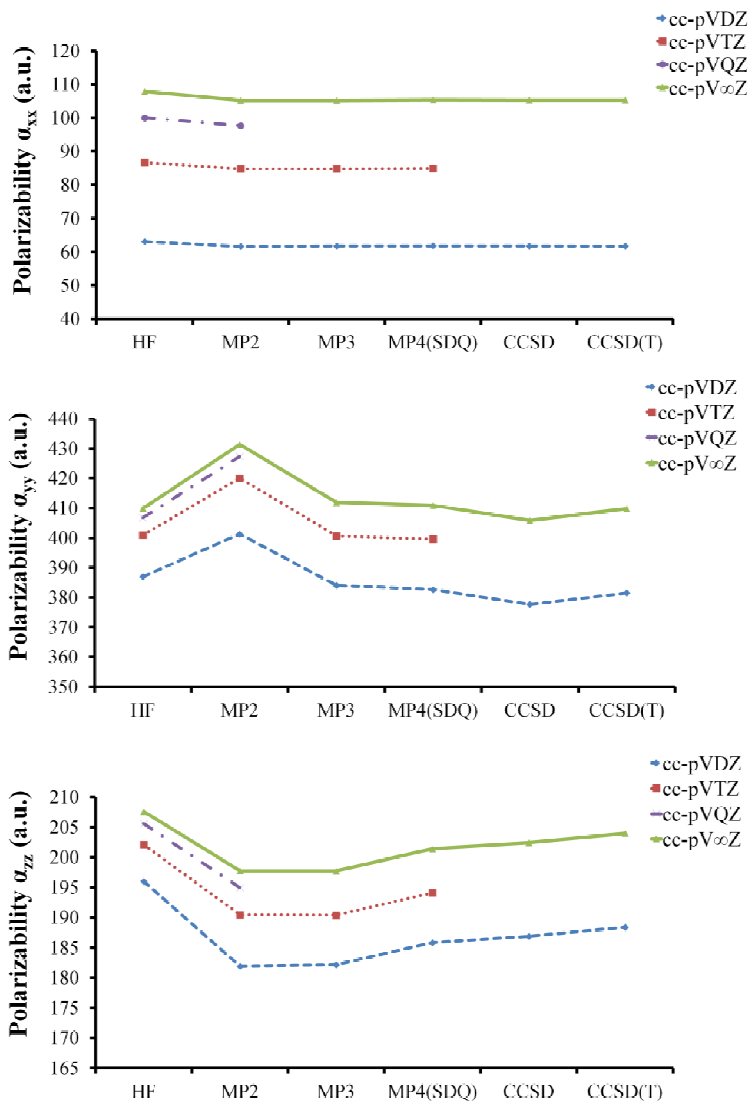


Figure 4. Evolution of the static electric dipole polarizability tensor of tetracene as a function of the theoretical level attained in the treatment of electron correlation using basis sets of improving quality. HF/cc-pV ∞ Z and MP2/cc-pV ∞ Z results were obtained by applying the Feller's and Schwartz's three point extrapolation formula on energies obtained using the cc-pVXZ ($X=D,T,Q$) basis sets. The MP3/cc-pV ∞ Z, MP4/cc-pV ∞ Z, CCSD/cc-pV ∞ Z and CCSD(T)/cc-pV ∞ Z (FPA-QZ) values are the results of FPA extrapolations of energies, according to equations 7, 8, 9 and 4, respectively.

In other words, the basis set appears to be the factor that dominates the quality of the computed electric polarizabilities. The α_{xx} component of the polarizability tensor is found to be essentially insensitive to the level attained in electron correlation. In contrast, the MP2 approach corresponds in general to maximal values for the other components (α_{yy} and α_{zz}) of the polarizability tensor-with the exception of the α_{zz} value reported for anthracene. We note that whereas Hammond *et al* considered that the effect of triple excitations for the static polarizabilities of benzene is not large enough to justify concern as to the validity of the CCSD calculations of the polarizabilities of larger oligacenes [11], we find that, compared with the CCSD results for naphthalene, anthracene and tetracene, the effect of the triple excitations on the α_{yy} and α_{zz} components of the polarizability tensor is very significant and grows with system size. It is clear therefore that a CCSD treatment is not sufficient for a computation of the polarizabilities of large *n*-acenes with relative accuracies better than a few %.

6.3.2 Naphthalene

The results of our most accurate [CCSD(T)] calculations of the electronic polarizabilities of naphthalene in its equilibrium B3LYP/cc-pVTZ geometry are summarized in Table 1. Our CCSD(T)/cc-pV ∞ Z and CCSD(T)/aug-cc-pV ∞ Z estimates of the isotropic value vary from 114.7 to 116.7 a.u. and are found to compare favorably with measurements that range from 102.57 a.u. [60] to 111.35 a.u. [16] and 117.42 a.u. [14]. The latest [14] of these values was obtained using Laser Stark spectroscopy, and is considered to be the most

accurate. In view of a D_{2h} symmetry point group, there is no permanent electric dipole moment and polarizability causes the dominant part to the Stark effect.

Table 1. Polarizability tensor (α_{xx} , α_{yy} , α_{zz}) and isotropic polarizability ($\bar{\alpha}$) of naphthalene at the CCSD(T) level (FPA results; all values are in a.u.).

α_{xx}	cc-pVXZ	aug-cc-pVXZ	Exp. ^d
CCSD(T)/X=D	36.7	65.3	
CCSD(T)/X=T	50.7		
CCSD(T)/X= ∞	64.0 ^a	64.3 ^b	
CCSD(T)/X= ∞	66.6 ^c		70.8
α_{yy}			
CCSD(T)/X=D	148.4	162.2	
CCSD(T)/X=T	156.1		
CCSD(T)/X= ∞	161.0 ^a	162.0 ^b	
CCSD(T)/X= ∞	163.2 ^c		162.0
α_{zz}			
CCSD(T)/X=D	109.3	120.0	
CCSD(T)/X=T	114.8		
CCSD(T)/X= ∞	119.0 ^a	120.1 ^b	
CCSD(T)/X= ∞	120.4 ^c		119.5
$\bar{\alpha}$			
CCSD(T)/X=D	98.1	115.8	
CCSD(T)/X=T	107.2		
CCSD(T)/X= ∞	114.7 ^a	115.5 ^b	
CCSD(T)/X= ∞	116.7 ^c		117.4

a) FPA-QZ estimate (eq. 6).

b) FPA-AQZ estimate (eq. 7).

c) FPA-5Z estimate (eq. 8).

d) Reference [14].

Compared with experiment (Table 1), the α_{yy} and α_{zz} components are slightly overestimated at the CCSD(T)/aug-cc-pV ∞ Z level, by 0.05 a.u. (0.03 %) and 0.60 a.u. (0.50 %), while the α_{xx} component is slightly underestimated, by 4.2 a.u. (5.9 %). This seems to be in line with the very smooth convergence of our results with the basis set, indicating relative accuracies of the order of 2% on theoretical side. The isotropic polarizability increases substantially from 98.1

to 114.7 a.u. when the basis set evolves from cc-pVDZ to cc-pV ∞ Z. In contrast, this property has already practically converged to the CBS value when using the aug-cc-pVDZ basis set: the isotropic polarizability of naphthalene indeed slightly decreases from 115.8 to 115.5 a.u. when the basis set evolves from aug-cc-pVDZ to aug-cc-pV ∞ Z. CBS estimates for all components of the polarizability tensor and for the isotropic polarizability obtained upon extrapolating results of calculations employing the cc-pV ∞ Z and aug-cc-pV ∞ Z basis sets do not differ by more than ~ 1 a.u., indicating again relative accuracies of the order of 1 to 2 % on theoretical side.

6.3.3 Anthracene

The reader is referred to Table 2 for an overview of CCSD(T) estimations of the polarizabilities of anthracene, using various basis sets and the principles of a FPA for extrapolations to the CBS limit. The most accurate CCSD(T)/cc-pV ∞ Z value for the isotropic polarizability (176 a.u.) derives from $S_{\text{MP2-5Z}}$ energy estimates, and compare most favorably with experimental values of 171 a.u. [20], 171.41 a.u. [19] and 175 a.u. [15], the latter value being the result of a measurement employing high-resolution laser Stark spectroscopy. With absolute (relative) deviations of the order of 17.28 a.u. (24.7%), 25.98 a.u. (8.6%), and 12.41 a.u. (8.1%), our best CCSD(T)/cc-pV ∞ Z theoretical estimates are also essentially in line with the experimental values for the α_{xx} , α_{yy} , α_{zz} components of the polarizability tensor which were inferred from the latter measurements [15], and which amount to 70, 302, and 153 a.u., respectively. CCSD(T)/cc-pV ∞ Z estimates obtained from extrapolations employing the cc-pVXZ (X=D,T,Q) and (X=T,Q,5) basis sets do not deviate by more than 1.86%.

In contrast with naphthalene, however, extrapolations to the CCSD(T)/cc-pV ∞ Z and CCSD(T)/aug-cc-pV ∞ Z limits give on the other hand significantly different results, which reflects an enhanced influence of diffuse functions onto the α_{xx} and α_{yy} components of the polarizability tensor.

Table 2. Polarizability tensor (α_{xx} , α_{yy} , α_{zz}) and isotropic polarizability ($\bar{\alpha}$) of anthracene at the CCSD(T) level (FPA results; all values are in a.u.).

α_{xx}	cc-pVXZ	aug-cc-pVXZ	Exp. ^d
CCSD(T)/X=D	49.3	55.1	
CCSD(T)/X=T	67.8		
CCSD(T)/X= ∞	85.3 ^a	67.0 ^b	
CCSD(T)/X= ∞	87.3 ^c		70
α_{yy}			
CCSD(T)/X=D	252.7	250.2	
CCSD(T)/X=T	265.6		
CCSD(T)/X= ∞	272.5 ^a	264.0 ^b	
CCSD(T)/X= ∞	276.0 ^c		302
α_{zz}			
CCSD(T)/X=D	148.3	159.9	
CCSD(T)/X=T	158.2		
CCSD(T)/X= ∞	161.1 ^a	163.8 ^b	
CCSD(T)/X= ∞	165.4 ^c		153
$\bar{\alpha}$			
CCSD(T)/X=D	150.1	155.1	
CCSD(T)/X=T	163.8		
CCSD(T)/X= ∞	173.0 ^a	164.9 ^b	
CCSD(T)/X= ∞	176.2 ^c		175

a) FPA-QZ estimate (eq. 6).

b) FPA-AQZ estimate (eq. 7).

c) FPA-5Z estimate (eq. 8).

d) Reference [15].

6.3.4 Tetracene

Our CCSD(T)/cc-pVDZ and extrapolated CCSD(T)/cc-pV ∞ Z values for the components of the polarizability tensor and isotropic polarizability of tetracene (or naphthacene) are listed in Table 3. In this case, convergence problems in finite field calculations prevented us to provide data at the CCSD(T) level of theory in conjunction with cc-pVXZ (X=T,Q,5) or aug-cc-pVXZ (X=D,T,Q) basis sets. An experimental value of 217.8 a.u. which has been reported in reference [8] for the isotropic polarizability of tetracene needs to be considered with the greatest caution, because it refers in this latter work to a study [61] of field ionization processes from benzene, naphthalene and anthracene in intense laser fields. In other words, the origin and nature of this experimental value cannot be identified. There is to our knowledge no other experimental information upon the polarizabilities of tetracene (naphthacene).

Table 3. Polarizability tensor (α_{xx} , α_{yy} , α_{zz}) and isotropic polarizability ($\bar{\alpha}$) of tetracene (naphthacene) at the CCSD(T) level (FPA results; all values are in a.u.).

α_{xx}	
CCSD(T)/X=D	61.7
CCSD(T)/X= ∞	105.3 ^a
α_{yy}	
CCSD(T)/X=D	381.5
CCSD(T)/X= ∞	409.7 ^a
α_{zz}	
CCSD(T)/X=D	188.4
CCSD(T)/X= ∞	204.0 ^a
$\bar{\alpha}$	
CCSD(T)/X=D	210.5
CCSD(T)/X= ∞	239.7 ^a

a) FPA-QZ estimate (eq. 6).

6.3.5 Vibrational corrections to electronic polarizabilities

Empirical contributions of thermally induced nuclear motions (merely molecular vibrations) at 298K to the polarizabilities of the target systems are supplied in Table 4, according to an averaging procedure resorting to Born-Oppenheimer dynamical simulations at the ω B97XD/aug-cc-pVDZ level (naphthalene) or ω B97XD/cc-pVDZ level (anthracene, tetracene), along with calculations at the same levels of analytic energy gradients and of polarizabilities at each computed point in the BOMD trajectories. The computed thermal corrections increase with system size. Quite remarkably, and in line with a similar study [34] on the same grounds of the polarizabilities of Ne, CO, N₂, F₂, HF, H₂O, HCN, and C₂H₂, adding these BOMD corrections to our CCSD(T)/aug-cc-pV ∞ Z estimates of the polarisabilities obtained at equilibrium geometries enables us to reproduce the latest experimental values reported from measurements [14,15] employing laser Stark spectroscopy for the isotropic polarizabilities [14,15] of naphthalene and anthracene within 1.5 and 6.2 a.u. absolute accuracy, i.e. 1.2 and 3.5 % in relative accuracy, respectively. Whereas for naphthalene the FPA-QZ, FPA-5Z and FPA-AQZ estimates of the isotropic polarizability at equilibrium geometry ($\bar{\alpha}_e$) make little difference, in the case of anthracene the most accurate insights into the latest experimental data are obtained when using the FPA-AQZ estimates of $\bar{\alpha}_e$, which emphasizes again the importance of incorporating diffuse functions in polarizability calculations on large conjugated systems.

Table 4. Comparison of Born–Oppenheimer Molecular Dynamical estimates of thermally averaged electronic isotropic polarizabilities ($\langle\bar{\alpha}\rangle$) with equilibrium ($\bar{\alpha}_e$) and experimental values (all results are in a.u.).

	$\bar{\alpha}_e(\text{FPA})$ result)	$\bar{\alpha}_e(\omega\text{B97XD})$	Δt (fs) ^f	$\langle\bar{\alpha}\rangle_{\text{BOMD}}$	(ωB97XD)	$\langle\bar{\alpha}\rangle_{\text{FPA}}$ ⁱ	Exp
					$\langle\bar{\alpha}\rangle_{\text{BOMD}} - \bar{\alpha}_e$		
naphthalene	114.66 ^a	119.31 ^d	1321	122.71 ^g	3.40	118.06	
	116.72 ^b	119.31 ^d	1321	122.71 ^g	3.40	120.12	117.42 ^j
	115.45 ^c	119.31 ^d	1321	122.71 ^g	3.40	118.85	102.6 ^k
anthracene	150.10 ^a	157.42 ^e	1167	162.40 ^h	4.98	155.08	
	176.24 ^b	157.42 ^e	1167	162.40 ^h	4.98	181.22	175 ^l
	164.95 ^c	157.42 ^e	1167	162.40 ^h	4.98	169.93	171.4 ^m
tetracene	239.67 ^a	222.04 ^e	1025	229.19 ^h	7.15	246.82	217.8 ⁿ

a) Results obtained using the cc-pVXZ (X=D,T,Q) basis sets.

b) Results obtained using the cc-pVXZ (X=T,Q,5) basis sets.

c) Results obtained using the aug-cc-pVXZ (X=D,T,Q) basis sets.

d) Results obtained using the aug-cc-pVDZ basis set.

e) Results obtained using the cc-pVDZ basis set.

f) Run time of BOMD simulations.

g) BOMD// ωB97XD /aug-cc-pVDZ simulations at 298 K.

h) BOMD// ωB97XD /cc-pVDZ simulations at 298 K.

i) Final estimate of vibrationally averaged isotropic values of electronic static dipole polarizabilities, based on the FPA values for $\bar{\alpha}_e$ and BOMD// ωB97XD results for the vibrational correction, i.e. $\langle\bar{\alpha}\rangle_{\text{BOMD}} - \bar{\alpha}_e$.

j) Reference [14].

k) Reference [60].

l) Reference [15].

m) Reference [19].

n) Reference [8]; the origin of this experimental value is unclear.

6.4 Conclusions

The static electric dipole polarizability tensors and isotropic polarizabilities of naphthalene, anthracene and tetracene have been inferred at the confines of non-relativistic quantum mechanics from second order energy derivatives with respect to the external electric field. Using the principles of a Focal Point Analysis for energy calculations, we have extrapolated these properties up to the CCSD(T) level of theory in conjunction with asymptotically complete cc-pV ∞ Z and aug-cc-pV ∞ Z basis sets. Including diffuse functions was found to reduce the dependence of results upon the cardinal number characterizing the employed Dunning's correlation consistent polarized valence basis sets. The basis set appears to be the factor that dominates the quality of the computed electric polarizabilities. Nevertheless, the selected compounds are strongly correlated systems, which imply that calculations of at least CCSD(T) quality are required for computing polarizabilities within a few % accuracy. The examples of naphthalene and anthracene demonstrate that relative accuracies of the order of 1.2 to 3.5% can be reached by adding to the isotropic polarizabilities inferred from a Focal Point Analysis corrections that account for thermally induced nuclear (merely vibrational) motions. In the present work, these corrections have been obtained from Born-Oppenheimer molecular dynamical simulations.

6.5 References

- [1] M. P. Bogaard and B. J. Orr, in *Molecular Structure and Properties*, edited by A. D. Buckingham (Butterworths, London, 1975); A. D. Buckingham, in *Intermolecular Interactions: From Diatomics to Biopolymers*, edited by B. Pullman (Wiley, New York, 1978), p. 1; K. Jankowski, in *Methods in Computational Chemistry*, edited by S. Wilson (Plenum, New York, 1992), Vol. 5; R.D. Amos, *Adv. Chem. Phys.* **67**, 989 (1987); C. F. Dykstra, S. Y. Liu, D. J. Malik, *Adv. Chem. Phys.* **75**, 37 (1989).
- [2] V. Librando, A. Alparone, *Environ. Sci. Technol.* **41**, 1646 (2007).
- [3] M. Schwartz, *Principles of Electrodynamics* (Dover Publications, New York, 1996) p.321.
- [4] R. Firouzi, M. Zahedi, *J. Mol. Struct. (THEOCHEM)* **862**, 7 (2008).
- [5] S. Millefiori, A. Alparone, *J. Mol. Struct. (THEOCHEM)* **422**, 179 (1998).
- [6] Z. G. Soos, E. V. Tsiper, and R. A. Pascal, Jr., *Chem. Phys. Lett.* **342**, 652 (2001).
- [7] H. Reis, M. G. Papadopoulos, P. Calaminici, K. Jug, and A. M. Köster, *Chem. Phys.* **261**, 359 (2000).
- [8] S. M. Smith, A. N. Markevitch, D. A. Romanov, X. Li, R. J. Levis, and H. B. Schlegel, *J. Phys. Chem. A*, **108**, 11063 (2004).
- [9] A. Hinchliffe, B. Nikolaidi, H.J.S. Machado, *Central Eur. J. Chem.* **3**, 361 (2005).
- [10] N. Matsuzawa, D. A. Dixon, *J. Phys. Chem.* **96**, 6241 (1992).
- [11] J. R. Hammond, K. Kowalski, W. A. deJong, *J. Chem. Phys.* **127**, 144105 (2007).

- [12] See J. R. Hammond, M. Valiev, W. A. deJong and K. Kowalski, *J. Phys. Chem. A*, **111**, 5492 (2007) and references therein.
- [13] A. J. Sadlej, *Collect. Czecj. Chem. Comm.* **53**, 1995 (1988).
- [14] S. Heitz, D. Weidauer, B. Rosenow, A. Hese, *J. Chem. Phys.* **96**, 976 (1992).
- [15] V. Bendkowsky, E. Heinecke, and A. Hese, *J. Chem. Phys.* **127**, 224306 (2007).
- [16] C. G. LeFèvre and R. J. W. LeFèvre, *J. Chem. Soc. (Lond.)*, 1641 (1955).
- [17] H. G. Kuball and R. Göb, *Z. Phys. Chem., Neue Folge* **63**, 251 (1969).
- [18] M. F. Vuks, *Opt. Spectrosc.* **20**, 361 (1966).
- [19] B. H. Ruessink and C. MacLean *J. Chem. Phys.* **85**, 93 (1986).
- [20] C. L. Cheng, D. S. N. Murthy, and G. L. D. Ritchie, *Aust. J. Chem.* **25**, 1301 (1972).
- [21] H. Meyer, K. W. Schulte, A. Schweig *Chem. Phys. Lett.* **31**, 187 (1975).
- [22] J. F. Ward and C. K. Miller, *Phys. Rev. A* **19**, 826 (1979).
- [23] P. W. Fowler, *Theory and Calculation of Molecular Properties*, Annual Report C (Royal Society of Chemistry, London, 1987) p. 3; A. A. Hasanein, *Adv. Chem. Phys.* **85**, 415 (1993); A. Hinchliffe, *Ab Initio Determination of Molecular Properties* (Adam Hilger, Bristol, 1987); C. E. Dykstra, *Ab Initio Calculation of the Structures and Properties of Molecules* (Elsevier, Amsterdam, 1988); D. M. Bishop, *Adv. Quantum Chem.* **25**, 1 (1994) (ScienceDirect); J. Olsen and P. Jørgensen, in *Modern Electronic Structure Theory*, edited by D. R. Yarkony (World Scientific, London, 1995) p. 857; Y. Luo, H. Ågren, P. Jørgensen, and K. V. Mikkelsen, *Adv. Quantum Chem.* **26**, 165 (1995); M. Nakano and K. Yamaguchi, in *Trends in Chemical Physics*, Vol. 5 (Research Trends, Trivandrum, 1997); D. Pugh, in *Chemical*

Modeling: Applications and Theory (Vol. 1), edited by A. Hinchliffe (The Royal Society of Chemistry, London, 2000) p. 1; D. M. Bishop and P. Norman, in *Handbook of Advanced Electronic and Photonic Materials*, edited by H. S. Nalwa (Academic, San Diego, 2000); B. Champagne and B. Kirtman, in *Handbook of Advanced Electronic and Photonic Materials*, edited by H. S. Nalwa (Academic, San Diego, 2000).

- [24] H-J. Werner, W. Meyer, *Mol. Phys.* **31**, 855 (1976); A. J. Sadlej, *Theoret Chim Acta*, **79**, 123 (1991).
- [25] N. Bloembergen, *Nonlinear Optics* (Benjamin, New York, 1965); D. C. Hanna, M. A. Yuratich, and D. Cotter, *Nonlinear Optics of Free Atoms and Molecules* (Springer, Berlin, 1979); Y. R. Shen, *Principles of Nonlinear Optics* (Wiley, New York, 1984); J.-M. André, J. Delhalle, J.-L. Brédas, *Quantum Chemistry Aided Design of Organic Polymers*, (World Scientific Publishing, Singapore, 1991).
- [26] A. L. L. East, W. D. Allen, *J. Chem. Phys.* **99**, 4638 (1993); S. J. Klippenstein, A. L. L. East, W. D. Allen, *J. Chem. Phys.* **105**, 118 (1996); N. L. Allinger, J. T. Fermann, W. D. Allen, H. F. Schaefer III, *J. Chem. Phys.* **106**, 5143 (1997); A. G. Császár, W. D. Allen, H. F. Schaefer III, *J. Chem. Phys.* **108**, 9751 (1998); G. Tarczay, A. G. Császár, W. Klopper, V. Szalay, *J. Chem. Phys.* **110**, 11971 (1999); E. F. Valeev, W. D. Allen, H. F. Schaefer III, A. G. Császár, A. L. L. East, *J. Phys. Chem. A*, **105**, 2716 (2001); A. Salam, M.S. Deleuze, *J. Chem. Phys.* **116**, 1296 (2002); N. D. Petraco, W. D. Allen, H. F. Schaefer III, *J. Chem. Phys.* **116**, 10229 (2002); S. P. Kwasniewski, L. Claes, J.-P. François, M. S. Deleuze, *J. Chem. Phys.* **118**, 7823 (2003); E. Czinski, A. G. Császár, *Chem. Eur. J.* **9**, 1008 (2003); A. G. Császár, M. L. Leininger, V. Szalay, *J. Chem. Phys.* **118**, 10631

- (2003); K. Kahn; T. C. Bruice, *Theor. Chem. Acc.* **111**, 18 (2004); S. E. Wheeler, W. D. Allen, H. F. Schaefer III, *J. Chem. Phys.* **121**, 8800 (2004); A. G. Császár, V. Szalay, M. L. Senent, *J. Chem. Phys.*, **120**, 1203 (2004); M. S. Schuurman, S. R. Muir, W. D. Allen, H. F. Schaefer III, *J. Chem. Phys.* **120**, 11586 (2004); K. Kahn, T. C. Bruice, *Chem. Phys. Chem.* **6**, 487 (2005); K.-C. Lay, C. Y. Ng, *J. Chem. Phys.* **122**, 224310 (2005); K. Kahn, I. Kahn, *J. Comp. Chem.* **29**, 900 (2008); J. Demaison, J. Liévin, A. G. Császár, C. Guttle, *J. Phys. Chem. A*, **112**, 4427 (2008); O. S. Bokareva, V. A. Bataev, *Int. J. Quantum Chem.* **108**, 2719 (2008); T. Szidarovszky, G. Czakó, A. G. Császár, *Mol. Phys.* **107**, 761 (2009); J. J. Wilke, M. C. Lind, H. F. Schaefer III, A. G. Császár, and A. D. Allen, *J. Chem. Theor. Comp.* **5**, 1511 (2009); R. M. Balabin, *Chem. Phys. Lett.* **479**, 195 (2009); E. V. Rastotseva, V. A. Bataev, I. A. Godunov, *J. Mol. Struct (THEOCHEM)* **905**, 86 (2009).
- [27] M. S. Deleuze, L. Claes, E. S. Kryachko, J.-P. François, *J. Chem. Phys.* **119**, 3106 (2003).
- [28] B. Hajgató, M. S. Deleuze, D. J. Tozer, F. De Proft, *J. Chem. Phys.* **129**, 084308 (2008).
- [29] B. Hajgató, D. Szieberth, P. Geerlings, F. De Proft, M. S. Deleuze, *J. Chem. Phys.* **131**, 224321 (2009); B. Hajgató, M. Huzak, M. S. Deleuze, *J. Phys Chem. A*, **115**, 9282 (2011).
- [30] M. Huzak, B. Hajgató, M. S. Deleuze, *J. Chem. Phys.* **135**, 104704 (2011).
- [31] Y.-W. Son, M. L. Cohen, S.G. Louie, *Nature*, **444**, 347 (2006).
- [32] K. Raghavachari, G. W. Trucks, J. A. Pople and M. Head-Gordon, *Chem. Phys. Lett.* **157**, 479 (1989); R. J. Bartlett, J. D. Watts, S. A. Kucharski and

- J. Noga, Chem. Phys. Lett. **165**, 513 (1990); J. F. Stanton, Chem. Phys. Lett. **281**, 130 (1997).
- [33] C. J. Jameson, P. W. Fowler, J. Chem. Phys. **85**, 3432 (1986); P. G. Jasien and G. Fitzgerald, J. Chem. Phys. **93**, 2554 (1990); F. Sim and D. R. Salahub, Int. J. Quantum Chem. **43**, 463 (1992); J. Guan, P. Duffy, J. T. Carter, D. P. Chong, K. C. Casida, M. E. Casida, and M. Wrinn, J. Chem. Phys. **98**, 4753 (1993); D. A. Dixon and N. Matsuzawa, J. Phys. Chem. **98**, 3967 (1994); N. Matsuzawa and D. A. Dixon, J. Phys. Chem. **98**, 2545 (1994); J. Guan, M. E. Casida, A. M. Köster, and D. R. Salahub, Phys. Rev. B **52**, 2184 (1995); S. A. C. McDowell, R. D. Amos, and N. C. Handy, Chem. Phys. Lett. **235**, 1 (1995); N. Matsuzawa, M. Ata, and D. A. Dixon, J. Phys. Chem. **99**, 7698 (1995).
- [34] R. Monten, B. Hajgató, M. S. Deleuze, Mol. Phys. **109**, 2317 (2011).
- [35] T. Helgaker, E. Uggerud and H. J. A. Jensen, Chem. Phys. Lett. **173**, 145 (1990); E. Uggerud and T. Helgaker, J. Am. Chem. Soc. **114**, 4265 (1992); K. Bolton, W.L. Hase and G.H. Peslherbe, *Modern Methods for Multidimensional Dynamics Computation in Chemistry*, edited by D. L. Thompson (World Scientific, Singapore, 1998).
- [36] J. Oddershede, Adv. Quantum Chem. **11**, 275 (1978); J. Oddershede, P. Jørgensen, D. L. Yeager, Comput. Phys. Rep. **2**, 33 (1984); K. L. Bak, H. Koch, J. Oddershede, O. Christiansen, and S. P. A. Sauer, J. Chem. Phys. **112**, 4173 (2000).
- [37] M. Deleuze, M. J. Packer, B. T. Pickup, D. J. Wilton, J. Chem. Phys. **102**, 6128 (1995); M. S. Deleuze, B. T. Pickup, Int. J. Quantum Chem. **63**, 465 (1997); M. S. Deleuze, B. T. Pickup, D. A. Wilton, Int. J. Quantum Chem. **77**, 625 (2000).

- [38] R. Dreizler, E. Gross, *Density Functional Theory* (Plenum Press, New York, 1995).
- [39] C. Lee, W. Yang, R. G. Parr, *Phys. Rev. B* **37**, 785 (1988); A. D. Becke, *J. Chem. Phys.* **98**, 5648 (1993).
- [40] T. H. Dunning Jr., *J. Chem. Phys.* **90**, 1007 (1989).
- [41] Gaussian 09, Revision A.1, M. J. Frisch, G. W. Trucks, H. B. Schlegel, G. E. Scuseria, M. A. Robb, J. R. Cheeseman, G. Scalmani, V. Barone, B. Mennucci, G. A. Petersson, H. Nakatsuji, M. Caricato, X. Li, H. P. Hratchian, A. F. Izmaylov, J. Bloino, G. Zheng, J. L. Sonnenberg, M. Hada, M. Ehara, K. Toyota, R. Fukuda, J. Hasegawa, M. Ishida, T. Nakajima, Y. Honda, O. Kitao, H. Nakai, T. Vreven, J. A. Montgomery, Jr., J. E. Peralta, F. Ogliaro, M. Bearpark, J. J. Heyd, E. Brothers, K. N. Kudin, V. N. Staroverov, R. Kobayashi, J. Normand, K. Raghavachari, A. Rendell, J. C. Burant, S. S. Iyengar, J. Tomasi, M. Cossi, N. Rega, J. M. Millam, M. Klene, J. E. Knox, J. B. Cross, V. Bakken, C. Adamo, J. Jaramillo, R. Gomperts, R. E. Stratmann, O. Yazyev, A. J. Austin, R. Cammi, C. Pomelli, J. W. Ochterski, R. L. Martin, K. Morokuma, V. G. Zakrzewski, G. A. Voth, P. Salvador, J. J. Dannenberg, S. Dapprich, A. D. Daniels, Ö. Farkas, J. B. Foresman, J. V. Ortiz, J. Cioslowski, and D. J. Fox, Gaussian, Inc., Wallingford CT, 2009.
- [42] H. H. Jaffé and M. Orchin, *Symmetry in Chemistry* (John Wiley & Sons, New York, 1965).
- [43] A. Szabo, N. S. Ostlund, *Modern Quantum Chemistry*, (McGraw-Hill, New York, 1982).
- [44] C. Møller, M. S. Plesset, *Phys. Rev.* **46**, 618 (1934).
- [45] M. Head-Gordon, J. A. Pople, and M. J. Frisch, *Chem. Phys. Lett.* **153**, 503 (1988).

- [46] J. A. Pople, R. Seeger, and R. Krishnan, *Int. J. Quant. Chem. Symp.* **11**, 149 (1977).
- [47] R. Krishnan, and J. A. Pople, *Int. J. Quant. Chem.* **14**, 91 (1978).
- [48] G.D. Purvis III and R.J. Bartlett, *J. Chem. Phys.* **76**, 1910 (1982).
- [49] MOLPRO, version 2010.1, a package of ab initio programs, H.-J. Werner, P. J. Knowles, F. R. Manby, M. Schütz, P. Celani, G. Knizia, T. Korona, R. Lindh, A. Mitrushenkov, G. Rauhut, T. B. Adler, R. D. Amos, A. Bernhardsson, A. Berning, D. L. Cooper, M. J. O. Deegan, A. J. Dobbyn, F. Eckert, E. Goll, C. Hampel, A. Hesselmann, G. Hetzer, T. Hrenar, G. Jansen, C. Köppl, Y. Liu, A. W. Lloyd, R. A. Mata, A. J. May, S. J. McNicholas, W. Meyer, M. E. Mura, A. Nicklass, P. Palmieri, K. Pflüger, R. Pitzer, M. Reiher, T. Shiozaki, H. Stoll, A. J. Stone, R. Tarroni, T. Thorsteinsson, M. Wang and A. Wolf, see [http:// www.molpro.net](http://www.molpro.net).
- [50] T. H. Dunning Jr, *J. Chem. Phys.* **90**, 1007 (1989); D. E. Woon and T. H. Dunning Jr, *J. Chem. Phys.* **100**, 2975 (1994).
- [51] R. A. Kendall, T. H. Dunning Jr and R. J. Harrison, *J. Chem. Phys.* **96**, 6796 (1992); A. K. Wilson, T. van Mourik and T. H. Dunning Jr, *J. Mol. Struct. (THEOCHEM)* **388**, 339 (1998).
- [52] D. Feller, *J. Chem. Phys.* **96**, 6104 (1992); *ibid* **98**, 7059 (1993).
- [53] J. M. L. Martin, in *Energetics of Stable Molecules and Reactive Intermediates*, NATO ASI Symposium Series, edited by M. E. Mirrasda Piedade and K. K. Irikura (Kluwer, Dordrecht, 1999).
- [54] C. Schwartz, *Methods in Computational Physics*, Vol. 2. edited by B. Alder (Academic, New York, 1963).
- [55] J.-D. Chai and M. Head-Gordon, *Phys. Chem. Chem. Phys.* **10**, 6615 (2008).

- [56] D. L. Bunker, *Meth. Comp. Phys.* **10**, 287 (1971); L. M. Raff and D. L. Thompson, *Theory of Chemical Reaction Dynamics*, edited by M. Baer (CRC, Boca Raton, FL, 1985); *Advances in Classical Trajectory Methods*, Vol. 1-3, edited by W. L. Hase (JAI, Stamford, CT, 1991); D. L. Thompson, *Encyclopedia of Computational Chemistry*, edited by P. v. R. Schleyer, N. L. Allinger, P. A. Kollman, T. Clark, H. F. Schaefer III, J. Gasteiger, and P. R. Schreiner (Wiley, Chichester, 1998).
- [57] W. Chen, W. L. Hase, and H. B. Schlegel, *Chem. Phys. Lett.*, **228**, 436 (1994); J. M. Millam, V. Bakken, W. Chen, W. L. Hase, and H. B. Schlegel, *J. Chem. Phys.*, **111**, 3800 (1999); X. Li, J. M. Millam, and H. B. Schlegel, *J. Chem. Phys.*, **113**, 10062 (2000); W. L. Hase, R. J. Duchovic, X. Hu, A. Komornicki, K. F. Lim, D.-H. Lu, G. H. Peslherbe, K. N. Swamy, S. R. V. Linde, A. Varandas, H. Wang, and R. J. Wolfe, "VENUS96: A General Chemical Dynamics Computer Program" *QCPE*, **16**, 671 (1996).
- [58] R. Bulirsch, J. Stoer, *Introduction to Numerical Analysis* (Springer-Verlag, New York, 1991).
- [59] W. F. Press, B. P. Flannery, S. A. Teukolsky, W. T. Vetterling, Richardson Extrapolation and the Bulirsch-Stoer Method in: *Numerical Recipes in FORTRAN: The Art of Scientific Computing*, 2nd ed. (Cambridge University Press, Cambridge, England, 1992) p. 718-725.
- [60] R. L. Calvert, G. L. D. Ritchie, *J. Chem. Soc. Faraday Trans. II* **76**, 1249 (1980).
- [61] M. J. DeWitt and R. J. Levis, *Phys. Rev. Lett.* **81**, 5101 (1998).

7 Summary and conclusions

In the first part of the present thesis we have re-investigated the issue of Half-Metallicity for zig-zag graphene nanoribbons (ZGNRs) of finite width and periodicity in one dimension as well as for zig-zag graphene nanoislands (ZGNIs), such as bisanthrene and tetrabenzo[bc,ef,kl,no]coronene. This issue is currently very popular among material scientists due to theoretical predictions published in major scientific journals (Nature [1], Physical Review B [2]) that are based on spin-unrestricted Density Functional Theory calculations, which invariably predict a symmetry-broken electronic wave function with spin-polarized edge states. Because these states are localized on opposite zig-zag edges, they respond differently to a transversal electric field, hence the very unusual property of half-metallicity, i.e. the coexistence of metallic nature for electrons with one spin orientation and insulating nature for the electrons of opposite spin. Based on these predictions a new generation of electronic devices exploiting the electron spin for carrying binary information is already envisioned. ZGNRs and ZGNIs would thus open the way to a new field in electronics, referred to as spintronics (i.e. *spin transport electronics*).

It has been made clear within the frame of this thesis that these views are the outcome of a too approximate treatment of electron correlation within a one-determinantal approach such as unrestricted Density Functional Theory (which has been introduced in **Chapter 2**, along with Hartree-Fock theory and many-body theories of improving quality). In the absence of a symmetry-breaking spin-dependent potential (e.g. spin orbit interactions), symmetry breakings in the spin densities of a system exhibiting a singlet state are necessarily artefactual in origin. In **Chapter 3**, the formalism of crystalline orbitals for

extended systems with periodicity in one dimension has been applied in order to demonstrate that any antiferromagnetic and half-metallic spin-polarization of edge states in n -acenes, and more generally in zig zag graphene nanoislands and nanoribbons of finite width, would imply a spin contamination ($\langle S^2 \rangle$) that increases proportionally to system size, in sharp and clear contradiction with the implications of Lieb's theorem for compensated bipartite lattices and the expected value for a singlet ($S=0$) electronic ground state. In support to these findings, it has been computationally verified with various many-body treatments employing Møller-Plesset perturbation theory or Coupled Cluster theory that half-metallicity in extended graphene nanoribbons will be quenched by an exact treatment of electron correlation, at the confines of non-relativistic many-body quantum mechanics. In this context, such as the size-extensive spin-contamination to which it relates, half-metallicity is thus most clearly nothing else than a methodological artefact. In extended systems with translation symmetry in one dimension and with a vanishing band gap, a physical symmetry breaking of spin-densities due to a spin-dependent potential or thermally induced spin flips may nonetheless still result into an intrinsic half-metallic transport behaviour. Further studies employing *many-body relativistic quantum mechanics* are therefore needed for verifying whether extremely weak spin-orbit coupling interactions, of the order of a few tenths μeV only [3], or anisotropic magnetic dipole-dipole interactions between unpaired electrons, could nevertheless be strong enough to induce a physical and effectively measurable spin-polarization of edge states in large enough, perfectly planar and undistorted ZGNRs, with vanishingly small excitation energies, in the absence of any external magnetic perturbation or complications like thermal excitations.

In **Chapter 4**, we have presented a benchmark theoretical study of the electronic ground state and of the vertical and adiabatic singlet-triplet (ST) excitation energies of n -acenes ($C_{4n+2}H_{2n+4}$) ranging from octacene ($n=8$) to undecacene ($n=11$), in continuation to a previous study [4] of the singlet-triplet energy gap of benzene and n -acenes ranging from naphthalene ($n=2$) to heptacene ($n=7$). These studies demonstrate that highly accurate insights into experimental observable are amenable for these strongly correlated systems, using a spin-restricted depiction. These studies exploit, by means of a Focal Point Analysis (FPA), the overall smooth and regular convergence of electronic energy differences with regards to the size of the basis set and to the level attained in correlation, in calculations employing the HF, MP2, MP3, MP4SDQ, CCSD, and CCSD(T) approaches, along with increasingly complete Dunning's correlation consistent polarized valence basis sets. Since the discrepancies between different FPA results for the vertical and adiabatic singlet-triplet excitation energies do not exceed 0.6 kcal/mol (0.026 eV), and considering that various criteria for multi-reference (i.e. static correlation) effects indicate that a single-reference depiction should prevail, we conclude that we have managed to grasp the lowest excitation energies of acenes up to undecacene in the vacuum within or close to chemical accuracy (1 kcal/mol, i.e. 43.4 meV). Further extrapolations of results obtained for benzene ($n=1$) and all studied n -acenes so far ($n=2-11$) indicate a vanishing singlet-triplet energy gap, in the limit of an infinitely large polyacene ($n \rightarrow \infty$), within an uncertainty of 1.5 kcal/mol (0.06 eV). Considering the trends that emerge from the calculations we have presented, it seems quite likely that finite acenes approaching the polymer limit would still possess a singlet electronic ground state with a total spin equal to zero. Further studies are nonetheless required for assessing the origin of a

rather large difference between our theoretical value for the singlet-triplet energy gap in the polymer limit (0.00 ± 0.06 eV) and the optical gap inferred in this limit (1.18 ± 0.06 eV) from an extrapolation of UV-Vis experimental data on finite acenes. A most likely explanation is that this large experimental band gap results from structural distortions left by the photogeneration of octacene and nonacene in a rigid solid argon matrix from twisted diketone precursors.

In **Chapter 5**, we have presented a benchmark theoretical study of the ionization energies, electron affinities and singlet-triplet energy gaps of azulene, phenanthrene, pyrene, chrysene and perylene. These various properties were again computed by applying the principles of a Focal Point Analysis onto a series of single-point calculations at the level of Hartree-Fock theory, second-, third-, and fourth-order Møller-Plesset perturbation theory, as well as coupled cluster theory including single, double and perturbative triple excitations, in conjunction with correlation consistent basis sets of improving quality. Results are supplemented with an extrapolation to the limit of an asymptotically complete basis set. In view of the complexity and strongly correlated nature of the selected molecular targets, our best estimates for the singlet-triplet energy gap support favorably the comparison with experiment, with discrepancies ranging from 0.046 eV (azulene) up to 0.24 eV (phenanthrene). Also our theoretical results for the electron affinities sustain most favorably the comparison with experiment, with discrepancies ranging from only 0.006 eV and 0.017 eV for pyrene and azulene, up to 0.075 and 0.1 eV in the case of chrysene and perylene, respectively. At last, when considering ionization energies, the discrepancies between theory and experiment vary from 0.04 eV, 0.05 eV and 0.05 eV, for azulene, pyrene and chrysene, up to 0.11 and 0.19 eV for phenanthrene and perylene. The latter very large discrepancy is probably

ascribable to the more strongly correlated nature of perylene, which a single-reference CCSD(T) treatment may fail to apprehend within chemical accuracy.

In **Chapter 6**, we have applied the principles of a Focal Point Analysis to finite field calculations in order to estimate the static electric dipole polarizabilities of naphthalene, anthracene and tetracene up to the level of Coupled Cluster theory including single, double and perturbative triple excitations [CCSD(T)] in the limit of an asymptotically complete basis set, again using a symmetry-restricted depiction. Thermal corrections to polarizabilities have been empirically estimated according to Born-Oppenheimer Molecular Dynamical simulations at 298K employing Density Functional Theory. The basis set appears to be the factor that dominates the quality of the computed electric polarizabilities. Confrontation with the latest experimental values for isotropic polarizabilities ultimately indicates relative accuracies of the order of 1.2 % (for naphthalene) to 3.5 % (for anthracene), provided diffuse functions are incorporated in the focal point analysis.

7.1 References

- [1] Y.-W. Son, M. L. Cohen, and S. G. Louie, *Nature (London)*, **444**, 347 (2006).
- [2] O. Hod, V. Barone, G. E. Scuseria, *Phys. Rev. B*, **77**, 035411 (2008).
- [3] M. Gmitra, S. Korschuh, C. Ertler, C. Ambrosch-Draxl, J. Fabian, *Phys. Rev. B*, **80**, 235431(2009).
- [4] B. Hajgató, D. Szieberth, P. Geerlings, F. De Proft, M.S. Deleuze, *J. Chem. Phys.* **131**, 224321 (2009).

8 Samenvatting en conclusies

In het eerste deel van de voorliggende thesis werd de Half-Metaalliciteit voor zig-zag grafeen nanolinten (ZGNLn) van eindige breedte en periodiciteit in één dimensie heronderzocht, alsook voor zig-zag grafeen nano-eilanden (ZGNE_n), zoals bisanthreen en tetrabenzo[bc,ef,kl,no]coroneen.). Dit thema staat momenteel zeer sterk in de belangstelling bij materiaalonderzoekers, wat zich uit in voorspellingen die gepubliceerd werden in prestigieuze internationale wetenschappelijke tijdschriften (Nature [1], Physical Review B [2]). Deze voorspellingen zijn gebaseerd op berekeningen gebruik makend van spin ongerestricteerde Dichtheid Functionaal Theorie, die op een steevaste manier een symmetrisch gebroken elektronen golf functie met spin gepolariseerde randtoestanden voorspellen. Omdat deze toestanden zich bevinden op tegengestelde zig-zag randen, reageren zij anders op een transversaal elektrisch veld, vandaar de zeer ongewone eigenschap van half-metaalliciteit, m.a.w. het naast elkaar bestaan van metallische natuur voor de elektronen met één spin-oriëntatie en isolerende natuur voor de elektronen van de tegengestelde spin. Op basis van deze voorspellingen, heeft men reeds een nieuwe generatie elektronische apparaten op het oog die de elektronenspin benutten om binaire informatie te dragen. ZGNLn en ZGNE_n zouden zo de weg vrijmaken voor een nieuw veld in de elektronica, waarnaar verwezen wordt als spintronica (Engels: "Spintronics", voor "*spin transport Electronics*").

Binnen het kader van deze thesis werd het duidelijk gemaakt dat deze visies het resultaat zijn van een onvolledige behandeling van elektronen correlatie binnen een benadering met één determinant zoals ongerestricteerde Dichtheid Functionaal Theorie (deze werd geïntroduceerd in **Hoofdstuk 2**,

samen met Hartree-Fock theorie en veel-deeltjes theorieën van stijgende kwaliteit). In de afwezigheid van een symmetrie brekende spinafhankelijke potentiaal (m.a.w. spin-orbitaal interacties), symmetrie breuken in de spin-dichtheden van een systeem, welke een singlet toestand toont, zijn in oorsprong een methodologische artefact. In **Hoofdstuk 3** werd het formalisme van kristallijne orbitalen voor uitgebreide systemen met periodiciteit in één dimensie toegepast om aan te tonen dat elke antiferromagnetische en half-metallische spin-polarisatie van randtoestanden in n -acenen, en meer algemeen in zig zag grafen nano-eilanden en nano-linten van eindige breedte, een spin-contaminatie ($\langle S^2 \rangle$) zou impliceren die proportioneel stijgt met de systeemgrootte. Dit is een scherpe en duidelijke tegenstelling met de implicaties van Lieb's theorema voor gecompenseerde tweedelige roosters en de verwachte waarde voor een singlet ($S=0$) elektronen grondtoestand. Ter ondersteuning van deze bevindingen, werd computationeel geverifieerd met verschillende veel-deeltjes behandelingen gebruik makend van Møller-Plesset's storingstheorie of van Coupled Cluster theorie dat half-metallische in uitgebreide grafen nanolinten zal uitgeschakeld zijn met een exacte behandeling van elektronencorrelatie, in het kader van niet-relativistische veel-deeltjes kwantummechanica. In deze context, zoals de "size-extensive" spin-contaminatie waar het aan verwant is, is half-metallische dus duidelijk niets meer dan een methodologisch artefact. In uitgebreide systemen met translatie symmetrie in één dimensie en met verdwijnende band gap, kan een fysische breuk van de symmetrie van spin-dichtheden te wijten aan een spin-afhankelijke potentiaal of thermisch geïnduceerde spin omkeringen, nog steeds resulteren in een intrinsieke half-metallisch transport gedrag. Verder onderzoek dat gebruik maakt van veel-deeltjes relativistische kwantummechanica is dus nodig om na

te gaan of extreem zwakke spin-orbitaal koppelings interacties, van de orde van slechts enkele tientallen μeV [3], of anisotropische magnetische dipool-dipool interacties tussen niet gepaarde elektronen, toch sterk genoeg kunnen zijn om een fysische en effectief meetbare spin-polarisatie van randtoestanden te induceren in voldoende groote, perfect vlakke en onvervormde ZGNLs met verdwijnend kleine excitatieenergieën, in afwezigheid van enige externe magnetische storing of complicaties zoals thermische excitaties [4].

In Hoofdstuk 4 werd een bench-mark theoretische studie van de elektronen grondtoestand en van de verticale en adiabatische singlet-triplet (ST) excitatie-energieën van n -acenen ($\text{C}_{4n+2}\text{H}_{2n+4}$) gaande van octaceen ($n=8$) tot undecaceen ($n=11$) gepresenteerd, voortbouwend op een voorgaande studie [4] van de singlet-triplet excitatie-energieën van benzeen ($n=1$) en n -acenen gaande van naftaleen ($n=2$) tot heptaceen ($n=7$). Deze studies tonen aan dat zeer accurate inzichten in experimentele waarden mogelijk zijn voor deze sterk gecorreleerde systemen, in het kader van een spin-gerectriceerde representatie. Focale Puntanalyse (FPA) maakt gebruik van de gladheid en de reguliere convergentie van elektronen energiever verschillen met betrekking tot de grootte van de basisset en tot het bereikte correlatieniveau, in berekeningen die de HF, MP2, MP3, MP4SDQ, CCSD, en CCSD(T) benaderingen aanwenden, samen met basissets van stijgende grootte. Omdat de discrepanties tussen verschillende FPA resultaten voor de verticale en adiabatische singlet-triplet excitatie-energieën 0.6 kcal/mol (0.026 eV) niet overtreffen, en rekening houdend dat verschillende criteria voor multi-referentie (statische correlatie) effecten er op wijzen dat een single-referentie representatie prevaleert, besluiten we dat we in staat waren om de laagste excitatie-energieën van acenen tot aan undecaceen in het vacuüm binnen of dicht bij chemische

accuraatheid (1 kcal/mol, i.e. 43.4 meV) te bepalen. Verdere extrapolaties van resultaten verkregen voor benzeen ($n=1$) en alle bestudeerde n -acenen ($n=2-11$) duiden een verdwijnende singlet-triplet excitatie-energie aan, in de limiet van een oneindig grote polyaceen ($n \rightarrow \infty$), binnen een onzekerheid van 1.5 kcal/mol (0.06 eV). Rekening houdend met de trends die ontstaan uit de berekeningen die gepresenteerd werden, lijkt het waarschijnlijk dat eindige acenen die de polymeer limiet benaderen nog steeds een singlet elektronen grondtoestand zouden bezitten met een totale spin gelijk aan nul. Desalniettemin is verder onderzoek nodig om de oorsprong van een eerder groot verschil te begrijpen tussen onze theoretische waarde voor de singlet-triplet excitatie-energie in de polymere limiet (0.00 ± 0.06 eV) en de optische gap verkregen in deze limiet (1.18 ± 0.06 eV) door een extrapolatie van UV-Vis experimentele data van eindige acenen. Een mogelijke verklaring is dat deze grote experimentele band gap resulteert uit structurele vervormingen als gevolg van fotogeneratie van octaceen en nonaceen in een rigide vaste argon matrix, uitgaande van verdraaide diketon precursors.

In **Hoofdstuk 5** werd een bench-mark theoretische studie over de ionisatie-energieën, elektronenaffiniteiten, en singlet-triplet energie gaps van azuleen, fenanthreen, pyreen, chryseen en peryleen gepresenteerd. Deze verschillende eigenschappen werden opnieuw berekend door de principes van een Focale Puntsanalyse toe te passen op een reeks van single-point berekeningen op het niveau van Hartree-Fock theorie, tweede-, derde- en vierde orde Møller-Plesset's storingstheorie, alsook coupled cluster theorie met enkele, dubbele en tripele excitaties (deze laatste via storingstheorie) inbegrepen, samen met correlatie consistente basissets met stijgende kwaliteit. Resultaten worden aangevuld met een extrapolatie tot de basisset limiet. In het licht van de

complexiteit en sterk gecorreleerde natuur van de geselecteerde moleculaire systemen, stemmen onze beste schattingen van de singlet-triplet energie gap vrij goed overeen met experimentele resultaten, met discrepanties gaande van 0.046 eV (azuleen) tot 0.24 eV (fenanthreen). Ook onze theoretische resultaten voor de elektronenaffiniteiten komen zeer goed overeen met de experimentele data, met discrepanties gaande van slechts 0.006 eV en 0.017 eV voor pyreen en azuleen, tot 0.075 en 0.1 eV in het geval van respectievelijk chryseen en peryleen. Ten slotte, de discrepanties tussen theorie en experimentele data gaan in het geval van ionisatie-energieën van 0.04, 0.05 en 0.05 eV, voor azuleen, pyreen en chryseen, tot 0.11 en 0.19 eV voor phenanthreen en peryleen. Laatstgenoemde zeer grote discrepantie is waarschijnlijk toe te schrijven aan de sterker gecorreleerde natuur van peryleen, waardoor een enkelvoudige-referentie CCSD(T) behandeling kan falen om chemische accuraatheid te bereiken.

In **Hoofdstuk 6** werden de principes van Focale Puntsanalyse toegepast op eindige veldberekeningen om zo de statische elektrische dipool polariseerbaarheid van naphthaleen, anthraceen en tetraceen te bepalen, tot op het niveau van coupled cluster theorie met enkele, dubbele en tripele excitaties inbegrepen (deze laatste via storingstheorie) [CCSD(T)], in de limiet van een asymptotisch volledige basisset, opnieuw gebruik makend van een symmetrisch beperkte beschrijving. Thermische correcties aan de polariseerbaarheid werden volgens Born-Oppenheimer's Moleculaire Dynamische simulaties empirisch geschat op 298 K, hierbij gebruik makend van de Dichtheid Functionaal Theorie. De basisset lijkt de factor te zijn die de kwaliteit van de berekende elektrische polariseerbaarheden domineert. De vergelijking met de laatste experimentele waarden van isotropische polariseerbaarheden resulteert in relatieve

accuraatheden van de orde van 1.2 % (voor naftaleen) tot 3.5 % (voor anthraceen), op voorwaarde dat diffuse functies geïncorporeerde zijn in de FPA.

8.1 References

- [1] Y.-W. Son, M. L. Cohen, and S. G. Louie, *Nature (London)*, **444**, 347 (2006).
- [2] O. Hod, V. Barone, G. E. Scuseria, *Phys. Rev. B*, **77**, 035411 (2008).
- [3] M. Gmitra, S. Konschuh, C. Ertler, C. Ambrosch-Draxl, J. Fabian, *Phys. Rev. B*, **80**, 235431(2009).
- [4] B. Hajgató, D. Szieberth, P. Geerlings, F. De Proft, M.S. Deleuze, *J. Chem. Phys.* **131**, 224321 (2009).

List of publications

- M. Huzak, B. Hajgató, M. S. Deleuze, "Half-Metallicity and Spin-Contamination of the Electronic ground State of Graphene Nanoribbons and Related Systems: an Impossible Compromise?" J. Chem. Phys., **135** (2011), 104704.
- B. Hajgató, M. Huzak, M. S. Deleuze, "Focal Point Analysis of the Singlet-Triplet Energy Gap of Octacene and Larger Acenes", J. Phys Chem. A., **115** (2011), 9282 - 9293.
- M. Huzak, B. Hajgató, M.S. Deleuze, "Benchmark Theoretical Study of the Ionization Energies, Electron Affinities and Singlet-Triplet Energy Gaps of Azulene, Phenanthrene, Pyrene, Chrysene and Perylene" Chem. Phys., **406** (2012), 55-64.
- M. Huzak, M.S. Deleuze, "Benchmark Theoretical Study of the Electric Polarizabilities of Naphthalene, Anthracene and Tetracene" J. Chem. Phys., **138** (2013), 24319.
- M.S. Deleuze, M. Huzak, B. Hajgató, "Half-Metallicity of Graphene Nanoribbons and Related Systems: a new Quantum Mechanical El Dorado for Nanotechnologies ... or a Hype for Materials Scientists?" J. Mol. Model., Accepted July (2012).

List of attended conferences

- 14th International Conference on Density Functional Theory, Athens, Greece, August 29 - September 2, 2011; poster presentation.
- WOG meeting on aromaticity, Ghent University, October 28, 2011; oral presentation.
- Quantum Chemistry in Belgium, Tenth Edition (QCB10), Vrije Universiteit Brussel, February 10, 2012; oral presentation.
- 2nd International Symposium on Electron Momentum Spectroscopy, Hasselt University (Royal Academy of Belgium for the Sciences and Arts, Brussels), Belgium, August 23-24, 2012.